The Role of Carbon-Based Materials for Fuel Cells Performance

Babak Jaleh [a,**], Mahmoud Nasrollahzadeh [b,***], Mahtab Eslamipanah [a], Atefeh Nasri [a], Ensiye Shabanlou [a], Nilesh R. Manwar [c], Radek Zboril [d,e], Paolo Fornasiero [f], Manoj B. Gawande [c,d,*]

[a] Department of Physics, Faculty of Science, Bu-Ali Sina University, 65174, Hamedan, Iran
[b] Department of Chemistry, Faculty of Science, University of Qom, Qom, 3716146611, Iran
[c] Department of Industrial and Engineering Chemistry, Institute of Chemical Technology, Mumbai-Marathwada Campus, Jalna, 431203, Maharashtra, India
[d] Regional Centre of Advanced Technologies and Materials, Czech Advanced Technology and Research Institute, (CATRIN), Palacký University Olomouc, Šlechtitelů 27, 779 00, Olomouc, Czech Republic
[e] CEET, Nanotechnology Centre, VŠB-Technical University of Ostrava, 17. Listopadu 2172/15, 708 00, Ostrava-Poruba, Czech Republic
[f] Department of Chemical and Pharmaceutical Sciences, INSTM Trieste Research Unit and ICCOM-CNR Trieste Research Unit, University of Trieste via L. Giorgieri 1, I-34127, Trieste, Italy

ARTICLE INFO

Keywords:
Carbon
Fuel Cell
Catalyst
Energy Storage

ABSTRACT

Global reduction of traditional fuel sources such as natural gases, coal, and petroleum has led researchers to seek prominent and beneficial energy conversion devices. Fuel cells are a newfound and upcoming energy generation systems that have progressed rapidly. Fuel cells are popular eco-friendly devices among different energy conversion devices due to their cost-effectiveness and high output. In a fuel cell composed of a cathode, anode, and electrolyte, the electrical energy is produced through chemical reactions. Various fuels such as H_2, alcohols, especially ethanol and methanol, and formic acid are applied in fuel cells. Large scale application of this technology mainly depends on two aspects, including one is the possibility to produce on a large scale and accessible cost-efficient catalytic materials (anodic and cathodic), and second is the stable and high performing membrane in fuel cells. Among various investigated materials, carbon supports and metal-free carbon materials are widely used in fuel cell devices, which increases their overall electrochemical surface area (ECSA) and performance. Carbon-based materials with high surface area, excellent electrical conductivity, and high porosity is known to be a primary substrate for electrochemical energy storage applications such as batteries, supercapacitors, and fuel cells. Herein, we have reviewed the efficacy of carbon-based materials on electrocatalytic activity, stability, and output performance of different fuel cells.

1. Introduction

Fossil fuels are the most significant energy source worldwide, leading to problems such as the rapid decline in fossil fuel reserves and increasing environmental impacts. Over the past few decades, the production of green fuels has been a significant challenge due to increasing global energy demand with the concomitant dramatic increase of environmental pollution and climate change. Hence, developing renewable systems for energy production is one of the most attractive categories for researchers. Fuel cells introduce as a conversion system, in which the chemical energy is converted to electrical energy by the oxidation of fuel. Fuel cells have the main advantages of high energy density, excellent efficiency, cost-efficient, and controllable emission [1]. Sir William Robert Grove invented the first fuel cell in 1838; however, the exploitation of fuel cells started in the 1950s by General Electric (GE) Company [2]. Hydrogen (H_2) is an abounded earth's element, and it is employed as fuel in fuel cells because of its high reactivity tendency. Furthermore, H_2 can derive from the electrochemical oxidation of hydrocarbon fuels such as methanol, formic acid and formaldehyde [1,3]. H_2 can quickly oxidize at the fuel cell's anode, and its chemical product

* Corresponding author. Department of Industrial and Engineering Chemistry, Institute of Chemical Technology, Mumbai-Marathwada Campus, Jalna, 431203, Maharashtra, India.
** Corresponding author.
*** Corresponding author.
E-mail addresses: jaleh@basu.ac.ir (B. Jaleh), mahmoudnasr81@gmail.com (M. Nasrollahzadeh), mb.gawande@marj.ictmumbai.edu.in (M.B. Gawande).

is only water [3]. However, H_2 must be produced sustainably, not from fossil fuels [4,5]. In a fuel cell based on H_2 fuel, H_2 enters the anode electrode and oxidizes by losing electrons. In this reaction, H^+ ion and electron generates. The transform of H^+ ions and electrons is carried out via electrolyte and an external circuit, respectively. The oxygen contained in the cathode reacts with the H^+ ions and the electrons, producing water [6]. Fuel cells can be classified based on their electrolyte and fuel used. Proton exchange membrane fuel cells (PEMFCs), phosphoric acid fuel cells (PAFCs), solid oxide fuel cells (SOFCs), alkaline fuel cells (AFCs), and molten carbonate fuel cells (MCFCs) are the main categories of fuel cells as depicted in Fig. 1 (a) [2]. Among all fuel cells, PEMFCs possess high power density and faster response. Based on fuel used, PEMFCs classify into two direct liquid fuel cells (DLFCs) and H_2-fueled PEMFCs [7]. Besides, biological fuel cells, including enzymatic biofuel cells (EFCs) and microbial fuel cells (MFCs), are attractive categories for researchers. Henceforth, the overall performance of carbon-based materials for PEMFCs, DAFCs, SOFCs, DFAFCs, and biological fuel cells are being examined in this review. Fuel cells has possess significant applications in vehicles, telecommunication, and portable electronic systems and devices of low power [3].

Nanomaterials or metal nanoparticles (MNPs) are one of the most promising materials which can be applied as efficient catalysts or materials in various fields [9-23]. Among them, MNPs such as platinum (Pt) and palladium (Pd) are widely employed as catalysts in fuel cell

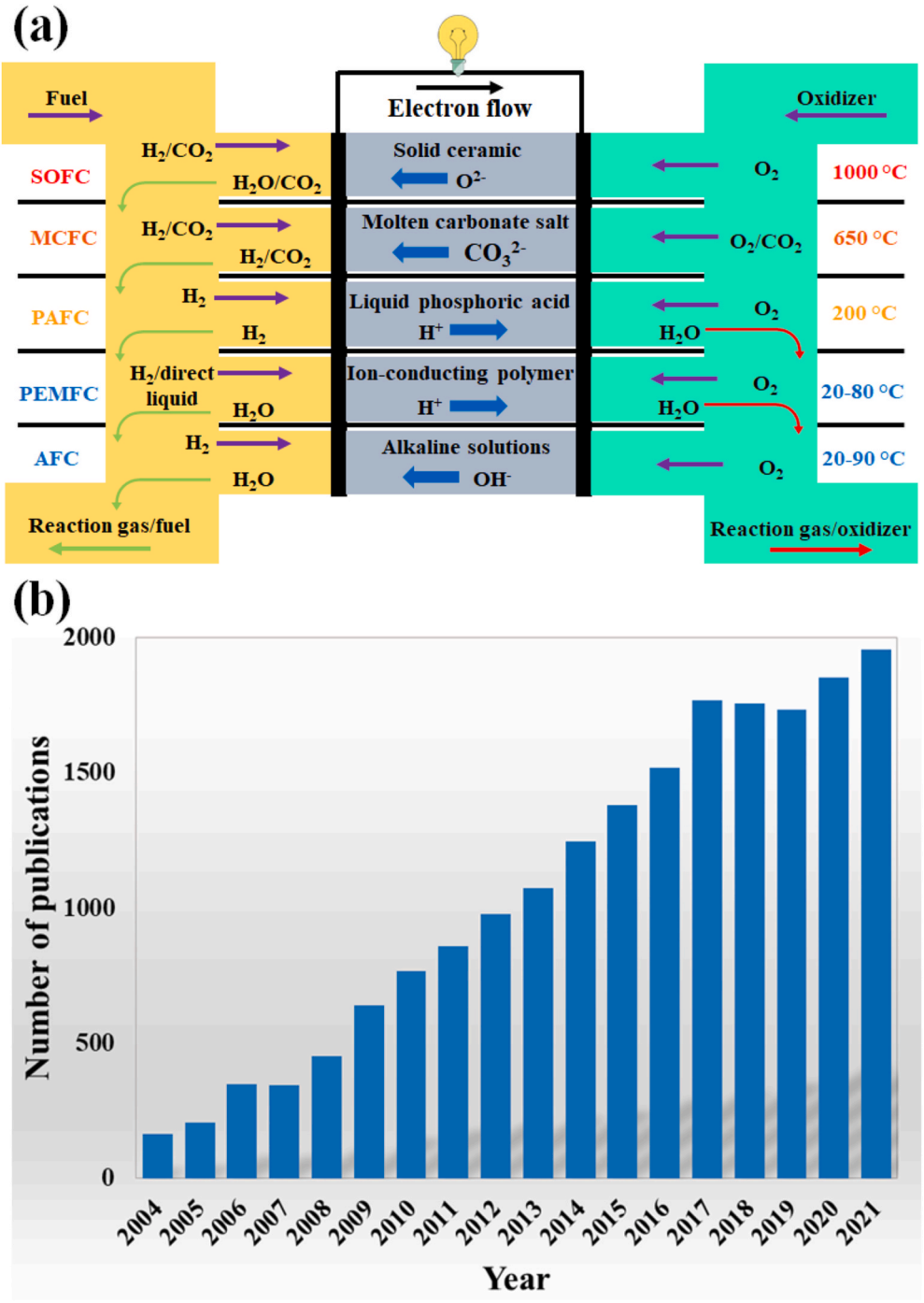

Fig. 1. (a) Diagram representation of fuel cell types. Modified from ref. [8]. (b) Publications recognized by search for "carbon materials for fuel cells" from 2004 to 2021 (Source: Web of Science core database).

applications [24-27]. However, catalytic activity enhancement is one of the most critical issues in fuel cell systems, and it is dependent on suitable catalyst supports. Support materials play a crucial role in determining the performance, cost of the electrocatalysts, and the overall fuel cell. Porosity, surface area, surface functional groups, electrical conductivity, and electrochemical stability are the main parameters for the investigation of support efficiency to prepare the appropriate electrocatalysts as anode or cathode materials for any type of fuel cell. With the increased surface area of the catalyst support, the dispersion of metallic NP grows on the suitable substrate, which enhances the catalytic activity [25,28,29]. However, owing to the features of high surface area, excellent porosity, chemical and mechanical stability, good conductivity, great interaction between catalyst and support, and significant biocompatibility of carbon-based materials such as graphene, carbon black (CB), carbon nanofibers (CNFs), and carbon nanotubes (CNTs) are suitable candidates for the loading of metallic NPs [30-40]. Superior interaction between the catalysts and the carbonaceous supports boosts the catalyst performance and reduces catalyst loss besides that controlling charge transfer [41-43]. They can enhance the catalyst dispersion and form an underlying structure to conduct electrons and gas diffusion. The underlying support improves the electrocatalytic properties because of affecting the form, size, and dispersion of the electrocatalysts and electronic interactions between catalyst and support [44,45]. The carbon support is made distinctive by segments of basal and edge planes exposed to the surface. Surfaces built up exclusively of basal planes are steady energetically and are known as homogeneous surfaces; however, the combination of the edge and basal planes is known as a heterogeneous surface [46,47]. These supports can also assist in adequately improving the electrocatalyst efficiency and stability by decreasing catalyst poisoning. In specific cases, they can influence the size of catalyst particles. To overcome the challenge of corrosion or oxidation of transition-metal electrocatalysts and their weak stability, carbonaceous materials could be employed to coat the surface of catalysts which prevent the direct contact between the transition metals and electrolyte, and also keep active sites, the catalytic performance, and so warranty the long-term durability of the electrocatalysts [48].

During the past decade, attention to the carbonaceous materials was increased in the field of fuel cells as a key material. Fig. 1 (b), plainly represents the significance of the carbon materials in the field of fuel cells and the increment of research in this field which is taken from the web of science with the keywords search “carbon materials for fuel cells”. In addition, carbon materials are also known as potential metal-free catalysts for fuel cells due to their high surface area and specific electrical structure. The presence of surface heteroatoms like nitrogen in carbon catalysts can improve 2D structures, which is essential for the catalytic process [49]. Thus, it is worth noting that defective carbon catalysts are more cost-efficient than metal catalysts and can quickly fabricate from organic waste materials and natural sources. Despite the advantages of carbon-based catalysts assisted by platinum-group-metal (PGM) material, PGM-metals such as Pt, Pd, or their alloys are expensive and scarce, which limits their usage in fuel cells. Therefore, non-precious materials in particular PGM-free catalysts can be replaced by those of PGM and develop the performance of fuel cells by designing new morphology, nanostructure, and doping of carbon materials [50]. In the past decades, different types of low-cost non-PGM catalysts were applied as ORR catalysts in either alkaline or acidic electrolyte. Among them, the catalysts fabricating by transition metal (Me: Fe, Co, Mn) and nitrogen species on carbon supports (introduced as Me-N-C) got more attention and were used in practical fuel cells owing to high ORR activity comparable with commercial Pt/C catalysts [51,52]. In 1989, pyrolysis approaches of metalloporphyrins were introduced as a cost-effective and easy synthesis method for increasing the activity and durability of ORR catalyst [51]. Me-N-C catalysts are often prepared by pyrolysis of metal, carbon, and nitrogen precursors such as polyaniline, metal salt, and metal-organic framework (MOF) [51,53]. Great efforts have been made to enhance the activity of new Me-N-C materials toward ORR, including the more creation of active sites with high density, the high durability in the acidic electrolyte, and the adjustable synthesis of active sites. The N-doped C or only N incorporated in metal could form various potential active metal-sites such as MeN_4, which are necessary to obtain high ORR performance in acidic media [50,51]. Hence, different Me-N-C catalysts are optimized by various strategies for improving fuel cells’ performance, and we have reviewed some of them in this paper.

However, carbon supports or carbon catalysts are not thermodynamically stable and can physically and chemically degrade at high potential, leading to carbon corrosion. Carbon corrosion usually happens due to potential changes at the high oxidizing potential. Carbon can electrochemically oxidize at the potential of $>$ 0.207 V by the water vapor as following reaction [54]:

$$C + 2H_2O \rightarrow CO_2 + 4H^+ + 4e^- \ (0.207\ V\ at\ 25^{\circ}C)$$

In addition, carbon corrosion can occur by water flooding. The produced water through water flooding in the PEMFCs cannot be removed in time, causing a barricade of contiguity of reaction gas with catalyst (starvation area). At the cathode, a hydrogen evolution reaction performs in the O_2 starvation area, creating heat. Penetrating O_2 to the anode through a proton membrane provides hydrogen-oxygen jointing, leading to high potential in the cathode, increasing carbon corrosion. Accordingly, carbon oxidation under water flooding increases compared with normal operation. Besides, the carbon corrosion advances by loading Pt NPs on a carbon support, causing the shedding of Pt NPs and a high electrolyte resistor [55-57]. In the presence of Pt NPs, the electrode potential is $>$ 0.6 V due to providing hydroxyl groups to the oxygen-consisting carbon surface groups and their fast transformation into CO_2. Although the carbon corrosion due to the normal operation is not serious compared to water flooding, it has an effect on the fuel cells performance during long-term operation. It is worth mentioning that the carbon oxidation increase with increasing operating temperature, water content, and the current density/potential [58]. However, the carbon corrosion is a strong dependence on the carbon materials properties such as the surface area and pore volume. Carbon modification is an important strategy for enhancing carbon corrosion resistance [59]. In addition, carbon materials can possess considerable impurities, changing their electrochemical behavior toward important reactions, e.g., oxygen reduction reaction (ORR) [60]. For instance, the electron-transfer rate in electrochemical responses is highly dependent on graphitic impurities on the electrode surface [61]. Among all carbon materials [62-77], the presence of impurities in CNTs and graphene have been widely studied because they are known as outstanding "metal-free" electrocatalysts [78, 79]. Commonly, synthetic methods lead to substantial metallic and carbonaceous impurities in the CNTs, containing remaining metal catalyst impurities, nano graphitic impurities, and amorphous carbon impurities [80,81]. The CNTs usually synthesized by chemical vapor deposition (CVD), and carbon structure forms on the metallic catalysts such as Ni, Fe, Co, and Mo. Carbon diffusion from carbon precursor creates tubular structures and nanotubes that encompass the metallic catalyst as metal impurities during the production process.

Meanwhile, nanocarbon such as nano graphite and amorphous carbon may be formed, which introduces as carbonaceous impurities [82]. Besides, graphene is typically synthesis by a top-down process of oxidation of graphite, exfoliation, and reduction steps. The used graphite as the primary precursor can obtain naturally or synthetic. Although the purification process can remove some purification of natural graphite, intercalation within graphite or graphene layer cannot remove. After purification, graphite is milled to acquire grain sizes. Hence, metallic mills are possibly caused to impurities in graphite particles. Synthetic graphite is commonly produced from carbon materials such as coal tar and petroleum cokes. According to precursor materials, synthetic graphite has 98-99.9% purity. Accordingly, synthetic graphite also consists of impurities graft to graphene layers [83,84]. Metallic

impurities are one of the vital contamination in natural and synthetic graphite. These metal impurities can consist of Fe, Ni, Co, Cu, *etc*. [85,86]. The produced amorphous carbon during graphene construction is another significant impurity in graphene. In addition, remaining oxygen groups on reduced graphene oxides (RGOs) are introduced as point impurities during the production of graphene [83]. However, the metallic impurities effects on graphene's catalytic activity and electronic features [87]. The carbon-based materials, including some metal impurities, have indicated better catalytic activity than metal-free carbon materials in electrochemical reactions. ORR is an essential reaction in fuel cells, and the most impressive and widely used catalyst for this reaction is Pt which has limited availability and high cost. Recently, carbon-based materials have been proposed as efficient alternative catalysts for catalytic reactions such as ORR. Several types of research confirm the presence of metallic impurities in carbon materials such as CNTs and graphene, which enhances the ORR activity [60,78,82,88,89].

In this context, the metal-free carbon catalysts and metallic catalysts supported on carbon-based materials are reviewed briefly for fuel cell applications. Firstly, we overviewed the basics of fuels cell performance to understand their electrochemical reactions. A brief explanation about PEMFCs, DAFCs and biological fuel cells properties was brought. In the main section, researchers about applying these carbon-based materials in different fuel cells discussed in detail. The essence of this review is to identify the potential role of various carbon materials for fuel cell applications. The performance of Pt catalyst supported carbon based materials was compared with commercial Pt/C catalyst. In addition, the performance of the supported affordable metallic catalyst on the carbon based materials was investigated and compared with carbon supported Pt catalyst. The effect of bimetallic catalysts supported carbon based materials on the fuel cell output was also reported. Subsequently, this review aims to summarize the applied research of carbon-based membranes for fuel cell applications. Current challenges and anticipated future outlooks are discussed in the end of this paper.

2. Basic fuel cell performance

A fuel cell acts as a factory with fuel input and electricity output which converts the chemical energy of the fuel to electrical energy. A fuel cell consists of cathode, fuel input at anode, and electrolytes [90]. Two positive and negative terminals introduce as cathode and anode, respectively. The fuel is perfused to the anode and an oxidant supplies to the cathode. Pure H_2 or gaseous hydrogenated compounds such as methanol and ethanol as fuels and pure O_2 or oxygenated gaseous compounds such as air or halogens like chlorine as oxidant use in fuel cells [2].

Three basic reactions (Rex) have happened in a fuel cell with acidic electrolytes [3], which are as following Rex (1) to (3). More specifically, at the anode, H^+ and electrons ions are released by the oxidation of H_2 [Rex (1)]. However, at the cathode, the water is formed by the combination O_2 with a gain of electron from the electrode and reduces the H^+ ions, which is derived from the electrolyte [Rex (2)]. Indeed, the overall reaction is presented in Rex (3).

$$\text{At Anode } 2H_2 \rightarrow 4H^+ + 4e^- \quad (1)$$

$$\text{At Cathode } O_2 + 4e^- + 4H^+ \rightarrow 2H_2O \quad (2)$$

$$\text{Overall reaction: } 2H_2 + O_2 \rightarrow 2H_2O + \text{heat} \quad (3)$$

It is noted that electrons produce at the anode and move to the cathode. Moreover, H^+ ions pass through electrolytes since an acidic electrolyte contains free H^+, and this reaction is easily carried out. Some polymers, Nafion being the most investigated and ceramics materials, could be used as compounds containing mobile H^+, called proton exchange membrane (PEM).

Although the overall reaction in a fuel cell with an alkaline electrolyte is similar to the acidic electrolyte, the oxidation (anodic) and reduction (cathodic) reactions are different [3]. The basic reactions in a fuel cell with alkaline electrolyte are given in Rex (4) to (6). In an alkaline solution the hydroxyl ions (OH^-) are freely and mobile, these ions react with H_2 and produce water, energy as heat and electrons losses at the anode. However, at the cathode, the reaction between O_2 and electrons obtained from the electrode, and water is performed, that produces the OH^- ions back into the electrolyte. The overall reaction is represented in Rex (6).

$$\text{At Anode } 2H_2 + 4OH^- \rightarrow 4H_2O + 4e^- \quad (4)$$

$$\text{At Cathode } O_2 + 4e^- + 2H_2O \rightarrow 4OH^- \quad (5)$$

$$\text{Overall reaction: } 2H_2 + O_2 \rightarrow 2H_2O + \text{heat} \quad (6)$$

The schematic representation of these fuel cells with acidic and alkaline electrolytes are depicted in Fig. 2a and 2b, respectively.

3. Application of carbon-based catalysts and membranes in different types of fuel cells

3.1. Proton exchange membrane fuel cell (PEMFC)

Proton exchange membrane fuel cell (PEMFC) is one of the most practical fuel cell types due to their advantages of high efficiency, high energy density, low pollutant and having fast response rate and thus widely used in vehicles and mobile applications [90,91]. PEMFCs device can be operated at low temperature, it is in the range of 60-80 °C [92]. It is worth noting that PEMFCs are known as polymer electrolyte membrane fuel cells. In PEMFCs, a solid polymeric membrane (as electrolyte) employs to transition protons from the anode to the cathode, and H_2 or gaseous hydrogenated compounds use as fuel [93]. At the anode, the H^+ ions and electrons produce by H_2 splitting. In the electrolyte, the hydrogen ions are transferred from the anode to the cathode. An external circuit utilizes for electrons transfer. At the cathode, water molecules form by combining hydrogen ions and electrons with O_2 [92,94]. The anodic and cathodic reactions that occur in a PEMFCs are described as follows [92,94]:

$$\text{At anode } 2H_2 \rightarrow 4H^+ + 4e^- \quad (7)$$

$$\text{At cathode } O_2 + 4H^+ + 4e^- \rightarrow 2H_2O \quad (8)$$

$$\text{Overall reaction: } 2H_2 + O_2 \rightarrow 2H_2O \quad (9)$$

In PEMFCs, the membrane electrode assembly (MEA) is the fuel cells' central core, which produces an electrical current. MEA is including of two parts of electrocatalyst and membrane. Perfluorosulfonic acid, named "Nafion," is a standard membrane in PEMFCs due to its specific conductivity and lifetime. Nafion with hydrophilic sulfonated groups can absorb water. In addition, proton conduction can create by splitting H^+ from sulfonated groups [95]. However, Nafion membrane is expensive, and hence, developing cost-efficient membranes with outstanding performance is needed [94]. Several studies have reported the use of carbon in PEMFCs [96-101].

Loading Pt catalysts on the porous carbon supports, including Vulcan carbon (VC), has a positive efficacy on the ORR catalytic activity in PEMFCs. However, coating Pt dispersed metal oxide on the VC showed better performance. A new oxygen reduction catalyst, Pt on a phase supported on VC (Pt/($TaOPO_4$/VC)), was introduced for ORR [102]. The presence of the tantalum oxide phosphate provided more sites to perform the reaction by barricading OH adsorption on the Pt. In comparison with Pt/C, the Pt/($TaOPO_4$/VC) presented better stability and lower loss of ECSA, probably due to the less Pt oxide formation on the Pt/($TaOPO_4$/VC). The high area-specific activity led to the higher mass-specific activity of Pt/($TaOPO_4$/VC) (0.46 A/mg_{Pt}) than Pt/C (0.20 A/mg_{Pt}). However, the supported Pt catalyst on the VC possibly causes reduced performance toward ORR, possibly due to the reduction of the free surface area of Pt nanonetwork (Pt NN) by strong adsorption of Pt

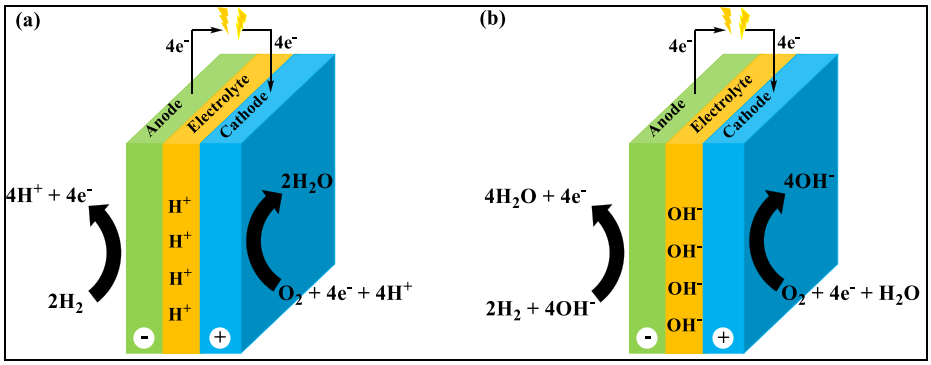

Fig. 2. Schematic representation of electrode reaction in the fuel cell with (a) acidic electrolyte and (b) alkaline electrolyte. Modified from ref. [3].

NN over the surface of the carbon [103]. In order to compare, the Tafel slope was investigated, suggesting 125 mV/dec and 135 mV/dec for Pt NN and Pt NN/VC catalysts. The Pt NN's agglomeration on VC by carbon corrosion led to high ECSA loss of Pt NN/VC. Nonetheless, the stability and catalytic activity of Pt NN/VC was preferable compared with Pt/C.

VC support has a low surface area incapable of incorporating high metal catalyst content with good dispersion. Hence, the active surface area of the deposited catalyst reduces at high catalyst deposition. Porous carbon with a high surface area and large pore size is an excellent alternative to VC for loading metal catalysts, enhancing ORR. The fabricated mesoporous carbon (MC) by soft colloidal template approach was showed 3.4 times the larger surface area and 2.3 larger pore volume than VC [104]. The ECSA of commercial Pt/Vulcan and Pt/MC catalysts was calculated in 0.5 M H_2SO_4 solution by investigating hydrogen adsorption/desorption, indicating 20 wt.% Pt/MC have higher ECSA (82.5 m^2/g) due to its smaller particles size. In addition, CO stripping analysis was performed by CO adsorption measurement on Pt/MC, showing 20 wt.% Pt/MC has the most ECSA (78.9 m^2/g). Although CB is the most usable support for loading metal catalysts due to its high surface area and its high ability to dispersion of metallic catalysts, it has non-uniform and hidden pores that enmesh catalysts. Application of anodic electrode the synthesized porous carbon loaded with various content of Pt in PEMFC indicated better performance due to the easy diffusion of Pt NPs inside the channels and limits the agglomeration of the particles [105]. The combination of Pd with Co can improve ORR catalytic activity, which is affordable compared with Pt-based catalysts. The examination of the ORR ability of carbon-supported Pd-Co electrocatalyst (Pd_{32}-Co_{68}/C and Pd_{62}-Co_{38}/C) suggested that the annealed samples at 300 °C have high ECSA due to lower particles size and agglomeration degree compared to the modified samples at 300, 500, and 700 °C [106]. Further, the tiny particles size of the annealed Pd_{32}-Co_{68}/C at 300 °C led to higher surface area and maximal catalytic activity toward ORR. Besides, alloying Pt NPs with metal oxides such as WO_3 and TiO_2 ameliorates CO tolerance than Pt alone. For instance, the application of Pt-WO_3/C, Pt-WO_3-TiO_2/C, and Pt/C anode catalysts in PEMFC indicated that Pt-WO_3/C anode has the highest power density of 221 mW/mg_{Pt}, which was better than commercial 10% Pt/C (111 mW/mg_{Pt}) and experimental 10% Pt/C (128 mW/mg_{Pt}) [107]. The ECSA of Pt-WO_3/C and Pt-WO_3-TiO_2/C was higher than Pt/C due to their small size of Pt NPs and high surface area. Both Pt-WO_3/C and Pt-WO_3-TiO_2/C catalysts exhibited excellent stability after a 200 h polarization study. The structural modification of CB into carbon microspheres causes good Pt NPs deposition, leading to increase catalytic activity. The as-prepared microspherical carbon with controlled morphology by spray-drying followed by impregnating of 10 wt.% of Pt NPs represented better ORR performance than commercial Pt/C [108]. Carbon-supported Pt NPs catalysts (Pt/C) with the erythrocyte-like and hollow-porous-microsphere structures named as dense-erythrocyte-like (DEL) and hollow-porous-microsphere (HPM), respectively. The ECSA of Pt/C_{HPM} (54.18 m^2/g) was higher than Pt/C_{DEL} (40.98 m^2/g), possibly due to its high specific surface area of 91.45 m^2/g and porous structure. In addition, the ORR mass activity of Pt/C_{HPM} was 239.57 mA/mg_{Pt}, whereas the Pt/C_{DEL} and Pt/C displayed values of 86.80 and 155.01 mA/mg_{Pt}, respectively [108].

Carbon graphitic structures with high stable sp^2 hybridized carbon have been displayed more stability to carbon corrosion. Carbon nanonetworks (CNNs) are one of the 3D hyperbranched graphitic carbon, which has shown attractive features as catalysts for fuel cells. High surface area, excellent electrical conductivity, and excellent oxidation resistance are some of the significant properties of graphitic carbon. The graphitic nature of CNNs can reduce or prevent carbon corrosion and no changes did not observe in reduction/oxidation CV tests before and after corrosion of CNNs. In comparison with commercial catalysts of PFSA-Pt/CNTs and Pt/C, the deposited Pt NPs stabilized perfluorosulfonic acid (PFSA) on CNNs presented suitable catalytic activity toward ORR. Although, ECSA of PFSA-Pt/CNNs (39 m^2/g) was lower than PFSA-Pt/CNTs (68 m^2/g) and Pt/C (59 m^2/g), probably due to Pt NPs agglomeration [109]. Comparison to Pt/C catalyst (19 mA/mg), the PFSA-Pt/CNNs catalyst had the higher mass activity of 29 mA/mg. However, its value was lower than PFSA-Pt/CNTs (37 mA/mg) due to its lower ECSA. The specific activity and Tafel slope of PFSA-Pt/CNNs catalyst were achieved 0.75 mA/cm^2 and -103 mV/dec, respectively, which were the maximum values compared with commercial catalysts.

Poly(2,2′-(2,6-pyridine)-5,5′-bibenzimidazole) (PyPBI) is a good candidate for dispersion of carbon supports and provide uniform sites for Pt NPs. In 2015, the ECSA, durability and high-temperature PEMFC performance of 3-dimensional nanoporous carbon/poly(2,2′-(2,6-pyridine)-5,5′-bibenzimidazole)/Pt (NanoPC/PyPBI/Pt) catalyst were compared with CB/Pt and CB/PyPBI/Pt catalysts [110]. TEM images indicated that Pt NPs were greatly dispersed on PyPBI wrapped NanoPC with a smaller diameter range of 2.2 ± 0.2 nm (Fig. 3a). The PyPBI as a proton conductor has been employed to create anchor sites for the Pt NPs after Pt NPs adding (Fig. 3b). In comparison to CB/Pt (60.6 m^2/g_{Pt}) and CB/PyPBI/Pt (46.8 m^2/g_{Pt}), the NanoPC/PyPBI/Pt catalyst demonstrated a higher ECSA value of 63.7 m^2/g_{Pt} due to the smaller loaded Pt NPs. Moreover, the electrochemical carbon corrosion tests showed the hydroquinone-quinone (HQ/Q) redox peaks at 0.5 V. The durability test of catalysts was carried out during 10000 cycles in N_2-saturated 0.1 M $HClO_4$ electrolyte, showing the ECSA of NanoPC/PyPBI/Pt was similar to the beginning value due to the deposition of more Pt NPs and larger micropores after carbon corrosion. While the ECSA loss of CB/PyPBI/Pt and CB/Pt was found 32 and 46%, respectively (Fig. 3c). Moreover, the power density polarization curves of catalysts were displayed that NanoPC/PyPBI/Pt has the maximum power density of 342 mW/cm^2 compared with CB/PyPBI/Pt (115 mW/cm^2) and CB/Pt (183 mW/cm^2), as shown Fig. 3d.

The application of Pt/C catalysts protected by nitrogen-doped carbon was reported to be beneficial for ORR [111]. The NC/Pt/C catalyst with an NC thickness of 1 nm (1.52 mA/cm^2) represented higher catalytic activity than 3 nm-thick NC (1.04 mA/cm^2). In addition, the ECSA loss

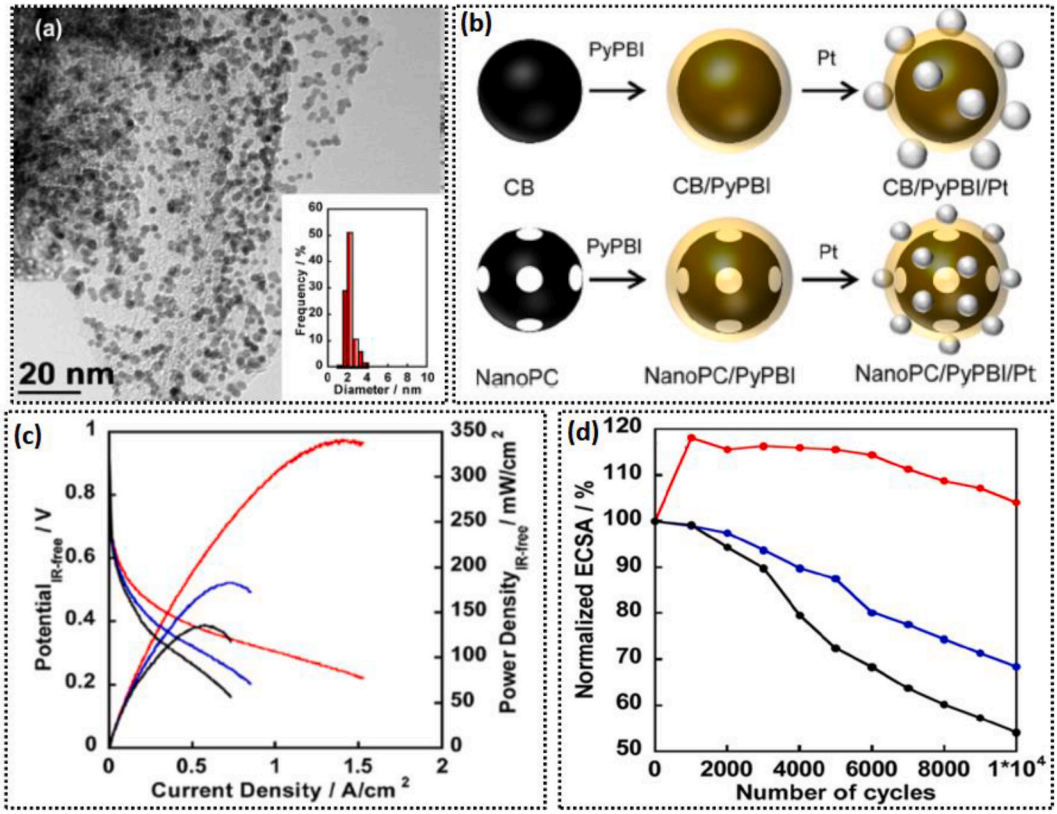

Fig. 3. (a) TEM image of NanoPC/PyPBI/Pt; (b) schematic representation of fabrication of CB/PyPBI/Pt and NanoPC/PyPBI/Pt electrocatalysts; (c) Normalized ECSAs of CB/Pt (black line), NanoPC/PyPBI/Pt (red line) and CB/PyPBI/Pt (blue line) as a function of the number of potential cycles in the range of 1.0-1.5 V vs. RHE and (d) I-V and power density polarization curves of MEAs based on CB/Pt (black line), NanoPC/PyPBI/Pt (red line), and CB/PyPBI/Pt (blue line) at 120 °C under a non-humidified atmosphere. Reproduced with permission from Ref. [110]. Copyright 2015, American Chemical Society.

of 1 nm-thick NC/Pt/C catalyst was lower than Pt/C, suggesting better durability of the catalyst. The annealed 1 nm-thick NC/Pt/C catalyst at 400, 500, 600, and 700 °C was employed as a cathode in low-temperature (75 °C) and high-temperature (120 °C) PEMFC in H_2O_2, indicating the highest current density of 1788 and 389 mA/cm^2 was achieved at 75 and 120 °C PEMFCs, respectively for NC/Pt/C-500 °C. After 10000 cycles, the current density of 1nm-thick NC/Pt/C (500 °C) was received to 1471 and 123 mA/cm^2 in PEMFCs at 75 and 120 °C, respectively. It is worth mentioning that the catalytic activity of NC/Pt/C was significantly increased compared with Pt/C, which was related to pyridinic N in the NC layers. Carbon aerogel (CA) is a highly porous carbon category that has presented high electrical conductivity and surface area. Loading of Pt NPs on the porous CA with various porous diameters of 6, 8, and 19 nm (CA6, CA8, and CA19) was homogenous without any significant agglomeration [112]. At decomposition temperature of 400 °C, Pt/CA19/400 showed the highest ECSA (126 m^2/g) in 10th cycles, whereas Pt/CA6/400 displayed the lowest ECSA (36 m^2/g). The ECSA loss of Pt/CA6/400, Pt/CA8/400, and Pt/CA19/400 were 19, 42, and 31% after 200 cycles. In addition, the Pt/CA19/400 electrocatalyst had mass and specific activity of 0.05 A/mg$_{Pt}$ and 0.06 mA/cm^2, respectively, which were higher than Pt/CA6/400 (0.02 A/mg$_{Pt}$, 0.04 mA/cm^2) and Pt/CA8/400 (0.03 A/mg$_{Pt}$, 0.03 mA/cm^2). The Pt NPs size was increased with increasing temperature from 400 °C (1.7 nm) to 1000 °C (5.3 nm). The ECSA, mass activity, and specific activity of Pt/CA19 were 30 m^2/g, 0.01 A/mg$_{Pt}$, and 0.16 mA/cm^2 when the Pt NPs size was 5.3 nm.

To ORR efficiency enhancement of metal-free catalyst, three-dimensional ultrathin N, P dual-doped carbon nanosheet (NPC-X-T; X is the ratio of N/P and T is pyrolytic temperature) catalyst was fabricated by Zhu et al. and then optimized using co-pyrolyzing with $ZnCl_2$ (NPC-X-T-Zn) [113]. The beginning potential of NPC-4-900, NPC-4-1000, and NPC-4-1100 were 0.82, 0.85, and 0.91 V, respectively, and NPC-4-800 demonstrated no ORR activity due to low graphitization degree and insufficient electronic conductivity. The NPC-4-1100 with a half-wave of 0.775 V and good stability had the best performance. However, the NPC-4-1100-Zn with a half-wave of 0.79 V exhibited better catalytic activity than NPC-4-1100. The lowest Tafel slope was achieved in NPC-4-1100-Zn catalyst, which was 56.9 mV/dec. In addition, the maximum power density of NPC-4-1100-Zn (579 mW/cm^2) was higher than NPC-4-1100 (393 mW/cm^2). After 72 h, the loss performance of NPC-4-1100-Zn was 21.5%, showing great stability of the catalyst. The above results were attributed to the porous structure and good electrical conductivity of NPC-4-1100-Zn and more active sites. Another metal-free ORR catalyst, nitrogen, sulfur, and fluorine tri-doped porous carbon (N-S-F/KB), was produced by Akula et al. [114]. A more positive shift (approximately 30 mV) was observed in the redox potential of N-S-F/KB compared with nitrogen-sulfur-doped carbon (N-S/KB) catalyst, which was attributed to synergistic between N, S, and F tri-doped with C-C band to absorb O_2 molecules. A positive shift of 50 mV appeared in half-wave potential (E1/2) of N-S-F/KB compared to $Pt_{20\%}$-C catalyst. The above results predicate the good ORR catalytic activity of N-S-F/KB. The stability of N-S-F/KB was examined during 10000 cycles, demonstrating a negative shift of 20 mV in its $E_{1/2}$ which was lower than that of Pt/C (160 mV). Therefore, N-S-F/KB had good stability. The mass activity, kinetic current density (i_k), and specific activity have been shown in Fig. 4a and 4b; it is clear that the loss of mass activity and i_k in N-S-F/KB was lower than Pt/C. According to MEA results (Fig. 4c), the power density of alkaline and acidic PEMFC with cathode catalyst of N-S-F/KB was obtained at 7.3 mW/cm^2 and 21 mW/cm^2, respectively.

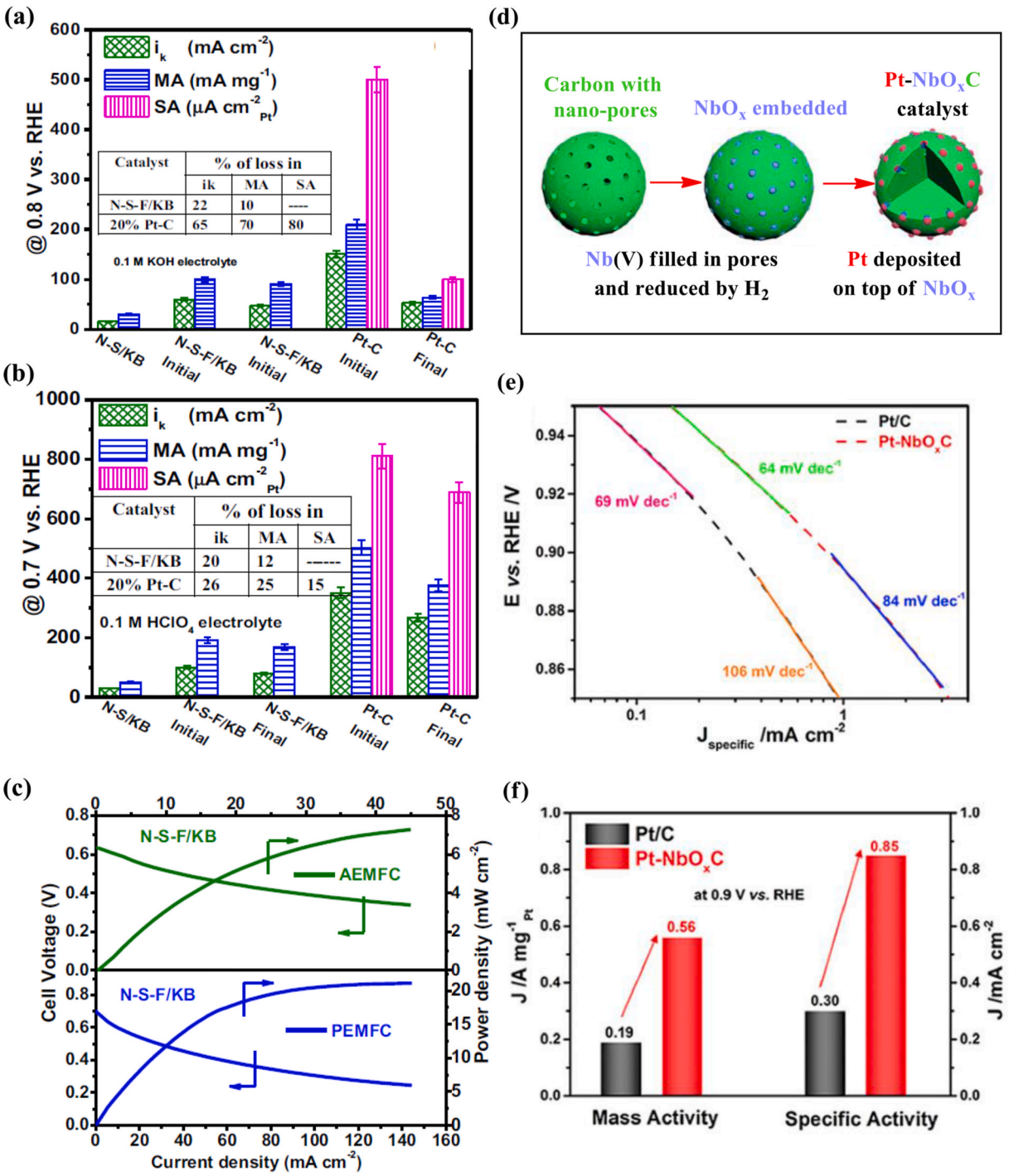

Fig. 4. (a) and (b) Kinetic current density (ik), mass activity and specific activity values for catalysts and initial and after 10000 repeated potential cycles for N-S-F/KB catalyst and 1000 cycles for Pt/C catalyst at 0.8 V in 0.1 M KOH and 0.7 V in 0.1 M $HClO_4$, respectively; (c) fuel cell polarization and power density data of 5 cm^2 active area in proton and anion exchange PEMFCs with Pt-C as anode and N-S-F/KB as cathode, respectively. Reproduced with permission from Ref. [114]. Copyright 2019, IOPscience; (d) schematic illustration of a ~40 nm carbon particle with 4-5 nm surface pores (left), low oxidation-state NbOx particles embedded into the surface pores on carbon (middle), and Pt-covered NbOx particles on carbon (right); (e) mass transport corrected Tafel plots based on specific current density obtained from ORR polarization curves, and (f) specific and mass activities at 0.9 V vs. RHE of Pt-NbO_xC and commercial Pt/C catalysts for ORR. Reproduced with permission from Ref. [119]. Copyright 2020, Elsevier.

Carbon nanofibers (CNFs) are useful carbonaceous materials as inexpensive catalysts or support in PEMFCs due to their stable crystalline structure under the oxidative condition of PEMFCs. However, doping metal and nitrogen into the crystal structure of CNFs leads to improve ORR; for instance, iron-nitrogen co-doped mesoporous CNFs (Fe-N-MCNFs) have been indicated high ORR catalytic activity compared with Pt/C, which was due to its high surface area [115]. The ORR polarization in acidic and alkaline solution exhibited that half-wave potential ($E_{1/2}$) of Fe-N-MCNFs (0.845 V) is higher than Fe-N-CNFs and commercial Pt/C in alkaline solution. However, the $E_{1/2}$ of Fe-N-MCNFs was reduced to 0.684 V in an acidic medium which was lower than $E_{1/2}$ of Pt/C. Hence, the ORR catalytic activity of Fe-N-MCNFs in alkaline solution was better than in acidic solution. To investigate PEMFC performance, 10 wt.% of Pt NPs were loaded onto

Fe-N-MCNFs. The beginning mass activity and ECSA of Pt/Fe-N-MCNFs were 0.141 A/mg_{Pt} and 78.4 m^2/g_{Pt}, respectively. After 2000 potential cycles, the ORR activity of Pt/Fe-N-MCNFs remained at 60% of beginning activity, while the activity loss of Pt/C catalyst was around 86%. In addition, the ECSA loss of Pt/Fe-N-MCNFs and Pt/C was 77 and 93%, respectively, after potential cycles. The excellent ORR activity of Pt/Fe-N-MCNFs was due to homogenous Pt dispersion on the Fe-N-MCNFs surface. Moreover, the high corrosion resistance of support led to the high stability of Pt NPs, causing significant ORR activity of Pt/Fe-N-MCNFs. In another report, the porous structure of CNFs with higher stability than that of CB was compressed with CB and then used to support Pt NPs loaded by microwave-assisted reduction approach [116]. It was found that the conductive networks form by hybridization of CNFs, which can enhance its catalytic prowess and fuel cell performance. The maximum of ECSA (108.2 m^2/g) and mass activity (0.272 A/mg_{pt}) were obtained in the presence of Pt/CNF50-CB50 (50 wt.% CNF:50 wt.% CB) which was higher than Pt/CB (50 m^2/g, 0.078 A/mg_{pt}) and Pt/CNF (51.9 m^2/g, 0.082 A/mg_{pt}). As expected, Pt/CNF50-CB50 with a power density of 907 mW/cm^2 displayed the best fuel cell performance. This excellent electrocatalytic activity was observed due to good Pt dispersion, electrical conductivity, and high mass transport.

Zeolitic Imidazolate Framework (ZIF) is a rich carbon metal-organic framework (MOF). The ZIF-derived porous carbon with suitable conductivity has exhibited notable ORR in alkaline medium, but its performance in acidic medium is poor. However, MOF is known great support for the low content of Pt NPs that enhances the ORR activity in acidic conditions. The fabricated PtNiCo/N-doped carbon (PtNiCo/NC) derived from bimetallic NiCo-ZIF containing Pt/Pt alloy as well as Pt single atoms was reported to be a significant catalyst for ORR [117]. The PtNiCo/NC has displayed an onset potential of 1.03 V and mass activity of 7.21 A/mg_{Pt} toward ORR, showing that the PtNiCo/NC has the better catalytic activity compared with Pt/C (0.98 V, 0.108 A/mg_{Pt}). At 70 °C, a single cell PEMFC with PtNiCo/NC cathode achieved the maximum peak power density of 1070 mW/cm^2. Carbon nano-onions (CNOs) are spherical fullerenes with concentric graphitic shells fabricated via different methods. These graphitic layers cause higher carbon corrosion resistance. Laser pyrolysis is a simple route for synthesizing CNOs with controllable size, morphology, and crystallinity. Compared with Pt/C, Pt/CNO was a more practical catalyst for PEMFC [118]. Although both catalysts showed similar primary performance, the loss performance of Pt/CNO was lower than Pt/C due to its resistance toward carbon corrosion. Pt/CNO and Pt/C displayed ECSA of 54.23 and 37.2 m^2/g_{pt}, respectively, which were reduced to 23.9 and 10.6 m^2/g_{pt} after the accelerated stress test (AST), respectively. MEA based on Pt/CNO (peak power densities of 510 mW/cm^2) and Pt/Vulcan XC-72 carbon (peak power densities of 520 mW/cm^2) displayed similar performance. However, after the AST, their peak power densities reduced to 477 (loss of performance of 6.5%) and 347 mW/cm^2 (loss of performance of 33.3%), respectively. The deposited Pt on top of the embedded NbO_x on the carbon showed good catalytic activity and durability toward ORR compared with commercial Pt/C (Fig. 4d) [119]. The ECSA of Pt-NbO_xC (66 m^2/g_{Pt}) was higher than that of the control electrode (63 m^2/g_{pt}). The Tafel slope of -64 mV/dec and -84 mV/dec was obtained for Pt-NbO_xC, whereas the commercial Pt/C had a lower Tafel slope (Fig. 4e). In addition, the mass activity of Pt-NbO_xC and Pt/C catalysts was about 0.56 A/mg_{Pt} and 0.19 A/mg_{Pt}, respectively. The specific activity of Pt-NbO_xC and Pt/C catalysts was achieved 0.85 mA/cm^2 and 0.3 mA/cm^2, respectively (Fig. 4f). This electrocatalyst was also showed good stability after 10000, 30000, and 50000 potential cycles; the loss of ECSA of Pt-NbO_xC was 15% after 50000 potential cycles, and the loss of mass activity of the catalyst was only 7.2%. The embedded NbO_x in carbon led to lower ECSA loss at high potential by preventing carbon corrosion by separating the contact of Pt NPs and carbon.

CNTs with high catalytic activity and prominent electronic, mechanical, and thermal features are more important for fuel cell application. However, their insolubility and a strong tendency to aggregate in an aqueous solution are two obstacles to applying CNTs which can be solved by noncovalent modification with polymers. The decoration of Poly(sodium 4-styrene sulfonate) wrapped CNTs (PSS-CNTs) surface by Pt nanoflowers (Pt NFs) increased the electroactive specific surface area (76.1 cm^2/mg) compared with the commercial catalyst of 20 wt.% Pt deposited CB (64.2 cm^2/mg) [120]. The oxygen reduction ability of Pt NFs/PSS-CNTs composite including 39.1 wt.% Pt NFs was examined in 0.5 M H_2SO_4. In the presence of oxygen, the electrocatalytic activity of composite was higher than the absence of oxygen. Using bimetallic catalysts has been reported to improve catalytic activity for ORR. Introducing Pd as a transition metal in bimetallic catalyst (multiwalled carbon nanotubes (MWCNTs) supported Pt-Pd) enhanced ORR [121]. The H_2 adsorption/desorption of electrodes was investigated in 0.1 M $HClO_4$ to the ECSA calculation, showing that a decorated electrode with the catalyst particle size of 1 nm has a better surface area (57 m^2/g) than the electrode with the catalyst particle size of 3 nm (41 m^2/g). The ORR activity measurement in O_2-saturated 0.1 M $HClO_4$ solution exhibited the optimal current density of 2.02×10^{-7} A for catalyst particle size of 3 nm. In fact, in the presence of small particles, the surface of the electrode was blocked by OH_{ad} or O_{ad}, which led to a reduction of active sites for the adsorption of O_2. However, Pt-based bimetallic catalysts may show instability and lose ORR catalytic activity due to the transition metals' leaching from the alloys. Although metal oxide conductivity is low, utilizing metal oxides loaded Pt catalyst can be a good alternative Pt-based bimetallic catalyst. Pt NPs loaded MWCNT supported ultrathin TiO_2 films (MWCNT@UT-TiO_2) demonstrated the highest ECSA of 285.5 m^2/g compared with Pt-C (153.4 m^2/g) and Pt-MWCNT (188.2 m^2/g), which is due to the uniform dispersion of small Pt NPs [122]. As depicted in Fig. 5, -OH and -COOH groups were formed on the MWCNTs surface by reflux method, and then TiO_2 was formed by slow addition water to a mixture of titanium tetrabutoxide and acid-treated MWCNT. The ORR measurement indicated that Pt-MWCNT@UT-TiO_2 catalyst has more positive potential (1.02 V) and thus displays higher electrocatalytic activity. The shells of TiO_2 are responsible for the improved catalytic prowess of Pt-MWCNT@UT-TiO_2 by creating protection to avoid carbon corrosion and improving Pt deposition on the surface.

Modification of CNTs by doping nitrogen atoms improved ORR catalytic activity and interaction with Pt NPs. As depicted in Fig. 6a-c, Pt NPs were well coated on nitrogen-doped carbon (NC) layer-coated nitrogen-doped CNTs (N-CNT) [123]. The beginning ECSA of N-CNT/Pt/NC was 75.5 $m^2/g_{Pt,}$ and ECSA of N-CNT/Pt/NC was received to 68.9 m^2/g_{Pt} after 4200 potential cycles, showing good durability of N-CNT/Pt/NC due to good dispersion of Pt NPs. The specific activity and mass activity of N-CNT/Pt/NC were 0.21 A/cm^2_{Pt} and 0.14 A/mg_{Pt}, respectively, due to the formation of sites to adsorption/desorption of oxygen species on the Pt surfaces in the presence of NC. In addition, the fuel cell performance was evaluated by MEAs analysis that showed a power density of 676 mW/cm^2, which was higher than CB/Pt (376 mW/cm^2) and N-CNT/Pt (539 mW/cm^2) catalysts. This high power density was due to the good activity of N-CNT/Pt/NC toward ORR.

Application of nitrogen coated graphene (N-G) and CNTs (N-CNT) as supports of Pt catalyst led to increasing surface area and electrical conductivity. The nitrogen-coated graphene/CNTs structure provides anchoring sites for metal catalysts on the substrate, causing high catalytic activity and stability [124]. Measurement of hydrogen oxidation charge resistor of anode catalysts by electrochemical impedance spectroscopy (EIS) indicated that the catalytic activity of Pt@G/N-CNT is higher than those of Pt@N-G/CNT, Pt@G/CNT, Pt@CNT, and Pt@G. In addition, the mixture of graphene and nitrogen doped CNT (G/N-CNT) had the highest anode capacitance of 4.02 mF/cm^2 and the lowest anode charge transfer resistance of 33 mΩ cm^2, which was due to its high surface area. The high conductivity and more porous structure of Pt@G/N-CNT caused the high mass activity of 0.91 A/cm^2, which was close to Pt@N-G/CNT (0.71 A/cm^2), whereas the normalized mass activity of Pt@G/N-CNT (36.4 A/g) was higher than Pt@N-G/CNT (5.63 A/g). Using a dual-template strategy for fabrication of nitrogen-doped

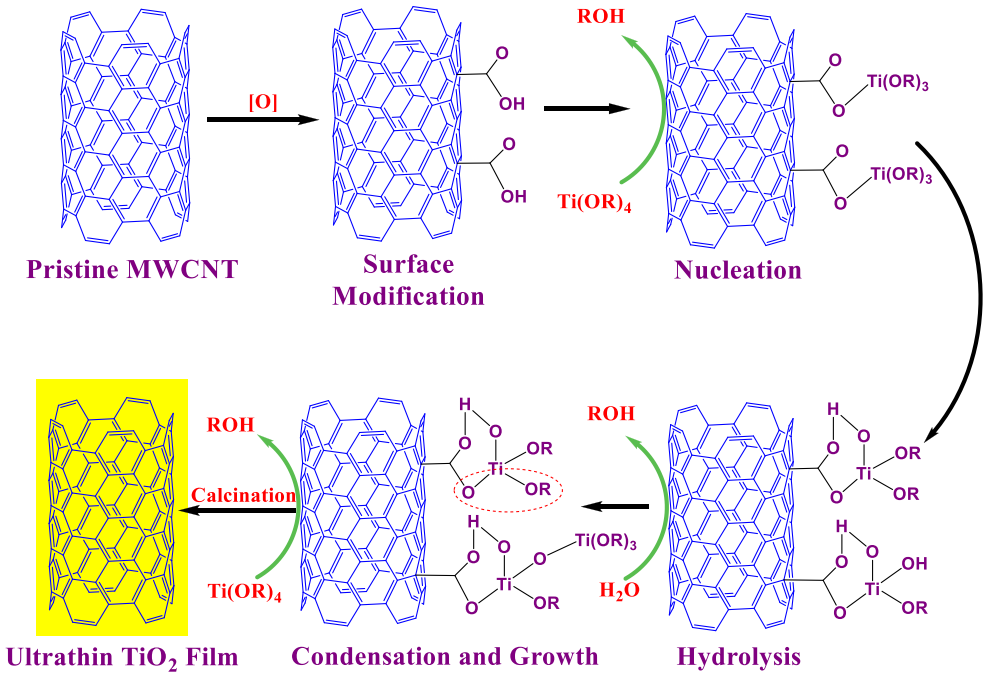

Fig. 5. Reaction scheme for the synthesis of MWCNT@UT-TiO_2. Reproduced with permission from Ref. [122]. Copyright 2012, Royal Society of Chemistry.

CNTs (N-CNTs) encapsulated cobalt NPs (Co@N-CNTs) catalysts increases specific surface area and reveals more active sites. Further, N-CNTs barricade the agglomeration and collapse of cobalt NPs and create electronic channels in the ORR process [125]. The calcinated Co@N-CNTs at 800 °C (Co@N-CNTs-800) displayed more positive cathodic ORR peak (0.77 V) with a current density of 3.00 mA/cm^2 in comparison with sample with only SiO_2 (hard template) colloidal suspension (0.71 V, 2.69 mA/cm^2) or F127 (soft template) (0.73 V, 1.88 mA/cm^2) and sample without any templates (0.64 V, 0.53 mA/cm^2). In addition, the ORR Tafel slope of Co@N-CNTs-800 was achieved 63 mV/dec, which was the smallest value. The highest ORR activity of Co@N-CNTs-800 may have corresponded to the uniform porous structure and high specific surface area, which sites for transportation of oxygen species. In addition, the charge transmission from cobalt NPs to graphitic carbon layers can be activated these layers.

Graphitic carbon nitride (g-C_3N_4) with high nitrogen content is an ideal metal-free catalyst toward ORR. The pyrolyzed CNTs supported g-C_3N_4 at high temperatures of 220, 600, 800, and 1000 °C indicated that the current density of samples was enhanced with increase temperature, suggesting that it was due to improving surface area and conductivity [126]. However, a slight reduction was observed in the current density of pyrolyzed catalyst at 1000 °C, attributed to surface area reduction. Hence, 800 °C was the optimum temperature to sample pyrolysis. In addition, the beginning potential of samples was in the range of 0.8-0.85 V, which was more positive compared with CNTs (0.43 V). 0.85 V was the best beginning potential, suggesting that ORR occurs mainly via a $4e^-$ pathway. Phosphotungstic acid (HPW), with two main properties of special Keggin-type structure and hydronium ion forms of protons, is a great filler for modification of PEM. In addition, mesoporous g-C_3N_4 (mg-C_3N_4) with a high surface area is a good candidate for immobilization of HPW and using sulfonated poly aryl ether sulfone (SPAES)/HPW/mg-C_3N_4 membrane has represented good fuel cell performance [127]. The SPAES/HPW/mg-C_3N_4 membrane showed the maximum proton conductivity of 203 mS/cm. The presence of mg-C_3N_4 in SPAES forms voids in SPAES/mg-C_3N_4 interfaces for absorption of water molecules; therefore, the water uptake was increased in SPAES/HPW/mg-C_3N_4 (50 ± 0.2% at 80 °C). The maximum power densities for the SPAES/HPW/mg-C_3N_4, SPAES/HPW, and SPAES membranes reached 584.2, 467, and 293.5 mW/cm^2 at 100% relative humidity (RH) and 80 °C, respectively. The outstanding fuel cell performance of SPAES/HPW/mg-C_3N_4 was due to its high proton conductivity.

Graphene nanosheets (GNS) with a two-dimensional sheet structure and excellent electrical conductivity is a prominent alternative of CB for loading Pt catalyst in PEMFC. In contrast to Pt/CB, GNS/Pt displays higher initial ECSA and lower ECSA reduction after 3000 cycles [128]. The hydrogen oxidation reaction (HOR) activity of Pt/GNS and PtRu/CB catalysts measurement exhibited that its HOR activity remained at 52% (0.44 mA/cm^2) and 45% (0.54 mA/cm^2) in pure H_2 and in H_2 with 500 ppm CO, respectively, possibly due to more sites and functional groups of GNS. The application of polymeric membranes, including sulfonated carbon nanostructures with Nafion and sulfonated polyether ether ketone (SPEEK), enhances fuel cell performance. Hence, Shukla et al. prepared sulfonated graphene nanoribbons (sGNR) from MWCNTs by synthetic hydrothermal pathway, and nanocomposite membrane was used based on sGNR and SPEEK [129]. The nanocomposite membranes with 0.05 and 0.10 wt.% sGNR value demonstrated cell power density of 550 and 625 mW/cm^2, respectively. It was due to their high proton conductivity and water uptake. To accelerate the durability test, open-circuit voltage (OCV) was measured during 200 h; the degradation of beginning OCV of SPEEK/sGNR (0.1 wt.%) was 11%, whereas it was found 70% after 100 h for pristine SPEEK membrane. Hence, the durability of SPEEK/sGNR (0.1 wt.%) was better than the pristine SPEEK membrane. Graphene-based supports with two-dimensional structure has high conductivity, and large surface provide more active sites for metal catalysts and enhance catalytic activity by improving the connection between catalysts. Colloidal reduction of exploited GO with Pt precursors such as tetraamine platinum(II) nitrate (TPN) and chloroplatinic acid (CPA) causes to the reduction of GO to RGO and Pt to Pt^0, simultaneously, leading to the formation of Pt/RGO [130]. In comparison with Pt/C, the synthesized Pt/RGO in the presence of CPA showed higher ECSA of 82 m^2/g_{Pt} owing to the sheets-like structure of RGO/Pt catalyst and high value of oxygenated groups on the RGO support. Good Pt distribution and high ECSA gave excellent cell performance for RGO/Pt. The assembled Pt catalyst with an average size of 1.2 nm on RGO-VC by liquid-phase self-assembly approach showed the narrow size

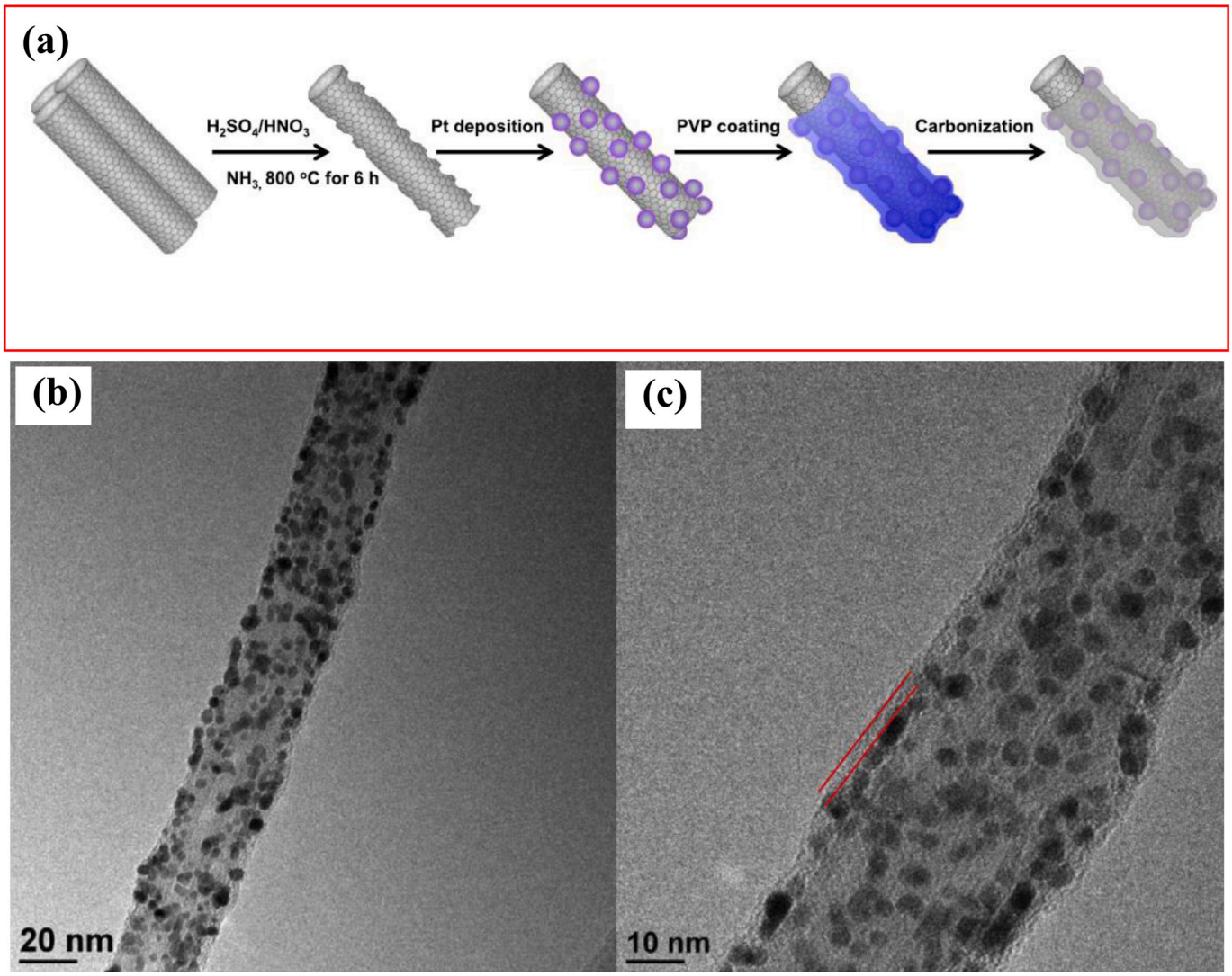

Fig. 6. (a) Schematic illustration of the fabrication of N-CNT/Pt/NC electrocatalyst; (b) TEM and (c) HRTEM images of N-CNT/Pt/NC electrocatalyst. Reproduced with permission from Ref. [123]. Copyright 2017, Elsevier.

and uniform distribution of Pt NPs [131]. In comparison with Pt/VC and Pt/RGO, the optimal ECSA (87 m^2/g) was observed with Pt/RGO-VC anode catalyst due to its better electron transfer and Pt NPs distribution. In the compound of Pt/RGO-VC, VC provides a distance between EGO, leading to more space for O_2 diffusion, and hence, the ORR catalytic activity improves. The PEMFC performance evaluation showed that the Pt/RGO-VC catalyst has the highest current density (1.10 A/cm^2) and power output (857 mW/cm^2) in comparison with Pt/VC (0.93 A/cm^2, 731 mW/cm^2) and Pt/RGO (0.95 A/cm^2, 694 mW/cm^2).

Graphite nanofibers (GNFs) are important carbon support due to their high graphitization degree and high interaction with metal nanoparticles. One of the best routes for increasing interaction GNFs with metal NPs is doping heteroatoms, inducing more catalytic active sites and increasing the electrochemical stability of metal NPs. In addition, the presence of metal NPs leads to the stability of the edge of carbon support toward corrosion. Evaluation of the catalytic activity of nitrogen and fluorine co-doped graphite nanofibers (NF-GNFs)-loaded Pt NPs (Pt/NF-GNF) toward ORR was revealed superior response [132]. The LSV recorded in 0.5 M H_2SO_4 solution displayed that the mass activity of Pt/C, Pt/GNF, Pt/N-GNF, and Pt/NF-GNF was 9.5, 12.2, 18.3, and 40.8 A/g_{pt}, respectively. The fuel cell power density of Pt/NF-GNF, Pt/N-GNF, Pt/C, and Pt/GNF cathode catalysts was 867, 775, 561, and 548 mW/cm^2. The excellent catalytic performance of Pt/NF-GNF was probably attributed to the homogeneous dispersion of small Pt NPs and ORR activity of F and N as well as the interaction between F and N with Pt NPs. In addition, the durability test of catalysts exhibited that the ECSA loss of Pt/NF-GNF is 12% after 10000 potential cycles. While the ECSA loss of Pt/N-GNF and Pt/GNF was 67 and 29%, respectively.

ZIFs 3D precursors were introduced as N and C sources for preparing Fe-N-C catalysts. Therefore, Fe ions doping into the network of ZIFs precursors were prepared by directly bonding Fe ions to imidazolate ligands within 3D frameworks [133]. The one-step thermal activation could provide the possibility of embedding well-dispersed atomic Fe sites into porous carbon particles and forming a complex like $Fe\text{-}N_4$ connecting with 3D framework nanocrystals. The number of PGM-free active sites could be increased by controlling the unique size of nanoparticles without changing chemical properties. Particle sizes of Fe-doped ZIF crystals were adjustable in the range of 20 to 1000 nm so that the catalyst with 50 nm illustrated the best size-dependent ORR activity with a half-wave potential of 0.85 V in 0.5 M H_2SO_4 as acidic media that was just 30 mV lower than the Pt/C catalysts (0.88 V). In another research, Fe-N-C was synthesized by electrospinning of nanostructured ZIF-8(Fe), resulting in the formation of 3D macroporous CNF web [134]. The catalyst showed mass activity of ~0.125 A/g at 0.8 V. The nano-ZIF-8(Fe) electrospun with PAN (E-ZIF-8(Fe)/PAN) indicated higher ORR activity with a current density and power density of 390

mA/cm^2 and 230 mW/cm^2 at 0.6 V, respectively, due to its useful morphology for mass transform. Carbon-supported iron single atom (FeSA) materials are appropriate PGEM-free catalysts for ORR in high temperature polymer electrolyte membrane fuel cells (HT-PEMFCs), but they need templates for avoiding iron atoms aggregation on carbon supports such as CNTs. Therefore, Yi Cheng et al. presented an easy template-free method for synthesizing iron single atoms supported CNTs [135]. FeSA catalyst exhibited a half-wave potential of 0.801 V and onset potential of 0.95 V toward ORR in O_2-saturated and 0.1 M $HClO_4$ electrolyte, which was comparable with Pt/C. This great catalytic activity is due to high-density atomic sites and the highly conductive CNTs-graphene networks. In addition, FeSA had been used in HT-PEMFCs as a cathode electrode with a peak power density of 266 mW/cm^2 with high stability at 240 °C. Doping the content of Fe into (ZIF)-8 precursors and achieving uniform atomic dispersion of FeN_4 sites in partially graphitized carbon phases showed considerable PEMFC performance [136]. It found that the Fe-N-C catalyst with Fe content of 1.5 at.% (1.5Fe-ZIF) had the highest density of FeN_4 active sites resulting in the best ORR performance in acidic (0.5 M H_2SO_4) electrolyte with a half-wave potential of 0.88 ± 0.01 V. The 1.5Fe-ZIF catalyst was selected as MEAs in fuel cells on both O_2 and air and MEA with the 1.5Fe-ZIF catalyst cathode generated the current density of 145 mA/cm^2 at a reference voltage of 0.80 V under 1.0 bar O_2 partial pressure. Also, stability analyses showed that significant carbon corrosion leads to reduce ORR due to loss of Fe-N coordination and decomposition of FeN_4 sites. Phloroglucinol/2-pyrrolaldehyde porous organic polymer with $FeCl_3$ was successfully employed for the preparation of pyrolyzed Fe-N-C catalyst [137]. The content of iron precursor ($FeCl_3$), pyrolysis temperature (750-950 °C), and phenanthroline addition had a significant effect on the final Fe-N-C catalyst performance so that the addition of phenanthroline enhanced the material graphitization and durability and also pyrolysis of material at temperatures ≥850 °C, resulting high ORR catalytic activity. The pyrolyzed Fe-N-C at 850 °C (Fe-N-C-850) showed the highest limited current density of 3.82 mA/cm^2 at 0.2 V with half-wave and onset potentials of 0.69 and 0.82 V, respectively, which were due to its higher surface area and Fe content. The Fe-N-C-850 catalyst performed well as the cathode in H_2-air single-cell PEFC and exhibited a current density of 0.37 A/cm^2 at 0.5 V and a peak power density of 0.2 W/cm^2.

As mentioned above, the modified carbon structures are more attention as catalyst support for PEMFCs. Production mesoporous carbon and doping heteroatoms such as nitrogen or metals such as Fe and Co can improve the catalytic activity of carbon compositions. These are affordable for increasing the durability of catalysts and resistance to carbon corrosion in acidic mediums. Further, these modification processes can enhance interaction carbon-based supports with metal catalysts, leading to increase catalytic activity. The reports on the PEMFCs were focused on the uniform dispersion of metal catalysts on the porous carbon supports. In addition, the carbon-based catalysts provide a high surface area, which is an essential factor for ORR in PEMFCs. CNTs, graphene, and g-C_3N_4 are three more significant carbon structures for loading Pt NPs due to their high electrical conductivity and specific morphology. Other reports about using catalysts, including carbon-based materials, are summarized in Table 1.

3.2. Direct alcohol fuel cells (DAFCs)

Although PEMFCs have a high current density due to using pure H_2 fuel, the production and storage of pure H_2 are complex. Pure H_2 can be alternatives with the H_2 carrier compounds such as alcohols [239]. The fuel cells with direct alcohol feed, i.e., DAFCs, are energy resources with high output energy density and low operating temperature. DAFCs consist of liquid fuel of alcohols (methanol, ethanol, ethylene glycol, propanol, and glycerol) and polymer membrane electrolytes (acid PEM or anion-exchange membrane) [240]. Nafion is the best selection as a membrane because of its high thermal and chemical stability and high

Table 1
The PEMFCs consist of carbon-based catalysts.

Catalyst	Characteristic performance	Ref.
Pt/Cloth-type CNFs (Pt/C-CNFs)	Current density of 80 mA/cm^2 Power density of 22.72 mW/cm^2 Better performance compared with commercial catalysts The lowest mass transfer losses	[138]
Non-platinum cathode catalyst layer	Power density of 150 mW/cm^2 at 0.45 A/cm^2 under pressurized H_2/O_2 at 80 °C	[139]
Pt/carbon aerogel	The most fraction of metallic state platinum on a carbon surface in comparison with commercial catalystThe ECSA of 86.3 m^2/g	[140]
MWNT/PBI/Pt	High electrocatalyst behavior with ECSA of 44 m^2/g Higher utilization efficiency of 74% relative to 39% of pristine MWNT	[141]
Hierarchy carbon paper (CP)	Maximum power density of 377mW/cm^2 Current density of 750 mA/cm^2 at 0.5 V	[142]
Pt-Co/C	Higher ORR current density than that of Pt-Co/glassy carbon (GC) Good stability toward ORR compared with commercial catalyst	[143]
N-doped ordered porous carbon	The fuel cell current density of 0.6 A/cm^2 at 0.5 V	[144]
Carbon-supported Ir-V nanoparticle	The ECSA of 247.7 m^2/g Maximum power density of 1008 mW/cm^2 at 70 °C Current density of 1000 mA/cm^2 at 0.6 V	[145]
Ir-V/C	Maximum power density of 563 mW/cm^2 at 0.512 V and 70°C Current density of 1000 mA/cm^2 The ECSA of 221.1 m^2/g	[146]
Pt/MWCNTs	Power density of 636 mW/cm^2 at 80 °C Current density of 1596 mA/cm^2 at 0.4 V	[147]
Pt/CNTs	The ECSA of 55.6 m^2/g$_{Pt}$ Current density of 29 mA/cm^2 at 0.9 V	[148]
TiN/CB	High cathodic current of 1 μA in ORR The optimum output power of 208 mW/cm^2	[149]
Vertically aligned, nitrogen-doped CNTs	ORR current density of 2.62 × 10^{-3} A/cm^2	[150]
Pt/graphene nanoplatelets	The excellent electrochemical durability, 2-3 times that of Pt/CNT and commercial Pt/C	[151]
Templated Pt/C	Better ORR activity relative to commercial catalyst (10 wt.% Pt on Vulcan XC72) by controlled decoration and particle size of Pt	[152]
Vertically aligned carbon nano-filaments	The higher specific activity of Pt/VACNF at an optimum Pt loading and layer thickness made it useful for PEMFCs	[153]
PdCoNi-g-C_3N_4	High catalytic activity toward ORR Mass activity of 50 A/g$_{PGM}$	[154]
Nano-Pt loaded ACNT/Nafion/ACNT	Power density of 397.23 mW/cm^2 Current density of 605.88 mA/cm^2 at 0.65 V	[155]
Carbon supported on Pd-Ni nanoalloy	Higher ORR catalytic activity than Pd/C	[156]
Pt/CNT	Maximum power density of 595 mW/cm^2	[157]
Pt/MWCNTs	The ECSA of 64 m^2/g Current density of 2300 mA/cm^2 at 0.4 V Power density of 1100 mW/cm^2 at 80 °C	[158]

(*continued on next page*)

Table 1 (*continued*)

Catalyst	Characteristic performance	Ref.
Pt-mesoporous carbons	Superior ORR activity and stability compared with commercial Pt/C	[159]
Pt/nano-silicon carbide/C	The ECSA of 48 m^2/g Better ORR activity and stability compared with Pt/nano-silicon carbide and Pt/C	[160]
Pt/MWCNTs	Power density about 1520 mW/cm^2 at 80 °C The excellent durability of the ECSA after 1500 cycles compared with Pt/C	[161]
Pt/MWCNTs	The peak power density of 950 mW/cm^2 at 8 °C High durability in comparison with commercial Pt/C	[93]
Platinum-vanadium-iron/C	The electrochemical active area (ECA) of 55 m^2/g Mass activity of 0.28 A/mg_{Pt} Power density of 0.82 W/cm^2 at 75 °C Current density of 1.81 A/cm^2 at 0.45 V	[162]
Pt/N-G nanoplatelets	Maximum power density of 440 mW/cm^2 toward ORR	[163]
Pt/C	The ECSA of 39.7 m^2/g Current density of 535 mA/cm^2 at 0.6 V Better fuel cell performance in comparison with commercial Pt/C at 60 °C	[164]
Pt/mesoporous carbon CMK-3	Mass activity of 229.9 A/g Pt, 3.6 times higher than Pt/WMC	[165]
$La_{1-x}Sr_xMnO_3$/CNTs (LSMO/CNT)	Superior oxygen reduction activity compared with LSMO/C, even in the presence of ethylene glycol	[166]
Pt/C	Better performance in fuel cell test with the mass activity of 48 A/Pt-g The ECSA of 86 m^2/Pt-g	[167]
Pt/fourth-generation hydroxyl-terminated poly (amidoamine) dendrimer-C	ORR mass activity of 0.11 A/mg_{Pt} at 0.9 V Electrochemical surface area of 76 m^2/g Power density of 830 mW/cm^2	[168]
Pd-polypyrrole (PPy)/C	Power density of 280 mW/cm^2	[169]
Carbon-supported multiarmed starlike Pt nanowire	Mass activity of 0.135 mA/μg Pt at 0.9 V The specific ORR activity of 0.611 mA/cm^2_{Pt} at 0.9 V	[170]
Nitrogen-doped graphene (N-G)-supported carbon-containing iron nitride	Current density of -3.53 mA/cm^2 at 0.05 V	[171]
Carbon supported on nanoscale tantalum oxide (Ta_2O_5/C)	Increasing area-specific current density, 35% than that of the baseline Pt/C catalyst, increased the loading of the active material five-fold	[172]
Pt/MWCNT	The average ORR intrinsic activity of 0.95 mA/cm^2 at 0.9 V, 3-fold higher than Pt/C Mass activity of 0.48 A/mg_{Pt} at 0.9 V	[173]
Pt/solar exfoliated graphene-MWCNTs (pt/sG-MWCNT) hybrid	The electrochemically active surface area (ECSA) of 82 m^2/g Maximum power densities of 675 mW/cm^2 at 60 °C	[174]
Pt-iron nitride-CNFs	The ECSA of 64.6 m^2/g The optimum power density of 447 mW/cm^2 Current density of 0.081 A/cm^2 at 0.8 V	[175]
FeCo triethylenetetramine/carbon	Maximum power density of 256 mW/cm^2 Current density of 514 mA/cm^2 at 50 °C at 0.5 V	[176]
Pt/Vulcan XC72 carbon-SiO_2	Mass current density of 0.41 A/mg_{pt} at 60 °C at 0.85 V	[177]
carbon-supported Co_3O_4		[178]

Table 1 (*continued*)

Catalyst	Characteristic performance	Ref.
	Current density of 3.54 mA/cm^2 at -0.6 V, higher than the carbon-supported noble Pd catalyst	
Au@Pt/C	Maximum power density of 479 mW/cm^2 at 80 °C The ORR current density of 4.0 mA/cm^2 is as high as that of the commercial Pt/C	[179]
Pt/CNTs/GO	The peak power density of 2.32 kW/g at 75 °C	[180]
Carbon supported Pt	Mass activity of 143 A/mg_{Pt} at 0.9 V The ECSA value of 120 m^2_{Pt}/g_{Pt}	[181]
Pt/Nb-TiO_2/C	The peak power density of 0.34 W/cm^2 at 75 °C Mass activity of 17 A/g_{Pt} Current density of 2 mA/cm^2	[182]
Pt monolayer-shell Pd nanowires/nanorods-core supported on carbon	Higher ORR activity than Pt/C	[183]
Pt/C	The max power density of 0.64 W/cm^2 at 60 °C Current density of 1.3 A/cm^2 at 0.5 V	[184]
Pt/SnO_2-mesopourse carbon	The electrochemically active surface area of 53.2 m^2/g The ORR current density of 3.40 mA/cm^2 at 0.9 V	[185]
Pt/C	Maximum power density of 897 mW/cm^2	[186]
Pt/decorated modified RGO-MWCNTs sandwich	The ECSA value of 50.7 m^2/g_{Pt} Current density of 613 mA/cm^2 at 0.6 V Maximum power density of 495 mW/cm^2 at 60 °C	[187]
Pt- graphitized CNFs	The ECSA value of 44 m^2/g Mass activity of 284 A/g_{Pt}	[188]
Pt/Vulcan XC-72-Pt/CNTs-Pt/coiled CNTs	The ECSA value of 111 m^2/g_{Pt} Current density of 4.7 mA/cm^2 at 0.7 V	[189]
Pt-pyridine-modified-polybenzimidazole/CNTs	The ECSA of 46.8 ± 2 m^2/g Current density of 200 mA/cm^2 at 160 °C	[190]
Pt/Marimo-like carbon	ECSA of 30 m^2/g Higher electrochemical stability and less surface oxidation than that of the conventional CB	[191]
Pt/Nitrogen and carbon doped TiO_2	Mass activity of 5.5 A/g_{Pt} at 0.8 V ECSA of 30 m^2/g ORR limiting current density of 5.4 mA/cm^2	[192]
Pt/CNFs graphitized	High output power density of 0.185 W/cm^2 compared to Pt/CNF (0.163 W/cm^2)	[193]
Vertically aligned CNTs	Improve cell performance by increasing the electronic conductivity and remarkable mass transportation	[194]
Nitrogen-doped SWCNTs	The ORR current density of -60 A/cm^2 at 0.27 V Good long-term durability after 11000 cycles	[195]
Pt/CNT	ORR current density of 0.26 mA/cm^2 at 0.65 V Mass activity of 504 A/g The highest ORR current density of 0.26 mA/cm^2	[196]
Pt/p-phenyl NH_2-graphene	The ECSA of 59.3 m^2/g_{Pt} ORR mass activity of 172.1 mA/mg_{Pt} at 0.9 V Better stability compared with Pt/graphene	[197]
Fe, N co-doped graphene nanoribbon/CNTs	ORR mass activity of 4.43 A/g at 0.9 V, 42% of commercial Pt/C (10.58 A/g) Good durability compared with Pt/C	[198]

(*continued on next page*)

Table 1 (*continued*)

Catalyst	Characteristic performance	Ref.
CNTs and nanohorn hybrid (CNT-CNH)	Current density of 550 mA/cm^2 at 0.6 V Maximum power density of 357 mW/cm^2	[199]
Graphene nanoribbons/Pt	ORR current density of 80 μg/cm^2 at 0.34 V Specific ECSA of 155 m^2/g Mass-specific activity of 1.04 at 0.9 V	[200]
PtFeCo/C	The ECSA of 156.2 m^2/g Power density of 841 mW/cm^2 at 80 °C Mass activity of 57.6 mA/mg$_{Pt}$ at 0.8 V	[201]
MWCNT/polyvinylpyrrolidone (PVA)/phosphotungstic acid (PWA)/Pt	The ECSA of 70 m^2/g Mass activity of 22.4 mA/mg at 0.45 V higher than MWCNT/PVP/Pt (5.86 mA/mg) Specific activity of 0.032 mA/cm^2 at 0.45 V, 3.6 times higher than MWCNT/PVP/Pt (0.01 mA/cm^2)	[202]
Pt/nitrogen-doped carbon	The ECSA of 24 m^2/g Power density of 365 mW/cm^2 at 60 °C	[203]
Fe-N-C	Current density of 115.2 mA/cm^2 at 0.8 V Power density of 325.7 mW/cm^2 at 0.6 V and 80 °C Greater ECSA than amorphous carbon catalyst supports	[204]
Fe-N-C	Current density of 44 mA/cm^2 at 0.85 V Maximum power density of 490 mW/cm^2	[205]
Fe/Cu-N-doped RGO/CNT	Better ORR performance and higher stability than the commercial Pt/C Power density of 185 mW/cm^2	[206]
Pt-Mn_3O_4/C	Excellent performance due to ECSA of 135.3 m^2/g-Pt Mass activity of 178.5 ma/mg-Pt at 0.8 V Maximum output power of 761 mW/cm^2	[207]
Dopamine@CNT	Better ORR activity than CNT Higher stability than that of Pt/C	[208]
Pt/niobium oxide-C	The ECSA of 80.8 m^2/g-Pt Good ORR activity with the mass activity of 351A/g-Pt compared with Pt/C	[209]
CNT/end-capped hyperbranched sulfonated macromolecules (E-HBM)/Pt	Displayed mass activity and durability 1.4 and 20 more than commercial CB/Pt Power density of 668 mW/cm^2 Higher durability than CB/Pt	[210]
N,S-co-doped nanocarbon	Higher ORR activity than Pt/C and co-doped nanocarbon The limiting current density of 3.99 mA/cm^2 Better long-term stability than Pt/C and co-doped nanocarbon	[211]
Pt/MWCNTs	Current density of 50 mA/cm^2 at 0.838 V Power density of 730 W/g and ECSA of 66 m^2/g	[212]
PtFe/N-doped porous carbon sheets	The specific ECSA of 111.58 m^2/g Mass activity of 0.533 A/mg$_{Pt}$, 3.04 times better than that of Pt/C (0.175 A/mg$_{Pt}$) Higher stability than Pt/C	[213]
PtCo supported carbon	Current density of 538.9 mA/cm^2 at 0.6 V	[214]
Pt/carbon aerogel	The ECSA of 73 m^2/g Power density of 536 mW/cm^2 at 0.6 V is obtained at 60 °C Better stability than commercial JM20	[215]

Table 1 (*continued*)

Catalyst	Characteristic performance	Ref.
Pt/Mn_3O_4-carbon	The ECSA of 127.4 m^2/g Mass activity of 1.17 mA/μg$_{Pt}$ Higher stability than those of Pt/C and Pt/Mn_3O_4	[216]
Carbon supported hollow Pt-Ag NPs	ORR specific activity of 1.11 ± 0.02 mA/cm^2 at 0.9 V	[217]
Pt/CNTs@C	The ECSA of 64 m^2/g Current density of 3.1 mA/cm^2 Higher durability than Pt/CNT	[218]
Polyaniline (PANI)-Fe-mesoporous carbon spheres	Kinetic current density of 0.29 A/cm^2 at 0.8 V Maximum power density was 0.83 W/cm^2 at 0.40 V The ECSA of 576.16 m^2/g	[219]
Co-N-C@Pluronic F127 block copolymer	Power density of 0.87 W/cm^2 comparable with Fe-N-C catalyst	[220]
PtCu/carbon arogel	Mass activity of 0.123 A/mg$_{Pt}$ ESA of 137 m^2/g	[221]
Pt/nitrogen-doped tantalum oxide (Ta_2O_5)/C	Mass activity of 0.252 A/mg$_{Pt}$ after 10,000 ADT cycles Excellent long-term durability compared with Pt/C Adequate catalytic activity for the ORR	[222]
Pt/SWCNTs	Stable oxygen adsorption Lower activation energy toward ORR at low loaded Pt (18.5 wt.%) than that of Pt/graphene (85.3 wt.% Pt)	[223]
Pt NPs on fluorinated graphitic CB	The ECSA of 35 m^2/g The initial currents of j_{H2} = 2.2 mA/cm^2 due to hydrogen permeation across the membrane	[224]
Pt-Pd/carbon xerogel reduced with methanol	The diffusional current density of 5.38 mA/cm^2 The mass activity of 188 mA/mg Pt at 0.75 V, 4 times higher than Pt/C	[225]
CdS/CNT/C	Greater electric current capacity than Pt/C Higher power density compared with Pt/C	[226]
Fe-Fe_3C-embedded Fe-N-codoped carbon	ORR mass activity of 6.80 A/g$_{cat}$ at 0.85 V Current density of 0.1 A/cm^2 at 0.8 V and 2.36 A/cm^2 at 0.3 V Peak power density of 0.76 W/cm^2	[227]
Fe-N-C	Geometric current density of 2.36 ± 0.12 mA/cm^2 at 0.9 V Mass activity of 2.95 ± 0.15 mA/mg at 0.9 V	[228]
Pt/nitrogen-sulphur co-doped partially exfoliating MWCNTs	The ECSA of 80.2 m^2/g$_{Pt}$, higher than Pt/C Mass activity of 121 mA/mg$_{Pt}$ toward ORR at 0.9 V, higher than Pt/C Maximum power density of 642 mW/cm^2 Greater durability compared with Pt/C	[229]
1-Octadecanethiol-Pt/C	Power density of 976 mW/cm^2, 8.3% higher than control (901 mW/cm^2)	[230]
Pt/nitrogen-doped carbon frameworks	The ECSA of 48 m^2/g Mass activity of 246 mA/mg$^2_{Pt}$ at 0.9 V, better than commercial Pt/C Power output of 646 mW/cm^2, 1.9 times higher than Pt/C	[231]
Fe-N-C	Kinetic current density of 0.465 ± 0.005 mA/cm^2 at 0.8 V	[232]
FeN_4-doped hierarchical ordered porous carbon (FeN_4/HOPC)	Current density of 0.75 A/cm^2 at 0.6V, 2-fold higher than FeN_4/C Power density of 0.42 W/cm^2 at 0.57 V	[233]
MWNT-COO^-/1^{Arg}/Nafion	Current density of 28 mA/cm^2 at 300 mV overpotential	[234]

(*continued on next page*)

Table 1 (*continued*)

Catalyst	Characteristic performance	Ref.
	Maximum power of 325 ± 2 μW/cm^2 at 415 mV	
Sulfur-doped Mn-N-C	Peak power density of 500 mW/cm^2 Mass activity of 1.85 mA/mg at 0.85 V Current density of 370 mA/cm^2 at 0.7 V	[235]
Co-N-C hydrogel	Current density of 0.47 A/cm^2 at 0.6 V Peak power density of 0.66 W/cm^2 at 0.41 V	[236]
Fe-N-C	Power density of 1.08 W/cm^2	[237]
Fe-N-C	Good ORR activity comparable with the Pt/C catalyst Peak power density of 0.837 W/cm^2 Excellent electrochemical stability	[238]

conductivity. However, the Nafion membrane reduces DAFCs performance, and hence it utilizes some fillers [95]. Comparatively, other alcohols, ethanol, and methanol are the most attractive fuels for DAFCs, it is due to their high energy density and safer handling [239,241]. Therefore, the role carbon based materials for direct methanol fuel cells (DMFCs) and direct ethanol fuel cells (DEFGs) is highlighted in the following.

3.2.1. *Direct methanol fuel cells (DMFCs)*

Methanol (CH_3OH) is a promising and cost-efficient liquid organic fuel used for DMFCs and it can obtain from fossil fuels and biomass. In comparison with ethanol, methanol has been indicated better selectively to CO_2 formation in electrochemical oxidation reactions [242]. DMFCs are the source of renewable energy which directly convert the chemical energy of methanol (as fuel) to electrical energy. They are suitable sources for mobile and portable applications as well as battery technology due to their outstanding properties of low emission pollutants, small size system, and easy storage fuel [243]. In addition, the operation temperature of DMFCs is <60 °C [2]. However, low fuel cell performance and low power density are important disadvantages of DMFCs [242,243]. The principal components of DMFCs are the anode, cathode, and membrane electrolyte. The performance of DMFCs is similar to PEMFCs; the mixture of water and methanol employs as fuel at the anode. Methanol is directly oxidized to CO_2 and released H^+, electrons, and heat. The constructed CO_2 leaves the cell by movement in the direction of the fuel tank. The released electrons and H^+ transform to the cathode through an external circuit and PEM. Finally, ORR is performs at the cathode by combining O_2, electrons, H^+, and water and heat form [6,7]. The following reactions that take place in a DMFC are:

$$\text{At anode } H_2O + CH_3OH \rightarrow 6H^+ + 6e^- + CO_2 \quad (10)$$

$$\text{At cathode } 3/2O_2 + 6H^+ + 6e^- \rightarrow 3H_2O \quad (11)$$

$$\text{Overall reaction: } CH_3OH + 3/2O_2 \rightarrow CO_2 + 2H_2O \quad (12)$$

There are certain reports based on carbon materials have significant impact on DMFCs performance [244-247].

Hollow carbon spheres (HCSs) with high surface area and pore volume are the beneficial substrates for loading catalysts. The supported Pt NPs on HCSs by hydrothermal and intermittent microwave heating methods has shown excellent catalytic activity for methanol oxidation compared with reference Pt/C electrode, which is due to the open microspores and nanochannels of HCSs [248]. According to Fig. 7a, HCSs have a size of 2 μm and a thickness of 150 nm. The uniform distribution of Pt NPs with an average size of 2 nm has been shown in Fig. 7b. The Pt/HCSs catalyst with microwave treated time of 3 min has the highest ECSA and methanol oxidation current density (115.2 mA/cm^2), which were better than that of Pt/C (Fig. 7c). Compared with Pt NPs supported on SWCNT, the supporting Pt NPs on carbon nanosheets (CNSs) showed

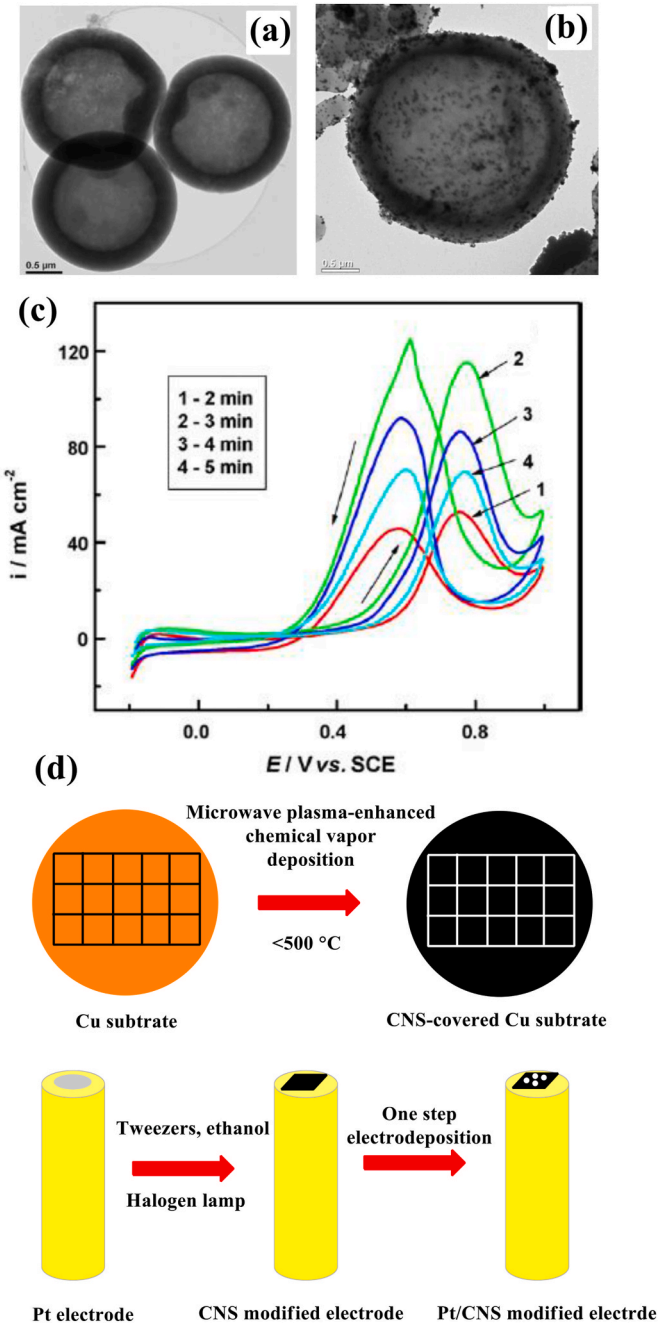

Fig. 7. TEM images of (a) HCSs and (b) Pt/HCS, (c) CV Pt supported on heat-treated HCSs at different times intervals in 0.5 mol/dm^3 H_2SO_4 + 1 mol/dm^3 CH_3OH solution Reproduced with permission from Ref. [248]. Copyright 2008, Elsevier. (d) CNS development and techniques for Pt NP deposition on CNSs. Reproduced with permission from Ref. [249]. Copyright 2012, Elsevier.

better methanol oxidation activity and CO tolerance. As depicted in Fig. 7d, the one-step electrodeposition method was used to load Pt NPs on the CNSs and SWCNTs [249]. Both Pt/CNSs and Pt/SWCNT had great catalytic activity due to their significant ECSA of 27.6 and 24.7 m^2/g, respectively. Both catalysts' methanol oxidation onset potential was similar, indicating the same Pt-O affinity. However, the Pt/CNSs displayed higher methanol oxidation current density and better CO tolerance, suggesting the prominent desperation of Pt NPs on the CNSs surface led to excellent stability and high electrocatalytic activity of the Pt/CNSs. Marimo nanocarbon (MNC) is a fibrous carbon material with a high density of carbon nanofilaments that indicated good fuel cell performance when employed as Pt support [250]. It was found that MNC

has more carboxyl and hydroxyl groups than VC and MWCNTs, leading to more active sites for metal-anchoring. The methanol oxidation current densities of 507, 400, and 240 mA/mg_{Pt} were achieved for Pt/MNC, Pt/Vulcan XC-72, and Pt/MWCNT, respectively. Therefore, the methanol oxidation activity of Pt/MNC was higher than other carbon-based catalysts. Single cells with both electrodes of Pt/MNC and Pt/Vulcan XC-72 displayed the highest current densities of 10.4 and 2.8 mA/cm^2, respectively. The output power of single-cell with Pt/MNC was four times higher than Pt/Vulcan XC-72.

One cost-efficient catalyst support for DMFCs is CNFs with high catalyst anchoring sites and long-term stability. Although Pt supported on tubular CNF (Pt/tCNF) has indicated suitable catalytic activity, deposition of Pt catalyst on the grown platelet CNFs (pCNFs) on graphite paper by CVD showed higher ECSA and stability due to its specific morphology and good metal clusters dispersion [251]. The CV in H_2SO_4 after electrode cycling in methanol (200 cycles) exhibited lower ECSA loss of Pt/pCNF electrodes than Pt/ tubular CNF (Pt/tCNF), which indicated better the tolerance of the Pt/pCNF electrodes to CO poisoning. In addition, the stability of electrodes was tested by repeating CV 200 times in $H_2SO_4 + CH_3OH$; the beginning mass surface activity of electrodes was increased and then reached a pseudo-plateau. SnO_2 is a metal oxide that can provide oxygen-containing species and help remove CO species at low potentials. Furthermore, SnO_2 can increase the dispersion of Pt catalyst over supports. It is reported that the coated SnO_2 layer on CNF by two atomic layer deposition (ALD) routs, static ALD, and dynamic ALD can be enhanced methanol oxidation activity CNF [252]. Uniform SnO_2 layer was created on CNFs using Al_2O_3 pre-inserting layer by static ALD method whereas SnO_2 layer was formed on the CNF whitout pre-inserting. The island-shaped SnO_2 layer on CNF by static ALD has exhibited the highest current efficiency of 575 mA/mg_{Pt} due to good Pt dispersion and its bi-functional effect. Incorporating metal oxides with Pt catalyst can improve the dissociation of water at low potential, enhancing the CO tolerance of DMFC. Hence, to improve CO tolerance and methanol oxidation of Pt catalyst, RuO_2-MnO_2/MWCNTs were chosen as support [253]. The onset potential of Pt/RuO_2-MnO_2/MWCNTs (0.29 V) was lower than Pt/RuO_2/MWCNTs (0.31 V), Pt/MnO_2/MWCNTs (0.49 V), and Pt/MWCNTs (0.56 V). The ECSA and methanol oxidation current peak of Pt/RuO_2-MnO_2/MWCNTs were 137 m^2/g_{Pt} and 865 A/g_{Pt}, respectively, which were the highest values. Indeed, the presence of MnO_2 and RuO_2 can be enhanced proton conductivity and Pt dispersion, respectively, while MWCNTs form electron channels. Hence, the Pt/RuO_2-MnO_2/MWCNTs had the best anode catalyst for methanol oxidation. The methanol oxidation in acidic medium by Pt-Ru/MWCNT (prepared by flashlight irradiation) catalyst has been higher than Pt/ MWCNT [254]. The ECSA of Pt-Ru/MWCNT (566.63 ± 2.9 cm^2/mg) was higher than Pt/MWCNT (484.38 ± 2.2 cm^2/mg), possibly was due to the formation of homogeneous Pt-Ru NPs and stronger bonding of MWCNTs with Pt-Ru NPs. In addition, the onset potential of Pt-Ru/MWCNT (0.105 ± 0.02 V) catalyst was lower than that of Pt/MWCNT (0.145 ± 0.02 V), which was due to the formation of $Ru(OH)_{ads}$ species at the lower potential. The application of polymer-based support can improve CO tolerance and durability of Pt catalysts. However, finding water-soluble polymer without any coverage on the Pt surface and reducing its catalytic activity is an important issue. The methanol oxidation activity of deposited Pt NPs on wrapped CNTs by dihydroxy-polybenzimidazole (2OH-PBI) was better than commercial CB/Pt [255]. Fig. 8a shows the schematic of MWCNT/2OH-PBI/Pt fabrication. According to Fig. 8b, Pt NPs with the size distribution of 4.1 ± 0.5 nm were uniformly dispersed on MWCNT/2OH-PBI due to the formation of Pt-N bond. After 100000 potential cycles, the mass activity and ECSA of the synthesized MWCNT/2OH-PBI/Pt were decreased by 50 and ~10%, respectively, whereas commercial CB/Pt displayed more reduction of ~46 and 50% after 10000 potential cycles due to its low carbon corrosion resistance. These results indicated that MWCNT/2OH-PBI/Pt has higher catalytic activity compared with CB/Pt. The MWCNT/2OH-PBI/Pt demonstrated

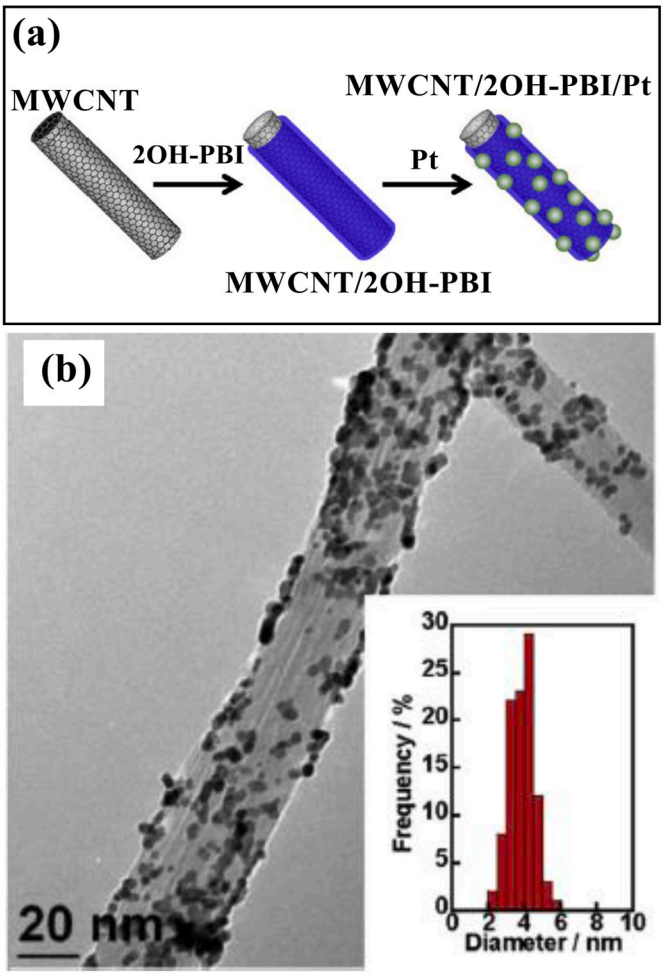

Fig. 8. (a) Schematic of MWCNT/2OH-PBI/Pt fabrication and (b) TEM image of MWCNT/2OH-PBI/Pt. Reproduced with permission from Ref. [255]. Copyright 2017, Elsevier.

that the onset potential of the methanol oxidation is lower than CB/Pt, and hence methanol can be quickly oxidized by MWCNT/2OH-PBI/Pt. In addition, CO-stripping measurement confirmed that the CO-tolerance of MWCNT/2OH-PBI/Pt was 1.5 times higher than CB/Pt owing to –OH groups on the 2OH-PBI and formation of Pt-OH.

To ease charge transfer and good dispersion of Pt catalyst, Liang et al. developed a nitrogen doped CNTs at low temperatures [256]. As shown in Fig. 9a, a hydrothermal system for making nitrogen-doped oxidized CNTs (N-OCNTs) at a low temperature by reaction NH_3H_2O with acid-treated CNTs and then byproducts (N-LOCNTs, N-MOCNTs, and N-HOCNTs; where L, M, and H stand for lowly, moderately, and highly oxidized, respectively) were used to loading Pt NPs. A negative shift was observed for CO oxidation potential, especially Pt/N-MOCNTs, which can explain by a positive shift in the binding energy of Pt *4f* after doping N into CNTs and electron transfer from Pt to N. The electrochemical tests revealed that the highest methanol oxidation current density value (1000 mA/mg_{Pt}) belongs to Pt/N-MOCNTs (Fig. 9b). The chronoamperometric (CA) results demonstrated good stability of nitrogen-doped CNTs based catalysts compared with Pt/pristine CNTs (Fig. 9c). In order to find the best support for Pt-based alloy catalysts, Ru, Pt, Fe were loaded on SWCNTs and MWCNTs, and graphene (Gr) [257]. The methanol oxidation current density of catalysts was as followed: PtRuFe/SWCNT (13.2 mA/cm^2)> PtRuFe/Gr (11.6 mA/cm^2)> PtRuFe/MWCNT (4 mA/cm^2)> commercial Pt/C (2.7 mA/cm^2). The calculated ECSA of catalysts indicated that PtRuFe/SW-CNT has the highest value of 212.2 m^2/g_{Pt}. Moreover, the maximum value of mass

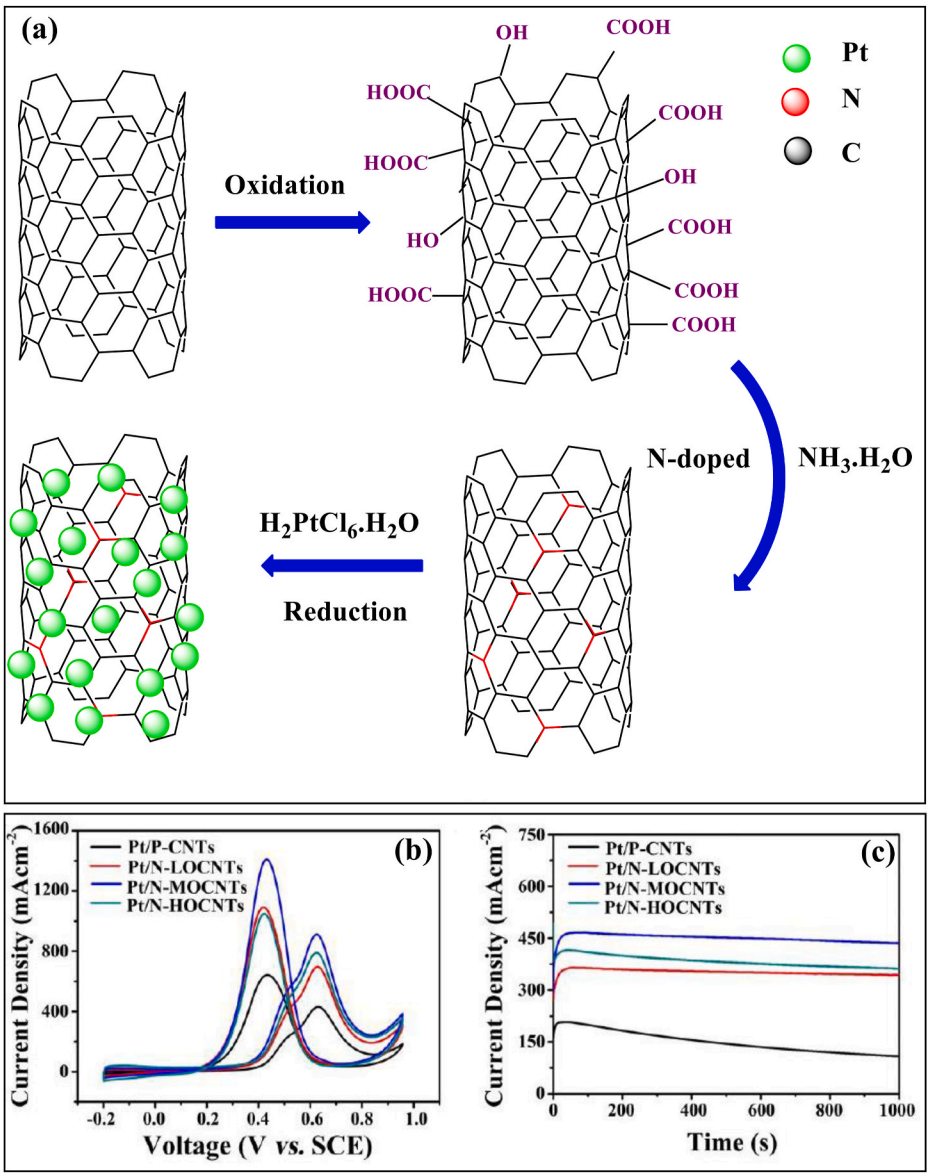

Fig. 9. (a) Schematic of the fabrication of the Pt/N-OCNTs, (b) CVs, and (c) CA curves in 0.5 M H_2SO_4 + 1 M CH_3OH at 0.5 V. Reproduced with permission from Ref. [256]. Copyright 2019, Elsevier.

activity belonged to PtRuFe/SW-CNT (827 A/g) catalyst. The above results imply excellent methanol oxidation catalytic activity of PtRuFe/SW-CNT, and hence it was chosen as optimum anode for the methanol fuel cells. The cell with PtRuFe/SW-CNT had a current density of 40 mA/cm^2, whereas the cell including Pt/C displayed a value of 27 mA/cm^2.

Graphitization of carbon supports at high temperatures affords excellent carbon corrosion resistance due to the reduction of oxygen groups which can be the reason for carbon corrosion in fuel cells. Hence, compared with CNTs, graphene is more affordable support with high electrical conductivity and corrosion resistance. However, graphite nanoplatelets are more available than graphene and GO. In addition, its highly graphitic structure increases the anchoring sites of catalysts, leading to more interactions between metal and carbon support. The loaded Pt NPs on exfoliated graphite nanoplatelets substrate (Pt/GnP) via a microwave process in the presence of room-temperature ionic liquids was showed better methanol oxidation activity than commercial Pt/XC-72R catalyst [258]. Good Pt NPs dispersion on GnP and large surface area of Pt/GnP catalyst were main factors of catalytic activity increase. The methanol oxidation mass activity of 1090 mA/mg$_{Pt}$ and high long-term stability was obtained for Pt/GnP catalyst, which was better than commercial Pt/XC-72R (mass activity of 577 mA/mg$_{pt}$).

One of the best strategies for enhancing ORR activity is the loading of metal catalysts on practical support, which having high electrical conductivity and reasonable surface area. Therefore, RGO was decorated with Pt and Pd catalysts to prepare a low-cost fuel cell electrode. RGO and VC have been chosen as the substrate to deposition Pd and Pt NPs and used for direct methanol fuel cells at three different temperatures (303, 343, and 363 K) [259]. Tafel slopes of 60, 61, 71, and 65 mV/dec were calculated for Pt/RGO, Pt/C, Pd/RGO, and Pd/C catalysts, respectively, and hence the ORR activity of Pd-based catalysts was lower than that of Pt-based catalysts. The best performance of fuel cell based on cathode catalysts was achieved at 343 K; the maximum power densities of Pt/RGO, Pt/C, Pd/RGO, and Pd/C were 10.21, 11.24, 2.75, and 1.9 W/g$_{Pt\ or\ Pd}$, respectively. Hence, inexpensive Pd catalyst has high electrocatalytic activity when supported on the RGO due to its good dispersion on RGO. In another report, Pt-decorated graphene aerogel (Pt/GO) with high stability as a porous electrode was fabricated by solvothermal reduction and used in direct methanol microfluidic fuel cell [260]. The Pt/GO electrode displayed the maxim of the

electroactive surface area of 1882 cm^2/mg_{Pt}. In contrast, its value was obtained 211 cm^2/mg_{Pt} for Pt/C, which can attribute to non-agglomeration and the small particle size of Pt/GO. Compared to commercial Pt/C, Pt/GO had a significantly better catalytic activity toward methanol oxidation in alkaline and acidic mediums. As opposed to the Pt/C anode, the Pt/GO electrode had a 358% improvement in specific power of 9.39 mW/mg_{Pt}. After 20 cycles, the maximum specific power of Pt/GO was received to 8.43 mW/mg_{Pt}. Loading bimetallic core-shell of Pd@Au on RGO has been presented effective catalytic activity toward ORR that was performed using two steps: firstly, Pd@Ag NPs were synthesized on RGO by reduction of Pd^{2+} and Ag^{+} with methyl ammonia borane, and then Pd@Au NPs were formed on RGO substrate using oxidation Ag and reduction of Au^{3+} (Fig. 10) [261]. Pd@Au/RGO with an onset potential of 183 mV had a higher ORR current density of 6.24 mA/cm^2 than Pd/RGO, Au/RGO, and commercial Pt/C. This higher catalytic activity of Pd@Au/RGO was probably due to the electronic structure modification of underlying palladium by the surface gold atoms favoring the electron exchange between oxygen and palladium to increase the oxygen reduction through enhanced oxygen adsorption. Furthermore, the non-agglomeration of Pd@Au on RGO increased the surface area for oxygen adsorption. In addition, the recorded ORR in 1 M methanol demonstrated that methanol tolerance of Pd@Au/RGO was higher than other catalysts, showing Pd@Au/RGO can be used as a promising catalyst in DMFCs.

In another report, the low supported content of Pt catalyst (5.3 wt.%) on graphene (GrPt) was effective for methanol oxidation; the methanol oxidation current density was 939 mA/mg_{Pt} in alkaline medium [262]. In addition, the GrPt electrode with an onset potential of -0.51 V revealed a higher methanol oxidation current density compared with the commercial Pt/C electrode. In addition, GrPt showed more excellent stability after 500 cycles; 34.7 and 8.9% of activity were remained in the presence of GrPt and Pt/C, respectively. The formation of Pt-OH species and the CO oxidation at the graphene sheets are reasons for the good electrocatalytic activity of GrPt. Recently, using conductive polymers such as polyaniline (PANI) can be alternative Pt-based catalysts. With good chemical stability, low cost, and high conductivity, PANI is one of the best conductive polymer known for fuel cells. In addition, the presence of PANI in hybrid catalysts has been led to increase electron transfer, homogeneous dispersion of metallic catalysts, and stability catalysts. For instance, a superior methanol oxidation ability was found for the nanohybrid structure of g-C_3N_4/PANI/Pd NPs, which was deposited on the screen-printed electrode (SPE) as illustrated in Fig. 11a [263]. SEM images of the fabricated electrode are shown in Fig. 11b and c; Pd NPs with a diameter of 100 nm and PANI needle-like nanostructure were successfully distributed on the g-C_3N_4 matrix. The recorded CV of g-C_3N_4/PANI/PdNPs and commercial Pd/C in alkaline medium showed that the catalytic activity of g-C_3N_4/PANI/PdNPs toward methanol oxidation was higher than Pd/C (Fig. 11d); the highest current density of 3.42 mA/cm^2 was obtained for g-C_3N_4/PANI/PdNPs. According to Fig. 11e, the current density of the as-prepared nanohybrid catalyst is three times better than the commercial Pd/C catalyst after 1000 s.

The iron-nitrogen-carbon (Fe-NCB) catalyst has been introduced as a highly active ORR PGM-free catalyst in the presence of alcohols like ethanol and methanol [264]. Fe-NCB catalyst achieved from pyrolysis of nicarbazin (N,N′-bis(4-Nitrophenyl) urea with 4,6-dimethyl-2-pyrimidinone and iron salt. The structure of this catalyst is well-coordinated with Fe atoms for achieving Fe-N_4 and Fe-N_2C_2 active sites. The ORR polarization curve of Fe-NCB did not have a remarkable shift (less than 10 mV) even in the presence of 2 M alcohols, indicating excellent alcohol tolerance of Fe-CNB. While the ORR half-wave potential was shifted to 300 mV (2 M methanol) in the presence of Pt/C catalyst. According to density functional theory (DFT) calculations, these best active sites (Fe-N_4 and Fe-N_2C_2) at the cathode side indicated much stronger oxygen adsorption and higher methanol tolerance than metal-free pyridinic nitrogen and graphitic nitrogen sites. The DAFCs operation had been done based on a high methanol concentration of 10 M by using Fe-NCB cathode catalyst with a high performance of 60 mW/cm^2. It was suggested that using PGM-based catalysts at the anode side and Fe-NCB at the cathode due to their active sites are the suitable selection for optimizing DAFCs components. Although Fe-N-C catalyst including FeN_4 active sites represented significant ORR activity, the modification of its morphology and atomic structure can enhance the stability and activity of Fe-N-C. Hence, a dual-metal site Fe/Co-N-C catalyst containing FeN_4 and CoN_4 active sites was designed with a two-step chemical doping and adsorption technique and tested for ORR in methanol-containing acidic electrolytes [265]. The Fe/Co-N-C catalyst enhanced the high ORR catalytic activity and stability with the half-wave potential of 0.85 V in an acidic electrolyte (0.5 M H_2SO_4) and exhibited peak power densities of 135 mW/cm^2, which was higher than the power density of Fe-N-C (124 mW/cm^2) in the same conditions of the methanol-air fuel cell.

As reviewed, using Pt catalyst for methanol oxidation was more common than other metallic catalysts. Pt NPs improve CO tolerance and catalytic activity. In addition, the composition of Pt with Ru and metal oxides can improve catalytic activity. However, Pd and bimetallic catalysts were also successful for the methanol oxidation. These catalysts were more affordable compared with Pt catalysts. Among carbon supports, CNTs and graphene are used more than those of other CB and g-C_3N_4 due to good catalyst dispersion and conductivity. Moreover, using polymers such as PANI and 2OH-PBI in compositions is improved conductivity and metal-OH formation, leading to increase catalytic activity toward methanol oxidation.

The effect of the other composites, including carbon used in DMFCs is illustrated in Table 2.

In addition, carbon-based materials can be used in membranes. Table 3 is summarized of DMFCs with membranes, including carbon materials.

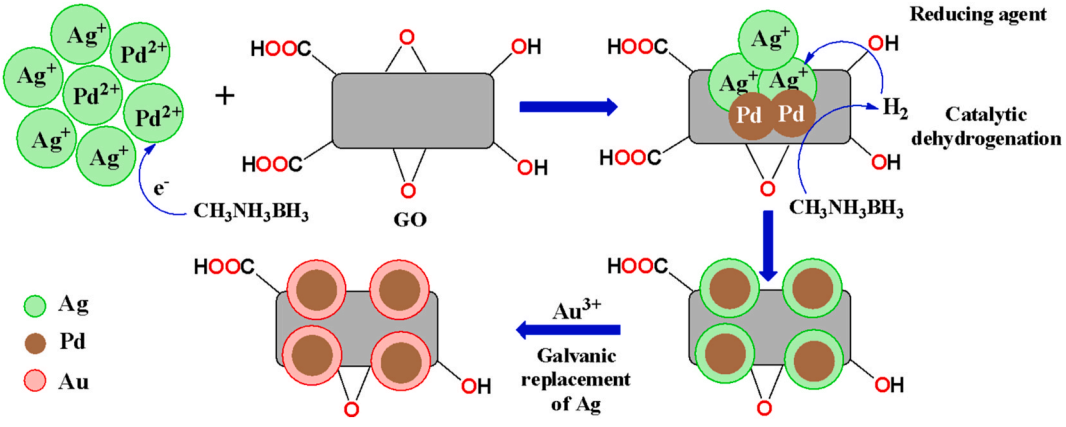

Fig. 10. Schematic presentation of Pd@Ag/RGO and Pd@Au/RGO core-shell NPs. Reproduced with permission from Ref. [261]. Copyright 2018, Elsevier.

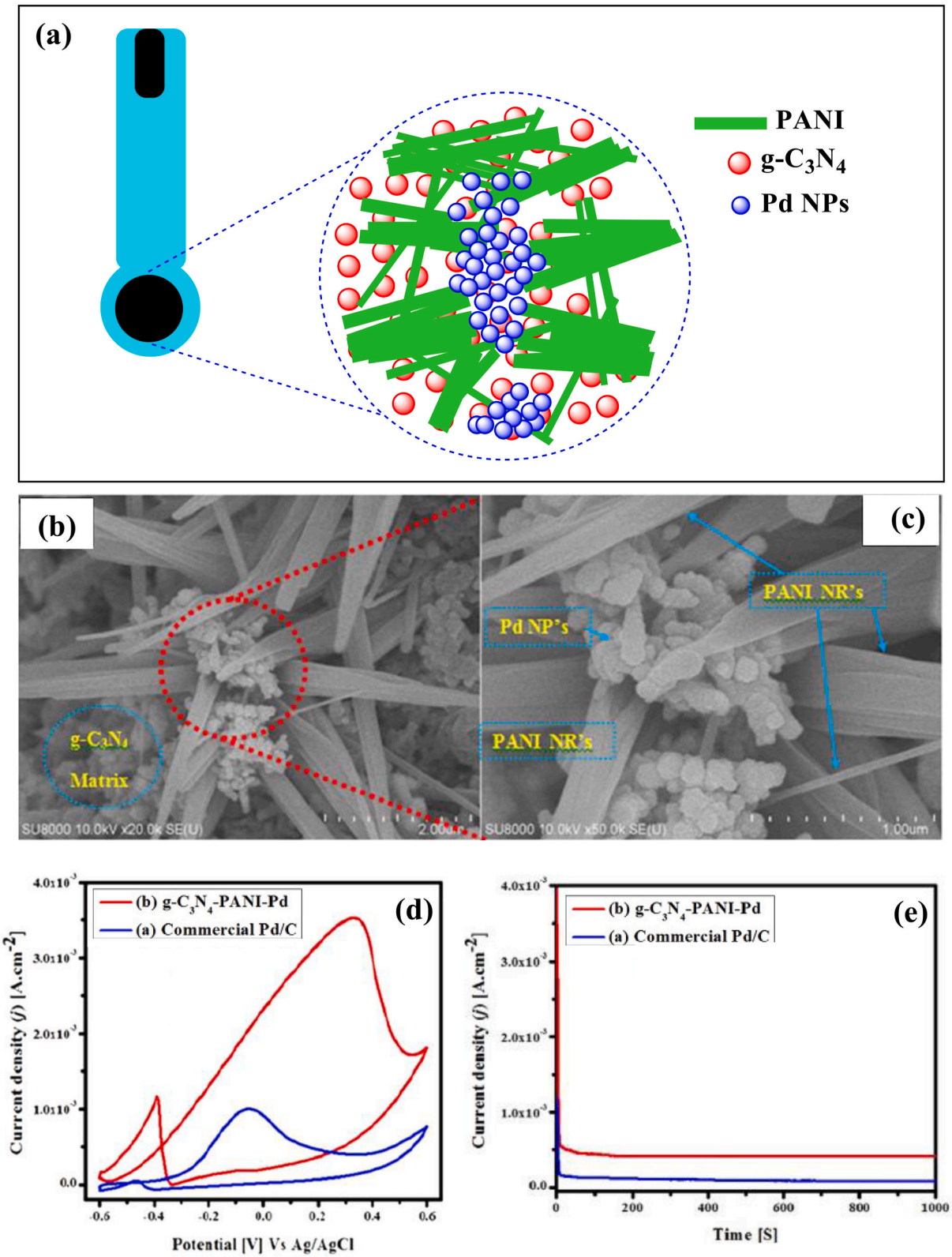

Fig. 11. (a) Scheme representation of the fabrication of the proposed electrode by electrochemical co-deposition method, (b and c) SEM images of ASPE-g-C_3N_4/PANI/Pd nanohybrid, (d) CV performance of ASPE-g-C_3N_4/PANI/Pd nanohybrid in 0.5M KOH + 1 M CH_3OH at a scan rate of 50 mV/s at room temperature and (e) chronoamperometric curves 1 M CH_3OH with a scan rate of 50 mV/s at 0.24 V at room temperature in 0.5 M KOH. Reproduced with permission from Ref. [263]. Copyright 2019, Elsevier.

Table 2
The DMFCs consist of carbon-based catalysts.

Composite catalysts	ECSA (m^2/g)	Current density/Mass activity	Potential of current density/Mass activity (V)	Power density (mW/cm^2)	Temp. (°C)	Ref.
Pt-Ru/C	-	213 mA/mg $_{Pt-Ru}$	0.5	-	-	[266]
Pt/GCNFs/graphite	-	323 A/g	0.5 and 0.75	-	-	[267]
Pt/MWCNT	73.6	51.5 mA/cm^2	-	-	25	[268]
Carbon-supported Pd-Mo	-	1.3 mA/cm^2	-	-	80	[269]
CNF interlayer between the PtRu black catalyst layer and the CP	-	-	-	130	80.8	[270]
Pt-Ru/AS (arc-soot nano carbon)	-	-	-	20	-	[271]
PtSn/C	28.5	56.7 mA/mg	0.86	-	25	[272]
Pt/C-HAC	93.9	7.54 mA	0.882	-	-	[273]
Se/(Ru-Mo)/C	-	-	-	118	80	[274]
PtRu/TFC (thin-film carbon)	105.18	410.0 mA/mg_{PtRu}	0.5	-	60	[275]
PdNi/C	-	Higher than Pd/C	-	-	-	[276]
Pt/ACNC	327	-	-	-	-	[277]
Single wall nanohorns (SWNH)	-	-	-	Higher 60 % than carbon black	50	[278]
Pt-Fe/C	46.2	19.8 A/g_{Pt}	0.660	120	90	[279]
Pt/SWNTs	-	12.1 mA/cm^2	0.6	-	-	[280]
Pt/Coral-C	102.5	230 mA/cm^2	0.070	21	60	[281]
Pd-MnO_2/MWCNTs	35.57	431.02 A/g	-0.2	-	25	[282]
Pt/CNF	181 cm^2/mg	-	-	-	RT	[283]
PtRu/(f-Gef-MWNT)	-	-	-	68	80	[284]
PtRuP/TCF (mesoporous carbon thin film)	-	385 mA/mg_{PtRu}	0.5	-	-	[285]
Pd/PHCS	-	Higher than Pd/C	-	-	30	[286]
Pt/CMK-3	84	185 mA/mg Pt	0.7	-	-	[287]
EDTA-RGO/Pt-NPs	-	6.3 mA/cm^2	0.67	-	-	[288]
Pt/CNT	32.4	381 A/g	0.68	-	-	[289]
Pt/WO_3/CNT	-	4.82 mA/cm^2	0.6	-	-	[290]
PdNi/MC	18.8	-	-	-	-	[291]
Pt/SiC@C	108.1	554 mA/mgPt	0.4	-	-	[292]
AuPd/C	43.5	-	-	-	-	[246]
PtAu/pCNF	49	-	-	-	-	[293]
Pt-TiO_2/CNT	23.4	5.48 mA/cm^2	-	-	-	[294]
Pd-graphene	26.2	112 A/g Pd	0.8	-	-	[295]
PtRu/GNF	-	1.37 mA/cm^2	0.4	-	-	[296]
NCN	-	20% higher than Pt/C	-0.45	-	-	[297]
G-Pd/CC	24.2	Higher than Pd/CC	0.3	-	-	[298]
Pt-G-CNF	123.1	560 mA/mg	-	-	-	[299]
Pt/CS (carbonized soybean)	-	Higher than Pt/XC-72	-	-	-	[300]
Pt/L.MWCNTs	-	-	-	5.7	25	[301]
Pt/TCN (titania nanowires coated by carbon)	91.4	272.9 mA/cm^2	-	33.6	80	[302]
Fe-N-C	-	255 mA/cm^2	0.22	48	90	[303]
ZnO/CeO_2 dots@CNFs	-	16.3 mA/cm^2	0.4			[304]
BCNMs@C (carbon-boron core-shell microspheres)	-	1.2 mA/cm^2	0.170	-	-	[305]
Pd-OMC (ordered mesoporous carbon)	-	50.0 mA/mg	0.3	-	-	[306]
3D porous N-G	-	7.15 mA/cm^2	0.6	-	RT	[307]
PtPdPt/graphene	142.9	25.63 mA/cm^2	0.679	-	-	[308]
PdSn/β-cd-CNT	-	-	-	15.2	RT	[309]
Pd/C-DEG (diethylene glycol)	93.6	3.9 times higher than Pd/C-EG	-0.2	-	-	[310]
Pt/CNTs@TiCoN	55.9	0.92 A/Mg_{Pt}	-	-	-	[311]
Pt/N-C	65.3	385.2 A/g Pt	-	-	-	[312]
GC/PdNPs-$LaNi_{0.5}Fe_{0.5}O_3$ NPs-CH	6.63	23.51 mA/cm^2	-0.14	49.47	70	[313]
PteRu/GC-500	-	69.9 mA/cm^2	-	13.7	RT	[314]
Pd-Mo/Vulcan XC-72R carbon	-	71.2 mA/cm^2	-0.3	-	-	[315]
Pt/CN_x	68	310 mA/mg_{Pt}	0.64	-	-	[1]
Pt-FAU-C SG (Pt-faujasite zeolite with carbon-sol gel)	2.28	1.07 mA/cm^2	-	-	-	[316]
Ni-C-Pt	22.18	151.9 mA/mg	0.651	-	-	[317]
Pt/S-MWCNTs	161.4	803.9 mA/mg_{Pt}	0.42	-	-	[318]
Pt-Ru/MCN	-	65 mA/cm^2	0.62	56.30	80	[319]
Pt@RFC (resorcinol-formaldehyde carbon spheres	80.8	-	-	58.5	60	[320]
Pt/YBCPE (doped carbon paste electrode)	65.9	176 mA/mg	0.91	-	RT	[321]
Pt@NC/Ni	-	744 mA/mg_{Pt}	0.65	-	-	[322]
Pt/*f*-CB	-	50 mA/cm^2	0.88	-	-	[323]
PtCMs	-	0.2 mA/cm^2	0.55	-	-	[324]
$Co_4(PW_9)_2$@N-CNT	-	Higher than Pt/C	0.86	-	-	[325]
G-PdAg/CC	-	7 times higher than G-Pd/CC	-	-	-	[326]
Ni@Pd/MWCNTs	-	-	-	67	60	[327]
Pt Core/Carbon Shell	34	473.2 mA/mg	-	-		[328]

(*continued on next page*)

Table 2 (*continued*)

Composite catalysts	ECSA (m^2/g)	Current density/Mass activity	Potential of current density/Mass activity (V)	Power density (mW/cm^2)	Temp. (°C)	Ref.
Pd/Ag/CNT	46	27 mA/cm^2	0.35	-	RT	[329]
Pt/ATO-C	66	0.737 A/g_{Pt}	-	-	-	[330]
Pt/polythiophene-carbon	98	0.027 mA/cm^2	0.65	-	-	[331]
Pt-Ru/carbon aerogel	36.2	-	-	100	RT	[332]
RGO-CNT/Pt	501.87	407.71 mA/mg	0.614	-	-	[333]
PtNi/NC (natural graphitic-nano-carbon)	58	1500 mA/mg_{Pt}	-	-	RT	[334]
Pd/CNH (single-walled carbon nanohorns)	-	1910.6 mA/mg	-0.2	-	-	[335]
Fe-N-C	-	220-25 mA/cm^2	0.3	72-32	90	[336]
Fe/Co-N-C	-	100 mA/cm^2	-	100	75	[337]

Table 3
The DMFCs with membranes consist of a carbon filler.

Membrane	Proton conductivity (S/cm)	Power density (mW/cm^2)	Tensile strength (MPa)	Water uptake	Methanol permeability (cm^2/s)	Temp. (°C)	Ref.
PVA/CNT	11.76 $\times 10^{-2}$	39	-	2.94 g/g	2.99 $\times 10^{-7}$	60	[338]
PBI/CNT	0.035	104.7	96.6 ± 32.8	21.48%	1.85 $\times$ 10^{-8}	90	[339]
Nafion/CNF	-	21.90	-	-	-	27	[340]
SPEEK/CN	0.183	-	51.31	59.50% ± 1.46	-	55	[341]
CNTs/ graphene oxide nanoribbon (CNT/GONR) nafion	0.18	-	-	-	8.61 $\times$ 10^{-9}	120	[342]
Naf-SWy-oxCNT-RSO_3H	7 $\times$ 10^{-2}	205	-	Reduced	Reduced	110	[343]
SA/SGO (sodium alginate/sulfonated graphene oxide)	0.034	13.6	9.7	137%	2.42 $\times 10^{-7}$	25	[344]

3.2.2. *Direct ethanol fuel cells (DEFCs)*

Ethanol (C_2H_5OH) as a renewable fuel can be widely produced from biomass such as sugarcane, corn, and beetroot [345]. Ethanol fuel has displayed less toxicity and higher energy density than methanol fuel, and hence it is a good candidate for fuel cells [240]. The fuel cells with ethanol fuel are named direct ethanol fuel cells (DEFCs), which belong to the PEMFCs category. The DEFCs performance is similar to DMFCs. The liquid ethanol oxides and H^+, electron, and CO_2 produce at the anode. The protons are diffused through the membrane and transferred to the cathode. At the cathode, water molecules form through the reaction of O_2 with H^+ and electrons. For a DEFCs, the reactions are described by the following:

$$\text{At anode } 3H_2O + C_2H_5OH \rightarrow 12H^+ + 12e^- + 2CO_2 \quad (13)$$

$$\text{At cathode } 3O_2 + 12H^+ + 12e^- \rightarrow 6H_2O \quad (14)$$

$$\text{Overall reaction: } C_2H_5OH + 3O_2 \rightarrow 2CO_2 + 3H_2O \quad (15)$$

The ethanol oxidation reaction releases 12 H^+, which is more than methanol oxidation (6 H^+). Therefore, the power output of DEFCs is higher than DMFCs. Although more CO_2 will be produced in DEFCs than DMFCs, the released CO_2 does not have a negatively impact on the environment because the ethanol can be taken from plants that grow by consumption of CO_2 during the photosynthesis process [95].

The comparison of ethanol and methanol electrooxidation ability of Pd-Ni-C electrocatalyst indicated that the ethanol oxidation rate of this catalyst is higher than the methanol. The ethanol oxidation current was 525 mA/mg, whereas the current of 198 mA/mg was obtained for the methanol oxidation reaction [346]. These appropriate electrocatalytic activities were due to the higher ionic potential of Ni^{2+}, which can reduce the electron density on Pd. Hence, Pd-CO bonding energy was reduced, and oxidation of CO was increased. In addition, ethanol oxidized to acetic acid and transformed into acetate ion in the alkaline environment of the reaction. The loaded Pd catalyst on the mesoporous hollow carbon hemispheres (HCHs), synthesized using glucose and solid core mesoporous shell silica template, revealed better ECSA relative to Pd/C [347]. Furthermore, the mass transfer for the electrochemical reaction was enhanced when the HCHs were selected as support, corresponding to the large porosity of HCHs. Therefore, the ethanol oxidation current density of Pd/HCH was three times higher than Pd/C, attributed to Pd good dispersion on HCHs support. However, the supported Pd NPs on two carbon substrates of Vulcan carbon (C_v) and Selectivity carbon (C_s) to catalyze ethanol electrooxidation indicated that Pd/C_v (45 m^2/g) has higher ECSA than Pd/C_s (18 m^2/g) [348]. The ethanol oxidation reaction was begun at -0.5 V on Pd/C_v and -0.4 V on Pd/C_s, revealing that the former has a lower activation loss for the ethanol oxidation reaction. Furthermore, considering the oxidation current, Pd/C_v has 2.4 times the mass activity of Pd/C_s. Regarding the results of analyses, VC acted better than selectivity carbon because VC has better textural and structural properties, and the high crystalline structure of C_v enhanced interaction of Pd with support. In addition, Pd/C_v was fixed at a higher current than Pd/C_s after 900 s, suggesting high stability of Pd/C_v. Using bimetallic-based Pt catalysts for electrooxidation of ethanol has been presented to be efficient. The produced HNO_3-functionalized acetylene black carbon-supported Pt-Ru (Pt-Ru/C_{AB}) nano electrocatalysts through polyol reduction and formic acid reduction methods (Pt-Ru/-C_{AB}-PLM and Pt-Ru/C_{AB}-FAM, respectively) revealed higher power output compared with commercial Pt-Ru/C_{AB} [349]. The Pt-Ru/CAB-PLM had the highest current density (34.71 mA/cm^2) among all anode catalysts toward ethanol oxidation. The as-synthesized catalysts were employed as an anode in a single DEFC. Commercial Pt-Ru/C_{AB} and Pt-Ru/C_{AB}-PLM at temperature of 35 °C achieved the maximum power density of 5.13 mW/cm^2 and 6.02 mW/cm^2 at a current density of 18.70 and 19.52 mA/cm^2, respectively. This good performance attributes high electrical conductivity, large pore volume of C_{AB}, and homogenous distribution of the ionomer in the electrocatalyst layer. It is worthwhile to mention that the highest DEFC performance significantly developed by increasing temperature to 80 °C, maximum power density of 13.04 mW/cm^2 at a current density of 44.8 mA/cm^2. One affordable approach for increasing catalytic activity is the preparation of alloys with core/shell structure, including noble metal as shell and transition metal as a core. It is found that the dispersed core/shell Ni@Pd on MWCNTs (Ni@Pd/MWCNTs), which has been fabricated via replacement method (Fig. 12a), has been indicated significant catalytic activity toward ethanol oxidation, as depicted in Fig. 12b [350]. The mass activity of ethanol oxidation for Ni@Pd/MWCNTs and Pd/MWCNTs was 3495 and 1539 mA/mg_{Pd}, respectively (Fig. 12c).

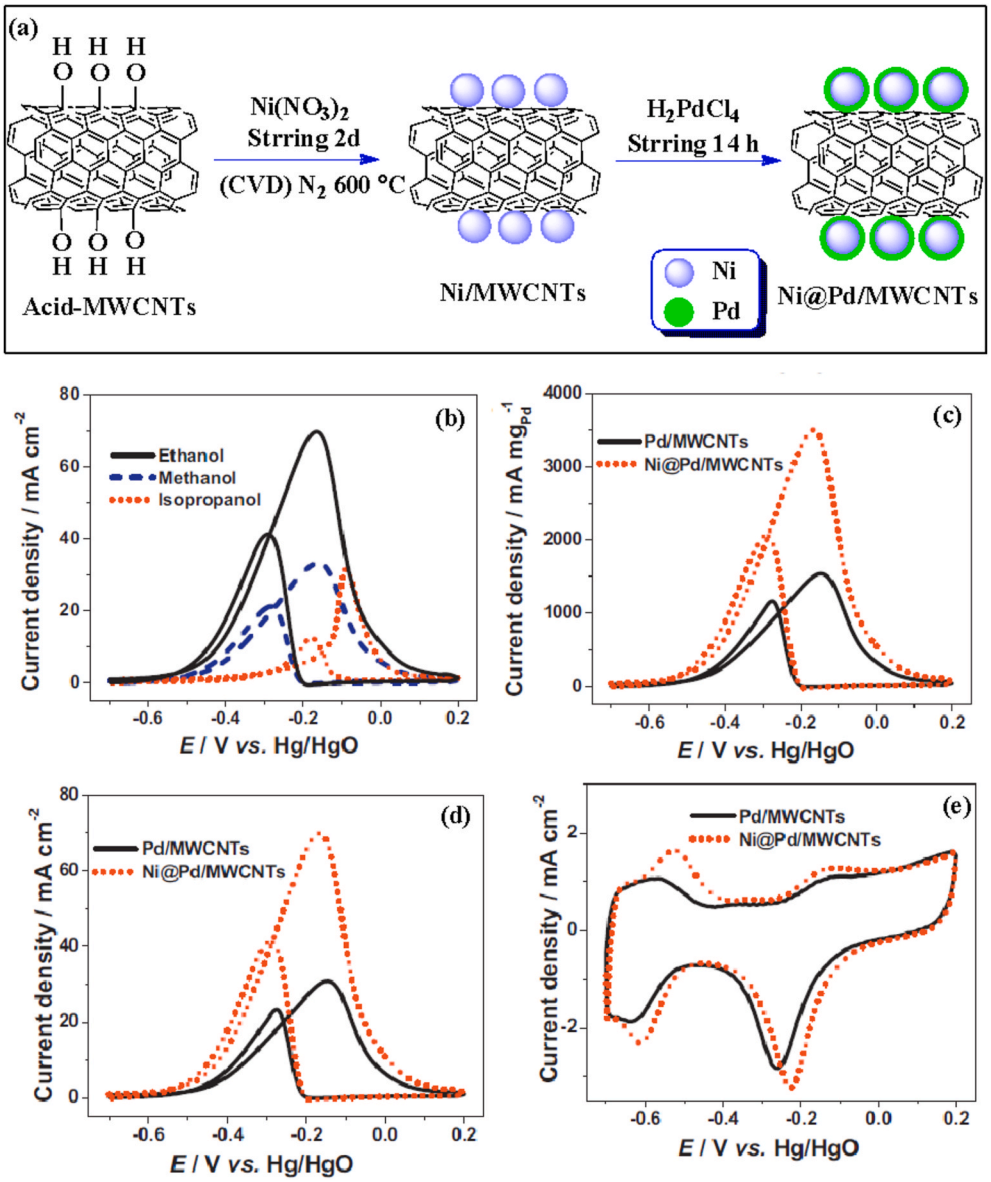

Fig. 12. (a) Schematic of the fabrication of Ni@Pd nanocatalysts on MWCNTs, (b) CV of different alcohol oxidation on Ni@Pd/MWCNTs electrode, in 1.0 mol/dm^3 KOH/1.0 mol/dm^3 alcohol solution at 303 K, scan rate: 50 mV/s, (c) and (d) CV of ethanol oxidation on Ni@Pd/MWCNTs and Pd/MWCNTs electrodes in 1.0 mol/dm^3 KOH/1.0 mol/dm^3 ethanol solution at 303 K, scan rate: 50 mV/s and (e) CV of Ni@Pd/MWCNTs and Pd/MWCNTs in 1.0 mol/dm^3 KOH solution at 303 K, scan rate: 50 mV/s. Reproduced with permission from Ref. [350]. Copyright 2012, Elsevier.

Moreover, the onset potential of Ni@Pd/MWCNTs was lower than Pd/MWCNTs. The ECSA and ethanol oxidation current density and Ni@Pd/MWCNTs were 1.2 and 2.3 times higher than Pd/MWCNTs (Fig. 12d and e). These great catalytic activities of ethanol were probably attributed to the electric synergistic effect between Pd and Ni and the uniform dispersion of Ni@Pd NPs on the MWCNTs. The alloyed catalysts can desorp toxic byproducts such as CO due to the ligand effect. In addition, the presence of Ni is created the downshift in the d-band energy center of the noble metal, leading to weak CO adsorption. Therefore, the catalytic activity and core/shell catalyst stability are improved.

Using metal-based catalysts consisting of CNTs, and metal oxides has shown significant ethanol oxidation catalytic activity due to its ability to remove CO. Manganese oxide with high proton conductivity and increasing employment of catalysts is widely used as support of catalysts. For instants, deposition Pt NPs on manganese oxide-CNTs (Pt/MnO_x-CNTs) by a microwave-assisted polyol route has possessed significant results toward ethanol oxidation, which was 1.82 times higher than Pt/CNTs [351]. The ECSA were 44.5 and 67.0 m^2/g for Pt/CNTs and Pt/MnO_x-CNTs, respectively. In addition, the current density reduced to 62.1 mA/mg_{Pt} on Pt/MnO_x-CNTs after 1800 s, whereas the Pt/CNTs displayed a current density of 11.6 mA/mg_{Pt}. Hence, Pt/MnO_x-CNTs indicated excellent catalytic activity and stability toward ethanol oxidation. However, the ethanol oxidation activity was reduced when the content of MnO_x was increased on the CNTs, and hence, the optimum content must be considered. In another report, copper oxide was introduced as an attractive semiconductor due to its high electrochemical activity and CO oxidation ability. The electrochemically synthesized Pd NPs/copper oxide/MWCNTs (Pd/Cu_2O/MWCNT) showed higher ECSA of 213.4 cm^2/mg compared with Pd/MWCNTs (34.9 cm^2/mg) [352]. In comparison with Pd/MWCNT, the onset potential of Pd/Cu_2O/MWCNT was shifted to the negative value of 120 mV. Pd/Cu_2O/MWCNT catalyst exposed a peak current density of 101 mA/cm^2, almost two times more than Pd/MWCNT (49 mA/cm^2). The results indicated that the addition of Cu_2O dramatically developed the stability and tolerance of the Pd to CO poisoning during ethanol electrooxidation.

The application of composed functionalized CNTs (m-CNTs) with PVA as membrane electrolyte in alkaline DEFC was reported as a great strategy for improving ionic conductivity and fuel cell performance [353]. The as-prepared composite indicated higher water uptake and water diffusivity than pure PVA. The ethanol permeability of

PVA/m-CNTs was 5.7-22.4% lower than pure PVA. The highest ionic conductivity was observed for the membrane at the temperature of 60 °C, due to its high water uptake and free fractional volume level. Meanwhile, PVA/m-CNTs have microchannel hydroxide and water transport, which improves ionic conductivity. The cell performance of PVA/m-CNTs was determined in different temperatures, ethanol concentration, KOH concentration, fuel flow rate, and oxygen gas flow rate; the optimum power density of 65.2 mW/cm^2 was achieved by 3 M ethanol in 5 M KOH at a flow rate of 5 mL/min with humidified oxygen fed at 100 mL/min at 60 °C. Adding polymeric materials to CNTs matrix increases their stability and acts as a charge transfer channel between the matrix and deposited metal NPs. Furthermore, the interaction between polymer and metal NPs improves poison tolerance in fuel cell reactions. As exposed, the uniformly dispersed Pt catalyst over the CNT-PANI composite exhibited excellent ethanol oxidation activity compared with Pt/C and CNT/Pt electrodes, showing that embedded Pt on CNT-PANI possesses high ECSA [354]. Fig. 13a represents a schematic of the ethanol oxidation process on CNT-PANI/Pt. The voltammograms of the acidic ethanol solution displayed that the anodic peak of CNT-PANI/Pt is two times that of Pt/C, as depicted in Fig. 13b. According to polarization curves, the overpotential for ethanol oxidation was the lowest value in the presence of the CNT-PANI/Pt. The performance anode matrix by diffusion coefficient and relative stability seems to be CNT-PANI/Pt 7.49 × 10^{-14} cm^2/s > CNT/Pt 4.3 × 10^{-14} cm^2/s > C/Pt 1.8 × 10^{-15} cm^2/s catalyst. The π-π interaction between PANI and CNT structure, hydrogen bonding between -OH group of CNT and -N of aniline, and the electrostatic interactions led to electron transfer and stability of catalyst against poisoning. In contrast, the embedded tri-metallic Pt-Ru-Re nano-electrocatalyst on the functionalized MWCNT (f-MWCNT) showed better power output [355]. By a facile route, modified polyol reduction process, bi-metallic Pt-Ru, Pt-Re, and tri-metallic Pt-Ru-Re nano electrocatalysts embedded on functionalized MWCNTs (f-MWCNT) were successfully fabricated for ethanol electro-oxidation. The highest ECSA value of 150.77 m^2/g$_{Pt}$ was obtained for tri-metallic Pt-Ru-Re (1:1:0.5)/f-MWCNT. The analysis indicated that tri-metallic Pt-Ru-Re (1:1:0.5)/f-MWCNT with the lowest onset potential (0.1 V) and the maximum peak current density of 83.34 mA/cm^2, provides the best ethanol oxidation activity among other synthesized electrocatalysts as following: Pt-Ru-Re (1:1:1)/f-MWCNT (65.46 mA/cm^2), Pt-Ru-Re (1:1:0.25)/f-MWCNT (57.94 mA/cm^2), Pt-Re (1:1)/f-MWCNT (23.60 mA/cm^2) and Pt-Ru (1:1)/f-MWCNT (48.76 mA/cm^2). The single-cell performance was tested, indicating that the Pt-Ru-Re (1:1:0.5)/f-MWCNT anode has the highest power density of 9.52 mW/cm^2, corresponding to the current density 38.40 mA/cm^2 at the temperature of 30 °C. It was observed that the fuel cell performance improves by increasing temperature from 30 to 80 °C.

Electrospinning synthesizes of porous carbon fibers (CFs) supported Pt-SnO_2 with polyacrylonitrile (PAN) and polyvinylidene fluoride (PVDF) as the carrier and pore-forming agent, respectively, represented good ethanol oxidation activity [356]. The best ethanol oxidation activity was observed for the prepared catalyst with PAN/PVDF weight ratio of 1:0.8. A peak current of 140.14 mA/cm^2 and an ECSA of 54.296 m^2/g for ethanol oxidation were achieved, probably due to homogenous particle size and good dispersion of Pt NPs on the surface of the CFs. Additionally, an increase in temperature led to an increase in power density; the power density peak reached 18.1 mW/cm^2 at 80 °C but 3.5 mW/cm^2 at 30 °C. Since Pd NPs are known as a cheap alternative of Pt NPs and GO, or RGO doped heteroatom provides a reduced anion poisoning effect and high alcohol oxidation, Pd/RGO and Pd/N-doped RGO (Pd/N-RGO) were prepared *via* an electrochemical process followed by solvothermal method [357]. The ECSA of Pd/RGO and Pd/N-RGO was 41 and 53 m^2/g, respectively. The highest ECSA of Pd/N-RGO was probably due to the uniform dispersion of Pd. The ORR kinetic was evaluated for each catalyst by measuring the Tafel slope; the Tafel slope of Pd/N-RGO was the lowest value, suggesting a fast electron transfer of the initial adsorbing oxygen adsorption step. Furthermore, the onset potential (-0.605 V, *vs.* Ag/AgCl) and mass activity (1422.5 mA/mg$_{Pd}$) of Pd/N-RGO toward the ethanol oxidation process were greater than Pd/RGO. The I_f/I_b for Pd/N-RGO was more than Pd/RGO, which means that Pd/N-RGO has better poisoning-tolerant behavior, better catalytic efficiency, and more effective removal of CO. The maximum power density was 31.5 mW/cm^2. The obtained result can be related to unique structures of N-RGO with a high specific surface area. It was found that CNTs are more useful for loading metal catalysts due to providing conductive channels and high ECSA. However, the metal-free carbon catalyst was not applied for the ethanol oxidation reaction. Using compounds of Pd NPs or Pd-based alloys as cheap alternatives of Pt NPs with carbon materials revealed significant catalytic activity toward ethanol oxidation due to the excellent dispersion of Pd-based catalyst on the carbon supports and high CO removal ability of the compound. Other carbon-based catalysts for DEFCs performance are listed in Table 4.

3.2.3. *Direct glycerol fuel cells (DGFCs) and direct ethylene glycol fuel cells (DEGFCs)*

Biomass-derived alcohols as renewable fuels are charming choices compared to methanol due to their lower poisonous and effortlessly preparation from biomass with well-established technology [382].

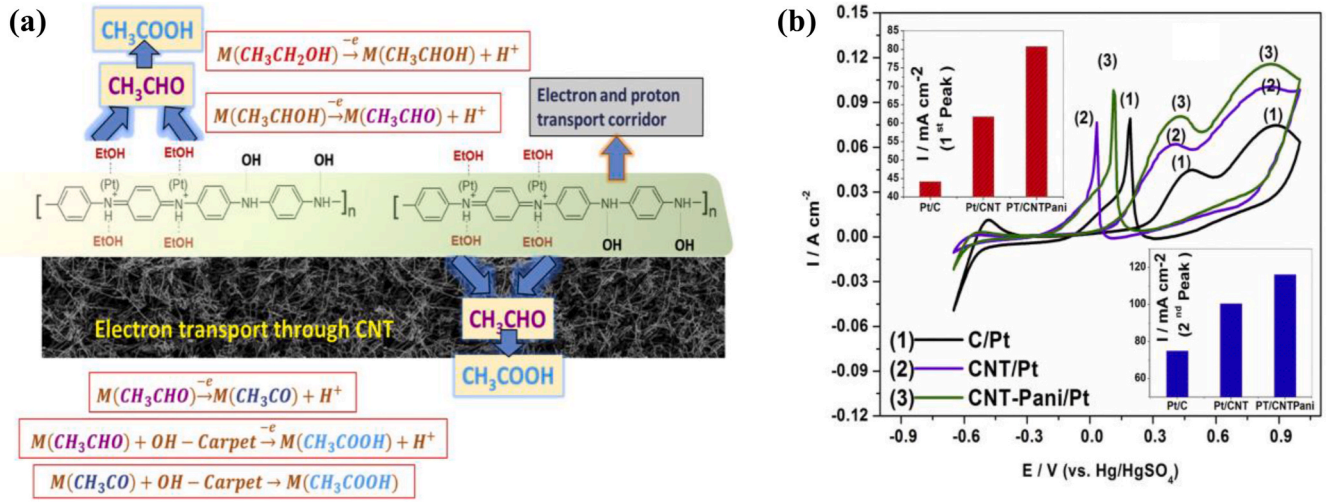

Fig. 13. (a) Ethanol electro-oxidation on CNT-PANI/Pt catalyst and (b) CV in 1 M Ethanol containing 0.5 M H_2SO_4 solution of the C/Pt, CNT/Pt, and CNT-PANI/Pt catalysts. Scan rate 50 mV/S. Reproduced with permission from Ref. [354]. Copyright 2017, Elsevier.

Table 4
The DEFCs consist of carbon-based catalysts.

Catalyst	ECSA (m^2/g)	Current density (mA/cm^2)	Potential of current density (V)	Power density (mW/cm^2)	Temp. (°C)	Ref.
PtSn/C	-	146	-	60	90	[358]
Pd/MWCNT treated with dilute hydrofluoric acid	-	0.18	-	-	-	[359]
Pt/mesoporous carbon CMK-3	39.0	48.43	-	-	60	[165]
PtAuSn/C	-	34.21	-	-	RT	[360]
Pt-bamboo shaped CNTs (BCNTs)	-	Higher than Pt-MWNTs	0.43	-	RT	[361]
PtPdAu/C	-	4.24 times higher than Pt/C	-	-	RT	[362]
Pd/porous hollow carbon spheres (PHCS)	-	3.1 times higher than Pd/C	-	-	40	[286]
Pt-Ir-Sn/C	-	32	0.761	29.13	90	[363]
PtSnNi/C	-	60.28 ± 14.80	0.781	-	25	[364]
Pd–CeO_2/C	-	106	0.82	140	80	[365]
Pd-helical CNFs (HCNFs)	-	Higher than Pd/XC-72	-	-	22	[366]
Pd-Ni NPs/C	-	19.83	-	-	-	[367]
CNTs/PtSn	-	35	0.5	-	-	[368]
Pt-Ru/ mesoporous g-C_3N_4	-	222	0.308	61.1	100	[369]
Pd/Mn_3O_4/plait-like carbon nanocoils (CNCs)	585.24	700.2 mA/mg	-	-	-	[370]
NiCo-doped CNFs	-	142	0.86	-	25	[371]
PdNi/C	53.9	-	-	31	40-80	[372]
Pd/1H-benzotriazole functionalized-C	58.3	0.18 A/mg $_{Pd}$	-0.56	-	-	[373]
Pd-CeO_2/C	-	85.5	0.82	47	RT	[374]
PdSn/β-cd-CNT	-	51.79	-	16.1	RT	[309]
Pd-Mo/Vulcan XC-72R carbon	-	121.2	-	-	-	[315]
Pt-FAU-C SG (Pt-faujasite zeolite with carbon-sol gel)	2.28	2.7	-	-	RT	[316]
CP/TiO_2/Pt	29	29	-	-	RT	[375]
Pd/TiO_2-nitrogen-doped carbon (NC)	-	5.18 mA	-0.102	-	25	[376]
PtRh/TiO_2-C	49.38	1039.5 mA/mg $_{Pt}$	0.877	-	25	[377]
Pt/nitrogen-sulfur (NS)-rGO/double wall CNT (DWCNT)	27.3	0.088	0.5	-	70	[378]
Ni-Co-N/HC (honeycomb carbon)	-	20	-	42.2	-	[379]
Pd@C-Ni	121.8	160	-	202	60	[380]
PdNiBi	549 ± 72 cm^2/mg	105.7	-	-	-	[381]

Glycerol and ethylene glycol are a member of the biomass-derived alcohol group. Contrary to methanol and ethanol, which are produced from biomass fermentation, the biomass-derived glycerol is mainly synthesized as a waste byproduct in biodiesel production by a trans-esterification reaction. So it is considered a cost-effective, eco--friendly, and non-toxic fuel for DAFCs instead of methanol or ethanol. Ethylene glycol can also be directly obtained from catalytic conversion of cellulose derivatives with great yields. The features such as high boiling point, great theoretical charge capacity, and excellent performance of electric power conversion lead to propose the ethylene glycol as a promising fuel in DAFCs [383-385]. The cogeneration of electrical energy and valuable chemicals, namely glycolic acid, oxalic acid, mes-oxalic acid, tartronic acid, glyceric acid, and 1,3 dihydro-acetone occur from the electrooxidation of glycerol and ethylene glycol in both passive and active alkaline DAFCs. These valuable oxygenates are generally generated via expensive and non-eco-friendly stoichiometric oxidation or slow fermentation proceeding with low yields. Hence, cogeneration of electrical energy and these valuable chemicals by DAFCs is a cost-competitive and environment-friendly approach [386,387].

The reactions occur in a DGFC are as follow [388]:

$$\text{At anode } 3H_2O + C_3H_8O_3 \rightarrow 14H^+ + 14e^- + 3CO_2 \quad (16)$$

$$\text{At cathode } 3/2O_2 + 6H^+ + 6e^- \rightarrow 3H_2O \quad (17)$$

$$\text{Overall reaction: } C_3H_8O_3 + 7/2O_2 \rightarrow 3CO_2 + 4H_2O \quad (18)$$

And the reactions for a DEGFC are described as follow [389]:

$$\text{At anode } C_2H_6O_2 + 10OH^- \rightarrow (COO^-)_2 + 8e^- + 8H_2O \quad (19)$$

$$\text{At cathode } 4H_2O_2 + 8H^+ + 8e^- \rightarrow 8H_2O \quad (20)$$

$$\text{Overall reaction: } C_2H_6O_2 + 4H_2O_2 + 8H^+ + 10OH^- \rightarrow (COO^-)_2 + 16H_2O \quad (21)$$

In spite of the fact that both glycerol and ethylene glycol have the standards for effective fuels (namely cost-effectively, availability, and high boiling point to utilize at temperatures above 100 °C under ambient pressure), there are challenges for complete electro-oxidation of them to CO_2 (carbonates in alkaline media) owing to hardly breaking of strong C–C bond by metallic catalyst [390,391]. Therefore, as a remedy to improve the fuel performance, active catalysts with sufficiency to cleave C–C bond in glycerol and ethylene glycol are enormously gained attention. In 2009, Bambagioni et al. reported the first utilizing of a Pd catalyst in a real DAFC [392]. Earlier than, studies have been restricted to oxidation of alcohol in half cells. Pd and Pt-Ru NPs supported on MWCNTs were synthesized using the impregnation reduction procedure and used as an anode for the electro-oxidation of methanol, ethanol, and glycerol in 2 M KOH solution in half cells. The catalysts were highly active for the oxidation of all alcohols, with glycerol indicating the best performance with respect to the current density (53.7 mA/cm^2) and ethanol demonstrating the lowest onset potential (-0.55 V). Glycolate, glycerate, tartronate, oxalate, formate, and carbonate were produced from the glycerol oxidation. The considerable electrocatalytic activity of Pd/MWCNT has been related to the great dispersion of the Pd NPs on MWCNTs. In another report, MWCNTs bearing carboxylic (MWCNT-COOH) and sulfonic acid (MWCNT-SO_3H) were used as a support to the synthesis of Pd-based ternary core-shell (FeCo@Fe@Pd) nanocatalyst [383]. The electrocatalytic behavior of as-prepared nano-catalyst was studied for electro-oxidation of glycerol and ethylene glycol in an alkaline medium. Physico-chemical properties of the nanocatalyst for electro-oxidation reactions were immensely affected by the surface functional groups of MWCNTs. The –COOH surface groups had more effective due to lower NPs size, more uniform dispersion on the support, high electrochemically active surface area, and increased electro-catalytic activity of FeCo@Fe@Pd/MWCNT-COOH in comparison with FeCo@Fe@Pd/MWCNT-SO_3H. The exhaust products in the AEM-DEGFC

and AEM-DGFC in the presence of FeCo@Fe@Pd/MWCNT-COOH nanocatalyst indicated the high selectivity level for complete oxidation of both alcohols. The high electrocatalytic performance and the sufficiency of the FeCo@Fe@Pd/MWCNT-COOH to competently cleave the C–C bonds resulted from the electronic properties improvement coupled with the strong affinity of its –COOH surface groups with the catalyst species. Ethylene glycol oxidation reaction generated a high amount of glycolate, a precious product for a wide variety of commercial applications, from pharmaceuticals to textiles industries. One more report in 2015 studied the synthesis of Pt-supported CNT (Pt-CNT) by microwave-induced reaction for glycerol and ethylene glycol oxidation [393]. The Pt-CNT electrocatalyst exhibited an onset potential of -0.44 V and a current density of 1.23 mA/cm^2 in the glycerol oxidation. In addition, the Pt-CNT had superior catalytic activity toward ethylene glycol oxidation; the onset potential and current densities were -0.49 V and 9.5 mA/cm^2, respectively. The Pt-CNT current density was six-folds and 33 folds higher than the Pt-C catalyst in the glycerol oxidation reaction and ethylene glycol oxidation reaction, respectively, due to its strong conductivity and electronic relay. The MWCNTs can be functionalized with 1-pyrenecarboxylic acid (PC), which has a large π-conjugated system and own the great content of carboxylic acid groups and can act as a molecular building block. PC is self-assembled on MWCNTs by the π- π stacking of pyrene structure and the graphitic surface of nanotubes. Yuan and coworkers synthesized PC-MWCNTs and then used microwave-assisted self-assembly for deposition of ultrafine CeO_2 NPs (<2 nm) on MWCNTs [394]. Au NPs were decorated on CeO_2/MWCNT during the alcohol reduction procedure. The great activity and durability were reported for the glycerol oxidation reaction by this electrocatalyst in terms of the peak current density 28.2 folds higher than that of the commercial Pt/C catalyst and the current density 1.6 times as high as that of Pt/C at a practical fuel cell operation potential of -0.3 V. Hence, as-prepared electrocatalyst is superior alternative electrocatalyst for Pt-based ones for DGFCs. In another work, the use of CNs was reported to deposit the Pd and Ag NPs by an aqueous-phase reduction process with no surfactant [395]. The excellent fuel efficiency was achieved for DAFCs by PdAg/CNT electrocatalyst as an anode and breaking the C-C bond of glycerol, more effectually compared to Pd/CNT. In a half-cell system with 1 M KOH and 0.1 M alcohol (ethanol, methanol, ethylene glycol, and glycerol) electrolyte, the best performance was reported for glycerol and ethylene glycol with the power densities of 276.2 mW/cm^2, and 245.2 mW/cm^2, respectively. CNTs possess great electrical conductivity, significant mechanical and thermal stabilities, and can form 3D electrode structures to increase the mass transfer of alcohol and OH-, so increase the catalytic performance for actual fuel cell operation. Ag@C nanocables can outperform MWCNTs-based nanocatalyst. The Ag@C nanocables were effectively fabricated *via* a hydrothermal self-assembly route to use as the supporting material for uniformly Pt deposition, according to Fig. 14a [396]. Fig. 14b,c show that the nanocables had different diameters, about 100-220 nm, and an average shell thickness of 30 nm. Also, it can be seen that Ag@C nanocables are well-dispersed. The Pt/Ag@C electrocatalyst behaved highly more active and more stable with a peak current density of 1079 mA/mg$_{Pt}$ compared to Pt/MWCNTs (260 mA/mg$_{Pt}$) and Pt/C-shell (142 mA/mg$_{Pt}$). It is concluded that Pt/Ag@C electrocatalyst should be a supreme possible anode catalyst for DGFCs.

Awasthi et al. studied ethylene glycol and glycerol oxidations performance in the presence of synthesized (100-x)% Pd-x % Ni (x = 1, 2, 5, 10, and 20) and (90-y)%Pd-10%Ni-y%C (y = 0.5, 1, 2, 5, and 10) catalysts in 1 M KOH solution [346]. The maximum catalytic activity of (100-x)% Pd-x% Ni composites was observed in the presence of 10% Ni

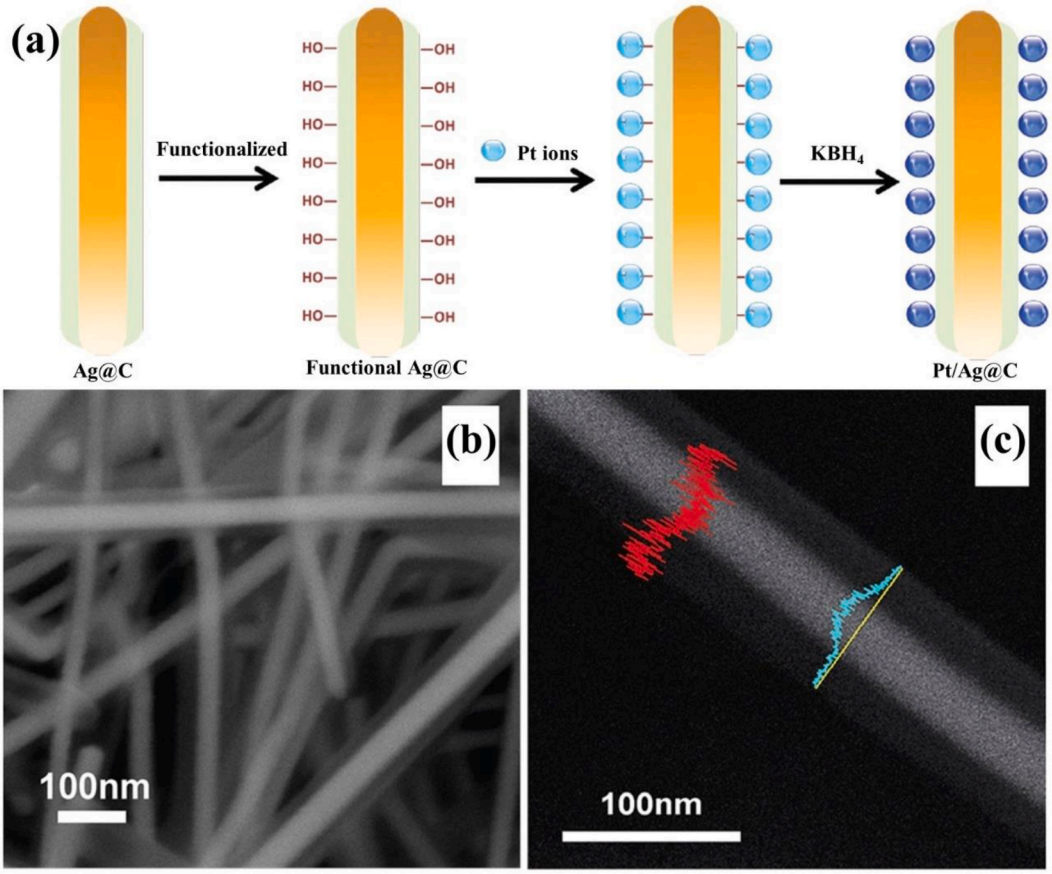

Fig. 14. (a) Schematic illustration of the Pt/Ag@C electrocatalyst formation, and (b,c) FESEM images with two different scales of the Ag@C nanocables. Reproduced with permission from Ref. [396]. Copyright 2016, Royal Society of Chemistry.

due to higher ionic potential of Ni^{2+}, and thus reduction of electron density on Pd; the ethylene glycol and glycerol oxidation current peaks at -0.20 V was 101 and 93 mA/mg, respectively. The addition of different C content enhanced the electrocatalytic activity of composites. However, the highest ethylene glycol and glycerol oxidation current were achieved with 5% C, which was 129 mA/mg and 192 mA/mg at -0.20 V, respectively. In one more work, Ni foam anodes were coated with a Pd-(Ni-Zn)/C catalyst and the cathodes were FeCo/C (C=Ketjen Black) catalyst to study the glycerol and ethylene glycol electrooxidation in a half cell [397]. The great electrocatalytic efficiency of Pd-(Ni-Zn)/C was reported with respect of the peak current density of 3300 A/g_{Pd} for ethylene glycol and 2150 A/g_{Pd} for glycerol. Producing valuable chemicals containing glycolate, tartronate, glycerate, formate, oxalate, and carbonate, was more found from the glycerol oxidation by both Pd/C and Pd-(Ni-Zn)/C compared to ethylene glycol oxidation with no observation side products of glycerol oxidation such as dihydroxyacetone, hydroxypiruvate, and mesoxalate. The notable electrocatalytic performance of Pd-(Ni-Zn) can be affiliated to both the uniform dispersion of the metal NPs and to the natural properties of the Ni-Zn phase that should enhance the content of OH_{ads} groups on the surface of the catalyst, which are involved for the carboxylic acid formation.

Since some carbide materials are suitable as an electrocatalyst, Zhang and coworkers used binary molybdenum carbide-tungsten carbides/carbon aerogel (Mo_2C-WC/C) loaded Pd NPs catalyst for ethylene glycol oxidation [398]. The electrocatalytic activity of the Pd/WC electrode was enhanced in the highest concentration of 2 M ethylene glycol (Fig. 15a). According to Fig. 15b, the maximum current density of ethylene glycol oxidation (600 mA/mg_{Pd}) was achieved on Pd/WC-Mo_2C, which was ten times higher than Pd/C with the same loaded Pd NPs. In addition, the onset potential of Pd/WC-Mo_2C was -0.6 V while it was -0.4 V on Pd/C. The superior electrocatalytic activity of Pd/WC-Mo_2C was due to the synergistic effect between Pd and carbides. Qi et al. employed the Au NPs catalyst supported on carbon for selective glycerol oxidation to tartronate and electrical energy generation [399]. The cogeneration of tartronate with an excellent performance of 61.8% and electrical energy of 1527 J for 12 h was achieved. Au/C synthesized by organic phase nanocapsule procedure (Au/C-NC) with the average size of 3 nm (Fig. 15c) was evaluated with an aqueous phase reduction procedure (Au/C-AQ) with an average size of 4.7 nm (Fig. 15d), indicating the residual surfactants slightly affected on the tartronate yield.

Alloying of Pd with Cu can increase the electrooxidation of alcohols. Pd-Cu supported carbon (Pd-Cu/C) was prepared using wet synthesis with sodium hypophosphite reducing agent and compared with Pd/C catalyst for electrochemical oxidation of glycerol and ethylene glycol.

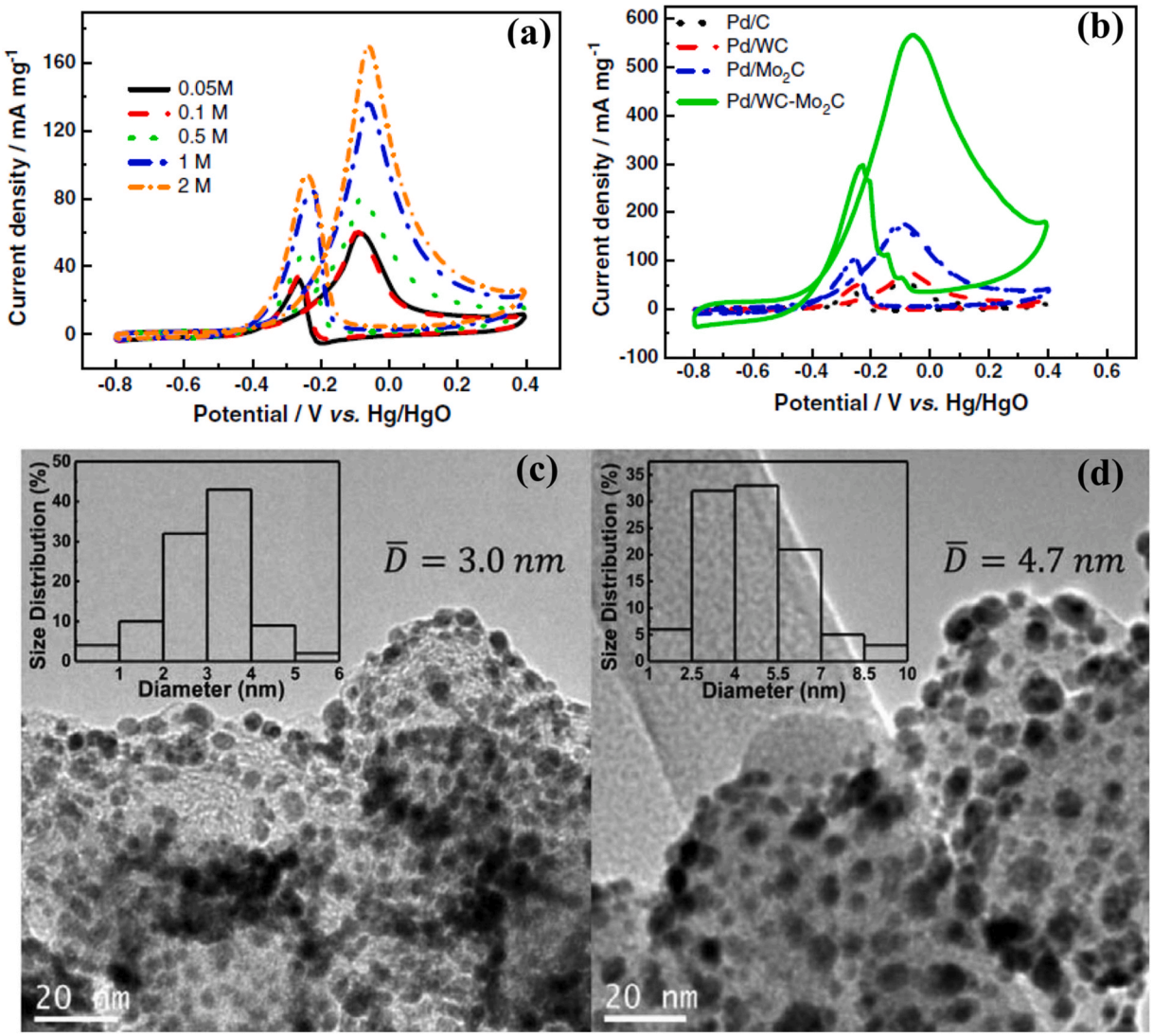

Fig. 15. (a) CV of different concentrations of ethylene glycol in 0.5 M KOH on Pd/WC electrode at 50 mV/s and 25 °C and (b) the CVs of 0.5 M ethylene glycol oxidation on different electrocatalysts at 50 mV/s in 0.5 M KOH at 25 °C. Reproduced with permission from Ref. [398]. Copyright 2013, Elsevier. TEM images and particle size histograms of (c) Au/C-NC, (d) Au/C-AQ. Reproduced with permission from Ref. [399]. Copyright 2014, Elsevier.

The oxidation rate of ethylene glycol and glycerol in the presence of Pd-Cu/C was 4 and 3 times higher than that of Pd/C, respectively. The maximum power density for ethylene glycol was reported to be 75% higher, and for glycerol was 32% higher related to a power density of Pd/C. One more report discussed the effect of bimetallic alloy on the catalytic activity of carbon catalyst in the alkaline medium for DAFCs application. Pd and Pd-Mo with various ratios supported Vulcan XC-72R carbon (VC) to investigate ethylene glycol and glycerol oxidation reactions [315]. The ECSA of Pd-Mo/VC was lower than Pd/VC. However, the catalytic efficiency of bimetallic alloys was better than monometallic Pd due to decreasing the d-band position and changing electronic structure. The Pd_3Mo/VC catalyst presented the highest catalytic activity in 1 M KOH solution, and the current activities of ethylene glycol and glycerol oxidation were 234.8 and 182.6 mA/cm^2, respectively. After 5400 s, the current density of Pd_3Mo/VC catalyst for ethylene glycol oxidation (25 mA/cm^2) was fixed at a higher value compared with glycerol (17 mA/cm^2). Hence, this catalyst displayed better electrocatalytic activity for glycol oxidation due to a lower Mo content.

Meeting bimetallic nanocatalyst with RGO as support can enormously improve the electrocatalytic behavior of nanocatalyst owing to high electrochemical surface area and unique topological defects of RGO resulting in more catalytic active sites [400]. Among bimetallic nanocatalysts, AuPd nanocrystals have gained immense interest owing to their supreme catalytic efficiency in alcohol oxidation [401]. Feng and co-workers used the one-pot wet-chemical method to synthesize well-defined dendritic core-shell gold@gold-palladium nanoflowers supported on RGO (Au@AuPd NFs/RGO) conforming to the formation process illustrated in Fig. 16 [402]. The specific alloy core-shell architecture and the synergistic effects of the AuPd nanocatalyst improved the catalytic performance and durability for glycerol oxidation reaction compared to AuPd/RGO.

Although different noble metals and their alloys have behaved as powerful electrocatalysts in fuel cell applications, the catalytic activity of the Pt-based nanocatalysts remains still considered the best. To alleviate the limits of Pt, it is desirable to progress the synthesis of multimetallic alloys. Bhunia et al. offered a facile and one-step solvothermal manner to synthesize the trimetallic hybrid electrocatalysts by concurrent reduction of metal ions (Pt, Pd, and Ni) on RGO as support [403]. The decoration of Ni into the PtPd alloy led to altering the surface electronic structure of PtPd alloy, increasing the electrochemical surface area and altering the kinetics. Moreover, the intrinsically hydrophilic property of Ni boosts electrooxidation of alcohols (ethanol, glycerol, and ethylene glycol) and also remaining carbon impurities generated on the surface of the catalyst, resulting in reducing the catalyst poisoning. $Pt_{70}Pd_{24}Ni_6$/rGO electrocatalyst demonstrated a maximum catalytic

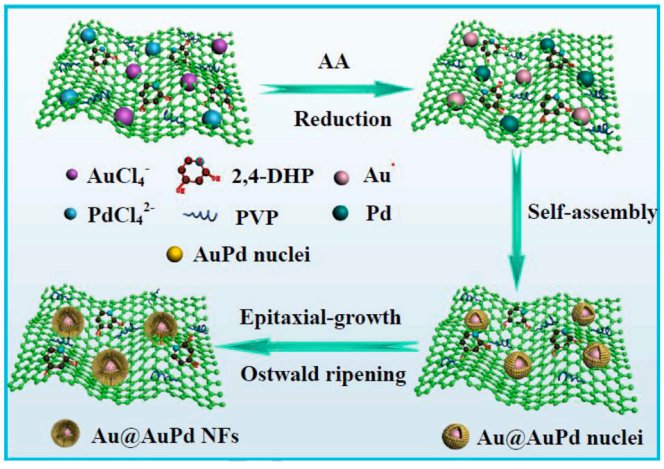

Fig. 16. Schematic presentation of the synthesis process of Au@AuPd NFs/RGO. Reproduced with permission from Ref. [402]. Copyright 2018, Elsevier.

efficiency with a lower onset potential of oxidation, a higher current density, and a higher mass activity. The best performance of this catalyst was associated with electrochemical oxidation of ethylene glycol with the mass activity of 7.75 A/mg, which was 4.96 folds as high as the mass activity of commercial Pt/C. Therefore, the alloy Pt-based is a favorable nanocatalyst for boosting electrochemical alcohol oxidation and reducing limits of Pt usage. Fig. 17 shows the synthesis of ultrafine Pt NPs decorated on flowerlike MoS_2/N-doped RGO (Pt@MoS_2/N-RGO) by a simple and cost-effective route, carried out through the hydrothermal procedure and subsequently by the wet-reflux system [404]. Pt@MoS_2/N-RGO was used as a potential electrocatalyst anode for alcohol fuel oxidation reaction. The Pt@MoS_2/N-RGO electrocatalyst exhibited excellent performance with high mass activities for electrooxidation of methanol (448 mA/mg$_{Pt}$), ethylene glycol (158 mA/mg$_{Pt}$), and glycerol (147 mA/mg$_{Pt}$) which were about 4.14, 2.82, and 3.34 times higher than that of a commercial Pt/C (20%) catalyst, respectively.

Recently, Krishnadevi and co-workers employed RGO to synthesize a new composite, non-covalent functionalized triazine framework using poly(cyanuric chloride-co-biphenyl) over RGO (Poly(CC-co-BP)-RGO) as a support material for deposition of Pt and Pt-Au NPs for the glycerol oxidation reaction in alkaline condition, as shown in Fig. 18a [405]. The results of glycerol oxidation reaction indicated that the Pt-Au/Poly (CC-co-BP)- RGO catalyst behaved more active and more stable with comparison to Pt/Poly(CC-co-BP)-RGO, Pt/Poly(CC-co-BP), and Pt/RGO catalysts. So the outperformed Pt-Au/Poly(CC-co BP)-RGO catalyst was applied as the electrode material to make the single test direct alkaline glycerol fuel cell, resulting in the power density of 122.96 mW/cm^2 (Fig. 18b) with the optimum glycerol concentration (2.0 M) at 70 °C. Several other reports on the carbon-based catalysts used for glycerol or ethylene glycol oxidation are summarized in Table 5.

In summary, real improvement can be totally ascribed to the amended mass transfer owing to the 3D-mesoporous framework generated by these materials, and also attributed to the superior electrical conducting properties and uniformly dispersing the NPs and great electroactive surface area values.

3.2.4. *Other alcohol fuel cells*

As mentioned above, other alcohol fuels such as isopropanol and n-propanol could be employed in the fuel cells. Isopropanol is a prominent chemical matter which can be applied as a good alternative fuel to methanol and ethanol in the DAFCs due to low toxicity, high energy density, and high boiling point. Further, the CO adsorption on the catalysts is lower during the isopropanol oxidation [435]. In 2011, ALD was utilized to Pd NPs distribution on porous carbon [436]. The isopropanol oxidation of the Pd/C (ALD) catalyst was examined, and resultant the commercial Pd/C catalyst presented a lower H_2 desorption peak compared to the synthesized Pd/C. The ECSA, onset potential and mass activity of isopropanol oxidation on Pd/C (ALD) electrode were 91.1 m^2/mg$_{Pd}$, 180 mV and 1247 mA/mg$_{Pd}$, respectively. On the commercial Pd/C catalyst, these parameters were 39.3 m^2/mg$_{Pd}$, 230 mV, and 493 mA/mg$_{Pd}$, respectively. Hence, the Pd/C (ALD) electrocatalyst displayed higher catalytic activity due to its smaller Pd NPs. The recorded chronoamperometric curves indicated that the beginning mass activity of isopropanol oxidation on both catalysts was reduced due to surface poisoning by acetone. However, the current of Pd/C (ALD) was higher than commercial Pd/C. In another work, MWCNTs were applied to load Pd catalyst [309]. Pd-based anode catalysts were fabricated using supports of MWCNT, carbon powder (C), β-cyclodextrin (β-cd) modified MWCNT (β-cd-MWCNT), and C (β-cd-C). The n-propanol and isopropanol oxidations activity of catalysts were survived in novel alcohol/Fe^{3+} fuel cells, as illustrated in Fig. 19a. The CV resultants indicated that the PdSn/β-cd-CNT catalyst has optimized catalytic activity compared with other catalysts. The chronoamperometry (CA) analysis confirmed that PdSn/β-cd-CNT affords the highest current density of alcohol oxidation (Fig. 19b and c). The cell power density for n-propanol

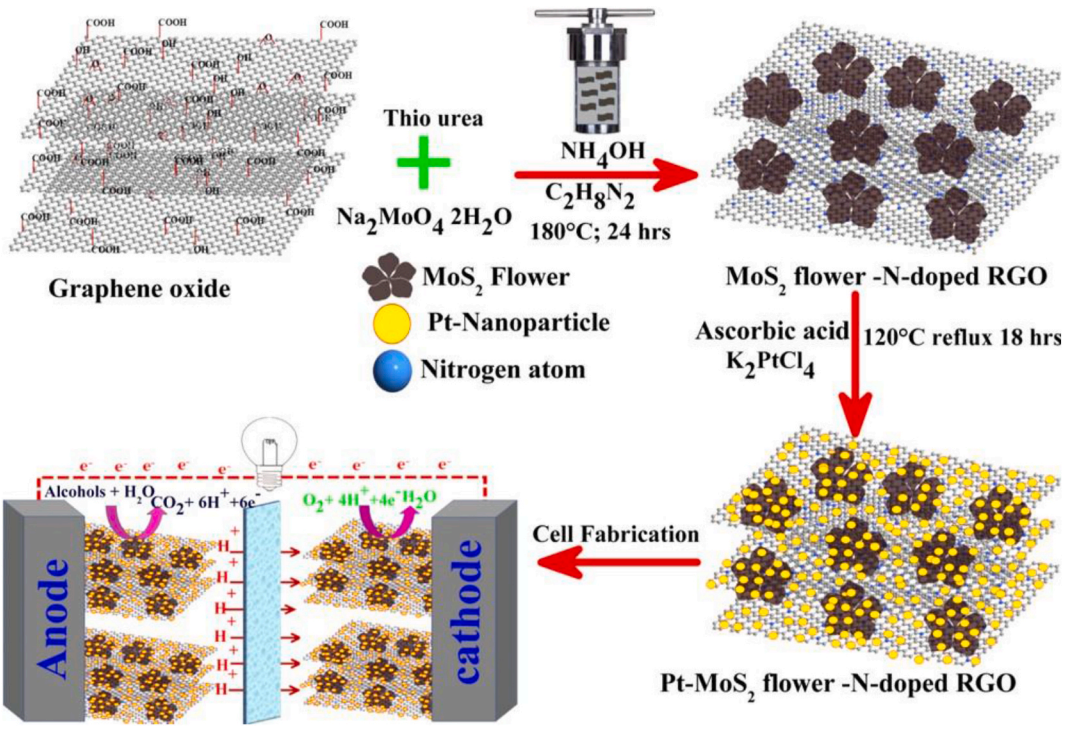

Fig. 17. Schematic image of the preparation process of Pt@MoS_2/N-RGO nanohybrid for DAFC applications. Reproduced with permission from Ref. [404]. Copyright 2019, American Chemical Society.

fuel and isopropanol fuel was 19.9 mW/cm^2 and 12.2 mW/cm^2, respectively. The cell performance of PdSn/β-cd-CNT was also investigated in the presence of different Fe^{3+} concentrations (0.5-1.5 mol/L) in the cell, showing the current density and power density of anode catalyst in n-propanol oxidation reaction was higher than isopropanol oxidation reaction.

In the use of Pd/carbon@functionalized CNT (Pd@C-f-CNT) for electrooxidation of Xylitol alcohol showed another significant catalytic activity [437]. The interaction of metal and support was increased by obtained carbon, which led to a high electrocatalytic performance in alkaline medium, it is in accordance to CV tests performed in 1 M H_2SO_4, 1 M KOH, and 1 M Na_2SO_4 solutions. The obtained electrochemical active surface area of the electrodes was 176.5, 263 and 97 mC/cm^2.mg in alkaline, acidic and neutral mediums, respectively. In addition, the xylitol oxidation of the electrode was tested in each medium; indicating three oxidation peaks appeared in the potential range of 0.4 V to 0.7 V. The maximum oxidation current density of 2.1 A/cm^2 was achieved at -0.05 V in 1 M KOH, which was ten times higher than H_2SO_4 and Na_2SO_2, resulting the Pd@C-f-CNT had better catalytic activity in alkaline solution.

In 2018, a new catalyst-based carbon was introduced using carbon with a honeycomb structure. The nanocomposites consisted of Ni-Co-N doped honeycomb carbon (HC) were prepared for n-propanol and isopropanol oxidation [379]. The arranged honeycomb structure of carbon increased the stability of the nanoparticles. The ORR activity of the synthesized Ni_3Co_1-N/HC-x (x is the metal mass presentation of 20, 30, and 40 wt.%) was tested by LSV, exhibiting Ni_3Co_1-N/HC-40 had the maxim electrocatalytic activity due to its high current density of 4.04 mA/cm^2. The alcohol fuel cell performance investigation of Ni_3Co_1-N/HC-40 cathode catalyst demonstrated that the highest current densities are 33 mA/cm^2 for n-propanol and 14.4 mA/cm^2 for isopropanol.

Organometallic fuel cells (OMFCs) are a type of DAFCs with an organometallic molecular complex anode catalyst, operating in alkaline media for electrooxidation of alcohols to the attributed alkali metal carboxylate, protons, and electrons [438,439]. The electrons move from the anode in the external circuit to the cathode, and the oxygen is converted to OH^-. Then, the hydrated hydroxyl group move from the cathode to the anode into an anion-exchange membrane closes the circuit. Organometallic molecular complexes can be easily incorporated in a broad range of conductive support nanomaterial, like functionalized fullerenes, nanofibers, and carbon nanotubes. The successfully formed molecular architecture with correspondent support can selectively oxidize polyalcohols into valuable chemicals without waste. Annen and co-workers deposited (Rh(OTf)($trop_2$NH)(PPh_3)) on the Vulcan XC-72 as anode electrocatalyst, indicating power density was 24 mW/cm^2, it is in an active cell in the presence of 2 M KOH with 10 wt% ethanol at 60 °C [439]. In another report, Bevilacqua et al. modified the peripheral molecular structure of the Rh complexes (Rh(Y)($trop_2$NH)(PPh_3)) (Y=OTf, OAc) by replacing the PPh_3 with P(4-n-BuPh)$_3$, resulting in the formation of amorphous materials at the same coordination environment and then deposited them on the Vulcan XC-72 (Cv) and Ketjenblack EC-600JD (Ck) [440]. The deposited 2(OAc) on Ck exhibited a larger surface area, more pore volume, and lower polarity than Cv. The 2(OAc)@Ck was employed as an anode material in a complete alkaline OMFC to convert ethanol into acetate, showing comparable substrate conversions (45%) in three galvanostatic cycles. The 1(OTf)@Cv electrocatalyst had a little higher power density of (24 mW/cm^2) than 2(OAc)@Ck (18 mW/cm^2) but had lower electrochemical stability.

3.3. *Direct formic acid fuel cells (DFAFCs)*

Formic acid (HCOOH), as a liquid fuel at room temperature, is a prominent fuel for application in liquid fuel cells, which possess features of easy handling, low cost, and availability [441]. Direct formic acid fuel cells (DFAFCs) are an attractive electronic power resource due to their outstanding properties of low operating temperature, enough high energy density, non-flammability, and less crossover of the formic acid thorough membrane [442,443]. One of the important advantages of DFAFCs is their high electromotive force which is higher than DMFCs [444]. The protons, electrons, and CO_2 are released during the dehydrogenation reaction of HCOOH at the anode, and then the formation of

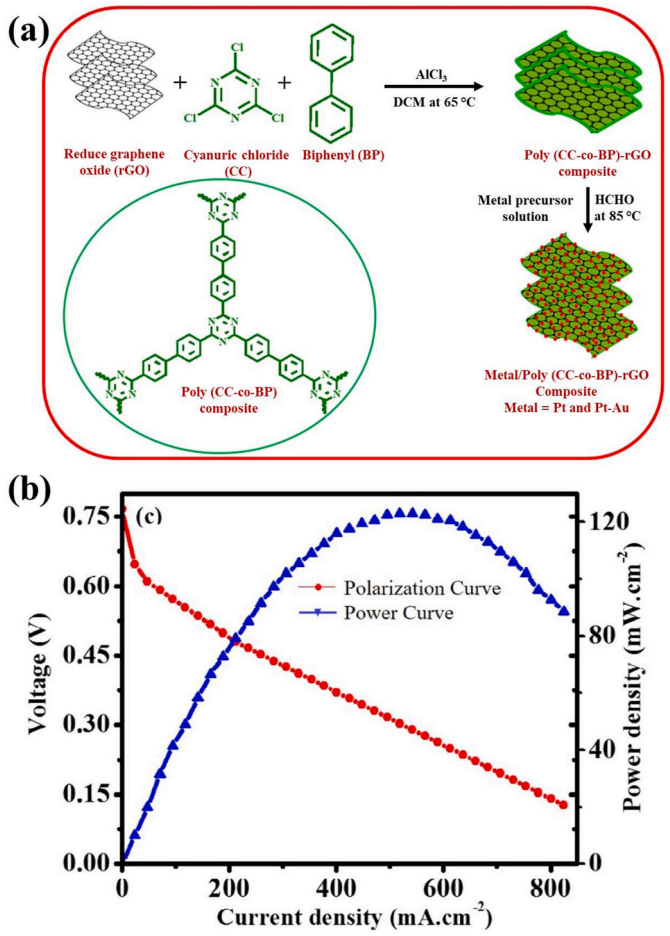

Fig. 18. (a) Schematically representation of the synthesis of Pt and Pt-Au NPs decorated on the Poly(CC-co-BO)-RGO composite and (b) Polarization and current density curves for fuel cell in the presence of the Pt-Au/Poly(CC-co-BP)-RGO electrocatalyst in 2.0 M glycerol + 1.0 M KOH solution at 70 °C. Reproduced with permission from Ref. [405]. Copyright 2022, Elsevier.

water molecules occurs at the cathode by the reaction of O_2 with transferred protons and electrons. The reactions that occur in the DFAFCs are:

$$\text{At anode } HCOOH \rightarrow 2H^+ + 2e^- + CO_2 \quad (22)$$

$$\text{At cathode } 1/2O_2 + 2H^+ + 2e^- \rightarrow H_2O \quad (23)$$

$$\text{Overall reaction: } 1/2O_2 + HCOOH \rightarrow H_2O + CO_2 \quad (24)$$

Carbon-based materials are efficient for DFAFCs due to their excellent conductivity and specific structure. The loaded Pt NPs on the CO and OH-annealed Pt/C have shown higher catalytic activity toward HCOOH oxidation than untreated Pt/C [445]. By CO-annealed catalyst, HCOOH oxidation was performed from the direct pathway, whereas OH-annealed Pt/C was slightly improved HCOOH oxidation through a direct mechanism. The electrochemical oxidation measurement in 0.5 M formic acid displayed that the treated catalysts, especially CO-annealing, have a better oxidation rate than untreated catalysts due to small Pt domains appearance. Another research found that the mixture of α-Al_2O_3 and Vulcan XC-72 carbon support can enhance stability, corrosion resistance of carbon and activity toward formic acid oxidation due to the narrowest particle size distribution the supporting surface, and its current density was 36.97 mA/cm^2 [446]. A microwave-assisted polyol approach was used for Pd/α-Al_2O_3-Vulcan XC-72 CB (Pd/Al_2O_3-C) catalyst preparation. The catalytic activity of catalyst with α-Al_2O_3 matrix was lower than catalyst with Vulcan XC-72 carbon matrix due to its low conductivity. However, the Pd/Al_2O_3-C catalyst displayed higher stability and ability in HCOOH oxidation compared with Pd/C due to anti-corrosion of α-Al_2O_3 and a metal-support interaction between the Pd NPs and the α-Al_2O_3. Helical CNFs with significant conductivity and mechanical stability possess a higher surface area than CNFs. The fixed Pd NPs on functionalized helical CNFs (Pd-S-HCNFs) showed better DFAFC performance than commercial Pd/Vulcan XC-72 [366]. The formic acid oxidation current density of 29.8 mA/cm^2 (at 0.386 V) and 15 mA/cm^2 (at 0.418 V) were attributed to Pd-S-HCNFs and Pd/Vulcan XC-72, respectively, ascribed to the good conductivity of helical CNFs and the strong attachment of Pt catalyst on the surface of a support. Nanostructured carbon black (NCB) with a high surface area was chosen as affordable support for loading Pd catalysts to enhance the catalytic activity of Pd NPs. After deposition Pd/NCB on a carbon-ceramic electrode (CCE), its formic acid electrooxidation ability was compared with Pd/CCE, resulting in the maximum oxidation current density of 24.90 mA/cm^2 at 0.31 V was achieved with Pd/NCB/CCE catalyst [447]. High conductive network, well dispersion of Pd NPs on/in NCB, and high electrochemical activity of Pd NPs were practical factors in the catalytic activity of Pd/NCB/CCE. The catalyst performance stability of Pd/NCB/CCE was tested during 2000 s, and the current density was fixed at 20.7 mA/cm^2. Low stability of Pd in formic acid oxidation and low CO removal ability of Pt at low potentials caused the synthesis of alloying Pt or Pd. The various nanocatalysts based on carbon-supported Pt_x-Pd_y-Cu_z (Pt_x-Pd_y-Cu_z/C, where x, y, and z are atomic ratios of Pt, Pd, and Cu, respectively) revealed considerable formic acid oxidation activity [448]. $Pt_1Pd_4Cu_2$/C catalyst showed excellent performance towards formic acid oxidation. Its current density (3.02 A/$mg_{(Pt+Pd)}$) was the highest value due to the formation of much less CO. In addition, the isolation of Pt with Pd and Cu can help to direct oxidation of formic acid. In contrast, the as-prepared nitrogen-doped carbon dot/$Pt_{84}Pd_{16}$ (N-Cdot/$Pt_{84}Pd_{16}$) catalyst by chemical etching method showed the current density of 1919.5 mA/mg_{metal} corresponded to modification of its electronic structure and the unique nanonetwork structure [449]. The ECSA of N-Cdot/$Pt_{84}Pd_{16}$ was estimated at 89.9 m^2/g_{metal} by CV analysis. After the 1200 s test, the N-Cdot/$Pt_{84}Pd_{16}$ catalyst was fixed at a more current density value. Fig. 20 indicates a schematic of the fabrication of the catalyst. In order to form a homogenous deposition of Pd catalyst, CeO_2 metal oxide was employed [450]. Comparison of formic acid oxidation activity of Pd/CeO_2/C with two reference electrodes of Pd-CeO_2/C and Pd/C indicated that the ECSA was estimated to be 52.6, 38.7, and 25.5 m^2g for Pd/CeO_2/C, Pd-CeO_2/C, and Pd/C catalysts, respectively, which attributed to small particles size of Pd/CeO_2/C. The specific activity of Pd/CeO_2/C was 4.6 mA/cm, which was higher than those of Pd-CeO_2/C and Pd/C catalysts. The presence of CeO_2 in the vicinity of Pd NPs can reduce CO poisoning by holding -OH groups. The loaded Pd NPs on top of CeO_2 enhanced the resistance of carbon corrosion. This catalyst exhibited good stability such that its current density was fixed at 70% of the initial current density after 1000 cycles.

Since MWCNTs have higher electrical conductivity compared to Vulcan XC-72® carbon, the loaded Pd NPs on MWCNTs (Pd/MWCNTs) as an anode showed better HCOOH oxidation than Pd/V XC-72 at low formic acid concentration (0.1 and 0.5 M) fuel cell and the optimal power density of 3.3 mW/cm^2 was obtained by Pd/MWCNTs anode with a 50% less Pd NPs than Pd/V XC-72 [451]. In addition to the electrical features of MWCNTs, good distribution of Pd on the MWCNTs surface improved fuel cell performance. In another report, phosphomolybdic acid (HPMo)-poly(diallyl dimethylammonium chloride) (PDDA)--functionalized MWCNTs (HPMo-PDDA-MWCNTs) were employed as a substrate to support Pd NPs for formic acid oxidation application [452]. Compared with acid-treated MWCNTs/Pd and Pd/Carbon (Pd/C) catalyst, Pd/HPMo-PDDA-MWCNTs exhibited higher electrocatalytic activity. However, these three catalysts showed similar formic acid oxidation potentials, indicating a similar oxidation mechanism. The current oxidation peaks were about 945 mA/mg, 373 mA/mg, and 554 mA/mg

Table 5
Carbon-based catalysts for DGFCs and DEGFCs.

Catalyst	Power density (mW/cm^2)	Current density/mass activity	Potential of current density/mass activity (V)	Fuel	Temp. (°C)	Ref.
Pd-(Ni-Zn)/C	-	0.2 A	-	Glycerol	40	[406]
	-	0.2 A		Ethylene glycol		
Pd_9Bi_1/C	25	-	-	Glycerol	60	[407]
Pt/C	124.5	-	-	Glycerol	80	[408]
Au-RuO_2/C	-	6.69 mA/cm^2	-0.33V	Glycerol	-	[409]
Au/C	57.9	-	-	Glycerol	80	[410]
Pd/CNT-FLG (Pd/multi-walled carbon nanotubes-few layer graphene	-	1.84 $mA/\mu g_{Pd}$	-	Glycerol	RT	[411]
	-	3.7 $mA/\mu g_{Pd}$	-	Ethylene glycol		
$Pd_{50}Ni_{50}$/C	-	190 A/g_{Pd}	0.93	Glycerol	-	[412]
$Pd_{50}Ag_{50}$/C		263 A/g_{Pd}	1			
Ag/c	86	-	-	Glycerol	80	[413]
FeCo@Fe@Pd/C		4.5 mA/cm^2	-	Glycerol	-	[414]
		5.01 mA/cm^2	-	Ethylene glycol		
Pd_5Ru-PEDOT/C	-	4.3 mA/cm^2	-	Glycerol	-	[415]
Pd-CN_x/G (Pd-carbon nitride/graphene)	-	Higher than Pd/CB	-	Glycerol	-	[416]
PdAuSn/C 50:40:10	51	-	-	Glycerol	85	[417]
Pd-Cu/C	35	-	-	Glycerol	60	[418]
	29			Ethylene glycol		
Pb@Pt/C	-	5.08 mA/cm^2	-	Glycerol	-	[419]
PdAu/C	-	96.3 mA/cm^2	-0.155	Glycerol	-	[420]
PtAu/C	-	6.07 mA/cm^2	0.3	Glycerol	-	[421]
PdAu-NF/NG (PdAu nano-flower/N-doped graphene)	-	8.7 A/mg	-	Glycerol	RT	[422]
		12.8 A/mg	-	Ethylene glycol		
Pd-NiO_x-P/C	-	0.364 A/mg_{Pd}	-0.48	Glycerol	-	[423]
PdAg/CNT	214.7	43.4 mA/cm^2	0.16	Glycerol	80	[424]
PdAg/CNT	76.5	-	-	Glycerol	60	[425]
$CeO_2.xH_2O$/Pt/CNTs	-	1880 mA/mg	-	Glycerol	-	[426]
Pt/C-modified carbon paper	39.5	77.1 mA/cm^2	-	Glycerol	RT	[427]
	30.3	75 mA/cm^2	-	Ethylene glycol		
Pd/MGF (Pd/mesocellular graphene foam)	-	2.718 A/mg_{Pd}	-	Glycerol	-	[428]
		4.056 A/mg_{Pd}	-	Ethylene glycol		
PdAu/VGCNF (PdAurum/vapor grown carbon nanofiber)	7	0.08664 mA/cm^2	-	Glycerol	-	[429]
Fe/Pt/C	53.6	98 mA/cm^2	-	Glycerol	-	[430]
Pt/C	330	-	-	Glycerol	80	[431]
Au-Ni/C	142					
Pt/C	375	451 mA/cm^2	-	Glycerol	80	[432]
3D Ni-NMC (3D Ni-nitrogen-doped mesoporous carbon)	-	2.54 mA	-	Glycerol	-	[433]
P-D-$PdCo_3$/C (phosphate dealloyed palladium cobalt)	-	65.9 mA/mg	-0.05	Glycerol	-	[434]

for Pd/HPMo-PDDA-MWCNTs, Pd/C, and acid-treated MWCNTs/Pd, respectively. This high catalytic activity was found to be highly dispersed Pd. Furthermore, the interaction Pd with HPMo immobilized on PDDA-functionalized MWCNTs increases the HCOOH oxidation rate. While using the hydrothermal synthesis of nanocomposite based on Pd NPs supported on copper phthalocyanine 3,4',4",4"'-tetrasulfonic acid tetrasodium salt (TSCuPc)-functionalized MWCNTs (Pd/TSCuPc-MWCNTs) exhibited HCOOH oxidation current density of 1260.1 mA/mg, which was higher than Pd/acid-treated MWCNTs (Pd/AO-MWCNTs) [453]. In addition, the current of Pd/TSCuPc-MWCNTs was fixed at 86.5 mA/mg after 7200 s, while Pd/AO-MWCNTs showed a lower current (5.73 mA/mg). This better catalytic activity of Pd/TSCuPc-MWCNTs can explain by smaller particle size, better dispersion of Pd catalyst, and high CO oxidation ability.

Since the presence of oxygen-containing groups on to the graphene surface can facilitate Pd NPs deposition, the prepared low-defect graphene (LDG) sheets thorough exfoliation of bulk graphite was used to support Pd NPs with a 1-5 nm diameter, as shown in Fig. 21a [454]. This electrocatalyst had an ECSA of 83 m^2/g, higher than RGO/Pd, MWCNTs/Pd, and XC-72/Pd. The formic acid oxidation current density was acquired to be 61.6 mA/cm^2 at around 0.15 V. As shown in Fig. 21b, LDG/Pd displayed excellent formic acid oxidation performance among all samples, which is due to stability, conductivity, and large surface area of LDG. The catalytic performance investigation was confirmed the remarkable stability of LDG/Pd for formic acid oxidation (Fig. 21c); LDG/Pd catalyst retained the highest current after first decay. In another research, Pd nano-leaves were supported on modified GC by RGO (Pd nano-leaves/RGO/GCE), and then its formic acid oxidation ability was compared with Pd nano-leaves/GCE and commercial Pd/C/GCE [455]. The formic acid oxidation current density was obtained 19.5, 0.5, and 12.5 mA/cm^2 for Pd nano-leaves/RGO/GCE, Pd nano-leaves/GCE, and Pd/C/GCE, respectively, which is ascribed to higher ECSA of Pd nano-leaves/RGO/GCE (51.5 m^2/g) as well as improved electron transfer by RGO. After 2000 s, the current density loss of Pd nano-leaves/RGO/GCE was lower than other samples, suggesting the good poisoning-tolerance ability of Pd nano-leaves/RGO/GCE.

According to our investigation, modified carbon has been more attention for supporting metallic catalysts because of the modification process such as CO annealing, adding metal oxides caused to increase the ECSA and enhance formic acid oxidation. In addition, Pd-carbon

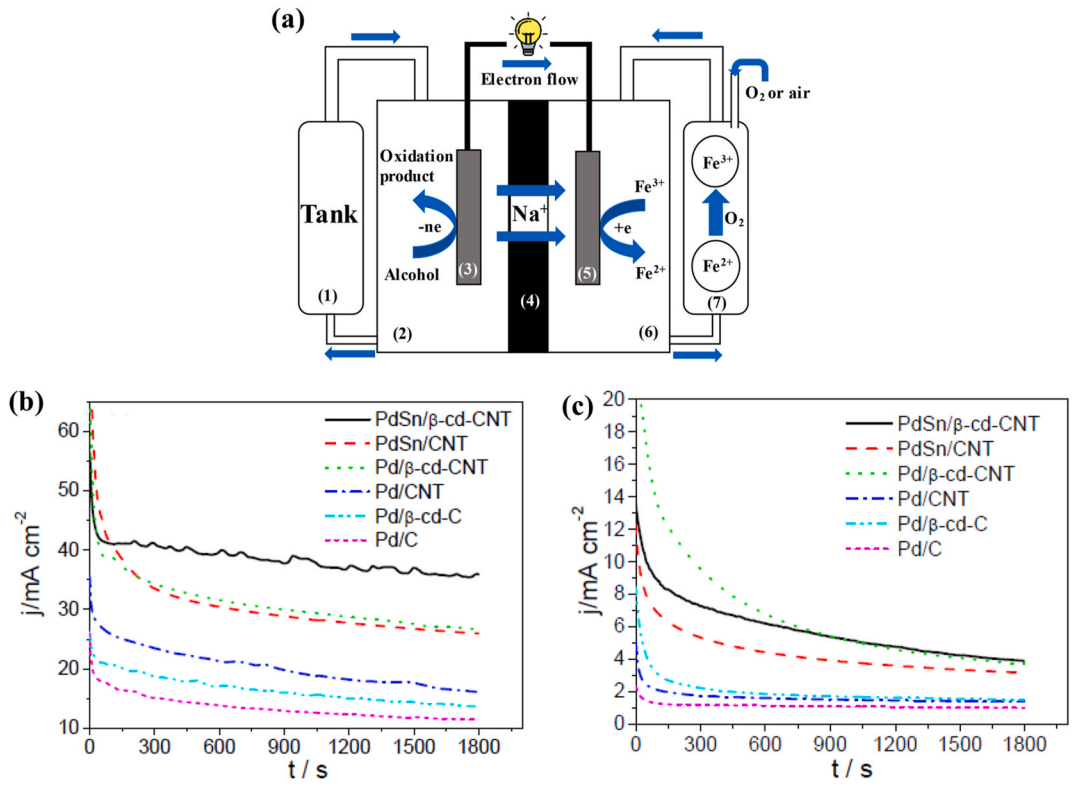

Fig. 19. (a) Schematic diagram of the presented cell. (1) anolyte storage tank; (2) anolyte (1.0 mol/L NaOH + 0.5 mol/L alcohol); (3) anode; (4) membrane; (5) cathode; (6) catholyte (0.5 mol/L NaCl containing $FeCl_3$); (7) conversion reactor of Fe^{2+} to Fe^{3+}; chronoamperometric responses of the prepared catalysts and Pd/C at -0.2 V in the presence of (b) 0.5 mol/L n-C_3H_7OH, (c) and 0.5 mol/L iso-C_3H_7OH. Reproduced with permission from Ref. [309]. Copyright 2016, Elsevier.

catalysts were used more than Pt-carbon catalysts, possibly due to Pd availability and low cost. Although CNTs are a great candidate for oxidation of HCOOH, graphene-based supports also showed significant catalytic activity due to their high conductivity and oxygen-containing groups.

Table 6 summarizes other carbon-based catalysts used in the DFAFCs.

The schematic representation of PEMFCs, DMFCs, DEFCs, and DFAFCs has been depicted in Fig. 22.

3.4. Biological fuel cells

This type of fuel cell works similarly to chemical fuel cells. There is a permanent fuel resource into the anode and a permanent oxidant resource into the cathode, and the electrical energy is produced through the electrochemical process by bio-electrocatalysts such as enzymes or microbial cells [464]. The electrons are generated during electrocatalytic oxidation at the anode and transferred to the cathode *via* an external electrical circuit. At the cathode, the transferred electrons act as a source for reducing the oxidizer. Fuel cells are known as green electricity generation devices due to their eco-friendly nature. Depending on the type of bio-electrocatalysts used, there are two types of biological fuel cells, named "Microbial fuel cells" and "Enzymatic biofuel cells" [465].

3.4.1. Microbial fuel cells (MFCs)

Microbial fuel cells (MFCs) are biological fuel cell that converts chemical energy to electrical energy *via* microorganism catalysts. Firstly, in 1911, Potter produced an electrical current from bacteria. However, MFCs were introduced as promising energy devices in the 1990s [466]. As depicted in Fig. 23, an MFC generally consists of anode and cathode chambers separated by a PEM. The organic material oxides at the anode and protons and electrons produce, and the produced electrons transfer to the cathode through PEM and external circuits. At the cathode, the water forms by reducing oxygen [467]. The MFCs possess different configurations, such as single-chamber and two-chamber MFCs. Single-chamber MFCs are a new design that reinforces power output by reducing internal resistance by removing PEM. A two-chamber MFC designed in "H" shape with two bottles connected by PEM. The two-chamber MFCs are affordable and popular compared with the single-chamber MFCs [468]. In MFCs, different compounds such as glucose, acetate, phenol, cellulose, wastewater, biomass, *etc.*, can be used for power production. Hence, MFCs are suitable for degrading wastewater and environmental pollutants [469]. Additionally, MFCs have different applications such as hydrogen production, industrial chemicals recovery, sensors, and microbial solar cells [468].

Modifying the anode and cathode using materials with high electrical conductivity, good biocompatibility, large surface area, chemical stability, and anti-corrosion features can enhance MFC's performance [466,468]. Carbon-based materials such as CP, carbon cloth (CC), activated carbon, *etc.*, with high conductivity and activity, can be applied to modify anode. However, the π electrons in carbon materials are inactive, which can be active by doping appropriate elements, leading to more O_2 adsorption. Doping N and boron into carbon NPs (NB-CPs) has been provided more catalytic activity toward ORR in MFCs. Both N and boron receive electrons from carbon and make a net positive charge, reducing chemisorption overpotential [470]. The preparation of NB-CPs was performed by in situ polymerizations of polydopamine (PDA) followed by binding with 3-aminophenyl boronic acid (ABA) and heat treatment. The electrochemical study revealed that the onset potential of NB-CPs is -0.02 V which has a positive shift compared with CPs and N-CPs catalysts. The Tafel slope of -0.121, -0.140, and -0.130 V/dec was achieved for NB-CPs, CPs, and N-CPs electrodes, indicating NB-CPs has an excellent catalytic activity toward ORR. This improved catalytic activity is attributed to charge transfer by N and boron atoms as catalytic sites. The maximum power density of MFC with NB-CPs cathode was 642

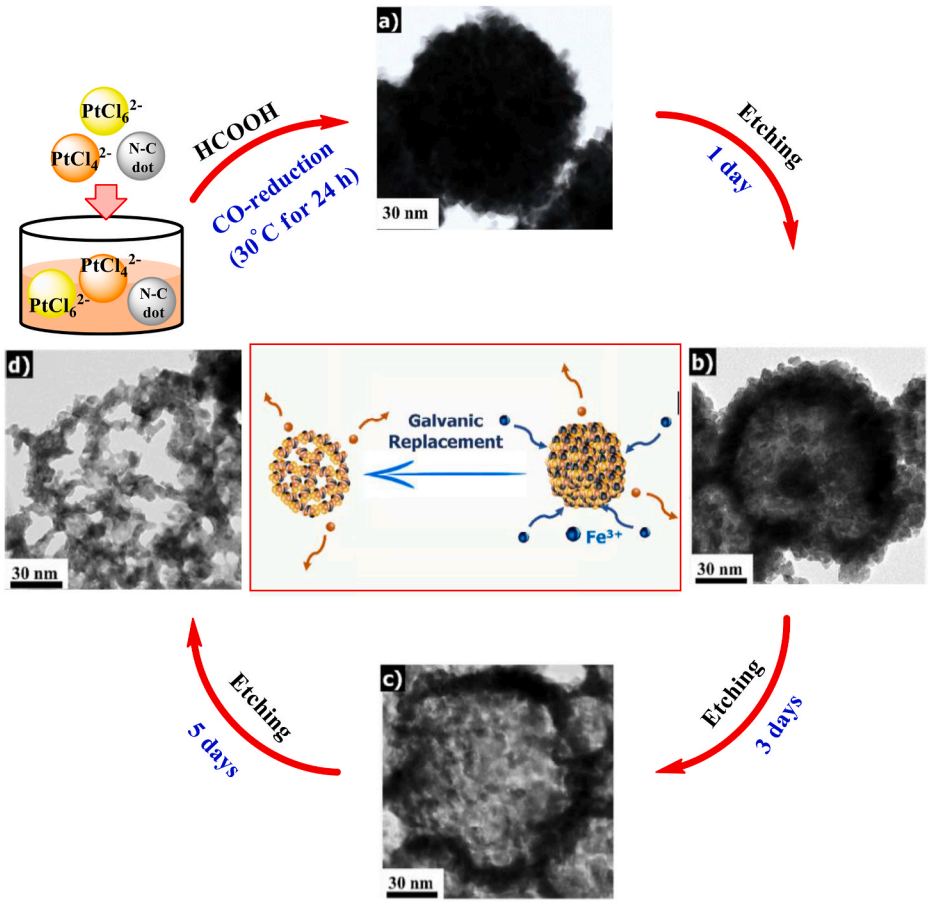

Fig. 20. Schematic illustration depicting the manufacturing procedure. TEM images of (a) N-Cdot/$Pt_{53}Pd_{47}$ nano-raspberries (b) N-Cdot/$Pt_{76}Pd_{24}$ porous nano-raspberries, (c) N-Cdot/$Pt_{81}Pd_{19}$ hollow porous nano-raspberries, and (d) N-Cdot/$Pt_{84}Pd_{16}$ nano-network. Reproduced with permission from Ref. [449]. Copyright 2018, Elsevier.

mW/m^2, which was higher than that of CPs (122 mW/m^2) and N-CPs (550 mW/m^2). In another report, a one-step carbonization process to fabricate N and Co-doped in porous carbon/nano Fe_3O_4 (noted as Fe_3O_4@N/Co-C) was represented to increase ORR in MFCs [471]. This three-dimensional catalyst with a 3-5 nm carbon layer thickness and well-distributed Fe_3O_4 NPs (20-50 nm) displayed that the power and current densities of Fe_3O_4@N/Co-C are approximately 918 mW/m^2 and -8.6 mA/cm^2, respectively, which were higher than Pt/C, Fe_3O_4@N-C, N/Co-C, and N-C. Metal-nitrogen-carbon compounds are another promising catalyst for ORR in MFCs. Among these catalysts, the iron-nitrogen-carbon catalyst shows better stability and catalytic activity. One of the low-cost methods for preparing Fe-N-C is the polymerization of nitrogen-rich polyaniline/graphene. In addition, adding graphene can effectively improve the conductivity of Fe-N-C. Using nanorods network anchored graphene (Fe-N-C/G) as an ORR catalyst in air-cathode MFC demonstrated significant results [472]. The Fe-N-C/G catalyst exhibited onset potential and overpotential of 0.224 V and 396 mV, respectively. Besides, a comparison between the LSV plot of Fe-N-C/G and Pt/C was carried out, suggesting the current exchange density of 11.11 and 10.13 mA/cm^2 was achieved for Fe-N-C/G and Pt/C, respectively. This high catalytic activity was ascribed to the formation of active sites of pyridinic-N, Fe-Nx, graphitic-N, and even unique Fe-Nx-C moiety, which have excellent adsorption ability of O_2 molecules. Moreover, the sandwich-like carbon nanorods network@-graphene@carbon nanorods network composites improve mass and charge transfer. To MFC performance study, Fe-N-C/G and Pt/C modified air-cathode MCF were examined. The output power density of Fe-N-C/G (1601 $\pm$ 59 mW/m^2) was enhanced compared with Pt/C MFC (1468 $\pm$ 58 mW/m^2). Fe-N-C catalyst as a new low-cost and highly stable PGM-free catalyst was successfully designed by a facile method for MFCs cathode. Fe-N-C catalyst cathode prepared by iron phthalocyanine that was supported on nitrogen-functionalized carbon black pearls (FeBP(N)) and then integrated into gas diffusion layer at hot pressing condition [473]. Although during MFC operation, the peak power density decreased due to the increasing charge and mass transfer resistances of ORR owing to agglomeration of biofilm at the cathode interface, the peak power density could be controlled with adjusting the hot pressing parameters resulting in the minimization of the kinetic and diffusional limitations of ORR at the cathode side of MFCs. The assembled MFCs at hot pressing parameters of the temperature of 120 °C and pressure of 2 MPa indicated the highest peak power density of 206.1+10.3 $\mu W/cm^2$ and good peak power stability over 100 days of MFC functioning compared to Pt-based cathodes. In another report, Fe-N-C catalyst cathode was synthesized via a single thermal conversion of Fe-doped ZIF-8 (a metal-organic framework (MOF) containing well-defined FeN_4 coordination) [474]. The Fe-N-C cathode presented a high ORR activity with an onset potential of 0.91 V in a 0.1 M KOH solution and illustrated a maximum power density of 1508 W/m^2. MOF structure created active sites, prevented particle aggregation and enhanced both mass transfer and ORR performance. The fabricated porous graphite with improved crystallinity was employed as a cathode catalyst in MFC [475]. A mixture of Mg and Cu powder was heated at 680 °C, MgO and then Cu were removed by 1.0 M HCl and 25% $NH_3.H_2O$ solutions. The byproducts were noted as C-Mg/Cu and C-Mg (prepared by Mg). The electrochemical performance of the as-prepared cathode catalysts was examined in MFC, indicating the current density of C-Mg/Cu catalyst was higher as much as 279% than that of C-Mg. Additionally, a 6.2% improvement was observed in the maximum power

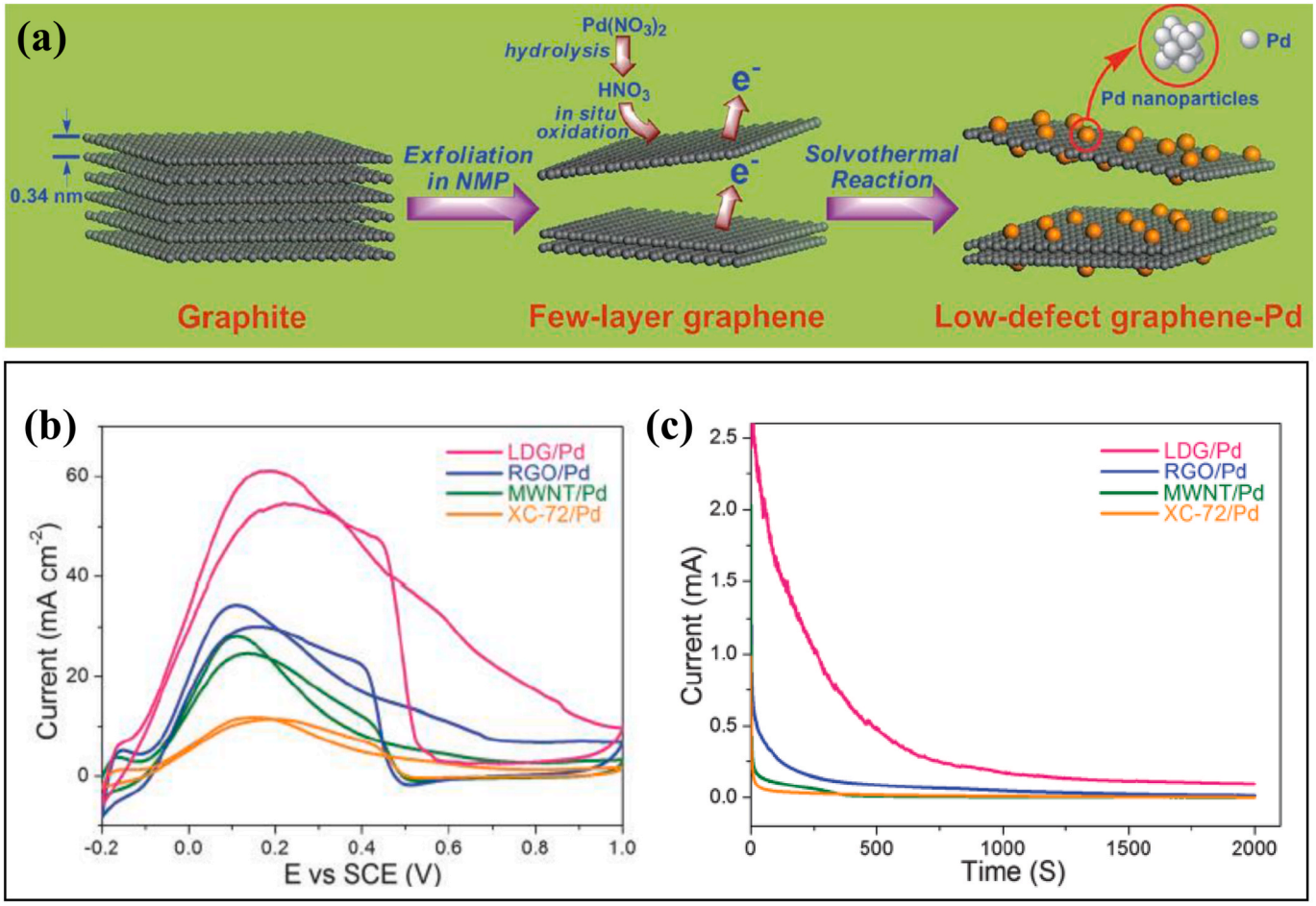

Fig. 21. (a) Illustration of the synthesis of low-defect graphene–Pd catalyst by our soft chemistry method; (b) CVs of LDG/Pd, RGO/Pd, MWNT/Pd, and XC-72/Pd and (c) Current-time dependence measured by chronoamperometry in 0.5 M H_2SO_4 with 0.5 M HCOOH. Reproduced with permission from Ref. [454]. Copyright 2012, Royal Society of Chemistry.

Table 6
DFAFCs consist of carbon-based catalysts.

Catalyst	ECSA	Specific Mass activity	FA oxidation current density	Potential of oxidation current density (V)	Power density (mW/cm^2)	Ref.
Pt-Os/carbon	-	-	Higher than Pt/C	0.34	-	[456]
Pd/vertically aligned CNTs	916.7 cm^2/mg_{Pd}	538 mA/mg_{Pd}	-	-	-	[457]
Pd/C	56 m^2/g	-	20.74 mA/cm^2	-	-	[458]
Pd/MWCNTs	46.2 m^2/g_{Pd}	-	159 mA/cm^2	0.32	-	[459]
Ru@PtPd/C	250.10 m^2/g	-	71.43 mA/cm^2	0.95	6.2	[460]
3D cubic ordered mesoporous carbon (CMK-8)/Pd	287 cm^2/mg_{Pd}	486.4 mA/mg_{Pd}	-	-	-	[461]
Pd-cobalt/ phosphotungstic acid-activated carbon	47.1 m^2/g	-	13.4 A/m^2	0.734	-	[462]
Pt/carbon nitrite	68 m^2/g_{Pt}	-	515 mA/mg_{Pt}	0.29	-	[1]
Pd/polyoxometalates/N,P-doped CFs	158.07 m^2/g	754.1 mA/mg_{Pd}	-	-	-	[463]

density of C-Mg/Cu compared with C-Mg, due to the high surface area of C-Mg/Cu. Candle soot-derived carbon NPs (CNPs) have mesoporous structure, high surface area, and significant electrical conductivity, which can be an outstanding alternative for graphitic matters in MFCs [476]. The spherical CNPs with the size of 30-50 nm are agglomerated and formed sponge-like 3D structures with rough surfaces, as shown in Fig. 24. The ORR catalytic activity of bare stainless steel (SS) and SS-supported CNPs were compared; the oxidation and reduction currents of SS were about one-sixth of that SS-supported CNPs. The maximum power density and limiting current density were 1650 ± 50 mW/m^2 and 7135 ± 110 mA/m^2 for SS-supported CNPs. The rough surface with high mesoporosity content of anode has good electrical conductivity due to the graphitic characteristic of the CNPs, and hence charge transfer was facilitated in ORR.

Using 3D materials as electrode provide a high surface area for bioelectrochemical systems. An ideal 3D structure electrode must be had a high number of open channels and conductive networks for electron transfer. Recently, metallic oxide-based nanowire/nanotube arrays on carbon-based matrix have been shown good catalytic activity in MFC [477]. This 3D nanostructure electrode was manufactured by developing self-supported N-doped carbon/Fe_3O_4-nanotube composite arrays onto the CF cloth (CC@N-C/Fe_3O_4), as depicted in Fig. 25a, which had a

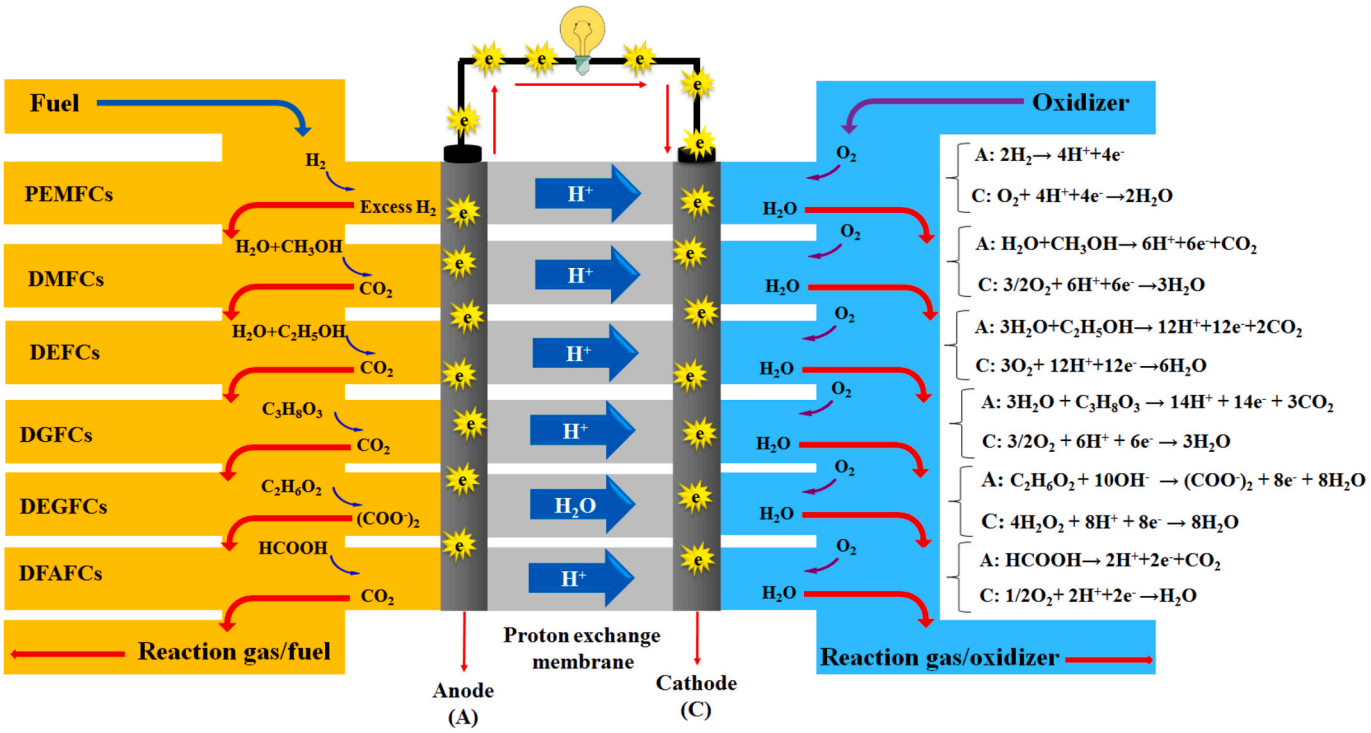

Fig. 22. Schematic representation of PEMFCs, DMFCs, DEFCs, DGFCs, DEGFCs and DFAFCs.

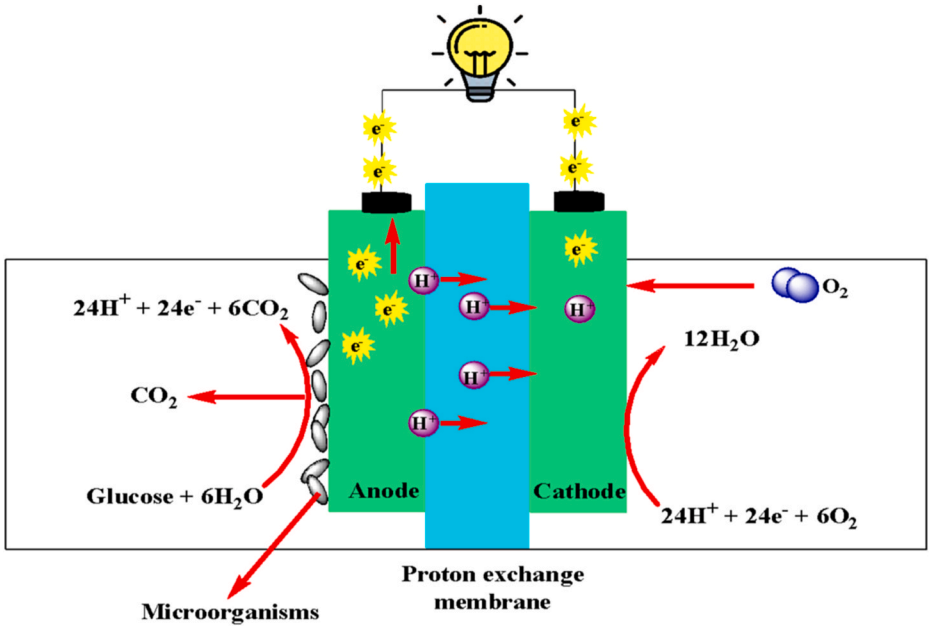

Fig. 23. Schematic representation of a two-chamber MFC.

uniform structure of nanotubes (Fig. 25). As seen in Fig. 25c, the bio-electrocatalytic behavior of the synthesized nanotube-based electrodes exhibited that CC@N-C/Fe_3O_4 has the highest current density of 4.27 mA/cm^2 after 5 cycles which was better than CC current density (1.95 mA/cm^2). These electrodes can be long-term used without damage because long-term stability tested suggested the current density of nanotube-based electrodes did not damage. The obtained coulombic efficiency of CC@N-C/Fe_3O_4 and CC electrodes was approximately in the range of 73.4-89 and 30.9-33.1%, respectively (Fig. 25d). The microbial fuel cell performance revealed that the highest voltage output and power density of CC@N-C/Fe_3O_4 anode was 671.4 mV and 1.21 ± 0.04 W/m^2, respectively (Fig. 25e).

The modification of graphene with a metal compound of copper selenide ($CuSe_2$) can enhance ORR performance. Furthermore, the composition of CNTs with graphene can prevent the aggregation of graphene sheets, improving the performance of graphene. Hence, the developed copper selenide (CuSe) on RGO and CNTs was employed as a cathode catalyst in MFC [478]. The electrochemical evaluation of CuSe@RGO-CNTs exhibited a more positive onset potential (-0.124 V) compared with CuSe@RGO (-0.132 V) and CuSe@CNTs (-0.136 V). Meanwhile, the current density of CuSe@RGO-CNTs (4.48 mA/cm^2) was approximately similar to Pt/C (4.62 mA/cm^2), which displayed good

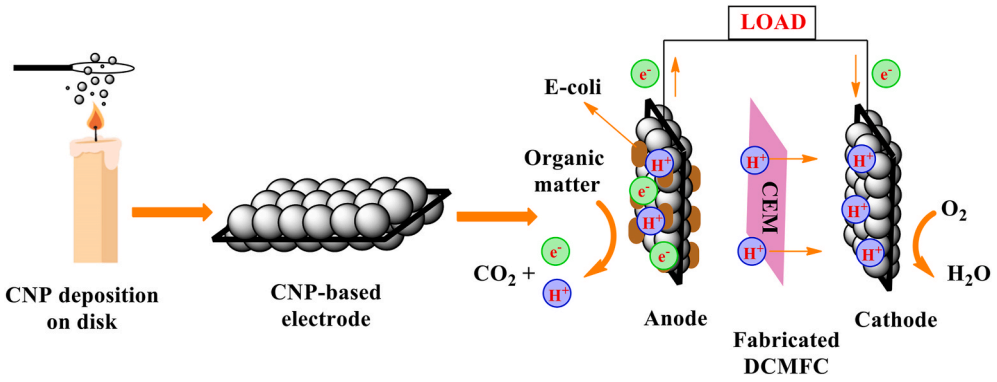

Fig. 24. Schematic illustration of the DCMFC process. Reproduced with permission from Ref. [476]. Copyright 2018, Elsevier.

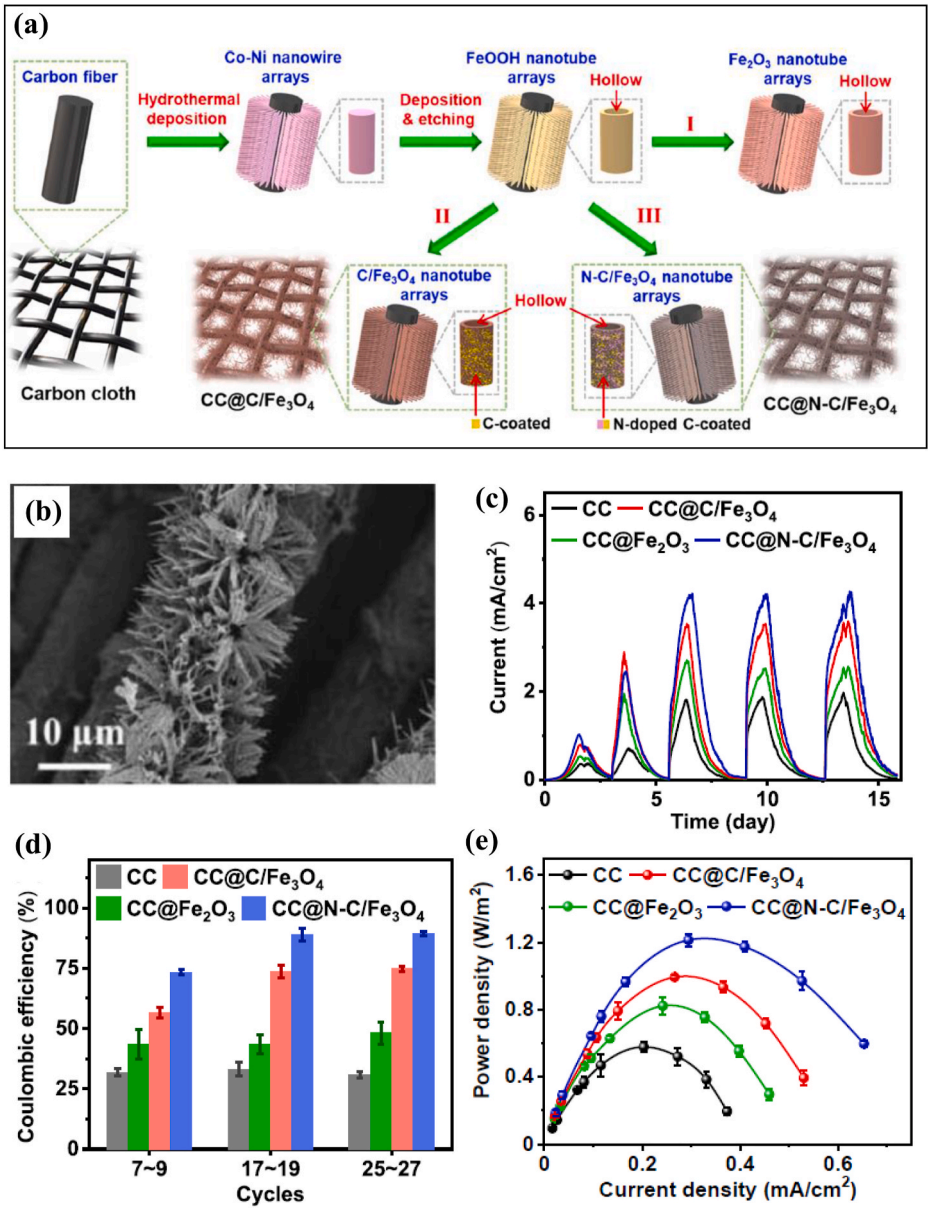

Fig. 25. (a) Schematic representation of self-supported Fe_2O_3, C/Fe_3O_4, and N-doped C/Fe_3O_4-nanotube arrays developed on CC. I: annealing at 500 °C; II: PDA-absorption and carbonization; III: glucose-absorption and carbonization, (b) SEM image of CC@N-C/Fe_3O_4, (c) Current density versus time curves and (d) coulombic efficiency of the bio-electrochemical system with CC, CC@Fe_2O_3, CC@C/Fe_3O_4, and CC@N-C/Fe_3O_4 electrodes and (e) polarization curves of the MFCs equipped with CC, CC@Fe_2O_3, CC@C/Fe_3O_4, and CC@N-C/Fe_3O_4 anodes during different operational cycles. Reproduced with permission from Ref. [477]. Copyright 2021, Elsevier.

ORR activity CuSe@RGO-CNTs. This excellent ORR activity can explain by the high charge transfer of its sandwiched network structure and the synergetic effect between CuSe and RGO-CNTs. Additionally, the Tafel slope was calculated to be 62.07, 64.05, and 71.90 mV/dec for CuSe@RGO-CNTs, CuSe@RGO, and CuSe@CNTs, respectively. The single-chamber MFC with the prepared cathodes was created for the

CuSe@RGO-CNTs performance study; the highest power density of 504 ± 5 mW/m^2 was acquired for MFC with CuSe@RGO-CNTs, which was better than CuSe@RGO (481 ± 7 mW/m^2) and CuSe@CNTs (430 ± 5 mW/m^2). Nanostructured manganese oxide (MnO_2) provides fast electrokinetics and remarkable catalytic activity due to its large number of active sites and lower toxicity and redox stability. Therefore, MnO_2 has potential for application in MFCs. However, MnO_2 has a low surface area which can resolve by supporting MWCNTs. The synthesized nanocomposite consists of MWCNTs, manganese oxide, and PPy (MWCNT/MnO_2/PPy) via an in-situ chemical technique used as an anode catalyst in MFC [479]. The EIS analysis indicated good electron transfer for modified CC electrode with MWCNT/MnO_2/PPy, and thus this nanocomposite can be a good candidate for application in MFCs. The MWCNT/MnO_2/PPy catalyst's MFC performance was evaluated for 30 days, and the maximum current and power density were obtained 3.35 ± 0.6 mA/m^2 and 1125.4 ± 5.5 mW/m^2, respectively. In addition, the calculated coloumbic efficiency of MFC with MWCNT/MnO_2/PPy and MWCNT-MnO_2 was ~59% and ~28%, respectively. The composition of 1D nanotubes with 2D nanosheets is produced coupled hybrids with high specific surface area, excellent electrical conductivity, and fluent mass transport pathways, which are suitable catalysts for MFCs. In addition, the encasement of Fe-based NPs into graphitic carbon materials leads to reduced carbon corrosion, improving the durability of carbon during the electrochemical process. For instance, Fe NPs-encapsulated bamboo-like N-doped CNTs on porous N-doped carbon nanosheets with hierarchical architecture (Fe@N-C NT/NSs) catalyst was synthesized by one-step pyrolysis technique and then assembled as cathode catalyst in MFC [480]. The ORR catalytic activity study was revealed that the cathodic peak of Fe@N-C NT/NSs is more positive than N-doped carbon, Fe@N-C NSs, and derived carbon material, suggesting that Fe@N-C NT/NSs had better catalytic activity. The Tafel slope of Fe@N-C NT/NSs was 69.6 mV/dec, which was similar to Pt/C. The MFC performance of Fe@N-C NT/NS was examined in phosphate buffer electrolyte, indicating the lower Tafel slope of 85.2 mV/dec compared with Pt/C (98.7 mV/dec). Moreover, the maxim power density of 900.18 mW/m^2 was observed for MFC with Fe@N-C NT/NSs, 1.61 times better than MFC based on Pt/C (558.07 mW/m^2). This great catalytic activity of Fe@N-C NT/NSs was observed due to enriched confined active sites, facilitated pathways for charge transfer, and improved diffusion kinetics.

In MFCs, different compositions of carbon-based materials such as graphene and CNTs with metal and metal oxide were used. Furthermore, doping N atoms into these materials enhances the performance of catalysts in MFCs. However, the metal-free carbon catalysts were less employed in MFCs. It is worth mentioning that Fe and Fe_3O_4 NPs were more attention than expensive Pt NPs to prepare cathode and anode catalysts.

Other carbon-based composites used in the MFCs are listed in Table 7.

3.4.2. *Enzymatic biofuel cells (EFCs)*

One of the most attractive biofuel cells (bioelectronic device) is EFCs because of their plainness and abundant redox enzyme sources. In 1964, the first EFC with glucose oxidase anode and Pt cathode was introduced, and after that, these green generation electrical devices were attractive for researchers [502]. Specific redox enzymes are employed as catalysts in an EFC to convert chemical energy to electrical energy [465]. Fig. 26 is a schematic of the EFC. At the anode, energy-rich organic matters such as glucose, alcohols, amines, *etc.,* oxidize by enzymes, and protons and electrons are released, the electrons are transferred to the anode surface. Meanwhile, the reduction reaction occurs in the presence of the enzymes and transferred electrons and protons at the cathode, generating electrical energy [503]. It is worth mentioning that the oxidative enzymes apply in the anode, whereas reductive enzymes use in the cathode.

Recently, it has been noted that the use of carbon-based nanomaterials such as CNTs or metal NPs linked to the oxidoreductase

Table 7
The MFCs consist of carbon-based compounds.

Composite Catalyst	Component of MFC	Type of MFC	Maximum power density (mW/m^2)	Ref.
Laccase modified cathode CP (10 wt.% Pt/C, E-TEK)	Cathode	Two-chamber	160	[481]
Mn_2O_3/C	Cathode	-	32 W/m^3	[482]
CNT-textile-Pt	Cathode	Two-chamber	837	[483]
Bacteria immobilized carbon NPs-coated CC	Anode	Two-chamber	269	[484]
CNT growth on silicon wafer	-	Two-chamber	3.6 μW/cm^2	[485]
MWCNTs	Anode	-	267.77	[486]
GN/SSFF	Anode	Two-chamber	2142	[487]
Carbon felt-supported Mo_2C/CNTs	Anode	Single-chamber	1.05 ± 0.0264 W/m^2	[488]
Nitrogen-decorated RGO/nano cobalt oxide	Cathode	-	713.6	[489]
CNP-coated biocarbon	Cathode	Single-chamber	703 ± 16	[490]
Urchin-like $NiCo_2O_4$ modified activated carbon (AC-NCO)	Cathode	Single-chamber	1730 ± 14	[491]
Nest-like oxygen-deficient $Cu_{1.5}Mn_{1.5}O_4$ doping activated carbon (AC-CMO)	Cathode	Single-chamber	1928 ± 18	[492]
Co-N-C/Pt	Cathode	-	1008 ±43	[493]
G/Co	Anode	Single-chamber	473.1	[494]
CP	Anode	Single-chamber	3.21	[495]
PANI-modified carbon foam	Anode	Single-chamber	1307	[496]
Iron aminoantipyrine-graphene nanosheets	Cathode	Single-chamber	(253 ± 1) × 10	[497]
Fe-N-C	Cathode	Single-chamber	(162 ± 3) × 10	[498]
Fe-N-C	Cathode	Two-chamber	1.3 × 10^{-3}	[499]
Fe-N-C	Cathode	Single-chamber	820	[500]
Activated carbon	Anode	Single-chamber	1626	[501]

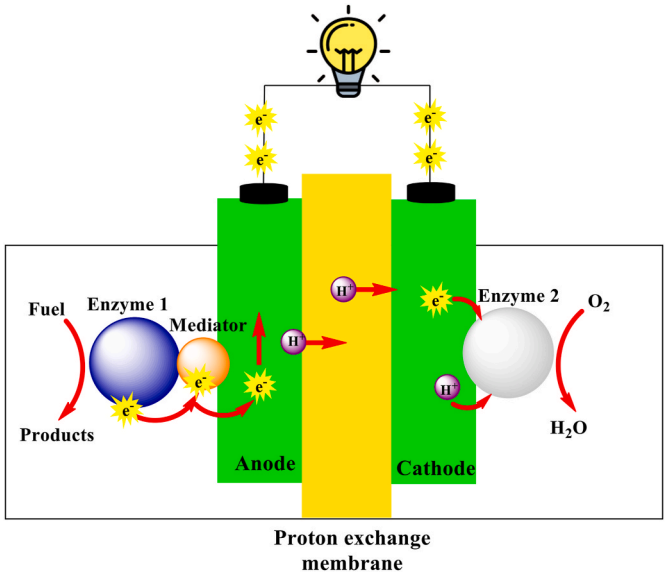

Fig. 26. Schematic representation of an EFC.

enzymes helps to facilitate the direct electron transfer from the active centers of the enzymes and electrodes [504-506]. Enzymes immobilization is an important issue for the preparation of biofuel cells because it can affect the bioanode lifetime. Polyamidoamine (PAMAM) dendrimers are good candidates for the immobilization of enzymes due to their highly functionalized terminal surface, larger uniformity, and organized structure. Besides, layer-by-layer (LbL) is a prominent strategy for the immobilization of enzymes onto layered thin films. In 2011, the electrostatic LbL process was used to immobilize enzymes and polyamidoamine (PAMAM) onto the carbon support, and the compound resultant was employed as bioanode in ethanol/O_2 biofuel cell. The presence of carbon support provided high surface area and increased electrical conductivity, leading to increase power output [507]. The power density of 0.063 and 0.12 mW/cm^2 was achieved for single and double enzymatic systems, respectively. Therefore, the LbL is suitable for enzyme immobilization with controllable enzyme arrangement on the anode surface. In another report, the affection of carbon NPs on the electron transfer and bio-electrocatalytic process in ethanol microfluidic biofuel cells was tested [508]. The large surface area and high electronic conductivity of carbon NPs increased the electrodes' reactive species loading and electron transfer rate.

Furthermore, carbon NPs with porous structures increased catalytic activity by offering closer proximity between the reactive species and the electrode surface and diffusion of ethanol and oxygen within the enzyme films. According to electrochemical tests, these bioanodes were exhibited the maximum power density was 90 μW/cm^2 at 0.6 V for Ethanol/O_2 microfluidic biofuel cell. Glucose oxidase (GOx) is one of the most usable biocatalysts for enzymatic biofuel cells. However, GOx has low electrochemical activity, which can be resolved by immobilizing nanomaterials with high surface area and electrical conductivity, such as carbon-based materials. To this aiming, the constructed GOx-graphitized mesoporous carbon (GMC) nanocomposite is used in enzymatic biofuel cells (Fig. 27a) [509]. Fig. 27b is a schematic of the prepared biofuel cell, including Pt-based air-breathing cathode and GOx-GMC nanocomposite anode. The electrochemical characterization of GOx-GMC exhibited high electrical conductivity with excellent charge transfer. The high electrical conductivity of GMC enhanced the electron transfer rate of the GOx-GMC nanocomposite. Thus, the GMC network can improve electrochemical performance with high enzyme loading. The glucose oxidation ability of GOx-GMC was survived for its electrochemical activity investigation; the optimal power density of 22.4 μW/cm^2 was achieved at 0.24 V. Using different carbon nanostructure substrates (CP, CF, or CC) covered with MWCNTs and laccase for biofuel cell electrode preparation indicated that CP has the best performance [510]. The maximum power density of 76.5 ± 6 μW/cm^2 at 0.31 V was observed for laccase biocathode and fructose dehydrogenase bioanode,

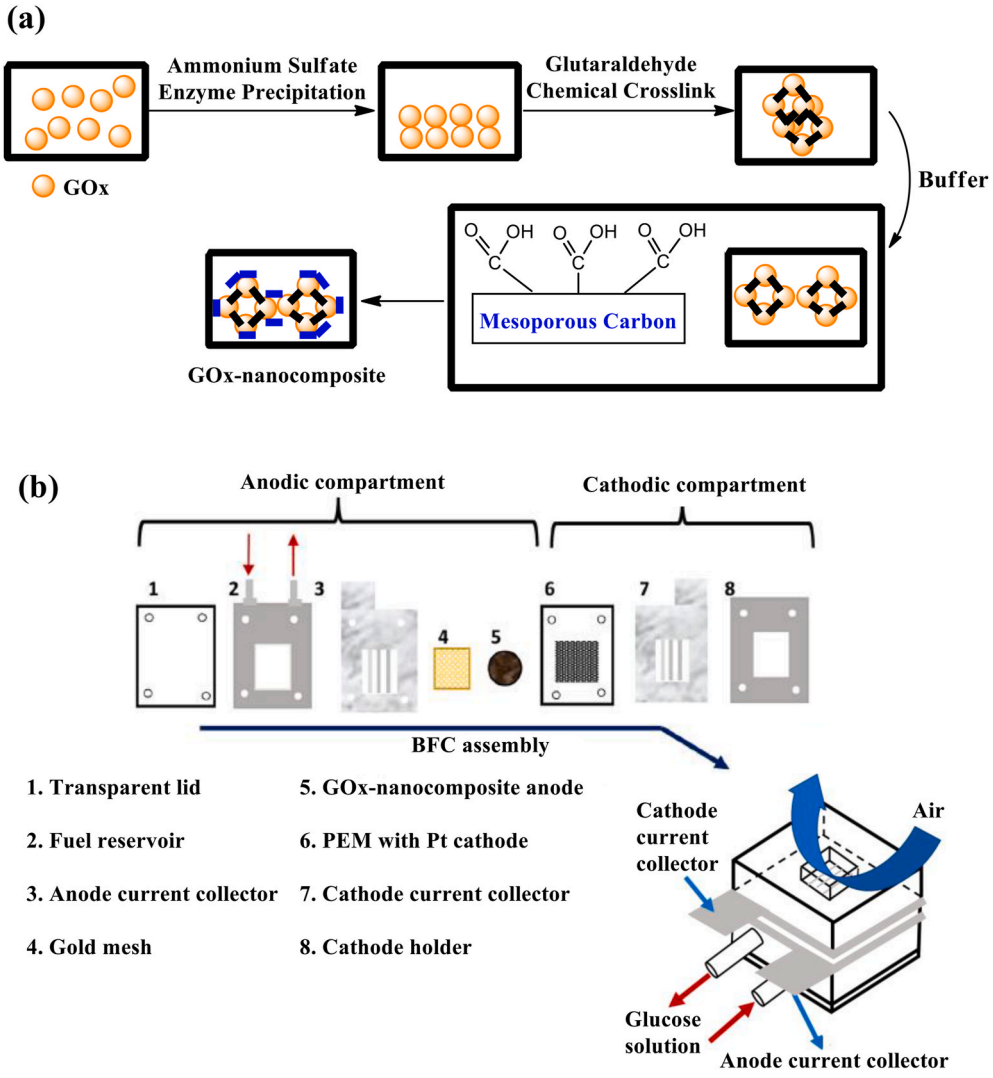

Fig. 27. (a) Schematic representation for the procedure to entrap cross-linked GOx aggregates within graphitized mesoporous carbon network and (b) components of the biofuel cell and its assembly. Reproduced with permission from Ref. [509]. Copyright 2016, Elsevier.

which were covered with 2 mg of MWCNT. At the same time, the maximum power of 1.65 ± 0.21 mW/cm^2 at 1.7 V was obtained for the Zn hybrid fuel cell. Single-walled carbon nanohorns (SWNHs) are affordable and novel carbon nanomaterials. Their use as catalyst supports has caused the rough surface and porous structure of SWNHs. Employing SWNHs as support in glucose/O_2 biofuel cell anode has been shown significant results [511]. GC was first speared by SWNHs suspension and then dried to the methylene blue (MB) electropolymerization. The mixed immobilized glucose dehydrogenase (GDH)/chitosan (CS) was coated on polyMB-SWNHs/GCE, and CS/GDH/polyMB-SWNHs/GCE bioanode was prepared. The f-TiO_2-Pt NPs were chosen as the cathode for the operation of the glucose/O_2 in a buffer solution of 30 mM glucose/10 mM NAD^+ (oxidized form of nicotinamide adenine dinucleotide) at 37 °C. The maximum power density (10.74 μW/cm^2) was obtained at 275 mV.

MWCNTs have more ability to immobilize enzymes, excellent biocompatibility, and the ability to electrically wire many redox proteins. A great current density of 0.55 mA/cm^2 was observed for the MWCNTs/tyrosinase electrode, which was fabricated by compression of the MWCNTs enzyme mixture [512]. In another report, the glucose/O_2 biofuel cell performance was examined using enzymatic carbon-based electrodes [513]; MWCNT, functionalized MWCNT (f-MWCNT), CNFs, and functionalized CNF (f-CNF) were used as carbon nanostructures for the fabrication of the electrodes. The biofuel cell based on CNF anode (glucose oxidation) and f-MWCNT cathode (oxygen reduction) has the highest power density of 210 μW/cm^2 at 0.44 V in the presence of 20 mM glucose solution.

The fabricated low-cost enzymatic biofuel cell biocathodes containing modified PANI, MWCNT, and laccase (Lac) enzymes were effective for application in enzymatic fuel cells [514]. Pencil graphite electrode (PGE)/MWCNT and PGE/PANI/MWCNT electrodes have similar surface morphology, and MWCNT was connected to the porous PANI substrate. However, the electrical conductivity of PGE/MWCNT was more than PGE/PANI/MWCNT. In addition, the Lac enzymes were uniformly dispersed on the PGE/PANI/MWCNT. The PGE/PANI/MWCNT/Lac bioelectrode was showed a maximum current density of 1209.23 μA/cm^2 compared with PGE/MWCNT and unmodified PGE electrodes. This significant current response was due to carboxyl groups on the surface.

As above mention, carbon-based materials have significant potential for immobilization of enzymes due to their high surface area. Furthermore, these materials have biocompatibility characteristics. In comparison to other carbon-based catalysts, CNTs, specially MWCNTs, have been indicated better fuel cell performance.

3.5. Other fuel cells

Carbon supported catalysts or metal-free carbon catalysts can also be used in other fuel cells such as solid acid fuel cell (SAFC), urea fuel cells, polymer electrode fuel cells (PEFC), direct hydrazine fuel cells (DHFCs), formaldehyde fuel cells, H_2-air fuel cells, metal-air fuel cells, anion exchange membrane fuel cells and direct borohydride fuel cells.

Carbon-supported MnOOH (MnOOH/C) and metal-free catalyst of N-doped graphene nanoribbons (N-GNR) in alkaline medium was significate catalytic activity toward ORR in alkaline electrolyte, suggesting that these catalysts can be applied in alkaline fuel cells [515,516]. The ORR activity of MnOOH/C indicated the kinetic current density of 0.0184 A/cm^2 in the presence of 72 wt.% MnOOH. However, the kinetic current density was reduced by increasing MnOOH content to 90 wt.%, probably due to electronic conductivity reduction with high MnOOH content. The LSV results showed that the catalytic activity of N-GNR is higher than GNR, which was attributed to the presence of N atoms on the GNR as active sites. The N-GNR with 8.3 wt.% nitrogen had more positive onset potential, showing prominent ORR activity. In addition, N-GNR with 8.3 wt.% lost 4.9% of its initial catalytic activity in durability tests during 5000 cycles, while the commercial Pt/C lost 9.5% of its catalytic activity.

Direct hydrazine fuel cells (DHFCs) are another attractive fuel cell due to zero carbon emissions, high theoretical energy density, and easy storage. CB-loaded Ni-B alloy NPs (Ni-B/C) was introduced as a suitable anode catalyst for DHFC application, which had better performance than Ni/C due to larger ECSA of Ni-B/C [517]. The recorded LSV in alkaline medium indicated that the mass current density of Ni-B/C and Ni/C was 1495 A/g and 500 A/g, respectively. Moreover, the onset potential of Ni-B/C was 0.05 V lower than Ni/C. The hydrazine oxidation activation energy of Ni-B/C (13.83 kJ/mol) was 33% lower than Ni/C (20.67 kJ/mol), suggesting the activity of Ni-B/C was higher than Ni/C. This great catalytic activity was achieved due to the excellent dispersion of Ni-B on CB, and the change of the electronic states of Ni by B. Carbon-based materials are more stable in hydrazine oxidation than low-cost metallic catalysts. Superaerophobic graphene as a metal-free catalyst was tested to hydrazine oxidation in the direct hydrazine fuel cells [518]. The plasma-enhanced chemical vapor deposition procedure performed growth vertical graphene nano-hills on SiO_2/Si substrate. The onset potential and the current density were -0.42 V and 13 mA/cm^2, respectively. Compared with flat/planar few-layer graphene on SiO_2/Si, the synthesized sample exhibited faster kinetic and lower activation energy (18.07 kJ/mol) toward hydrazine oxidation. In another report, the application of catalysts consisting of Cu NPs and functionalized MWCNTs (f-MWCNTs) for hydrazine oxidation in fuel cells showed considerable catalytic activity toward hydrazine oxidation which was better than Cu NPs, f-MWCNTs, and Cu@f-MWCNTs [519]. Using Cu@f-MWCNTs composite with 75 wt.% Cu NPs content as anode illustrated the maximum fuel cell performance; the power density cell was 3.57 mW/cm^2 at 0.89 V. Suggesting the synergistic between f-MWCNTs and Cu can be increased surface area and conductivity of Cu@f-MWCNTs.

Metal-air fuel cells are a cost-effective energy-releasing device that consists of a metal anode and an ORR catalytic cathode. Recently, metal oxides such as manganese oxides and $MnCo_2O_4$ have been introduced as a good alternative to Pt catalysts for metal-air fuel cells. However, metal oxides are compounds with conductive supports such as CNTs, leading to improved ORR. For instance, metal-air fuel cells based on deposited manganese oxides on CNTs-graphene (CMnCs) support was showed excellent performance [520]. The CMnCs with a mol ratio of $KMnO_4$ to CNTs of 3.2% (K/C = 3.2%, S1) have the highest catalytic activity toward ORR than pure CNTs, due to their conductivity and unique structure. The fuel cell performance investigation displayed that the current density of S1, S2 (K/C= 6.4%) and S3 (K/C= 12.8%) was approximately 152.8, 119 and 121.9 mA/cm^2, respectively. Moreover, the highest power density of 174.83 mW/cm^2 was achieved in a metal-air fuel cell with S1, whereas the power density of S2 (152.79 mW/cm^2) and S3 (159.91 mW/cm^2) was lower. In another research, metal oxide NPs of $MnCo_2O_4$ have loaded on 3D graphene (3D-G) substrate by a simple hydrothermal pathway [521]. The LSV curves of treated catalyst at 400 °C ($MnCo_2O_4$/3D-G-400) displayed a more positive onset potential of 0.98 V than those of $MnCo_2O_4$/RGO (0.94 V), $MnCo_2O_4$/CNTs (0.93 V), $MnCo_2O_4$/C (0.92 V), and Pt/C (0.97 V), indicating that $MnCo_2O_4$/3D-G-400 is the best electrocatalyst toward ORR. As expected, the Tafel slope of $MnCo_2O_4$/3D-G-400 (68.5 mV/dec) was smaller than $MnCo_2O_4$/RGO (75.4 mV/dec), $MnCo_2O_4$/CNTs (84.6 mV/dec), $MnCo_2O_4$/C (87.4 mV/dec), and Pt/C (70.2 mV/dec), suggesting the porous multilayer structure of 3D-G can be enhanced ORR in a metal-air fuel cell.

Using $Cs_{2.3}H_{0.7}PW_{12}O_{40}{\cdot}nH_2O$ deposited Pt nanoclusters and different CB content (0, 20, 30, 40, 46, 53, 59, and 75 vol%) as catalysts in H_2-air fuel cell has shown promising results [522]. The composite with 40 vol% of CB afforded higher catalytic activity in H_2 and air due to conductive cluster formation and high surface area between proton conductor and electronic materials in the catalysts. In addition, H_2-air fuel cell based on catalytic layer electrode of combined CNFs with gas diffusion layer (GDL) and Pt clusters (GDL/CNF/Pt) and hybrid

membrane (MF-4SC/SiO_2+$Cs_xH_{(3-x)}PW_{12}O_{40}$) showed higher performance than commercial Pt/C [523]. The as-prepared catalyst electrode had a higher ORR current density of 560 mA/cm^2 compared with Pt/C commercial catalyst (420 mA/cm^2).

Urea fuel cells are silent, efficient, and eco-friendly energy converter devices. Ni catalysts have been indicated good catalytic activity of urea oxidation, especially when Cd doped into Ni. Furthermore, the nanofiber structures can enhance the catalytic activity of Ni by improving electron transfer and mass transfer. The presence of Cd doping of Ni on carbon nano-fiber substrate was introduced as a great anode catalyst to urea oxidation in urea fuel cells [524]. The as-prepared samples were first activated in 0.5 M KOH during 100 cycles to form active urea oxidation sites (NiOOH). As seen in Fig. 28a, the current density of the urea oxidation peak at 0.67 V was improved from 35.3 to 67.2 mA/cm^2 by addition Cd. However, the sample with the highest Cd value revealed the lower performance, and hence, Cd can be acted as a co-catalyst but not as a stand-alone active catalyst (Fig. 28b and c). Fig. 28d shows the chronoamperometric at 0.6 V using 1 M urea to investigate catalysts stability, indicating the current was reduced from 65 to 25 mA/cm^2 after 5 h operation was due to mass transfer and urea concentration decline. In another research, using flexible anode catalyst including growth 3D hierarchical nickel cobaltite ($NiCo_2O_4$) architecture on CC fibers in the urea fuel cell has been demonstrated high performance compared with Co_3O_4/CC [525]. The measured urea oxidation catalytic activity of electrodes indicated that CC does not effect on urea oxidation. In contrast, the Co_3O_4/CC showed the oxidation peak at 0.46 V. However, $NiCo_2O_4$/CC catalysts had higher current density and lower onset potential due to their 3D structure and simple adsorption of urea by creating bonds of Ni-O and O-C between $NiCo_2O_4$/CC and urea. As expected, urea fuel cell based on $NiCo_2O_4$/CC catalyst displayed the highest power density of 18 mW/cm^2 and current density of 109 mA/cm^2 compared with Co_3O_4/CC catalyst.

Direct borohydride fuel cell (DBFC) is a converter device in which chemical energy stored in the borohydride ion (BH_4^-) directly changes into electricity by redox processes. Sodium borohydride ($NaBH_4$) is widely used as fuel in DBFCs. In the DBFCs, the OCV is 1.64 V which is higher compared to the H_2/O_2 PEMFCs (1.23 V) and the DMFCs, (1.21 V). In the PEMFCs and the DMFCs, the hydrogen and methanol oxidations produce two and six electrons, respectively, per molecule, but in the DBFCs, the direct oxidation of BH_4^- produces eight electrons. Accordingly, their specific energy is over 50% more than that of the DMFC, however, it does not achieve 30% of the specific energy of the H_2/O_2 PEMFC [526]. Carbon-supported PtAu (PtAu/C) electrocatalyst showed good $NaBH_4$ oxidation rate [527]. In the $NaBH_4$ electro-oxidation process, the highest current (297.6 mA/cm^2) and power (161 mW/cm^2) densities appeared in the presence of PtAu/C catalyst synthesized at pH = 7, which were due to uniform dispersion of PtAu particles. In addition, the prepared PtAu/C catalyst at 60 °C without pH adjustment exhibited the maxim current and power densities of 293.3 mA/cm^2 and 158.7 mW/cm^2, respectively. In another report, Pd NPs were supported on two carbon substrates, including commercial Vulcan XC72 (Pd/Vul) and synthesized carbon (Pd/c-PANI) by carbonization PANI doped with 3,5-dinitrosalicylic acid. To prepare carbon supports, two synthesis approaches were used (No1 and No2) [528]. As depicted in Fig. 29a, the oxidation peaks current density of Pd/c-$PANI_2$ and Pd/c-$PANI_1$ were 23 and 20 mA/cm^2, respectively, which was higher than Pd/Vul_1 (12 mA/cm^2) and Pd/Vul_2 (11 mA/cm^2), the higher specific surface area of c-PANI based catalysts can be caused to their high catalytic activity. However, the activation energy of Pd/Vul_1 (10.3 kJ/mol) was lower than that of Pd/c-$PANI_2$ (16.7 kJ/mol) for the

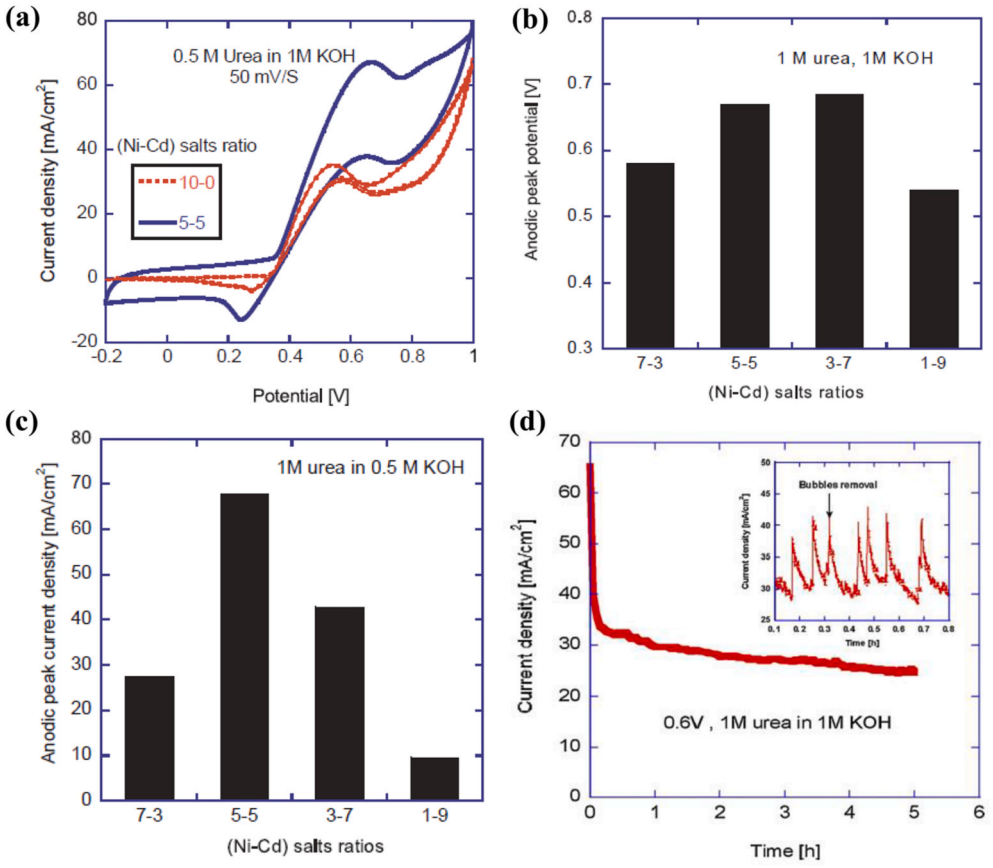

Fig. 28. (a) CV of (Ni-Cd) salt ratios of 10-0 and 5-5 in 1 M KOH containing 0.5 M urea at 50 mV/s, the effect of the (Ni-Cd) salt ratios on (b) Anodic peak potential and (c) Anodic peak current density using 1 M urea at 50 mV/s in 0.5 M KOH, (d) chronoamperometric measurement of 5-5 sample at 0.6 V using 1 M urea and 1 M KOH. Reproduced with permission from Ref. [524]. Copyright 2018, Elsevier.

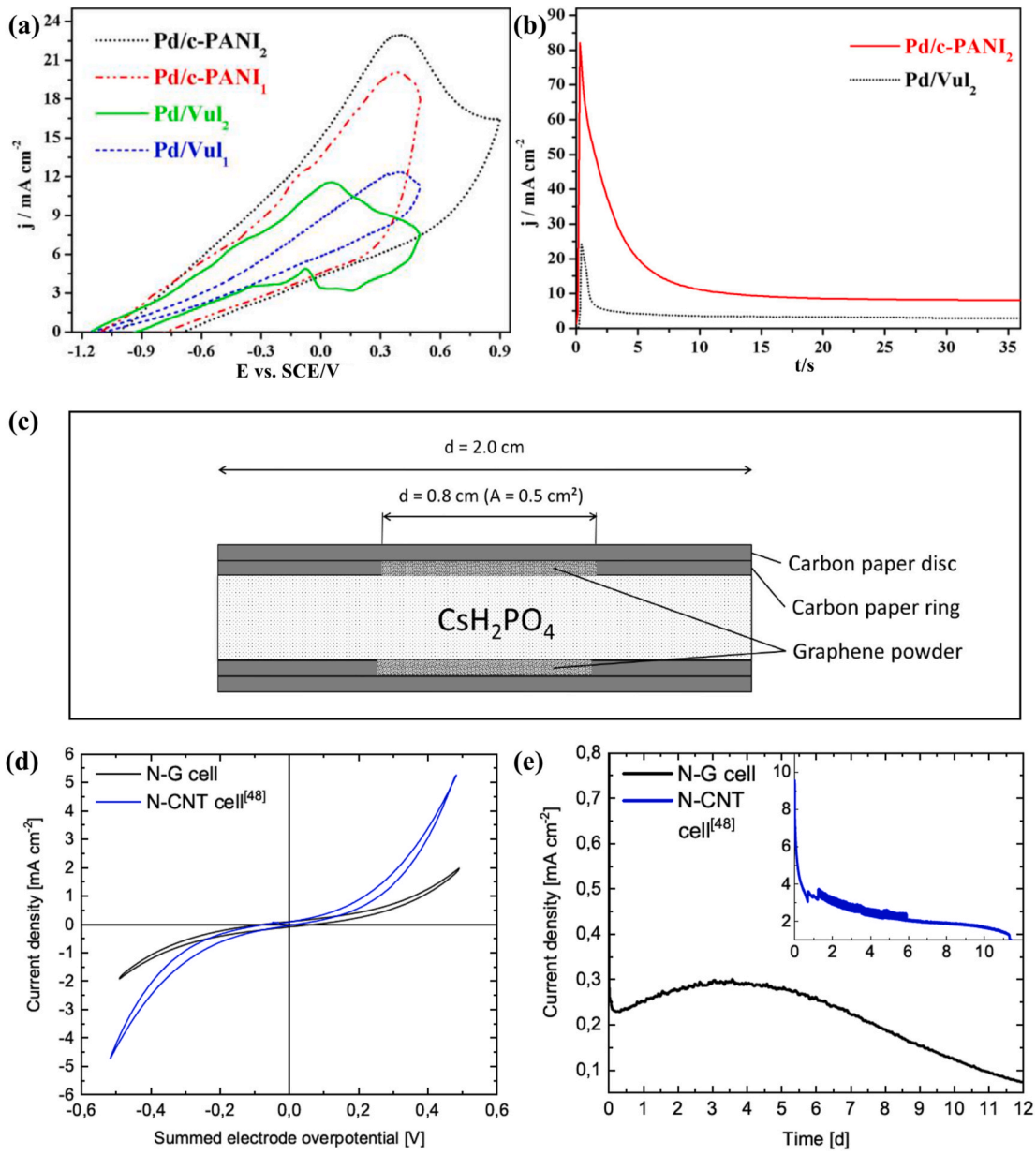

Fig. 29. (a) CVs of four studied electrocatalysts, (b) Chronoamperometric curves of Pd/c-PANI$_2$ and Pd/Vul$_2$ electrocatalysts in 0.03 M $NaBH_4$ + 2 M NaOH. Reproduced with permission from Ref. [528]. Copyright 2016, Elsevier. (c) Fuel cell schematic for symmetric (N-G | CDP | N-G) electrochemical cell, (d) CV curves of (N-G | CDP | N-G) and (N-CNT | CDP | N-CNT) cells, and (e) DC current density vs. time through symmetric (N-G | CDP | N-G) and (N-CNT | CDP | N-CNT) cells obtained during an AC impedance measurement with a 500 mV DC bias. Reproduced with permission from Ref. [548]. Copyright 2018, Royal Society of Chemistry.

borohydride oxidation reaction. Chronoamperometric (CA) data after 1 h demonstrated that the current of Pd/c-PANI became stable at a higher value than Pd/Vul (Fig. 29b), suggesting more durability of Pd/c-PANI. One of the most affordable metallic catalysts is silver (Ag). The carbon-supported Ag catalyst prepared by gamma irradiation-induced reduction with different content of poly(vinyl alcohol)/chitosan or poly(vinyl alcohol) polymer stabilizers has been demonstrated to be good catalytic activity toward borohydride oxidation, which was due to reduction on native Ag surface oxides [529]. The maxim current densities of borohydride oxidation were obtained for S5 (1 wt.% Ag, 1 wt.% C, and 0.5 wt.% polymers) and S3 (1 wt.% Ag, 1 wt.% C and 1 wt.% polymer) samples, showing their better catalytic activity to borohydride oxidation. The measured BOR onset potential was more negative than other Ag or Ag/C catalysts reports. PPy polymer is a good candidate for application in fuel cells due to its high stability and electrical conductivity. The supported Pt NPs on carbon composition with a conductive polymer of PPy was tested for borohydride oxidation reaction in an alkaline medium [530]. As a result, Pt/PPy-$C_{35\%}$ with a current density of 28 mA/cm^2 at 0.74 V displayed the best catalytic activity toward direct $NaBH_4$ oxidation, higher than commercial Pt/C (22 mA/cm^2 at 0.8 V). In contrast, the lowest current density of 7 mA/cm^2 was achieved for Pt/PPy-$C_{5\%}$ catalyst. In addition, the activation energy of Pt/PPy-$C_{5\%}$, Pt/PPy-$C_{12\%}$, Pt/PPy-$C_{20\%}$ and Pt/PPy-$C_{35\%}$ was obtained 18, 13, 15 and 10 kJ/mol, respectively. These catalytic activity resultants were due to the excellent dispersion of NPs on the PPy-C, which acts as a conductive network. PPy increases the stability of catalysts and improves morphology for good dispersion of Pt NPs. The stability of Pt/PPy-$C_{35\%}$ and Pt/PPy-$C_{12\%}$ was more than Pt/PPy-$C_{5\%}$ and Pt/PPy-$C_{20\%}$ electrode. The direct borohydride fuel cell performance revealed that the maxim power densities of 72.5, 83.7, and 59.6 mW/cm^2 were observed in fuel cells with Pt/PPy-$C_{35\%}$ as cathode, anode, and both cathode and anode, respectively. $NaBH_4$ should be in

high pH anolyte solutions. A strongly-alkaline anode chamber gives the possibility of non-precious materials utilization, for example, Ni and Cu as electrocatalysts for the BOR process [531]. The synthesis of RGO supported Pd_{10}-Ni_{45}-Co_{45} for electrooxidation of borohydride in a passive air-breathing DBFC, indicating the synergistic effect of Ni, Pd, and Co NPs plays a significant role in increasing the BOR activity [532]. In the fuel cell test, this prepared electrocatalyst showed a power density as high as 50.4 mW/cm^2.

In another work, nitrogen-doped reduced graphene oxide (N-rGO) was used for the synthesis of bimetallic Pd-Ni/N-RGO and Pd-Co/N-RGO nanocatalyst with a thermal solid-state method and polyol reduction [533]. They are utilized as an anode electrocatalyst for direct sodium borohydride-hydrogen peroxide fuel cells. The ECSA of Pd-Ni/N-rGO was as high as 166.38 m^2/g, which was more than 135.96 m^2/g for Pd-Co/N-rGO and 63.67 m^2/g for Pd/N-rGO. The current of BOR for Pd-Ni/N-rGO was 1.47 folds more than that of Pd-Co/N-rGO. The Pd-Ni/N-rGO outperformed in the direct borohydride-hydrogen peroxide fuel cell test with the power density of 353.84 mW/cm^2, at 60 °C in optimum conditions of H_2O_2 (2.0 M), and $NaBH_4$ (1.0 M). Noble-metal NPs, such as Pd NPs, are utilized as standard electrocatalysts due to their excellent activity toward BOR. Although the Pd NPs endure poisoning of catalysts due to strong binding with BH_x intermediates at a high BOR overpotential, leading to being inappropriate for high DBFC efficiency, but Ni NPs show a little catalyst poisoning owing to approximately weak binding of BH_x intermediates. Reducing H- and OH-binding energies on the surface of bimetallic PdNi electrocatalyst relative to each of them individually lead to generating further sites for adsorption of BH_4^- which plays a key role in a high BOR rate [534]. The bimetallic PdNi/C electrocatalyst presented more current densities at a 50-500 mM concentration of BH_4^- as compared to Ni/C and Pd/C. A DBFC with Pt/C, PdNi/C, and H_2O_2 as the cathode, anode, and oxidant, respectively, displayed an output of 466 ± 1.5 mW/cm^2 at 1.5 V, and an output of 630 ± 2 mW/cm^2 at 1.1 V. Also, Ni NPs with the combination of molybdenum nitride (MoN) were used to synthesize hierarchical sea urchin-like NiMoN@NC as a high efficient electrocatalyst for BOR [70]. NiMoN@NC as anode for DBFC exhibited a high power density of 67 mW/cm^2 under ambient conditions with significant stability. The carbon layer on the micropillar surfaces of NiMoN actually kept the active sites from oxidation or corrosion and warranted the high stability of NiMoN@NC. Ag-Co bimetallic catalysts supported on carbon were used as anode material for DBFCs [535]. The electrocatalysts were synthesized through three diverse metal loadings in aqueous solutions by a facile chemical reduction method. The electrocatalyst with a metal/carbon ratio of 10/90 outperformed with respect to maximum current density, best stability, and charge transfer resistance. The current density of this anodic electrocatalyst was reported to be 10.5 mA/cm^2 at 25 °C.

CNTs are also widely used as effective support of electrocatalyst for DBFCs. For example, CNT-G was employed as a support for the deposition of Pt, Au, and PtAu NPs [536]. The CNT and G incorporation could reduce the graphene sheet sticking because of π-π interactions and the better Pt NPs loading, leading to an increase in the electrocatalytic performance of electrocatalysts. As-prepared anodic electrocatalysts were used in a single $NaBH_4/H_2O_2$ fuel cell. The results indicated that the PtAu/CNT-G electrocatalyst displayed higher power densities (139 mW/cm^2), than that of Au/CNT-G (125 mW/cm^2) and Pt/CNT-G (113 mW/cm^2) electrocatalysts at 50 °C. The boosted $NaBH_4/H_2O_2$ performance can be associated with synergistic effects of Pt and Au NPs on CNT-G support. Furthermore, Au and Pd NPs were decorated on the surface of MWCNTs as bimetallic or individual catalysts [537,538]. The AuPd bimetallic electrocatalyst showed the best performance as an anode for $NaBH_4/H_2O_2$ fuel cells with Ni-based cathode in terms of the power density of 279.5 mW/cm^2 at approximately 52 °C. Recently, a MWCNTs-supported Ag-Ni electrocatalyst was synthesized to boost a new cathodic electrocatalyst for $NaBH_4/H_2O_2$ fuel cells [539]. Bimetallic $Ag_{41}Ni_{59}$/MWCNTs electrocatalyst gave the best power density (242.8 mW/cm^2) with great catalytic selectivity at high temperatures.

Anionic exchange membrane fuel cells (AEMFCs) embrace an anionic exchange membrane (AEM), which is an alternative for replacing common AFCs with liquid electrolytes. AEMFCs operate on the principle working of PEMFCs. However, in AEMFCs the OH^- ions migrate through the electrolyte from the cathode to the anode and react with hydrogen, generating water and releasing electrons. AEMs give notable advantages compared to liquid electrolyte systems for better CO_2 tolerance and decreased gas crossover [540]. Miller and co-workers offered a Pt-free AEMFC, equipped with a complex of Vulcan XC-72-CeO_2 supported Pd NPs (Pd/C-CeO_2) as an anode electrocatalyst [541]. The AEMFC was tested on dry H_2, and pure air resulted in peak power densities of higher than 500 mW/cm^2. This electrocatalyst could aid to weaken the Pd-H bonds and providing OH_{ad} from exophilic CeO_2 to the Pd-Had (HOR reaction sites), accelerating the overall hydrogen oxidation reaction (HOR). Similarly, the synthesis of a Pd-CeO_2/C electrocatalyst catalyst was reported with engineered Pd-to-CeO_2 interfacial contact [542]. The optimized Pd-CeO_2 interfacial contact gave an enhanced HOR activity resulted in peak power densities higher than 1.4 W/cm^2. In one more report, Pd-CeO_2/C electrocatalyst was utilized as an anode for HOR in the AEMFCs in which two different Pt and Pt-free cathodes were used [543]. The H_2/O_2 AEMFC operated with the peak power density of 2 W/cm^2 at 80 °C using a Pt/C cathode and a peak power density of 1 W/cm^2 at 60 °C (owing to thermal stability limitations of cathode) using a cost-competitive Fe/C cathode catalyst. AEMFCs are affordable due to the possibility to use abundant platinum group metal-free (PGM-Free) catalyst and a wide range of polymers as membranes. For improving the performance and durability of AEMFCs, carbon-support bimetallic nickel-molybdenum (NiMo/KB) catalyst as PGM-free hydrogen oxidation catalysts was prepared by thermal reduction of transition metal precursors on the surface of carbon support [544]. NiMo/KB catalyst investigated for the HOR activity in the 0.1 M NaOH electrolyte showed the mass activity of 4.5 A/g_{Me} comparable with Pt/C with similar particle size. The ECSA of 27 μA/cm^2 was achieved for NiMo/KB. The PGM-free anode in alkaline membrane fuel cells (AMFC) tests demonstrated a high power density of 120 mW/cm^2 at 0.5V under H_2/O_2 conditions. Also, the MEA was durable at the potential hold of 0.7 V for 115 h. Supporting $Ni_{95}Cu_5$-alloy NPs on mesoporous CB is another helpful PGM-free HOR electrocatalyst for AEMFC [545]. According to HOR CV studied, NiCu/KB illustrated the highest specific activity (1.8-3.6 times) compared to previously NiCu electrocatalysts. In addition, Ni-Co supported on CB catalyst was successfully integrated into an MEA resulting power density of 350 mW/cm^2 at 80 °C.

Glucose is a carbohydrate with high energy density which can apply as fuel in fuel cells. The assembled Pt-bismuth (PtBi) and Pt-Au NPs on carbon support were employed in a glucose fuel cell [546]. The highest current densities of glucose oxidation in the alkaline medium were 4.3 and 6.6 mA/cm^2 for PtAu/C and PtBi/C catalyst, respectively. The durability of catalysts was examined by chronoamperometry analysis during 3600 s, showing the current densities were reduced in the first 1500 s and received to a stable state. However, the PtBi/C catalyst illustrated a higher current density than PtAu/C. The fuel cell performance showed that the specific power densities of 1.25 and 1.6 mW/cm^2 mg were for PtBi/C and PtAu/C anodes, respectively. Unlike acidic salts, formate salts can be effortlessly stored and transported. They are not volatile (<100 °C) and also have low toxicity and fast kinetics of formate oxidation reaction (FOR) in alkaline media. A Pt-free alkaline direct formate fuel cell (DFFC) was provided with a commercial AEM, a Pd/C electrocatalyst synthesized by Vulcan XC-72 as an anode, and a Fe–Co/C cathode [547]. The maximum efficiency of the passive air-breathing DFFCs was obtained at room temperature with the power density of 96.33 mW/cm^2 and current density of 154.80 mA/cm^2 in 2 M KOH + 2 M formate. The maximum power density of an active air breathing DFFCs with 4 M KOH + 4 M formate, operating at a temperature of 60 °C, was reported to be 258 mW/cm^2. It can be commercially used as a

power source for portable electronic devices and remote control apparatus for power generation. Some fuel cells, such as solid acid fuel cells with an operating temperature of 230-250 °C, have limitation factors such as sluggish processes at the cathode, leading to large overpotentials. However, using MWCNTs and graphene has been effective in solid acid electrochemical cell performance [548]. Systematic electrochemical cells, including pressed solid acid electrolyte CsH_2PO_4 (CDP) between N-G electrodes (N-G | CDP | N-G), are illustrated in Fig. 29c. In comparison with N-doped MWCNT (N-CNT), the current density of N-G cells (1.98 mA/cm^2 at 490 mV) was lower than N-CNT cells (5.26 mA/cm^2 at 480 mV), which was owing to the higher surface area of N doped MWCNT (Fig. 29d). However, the long-term impedance results revealed that the degradation rate of N-CNT cells was higher than that of N-G cells (Fig. 29e).

4. Challenges and future perspective

Carbon-based materials are a prominent candidate for improving fuel cells performance. In the last decades, carbon materials such as CB, VC, CNTs, and CNFs have been widely employed to support metallic catalysts produced from different methods and sources. The hydrothermal synthesis approach is known as an attractive method for the preparation of carbon-based materials. Biomass, hydrocarbons, and polymers are excellent precursors with high carbon content. Despite, fabricating classic and new carbon-based materials have become challenging. Hence, future researchers should be focused on eco-friendly synthesis methods for the preparation of carbon-based materials. Moreover, using a combination of sp, sp^{2,} and sp^3 carbon atoms as support can instigate the fuel cells' performance. However, it is dependent on the uniform dispersion of metal catalysts. Thus, it is important to note that the synthesis of carbon-based supports should have a suitable control in their surface chemistry and its detailed, understanding is more important issue in future research.

Pt NPs are widely used as efficient electrocatalysts in fuel cells due to their high stability and catalytic activity. However, Pt NPs are low abundant and very expensive to afford for fuel cell devices. Therefore, the recent attentions are to replace these high-cost metallic catalysts (e.g., Pt, Au, Ag) with earth-abundant transition metals (e.g., Cu, Zn, *etc*.). In addition, the metallic catalysts can be produced via different chemical, physical, and biological methods. Although the chemical methods are the common routes and associated with some environmental pollutants, it is a primary challenge in their application. Hence, future research should focus on environmental benign methods for synthesizing metallic catalysts and needs to trigger the use of low-cost metallic catalysts.

The main challenge is accompanied with fuel cell device and their preparation cost of the overall fuel cell systems. The fuel cell system's durability is not yet as internal combustion engines. In the development of the catalytic activity of carbon-based catalysts, it is important to increase fuel cell power output. However, the reduced size of the fuel cells is another challenging task for applied transportation fields such as automobiles. The issues of air, thermal, and water management systems are needs to be resolved. Additionally, hydrogen fuel has safety risks, and the consumers must become familiar with hydrogen's properties and its handling risks.

5. Summary and future outlook

From the last few decades, the rise in the population and, following that, energy demand has caused environmental problems because of the high consumption of fossil fuel. One of the best resolving route is the use of fuel cell devices that can replace fossil fuels with cleanliness and high-power output energy resources. Fuel cells are associated with many advantages of high energy density, excellent efficiency, and cost-efficient electrical devices for converting chemical energy to electrical energy during catalytic reactions. However, increasing catalytic activity is the most important issue in fuel cells, and it is dependent on metal NPs and their supports. Herein, the role of carbon materials, carbon supports, and metal-free catalysts, in fuel cells was investigated. In this context, the effect of different compounds based on carbon materials in fuel cell's performance was compared with commercial Pt/C, indicating carbon based supports with high porosity, good electrical conductivity and high surface area can be improved fuel cell's output.

According to our review, different types of carbon materials such as CB, CNTs family, graphene family and g-C_3N_4 can be applied in fuel cells as metal-free catalysts and catalyst supports. In addition, comparison between carbon materials properties and its effect on fuel cell's performance showed that carbon materials with more pores structure have better output. However, CB has been one of the most useful supports for loading metal NPs such as Pt and Pd. However, CB has a microporous structure and low stability at high temperatures. Hence, replacement CB support with other carbon materials such as carbon nanohorns, GNS, carbon nitride, GO, *etc.,* are helpful reported in the last years. In addition, doping carbon with heteroatoms, especially nitrogen, enhances carbon's catalytic activity and can be employed as a highly efficient metal-free catalyst in fuel cells. Carbon aerogels, CNTs, and CNFs are other widely used supports after CB. Catalyst supported on carbon aerogels allows to increase the dispersion of catalyst, and thus the catalyst shows higher catalytic activity in fuel cells. CNTs are the most effective CB support replacement due to their high crystallinity, good stability, and high surface area. These carbon materials are unique catalyst supports, leading to the anchoring of the active phase for better catalysts dispersion. However, carbon corrosion at high potential is an important issue that affects the stability and performance of fuel cells. According to literature, nitrogen doping into carbon supports and loading metal and metal oxide NPs can enhance carbon resistance and hence can be effective for the stability of fuel cells in the long term. Metallic catalysts can easily reduce on these supports. In addition, surface of carbon materials consists of heteroatoms in the form of functional groups which cause to interaction carbon supports and catalyst, thus enhancing the catalyst dispersion. The impurities of carbonaceous material can also improve the catalytic activity and electronic features. Therefore, it is mandatory to pay careful attention to the use of reagents, electrolytes and materials of high purity, to fully characterize the systems with advanced techniques able to detect ppm and ppt levels of impurities before claiming metal-free components, and to reproduce in multiple and independent way the results [549]. Meanwhile, compounding polymers, especially Nafion, and carbon-based composites can also use as promising membranes in fuel cells. According to reports, the proton conductivity, mechanical properties, and water uptake of membranes consisting of carbon materials have enhanced. Pt NPs have been introduced as beneficial catalysts for expensive fuel cells. According to our research, the supported Fe, Pd, Ru, Au, MnO_2, Ag, SnO_2, and Ni on carbon-based materials have been acceptable output after deployment in fuel cells.

The loading metallic catalysts on the carbon materials led to increasing the current density and power output in different types of fuel cells. In fact, the metallic catalysts well disperse on the carbon supports, providing high specific surface area. Hence, the ECSA and mass activity can enhance by carbon materials, causing to improve fuel cells performance. PEMFCs with high power output and fast response are more attractive for researchers among other different fuel cells. Although, H_2 fuel can provide high power output without generated CO_2, its produce, store and transport are expensive. Even though, H_2 is abundant, it is hard to get and the environmental impurities generate during production H_2. Therefore, other fuels such as ethanol, methanol, ethanol, ethylene glycol and formic acid can be used in PEMFCs. These are renewable and low-cost fuels. In addition, overall use is ecofriendly due to less greenhouse emissions.

Although fuel cells are a great alternative to fossil fuels, different challenges need to study in the future:

- Improving carbon resistance toward corrosion during the electrochemical process.
- Providing convenient facilities for storage and carrier of H_2 for PEMFCs.
- Use of fuel cells at industrial scales, especially in automobile industry.
- Use of pure and contaminant-free fuels.
- Use of affordable and natural electrocatalysts instead of Pt catalysts.
- Increasing power output and lifetimes of fuel cells by controlling produced water.
- Understand the issues related to cathodic corrosion in the fuel cells.
- Studying the application of the carbon-based materials in the high temperature fuel cells such as SOFCs, MCFCs, and PAFCs performance.

Declaration of Competing Interest

The authors declare that they have no known competing financial interests or personal relationships that could have appeared to influence the work reported in this paper.

Data availability

No data was used for the research described in the article.

Acknowledgments

We gratefully acknowledge the Iranian Nano Council, Bu-Ali Sina University, and the University of Qom for the support of this work. RZ acknowledges the support from the Czech Science Foundation, project No. 19-27454X. This research was supported by the Ministry of Education, Youth and Sports of the Czech Republic (ERDF project No. CZ.02.1.01/0.0/0.0/16_019/0000754).

References

[1] M. Sadhukhan, M.K. Kundu, T. Bhowmik, S. Barman, Highly dispersed platinum nanoparticles on graphitic carbon nitride: A highly active and durable electrocatalyst for oxidation of methanol, formic acid and formaldehyde, Int. J. Hydrog. Energy 42 (2017) 9371–9383.
[2] V. Das, S. Padmanaban, K. Venkitusamy, R. Selvamuthukumaran, F. Blaabjerg, P. Siano, Recent advances and challenges of fuel cell based power system architectures and control-A review, Renew. Sust. Energ. Rev. 73 (2017) 10–18.
[3] A. Dicks, D.A.J. Rand, Fuel cell systems explained, third ed., Wiley Online Library, 2018.
[4] M. Eslamipanah, B. Jaleh, B.F. Mohazzab, S. Khazalpour, M. Nasrollahzadeh, M. Shokouhimehr, Facile synthesis and electrochemical hydrogen storage of bentonite/TiO_2/Au nanocomposite, Int. J. Hydrog. Energy 45 (2020) 33771–33788.
[5] B. Jaleh, M. Nasrollahzadeh, A. Nasri, M. Eslamipanah, A. Moradi, Z. Nezafat, Biopolymer-derived (nano) catalysts for hydrogen evolution via hydrolysis of hydrides and electrochemical and photocatalytic techniques: A review, Int. J. Biol. Macromol. 182 (2021) 1056–1090.
[6] M.H. Esfe, M. Afrand, A review on fuel cell types and the application of nanofluid in their cooling, J. Therm. Anal. Calorim. 140 (2020) 1633–1654.
[7] F. Samimi, M.R. Rahimpour, Direct methanol fuel cell, Methanol (2018) 381–397.
[8] J. Benz, B. Ortiz, W. Roth, D. Sauer, A. Steinhüser, Fuel cells in photovoltaic hybrid systems for standalone power supplies, 2nd European PV-Hybrid and Mini-Grid Conference, Kassel, Germany (2003) 232–239.
[9] M.R. Wang, L. Deng, G.C. Liu, L. Wen, J.G. Wang, K.B. Huang, H.T. Tang, Y. M. Pan, Porous organic polymer-derived nanopalladium catalysts for chemoselective synthesis of antitumor benzofuro [2, 3-b] pyrazine from 2-bromophenol and isonitriles, Org. Lett. 21 (13) (2019) 4929–4932.
[10] Y. Fu, H. Chen, R. Guo, Y. Huang, M.R. Toroghinejad, Extraordinary strength-ductility in gradient amorphous structured Zr-based alloy, J. Alloys Compd. 888 (2021), 161507.
[11] M. Hu, Y. Wang, Z. Yan, G. Zhao, Y. Zhao, L. Xia, B. Cheng, Y. Di, X. Zhuang, Hierarchical dual-nanonet of polymer nanofibers and supramolecular nanofibrils for air filtration with a high filtration efficiency, low air resistance and high moisture permeation, J. Mater. Chem. A 9 (24) (2021) 14093–14100.
[12] D. Zhang, C. Li, Y. Zhang, D. Jia, X. Zhang, Experimental research on the energy ratio coefficient and specific grinding energy in nanoparticle jet MQL grinding, Int. J. Adv. Manuf. Technol. 78 (5) (2015) 1275–1288.
[13] X. Zhang, C. Li, Y. Zhang, Y. Wang, B. Li, M. Yang, S. Guo, G. Liu, N. Zhang, Lubricating property of MQL grinding of Al_2O_3/SiC mixed nanofluid with different particle sizes and microtopography analysis by cross-correlation, Precis. Eng. 47 (2017) 532–545.
[14] D. Habibi, M. Nasrollahzadeh, H. Sahebekhtiari, Green synthesis of formamides using the Natrolite zeolite as a natural, efficient and recyclable catalyst, J. Mol. Catal. A Chem. 378 (2013) 148–155.
[15] Y. Orooji, M.H. Irani-Nezhad, R. Hassandoost, A. Khataee, S.R. Pouran, S.W. Joo, Cerium doped magnetite nanoparticles for highly sensitive detection of metronidazole via chemiluminescence assay, Spectrochim. Acta A Mol. Biomol. Spectrosc. 234 (2020), 118272.
[16] Y. Orooji, N. Han, Z. Nezafat, N. Shafiei, Z. Shen, M. Nasrollahzadeh, H. Karimi-Maleh, R. Luque, A. Bokhari, J.J. Klemeš, Valorisation of nuts biowaste: Prospects in sustainable bio (nano) catalysts and environmental applications, J. Clean. Prod. 347 (2022), 131220.
[17] Y. Orooji, B. Jaleh, F. Homayouni, P. Fakhri, M. Kashfi, M.J. Torkamany, A. A. Yousefi, Laser ablation-assisted synthesis of poly (vinylidene fluoride)/Au nanocomposites: crystalline phase and micromechanical finite element analysis, Polymers 12 (11) (2020) 2630.
[18] Y. Orooji, R. Mohassel, O. Amiri, A. Sobhani, M. Salavati-Niasari, Gd_2ZnMnO_6/ZnO nanocomposites: green sol-gel auto-combustion synthesis, characterization and photocatalytic degradation of different dye pollutants in water, J. Alloys Compd. 835 (2020), 155240.
[19] Y. Orooji, S. Mortazavi-Derazkola, S.M. Ghoreishi, M. Amiri, M. Salavati-Niasari, Mesopourous Fe_3O_4@SiO_2-hydroxyapatite nanocomposite: Green sonochemical synthesis using strawberry fruit extract as a capping agent, characterization and their application in sulfasalazine delivery and cytotoxicity, J. Hazard. Mater. 400 (2020), 123140.
[20] Y. Orooji, B. Tanhaei, A. Ayati, S.H. Tabrizi, M. Alizadeh, F.F. Bamoharram, F. Karimi, S. Salmanpour, J. Rouhi, S. Afshar, M. Sillanpää, R. Darabi, H. Karimi-Maleh, Heterogeneous UV-switchable Au nanoparticles decorated tungstophosphoric acid/TiO_2 for efficient photocatalytic degradation process, Chemosphere 281 (2021), 130795.
[21] Z. Taherian, A. Khataee, N. Han, Y. Orooji, Hydrogen production through methane reforming processes using promoted-Ni/mesoporous silica: a review, J. Ind. Eng. Chem. 107 (2021) 20–30.
[22] Z. Taherian, V.S. Gharahshiran, A. Khataee, Y. Orooji, Synergistic effect of freeze-drying and promoters on the catalytic performance of Ni/MgAl layered double hydroxide, Fuel 311 (2022), 122620.
[23] A. Nasri, B. Jaleh, S. Khazalpour, M. Nasrollahzadeh, M. Shokouhimehr, Facile synthesis of graphitic carbon nitride/chitosan/Au nanocomposite: A catalyst for electrochemical hydrogen evolution, Int. J. Biol. Macromol. 164 (2020) 3012–3024.
[24] N. Marković, T. Schmidt, V. Stamenković, P. Ross, Oxygen reduction reaction on Pt and Pt bimetallic surfaces: a selective review, Fuel cells 1 (2001) 105–116.
[25] P.P. Lopes, D. Strmcnik, H. Lv, R. Wang, N.M. Markovic, V.R. Stamenkovic, Trends in stability of Pt-based catalysts for PEM fuel cells, Meet, Abstr MA2019-02 (2019) 1595.
[26] J.D. Snyder, Y. Kang, D. Li, D. Strmcnik, N.M. Markovic, V.R. Stamenkovic, Advanced electrocatalysts for fuel cells, Meet, Abstr MA2014-01 (2014) 611.
[27] H. Xu, H. Shang, C. Wang, Y. Du, Recent Progress of Ultrathin 2D Pd-Based Nanomaterials for Fuel Cell Electrocatalysis, Small 17 (2021), 2005092.
[28] H. Chang, S.H. Joo, C. Pak, Synthesis and characterization of mesoporous carbon for fuel cell applications, J. Mater. Chem. 17 (2007) 3078–3088.
[29] H. Yang, Y. Ko, W. Lee, A. Züttel, W. Kim, Nitrogen-doped carbon black supported Pt-M (M= Pd, Fe, Ni) alloy catalysts for oxygen reduction reaction in proton exchange membrane fuel cell, Mater. Today Energy 13 (2019) 374–381.
[30] J. Tang, J. Liu, N.L. Torad, T. Kimura, Y. Yamauchi, Tailored design of functional nanoporous carbon materials toward fuel cell applications, Nano Today 9 (2014) 305–323.
[31] E. Antolini, Carbon supports for low-temperature fuel cell catalysts, Appl. Catal. B. 88 (2009) 1–24.
[32] P. You, S. Kamarudin, Recent progress of carbonaceous materials in fuel cell applications: An overview, Chem. Eng. J. 309 (2017) 489–502.
[33] Y. Shao, J. Sui, G. Yin, Y. Gao, Nitrogen-doped carbon nanostructures and their composites as catalytic materials for proton exchange membrane fuel cell, Appl. Catal. B 79 (2008) 89–99.
[34] E. Antolini, Structural parameters of supported fuel cell catalysts: The effect of particle size, interparticle distance and metal loading on catalytic activity and fuel cell performance, Appl. Catal. B 181 (2016) 298–313.
[35] K. Moore, W. Wei, Applications of carbon nanomaterials in perovskite solar cells for solar energy conversion, Nano Materials Science 3 (2021) 276–290.
[36] X. Wu, R. Liu, J. Zhao, Z. Fan, Advanced carbon materials with different spatial dimensions for supercapacitors, Nano Materials Science 3 (2021) 241–267.
[37] M. Nasrollahzadeh, B. Jaleh, A. Jabbari, Synthesis, characterization and catalytic activity of graphene oxide/ZnO nanocomposites, RSC Adv 4 (2014) 36713–36720.

[38] B.F. Mohazzab, B. Jaleh, Z. Issaabadi, M. Nasrollahzadeh, R.S. Varma, Stainless steel mesh-GO/Pd NPs: catalytic applications of Suzuki-Miyaura and Stille coupling reactions in eco-friendly media, Green Chem 21 (2019) 3319–3327.
[39] M. Nasrollahzadeh, M. Sajjadi, S. Iravani, R.S. Varma, Carbon-based sustainable nanomaterials for water treatment: State-of-art and future perspectives, Chemosphere 263 (2021), 128005.
[40] A. Omidvar, B. Jaleh, M. Nasrollahzadeh, H.R. Dasmeh, Fabrication, characterization and application of GO/Fe_3O_4/Pd nanocomposite as a magnetically separable and reusable catalyst for the reduction of organic dyes, Chem. Eng. Res. Des. 121 (2017) 339–347.
[41] N. Jha, A.L.M. Reddy, M. Shaijumon, N. Rajalakshmi, S. Ramaprabhu, Pt–Ru/multi-walled carbon nanotubes as electrocatalysts for direct methanol fuel cell, Int. J. Hydrog. Energy 33 (1) (2008) 427–433.
[42] G. Che, B.B. Lakshmi, C.R. Martin, E.R. Fisher, Metal-nanocluster-filled carbon nanotubes: catalytic properties and possible applications in electrochemical energy storage and production, Langmuir 15 (1999) 750–758.
[43] S. Sharma, B.G. Pollet, Support materials for PEMFC and DMFC electrocatalysts—A review, J. Power Sources 208 (2012) 96–119.
[44] X. Yu, S. Ye, Recent advances in activity and durability enhancement of Pt/C catalytic cathode in PEMFC: Part I. Physico-chemical and electronic interaction between Pt and carbon support, and activity enhancement of Pt/C catalyst, J. Power Sources 172 (2007) 133–144.
[45] M. Kim, J.N. Park, H. Kim, S. Song, W.H. Lee, The preparation of Pt/C catalysts using various carbon materials for the cathode of PEMFC, J. Power Sources 163 (1) (2006) 93–97.
[46] A. Wieckowski, E.R. Savinova, C.G. Vayenas, Catalysis and electrocatalysis at nanoparticle surfaces, CRC Press, 2003.
[47] B. Viswanathan, Architecture of carbon support for Pt anodes in direct methanol fuel cells, Catal, Today 141 (1-2) (2009) 52–55.
[48] J. Lu, S. Yin, P.K. Shen, Carbon-encapsulated electrocatalysts for the hydrogen evolution reaction, Electrochemical Energy Reviews 2 (2019) 105–127.
[49] D. Yu, E. Nagelli, F. Du, L. Dai, Metal-free carbon nanomaterials become more active than metal catalysts and last longer, J. Phys. Chem. Lett. 1 (2010) 2165–2173.
[50] H. Zhang, H. Osgood, X. Xie, Y. Shao, G. Wu, Engineering nanostructures of PGM-free oxygen-reduction catalysts using metal-organic frameworks, Nano Energy 31 (2017) 331–350.
[51] T. Tang, L. Ding, Z. Jiang, J.S. Hu, L.J. Wan, Advanced transition metal/nitrogen/carbon-based electrocatalysts for fuel cell applications, Sci. China Chem. 63 (2020) 1517–1542.
[52] U. Martinez, S. Komini Babu, E.F. Holby, H.T. Chung, X. Yin, P. Zelenay, Progress in the development of Fe-based PGM-free electrocatalysts for the oxygen reduction reaction, Adv. Mater. 31 (2019), 1806545.
[53] Y. Shao, J.P. Dodelet, G. Wu, P. Zelenay, PGM-free cathode catalysts for PEM fuel cells: a mini-review on stability challenges, Adv. Mater. 31 (2019), 1807615.
[54] J. Zhao, Z. Tu, S.H. Chan, Carbon corrosion mechanism and mitigation strategies in a proton exchange membrane fuel cell (PEMFC): A review, J. Power Sources 488 (2021), 229434.
[55] J. Zhao, X. Huang, H. Chang, S.H. Chan, Z. Tu, Effects of operating temperature on the carbon corrosion in a proton exchange membrane fuel cell under high current density, Energy Convers. Manag.: X 10 (2021), 100087.
[56] B. Chen, J. Wang, T. Yang, Y. Cai, C. Zhang, S.H. Chan, Y. Yu, Z. Tu, Carbon corrosion and performance degradation mechanism in a proton exchange membrane fuel cell with dead-ended anode and cathode, Energy 106 (2016) 54–62.
[57] A. Riese, D. Banham, S. Ye, X. Sun, Accelerated stress testing by rotating disk electrode for carbon corrosion in fuel cell catalyst supports, J. Electrochem. Soc. 162 (2015) F783.
[58] F. Maillard, W.O. Silva, L. Castanheira, L. Dubau, F.H. Lima, Carbon corrosion in proton-exchange membrane fuel cells: Spectrometric evidence for Pt-catalysed decarboxylation at anode-relevant potentials, ChemPhysChem 20 (2019) 3106–3111.
[59] V. Golovin, N. Maltseva, E. Gribov, A. Okunev, New nitrogen-containing carbon supports with improved corrosion resistance for proton exchange membrane fuel cells, Int. J. Hydrog. Energy 42 (2017) 11159–11165.
[60] L. Wang, C.K. Chua, B. Khezri, R.D. Webster, M. Pumera, Remarkable electrochemical properties of electrochemically reduced graphene oxide towards oxygen reduction reaction are caused by residual metalbased impurities, Electrochem. Commun. 62 (2016) 17–20.
[61] E.J. Stuart, M. Pumera, Impurities within carbon nanotubes govern the electrochemical oxidation of substituted hydrazines, Phys. Chem. Chem. Phys. 13 (2011) 10818–10822.
[62] S. Zheng, J. Zhang, H. Deng, Y. Du, X. Shi, Chitin derived nitrogen-doped porous carbons with ultrahigh specific surface area and tailored hierarchical porosity for high performance supercapacitors, J. Bioresour. Bioprod. 6 (2021) 142–151.
[63] J. Jjagwe, P.W. Olupot, E. Menya, H.M. Kalibbala, Synthesis and application of Granular activated carbon from biomass waste materials for water treatment: A review, J. Bioresour. Bioprod. 6 (2021) 292–322.
[64] X. Wu, J. Shi, X. Li, X. Huang, Q. Zhang, Flexural mechanical properties of carbon fiber reinforced polymer-bamboo scrimber composite, J. Forest. Eng. 5 (2020) 41–47.
[65] X. Li, Y. Liu, J. Hao, M Dun, W Wang, Flame retardancy of almond shell/high density polyethylene composites, J. Forest. Eng. 5 (2020) 80–88.
[66] M. Shi, H. Zhu, C. Yang, J. Xu, C. Yan, Chemical reduction-induced fabrication of graphene hybrid fibers for energy-dense wire-shaped supercapacitors, Chin. J. Chem. Eng. 47 (2021) 1–10.
[67] X. Zhang, Y. Tang, F. Zhang, C.S. Lee, A novel aluminum-graphite dual-ion battery, Adv. Energy Mater. 6 (2016), 1502588.
[68] Z. Feng, G. Li, X. Wang, C.J. Gómez-García, J. Xin, H. Ma, H. Pang, K. Gao, FeS_2/MoS_2@RGO hybrid materials derived from polyoxomolybdate-based metal-organic frameworks as high-performance electrocatalyst for ammonia synthesis under ambient conditions, Chem. Eng. J. 445 (2022), 136797.
[69] M. Yang, C. Li, Y. Zhang, D. Jia, R. Li, Y. Hou, H. Cao, J. Wang, Predictive model for minimum chip thickness and size effect in single diamond grain grinding of zirconia ceramics under different lubricating conditions, Ceram. Int. 45 (2019) 14908–14920.
[70] Z. Said, M. Jamei, L.S. Sundar, A. Pandey, A. Allouhi, C. Li, Thermophysical properties of water, water and ethylene glycol mixture-based nanodiamond+Fe_3O_4 hybrid nanofluids: An experimental assessment and application of data-driven approaches, J. Mol. Liq. 347 (2022), 117944.
[71] S. Arefi-Oskoui, A. Khataee, S.J. Behrouz, V. Vatanpour, S.H. Gharamaleki, Y. Orooji, M. Safarpour, Development of MoS_2/O-MWCNTs/PES blended membrane for efficient removal of dyes, antibiotic, and protein, Sep. Purif. Technol. 280 (2022), 119822.
[72] Y. Orooji, A.a. Alizadeh, E. Ghasali, M.R. Derakhshandeh, M. Alizadeh, M.S. Asl, T. Ebadzadeh, Co-reinforcing of mullite-TiN-CNT composites with ZrB_2 and TiB_2 compounds, Ceram. Int. 45 (16) (2019) 20844–20854.
[73] Y. Orooji, M.R. Derakhshandeh, E. Ghasali, M. Alizadeh, M.S. Asl, T. Ebadzadeh, Effects of ZrB_2 reinforcement on microstructure and mechanical properties of a spark plasma sintered mullite-CNT composite, Ceram. Int. 45 (2019) 16015–16021.
[74] Y. Orooji, H. Ghanbari Gol, B. Jaleh, M.R. Rashidian Vaziri, M. Eslamipanah, Large optical nonlinearity of the activated carbon nanoparticles prepared by laser ablation, Nanomaterials 11 (2021) 737.
[75] F. Besharat, F. Ahmadpoor, Z. Nezafat, M. Nasrollahzadeh, N.R. Manwar, P. Fornasiero, M.B. Gawande, Advances in carbon nitride-based materials and their electrocatalytic applications, ACS Catal 12 (2022) 5605–5660.
[76] Y. Orooji, E. Ghasali, M. Moradi, M.R. Derakhshandeh, M. Alizadeh, M.S. Asl, T. Ebadzadeh, Preparation of mullite-TiB_2-CNTs hybrid composite through spark plasma sintering, Ceram. Int. 45 (2019) 16288–16296.
[77] Y. Orooji, H. Khojasteh, O. Amiri, M. Amiri, S. Hasanifard, S. Khanahmadzadeh, M. Salavati-Niasari, A combination of hydrothermal, intercalation and electrochemical methods for the preparation of high-quality graphene: Characterization and using to prepare graphene-polyurethane nanocomposite, J. Alloys Compd. 848 (2020), 156495.
[78] L. Wang, C.H.A. Wong, B. Kherzi, R.D. Webster, M. Pumera, So-called "metal-free" oxygen reduction at graphene nanoribbons is in fact metal driven, ChemCatChem 7 (2015) 1650–1654.
[79] L. Wang, A. Ambrosi, M. Pumera, "Metal-free" catalytic oxygen reduction reaction on heteroatomdoped graphene is caused by trace metal impurities, Angew. Chem. 125 (2013) 14063–14066.
[80] A. Ambrosi, M. Pumera, Amorphous carbon impurities play an active role in redox processes of carbon nanotubes, J. Phys. Chem. C 115 (2011) 25281–25284.
[81] E.J. Stuart, M. Pumera, Nanographite impurities within carbon nanotubes are responsible for their stable and sensitive response toward electrochemical oxidation of phenols, J. Phys. Chem. C 115 (2011) 5530–5534.
[82] L. Wang, M. Pumera, Electrochemical catalysis at low dimensional carbons: graphene, carbon nanotubes and beyond–a review, Appl. Mater. Today 5 (2016) 134–141.
[83] M. Pumera, A. Ambrosi, E.L.K. Chng, Impurities in graphenes and carbon nanotubes and their influence on the redox properties, Chem. Sci. 3 (2012) 3347–3355.
[84] A. Ambrosi, C.K. Chua, B. Khezri, Z. Sofer, R.D. Webster, M. Pumera, Chemically reduced graphene contains inherent metallic impurities present in parent natural and synthetic graphite, Proc. Natl. Acad. Sci. U.S.A. 109 (2012) 12899–12904.
[85] C.K. Chua, M. Pumera, Carbocatalysis: the state of "metal-free" catalysis, Chem. Eur. J. 21 (2015) 12550–12562.
[86] S.Y. Chee, M. Pumera, Metal-based impurities in graphenes: application for electroanalysis, Analyst 137 (2012) 2039–2041.
[87] C.C. Mayorga-Martinez, Z. Sofer, D. Sedmidubský, J. Luxa, B. Kherzi, M. Pumera, Metallic impurities in black phosphorus nanoflakes prepared by different synthetic routes, Nanoscale 10 (2018) 1540–1546.
[88] V. Mazánek, J. Luxa, S. Matějková, J. Kučera, D. Sedmidubský, M. Pumera, Z. Sofer, Ultrapure graphene is a poor electrocatalyst: definitive proof of the key role of metallic impurities in graphene-based electrocatalysis, ACS Nano 13 (2019) 1574–1582.
[89] L. Wang, M. Pumera, Residual metallic impurities within carbon nanotubes play a dominant role in supposedly "metal-free" oxygen reduction reactions, Chem. Commun. 50 (2014) 12662–12664.
[90] R. O'hayre, S.W. Cha, W. Colella, F.B. Prinz, Fuel cell fundamentals, third ed., John Wiley & Sons, Hoboken, 2016.
[91] T. Zhang, P. Wang, H. Chen, P. Pei, A review of automotive proton exchange membrane fuel cell degradation under start-stop operating condition, Appl. Energy 223 (2018) 249–262.
[92] J.G. Carton, A.G. Olabi, Design of experiment study of the parameters that affect performance of three flow plate configurations of a proton exchange membrane fuel cell, Energy 35 (2010) 2796–2806.
[93] J. Lin, C. Mason, A. Adame, X. Liu, X. Peng, A.M. Kannan, Synthesis of Pt nanocatalyst with micelleencapsulated multi-walled carbon nanotubes as support for proton exchange membrane fuel cells, Electrochim, Acta 55 (2010) 6496–6500.

[94] S.J. Peighambardoust, S. Rowshanzamir, M. Amjadi, Review of the proton exchange membranes for fuel cell applications, Int. J. Hydrog. Energy 35 (2010) 9349–9384.

[95] K. Charoen, C. Prapainainar, P. Sureeyatanapas, T. Suwannaphisit, K. Wongamornpitak, P. Kongkachuichay, S.M. Holmes, P. Prapainainar, Application of response surface methodology to optimize direct alcohol fuel cell power density for greener energy production, J. Clean. Prod. 142 (2017) 1309–1320.

[96] S. Kaushal, A. Sahu, M. Rani, S. Dhakate, Multiwall carbon nanotubes tailored porous carbon fiber paper-based gas diffusion layer performance in polymer electrolyte membrane fuel cell, Renew. Energy 142 (2019) 604–611.

[97] S.M. Rao, Y. Xing, Simulation of nanostructured electrodes for polymer electrolyte membrane fuel cells, J. Power Sources 185 (2008) 1094–1100.

[98] K. Prehn, A. Warburg, T. Schilling, M. Bron, K. Schulte, Towards nitrogen-containing CNTs for fuel cell electrodes, Composites Sci. Technol. 69 (2009) 1570–1579.

[99] M. Shao, B. Merzougui, K. Shoemaker, L. Stolar, L. Protsailo, Z.J. Mellinger, I. J. Hsu, J.G. Chen, Tungsten carbide modified high surface area carbon as fuel cell catalyst support, J. Power Sources 196 (2011) 7426–7434.

[100] F. Barroso-Bujans, R. Verdejo, M. Arroyo, M.d.M. Lopez-Gonzalez, E. Riande, M. A. Lopez-Manchado, The development of proton conducting polymer membranes for fuel cells using sulfonated carbon nanofibres, Macromol. Rapid Commun. 29 (2008) 234–238.

[101] G. Zou, W. Wu, C. Cong, X. Meng, K. Zhao, Q. Zhou, Improved performance of poly (vinyl pyrrolidone)/phosphonated poly (2,6-dimethyl-1, 4-phenylene oxide)/graphitic carbon nitride nanocomposite membranes for high temperature proton exchange membrane fuel cells, RSC Adv 6 (2016) 106237–106247.

[102] Y. Garsany, A. Epshteyn, A.P. Purdy, K.L. More, K.E. Swider-Lyons, High-activity, durable oxygen reduction electrocatalyst: nanoscale composite of platinum-tantalum oxyphosphate on vulcan carbon, J. Phys. Chem. Lett. 1 (2010) 1977–1981.

[103] B. Narayanamoorthy, B.P. Kumar, M. Eswaramoorthy, S. Balaji, Oxygen reduction reaction catalyzed by platinum nanonetwork prepared by template free one step synthesis for polymer electrolyte membrane fuel cells, Mater. Res. Bull. 55 (2014) 137–145.

[104] S. Vengatesan, H.J. Kim, S.K. Kim, I.H. Oh, S.Y. Lee, E. Cho, H.Y. Ha, T.H. Lim, High dispersion platinum catalyst using mesoporous carbon support for fuel cells, Electrochim. Acta 54 (2008) 856–861.

[105] A. Vinu, Fabrication and electrocatalytic application of nanoporous carbon material with different pore diameters, Top. Catal. 53 (2010) 291–296.

[106] E.A. Zeid, D.S. Kim, H.S. Lee, Y.T. Kim, Temperature dependence of morphology and oxygen reduction reaction activity for carbon-supported Pd-Co electrocatalysts, J. Appl. Electrochem. 40 (2010) 1917–1923.

[107] M. Nagarajan, G. Paruthimal-kalaignan, G. Pathanjali, Novel anodes for fuel cell using nanostructured tungsten and titanium based electrocatalysts, Int. J. Hydrog. Energy 36 (2011) 14829–14837.

[108] R. Balgis, G.M. Anilkumar, S. Sago, T. Ogi, K. Okuyama, Nanostructured design of electrocatalyst support materials for high-performance PEM fuel cell application, J. Power Sources 203 (2012) 26–33.

[109] E. Negro, M.D. Vries, R. Latsuzbaia, G. Koper, Networked graphitic structures as durable catalyst support for PEM electrodes, Fuel Cells 14 (2014) 350–356.

[110] Z. Yang, I. Moriguchi, N. Nakashima, Durable Pt electrocatalyst supported on a 3D nanoporous carbon shows high performance in a high-temperature polymer electrolyte fuel cell, ACS Appl. Mater. Interfaces 7 (2015) 9800–9806.

[111] H.S. Kim, Y. Lee, J.G. Lee, H.J. Hwang, J. Jang, S.M. Juon, A. Dorjgotov, Y. G. Shul, Platinum catalysts protected by N-doped carbon for highly efficient and durable polymer-electrolyte membrane fuel cells, Electrochim. Acta 193 (2016) 191–198.

[112] Ş.B. Barım, A. Bayrakçeken, S.E. Bozbağ, L. Zhang, R. Kızılel, M. Aindow, C. Erkey, Control of average particle size of carbon aerogel supported platinum nanoparticles by supercritical deposition, Microporous Mesoporous Mater 245 (2017) 94–103.

[113] J. Zhu, M. Xiao, P. Song, J. Fu, Z. Jin, L. Ma, J. Ge, C. Liu, Z. Chen, W. Xing, Highly polarized carbon nano-architecture as robust metal-free catalyst for oxygen reduction in polymer electrolyte membrane fuel cells, Nano Energy 49 (2018) 23–30.

[114] S. Akula, S.G. Peera, A.K. Sahu, Uncovering N, S, F tri-doped heteroatoms on porous carbon as a metal-free oxygen reduction reaction catalyst for polymer electrolyte fuel cells, J. Electrochem. Soc. 166 (2019) F897.

[115] M. Kim, J. Lim, J. Bak, D. Song, S. Oh, E. Cho, Fe and N codoped mesoporous carbon nanofiber as a nonprecious metal catalyst for oxygen reduction reaction and a durable support for Pt nanoparticles, ACS Sustain. Chem. Eng. 7 (2019) 17544–17552.

[116] B. Yarar Kaplan, N. Haghmoradi, E. Jamil, C. Merino, S. Alkan Gürsel, Platinum nanoparticles decorated carbon nanofiber hybrids as highly active electrocatalysts for polymer electrolyte membrane fuel cells, Int. J. Energy Res. 44 (2020) 10251–10261.

[117] S. Hanif, X. Shi, N. Iqbal, T. Noor, R. Anwar, A. Kannan, ZIF derived PtNiCo/NC cathode catalyst for proton exchange membrane fuel cell, Appl. Catal. B 258 (2019), 117947.

[118] J.H. Yeon, S.J. Park, I. Choi, M. Choi, Generation of carbon nano-onions by laser irradiation of gaseous hydrocarbons for high durability catalyst support in proton exchange membrane fuel cells, J. Ind. Eng. Chem. 80 (2019) 65–73.

[119] Z. Ma, S. Li, L. Wu, L. Song, G. Jiang, Z. Liang, D. Su, Y. Zhu, R.R. Adzic, J. X. Wang, Z. Chen, NbO_x nano-nail with a Pt head embedded in carbon as a highly active and durable oxygen reduction catalyst, Nano Energy 69 (2020), 104455.

[120] W. Yang, Y. Wang, J. Li, X. Yang, Polymer wrapping technique: an effective route to prepare Pt nanoflower/carbon nanotube hybrids and application in oxygen reduction, Energy Environ. Sci. 3 (2010) 144–149.

[121] A.N. Golikand, M. Asgari, E. Lohrasbi, Study of oxygen reduction reaction kinetics on multi-walled carbon nano-tubes supported Pt–Pd catalysts under various conditions, Int. J. Hydrog. Energy 36 (2011) 13317–13324.

[122] N.G. Akalework, C.J. Pan, W.N. Su, J. Rick, M.C. Tsai, J.F. Lee, J.M. Lin, L.D. Tsai, B.J. Hwang, Ultrathin TiO_2-coated MWCNTs with excellent conductivity and SMSI nature as Pt catalyst support for oxygen reduction reaction in PEMFCs, J. Mater. Chem. 22 (2012) 20977–20985.

[123] Q. Zhang, X. Yu, Y. Ling, W. Cai, Z. Yang, Ultrathin nitrogen doped carbon layer stabilized Pt electrocatalyst supported on N-doped carbon nanotubes, Int. J. Hydrog. Energy 42 (2017) 10354–10362.

[124] E.J. Oh, R. Hempelmann, V. Nica, I. Radev, H. Natter, New catalyst supports prepared by surface modification of graphene-and carbon nanotube structures with nitrogen containing carbon coatings, J. Power Sources 341 (2017) 240–249.

[125] F. Liu, X. Zhang, X. Zhang, L. Wang, M. Liu, J. Zhang, Dual-template strategy for electrocatalyst of cobalt nanoparticles encapsulated in nitrogen-doped carbon nanotubes for oxygen reduction reaction, J. Colloid Interface Sci. 581 (2021) 523–532.

[126] S.M. Lyth, Y. Nabae, N.M. Islam, S. Kuroki, M. Kakimoto, S. Miyata, Oxygen reduction activity of carbon nitride supported on carbon nanotubes, J. Nanosci. Nanotechnol. 12 (2012) 4887–4891.

[127] Y. Liu, Y. Lu, A. Haragirimana, I.P. Buregeya, N. Li, Z. Hu, S. Chen, Immobilized phosphotungstic acid for the construction of proton exchange nanocomposite membranes with excellent stability and fuel cell performance, Int. J. Hydrog. Energy 45 (2020) 17782–17794.

[128] E. Yoo, T. Okada, T. Akita, M. Kohyama, I. Honma, J. Nakamura, Sub-nano-Pt cluster supported on graphene nanosheets for CO tolerant catalysts in polymer electrolyte fuel cells, J. Power Sources 196 (2011) 110–115.

[129] A. Shukla, S.D. Bhat, V.K. Pillai, Simultaneous unzipping and sulfonation of multi-walled carbon nanotubes to sulfonated graphene nanoribbons for nanocomposite membranes in polymer electrolyte fuel cells, J. Membr. Sci. 520 (2016) 657–670.

[130] L.P. Hoe, M. Boaventura, T. Lagarteira, L.K. Shyuan, A. Mendes, Polyol synthesis of reduced graphene oxide supported platinum electrocatalysts for fuel cells: Effect of Pt precursor, support oxidation level and pH, Int. J. Hydrog. Energy 43 (2018) 16998–17011.

[131] M.S. Yılmaz, B.Y. Kaplan, Ö. Metin, S.A. Gürsel, A facile synthesis and assembly of ultrasmall Pt nanoparticles on reduced graphene oxide- carbon black hybrid for enhanced performance in PEMFC, Mater. Des. 151 (2018) 29–36.

[132] S.G. Peera, A. Arunchander, A. Sahu, Platinum nanoparticles supported on nitrogen and fluorine co-doped graphite nanofibers as an excellent and durable oxygen reduction catalyst for polymer electrolyte fuel cells, Carbon 107 (2016) 667–679.

[133] H. Zhang, S. Hwang, M. Wang, Z. Feng, S. Karakalos, L. Luo, Z. Qiao, X. Xie, C. Wang, D. Su, Y. Shao, G. Wu, Single atomic iron catalysts for oxygen reduction in acidic media: particle size control and thermal activation, J. Am. Chem. Soc. 139 (2017) 14143–14149.

[134] J. Li, S. Bruller, D.C. Sabarirajan, N. Ranjbar-Sahraie, M.T. Sougrati, S. Cavaliere, D. Jones, I.V. Zenyuk, A. Zitolo, F. Jaouen, Designing the 3D architecture of PGM-free cathodes for H_2/air proton exchange membrane fuel cells, ACS Appl. Energy Mater. 2 (2019) 7211–7222.

[135] Y. Cheng, J. Zhang, X. Wu, C. Tang, S. Yang, P. Su, L. Thomsen, F. Zhao, S. Lu, J. Liu, S.P. Jiang, A template-free method to synthesis high density iron single atoms anchored on carbon nanotubes for high temperature polymer electrolyte membrane fuel cells, Nano Energy 80 (2021), 105534.

[136] H. Zhang, H.T. Chung, D.A. Cullen, S. Wagner, U.I. Kramm, K.L. More, P. Zelenay, G. Wu, High-performance fuel cell cathodes exclusively containing atomically dispersed iron active sites, Energy Environ. Sci. 12 (2019) 2548–2558.

[137] W. Kiciński, S. Dyjak, W. Tokarz, Carbon gel-derived Fe–N–C electrocatalysts for hydrogen-air polymer electrolyte fuel cells, J. Power Sources 513 (2021), 230537.

[138] M. Gangeri, G. Centi, A. La Malfa, S. Perathoner, R. Vieira, C. Pham-Huu, M. Ledoux, Electrocatalytic performances of nanostructured platinum-carbon materials, Catal. Today 102-103 (2005) 50–57.

[139] T.S. Olson, K. Chapman, P. Atanassov, Non-platinum cathode catalyst layer composition for single membrane electrode assembly proton exchange membrane fuel cell, J. Power Sources 183 (2008) 557–563.

[140] H.J. Kim, W.I. Kim, T.J. Park, H.S. Park, D.J. Suh, Highly dispersed platinum-carbon aerogel catalyst for polymer electrolyte membrane fuel cells, Carbon 46 (2008) 1393–1400.

[141] M. Okamoto, T. Fujigaya, N. Nakashima, Design of an assembly of poly (benzimidazole), carbon nanotubes, and pt nanoparticles for a fuel-cell electrocatalyst with an ideal interfacial nanostructure, Small 5 (2009) 735–740.

[142] C. Du, B. Wang, X. Cheng, Hierarchy carbon paper for the gas diffusion layer of proton exchange membrane fuel cells, J. Power Sources 187 (2009) 505–508.

[143] F. Kadirgan, A.M. Kannan, T. Atilan, S. Beyhan, S. Ozenler, S. Suzer, A. Yörür, Carbon supported nano-sized Pt-Pd and Pt-Co electrocatalysts for proton exchange membrane fuel cells, Int. J. Hydrog. Energy 34 (2009) 9450–9460.

[144] G. Liu, X. Li, P. Ganesan, B.N. Popov, Development of non-precious metal oxygen-reduction catalysts for PEM fuel cells based on N-doped ordered porous carbon, Appl. Catal. B 93 (2009) 156–165.

[145] B. Li, J. Qiao, J. Zheng, D. Yang, J. Ma, Carbon-supported Ir-V nanoparticle as novel platinum-free anodic catalysts in proton exchange membrane fuel cell, Int. J. Hydrog. Energy 34 (2009) 5144–5151.

[146] B. Li, J. Qiao, D. Yang, J. Zheng, J. Ma, J. Zhang, H. Wang, Synthesis of a highly active carbon-supported Ir-V/C catalyst for the hydrogen oxidation reaction in PEMFC, Electrochim. Acta 54 (2009) 5614–5620.

[147] K. Saminathan, V. Kamavaram, V. Veedu, A.M. Kannan, Preparation and evaluation of electrodeposited platinum nanoparticles on in situ carbon nanotubes grown carbon paper for proton exchange membrane fuel cells, Int. J. Hydrog. Energy 34 (2009) 3838–3844.

[148] M.S. Saha, R. Li, X. Sun, S. Ye, 3-D composite electrodes for high performance PEM fuel cells composed of Pt supported on nitrogen-doped carbon nanotubes grown on carbon paper, Electrochem. commun. 11 (2009) 438–441.

[149] J. Chen, K. Takanabe, R. Ohnishi, D. Lu, S. Okada, H. Hatasawa, H. Morioka, M. Antonietti, J. Kubota, K. Domen, Nano-sized TiN on carbon black as an efficient electrocatalyst for the oxygen reduction reaction prepared using an mpg-C_3N_4 template, Chem. Commun. 46 (2010) 7492–7494.

[150] W. Xiong, F. Du, Y. Liu, A. Perez Jr., M. Supp, T.S. Ramakrishnan, L. Dai, L. Jiang, 3-D carbon nanotube structures used as high performance catalyst for oxygen reduction reaction, J. Am. Chem. Soc. 132 (2010) 15839–15841.

[151] Y. Shao, S. Zhang, C. Wang, Z. Nie, J. Liu, Y. Wang, Y. Lin, Highly durable graphene nanoplatelets supported Pt nanocatalysts for oxygen reduction, J. Power Sources 195 (2010) 4600–4605.

[152] S. Pylypenko, T.S. Olson, N.J. Carroll, D.N. Petsev, P. Atanassov, Templated platinum/carbon oxygen reduction fuel cell electrocatalysts, J. Phys. Chem. C 114 (2010) 4200–4207.

[153] P. Ruvinskiy, A. Bonnefont, M. Houllé, C. Pham-Huu, E. Savinova, Preparation, testing and modeling of three-dimensionally ordered catalytic layers for electrocatalysis of fuel cell reactions, Electrochim. Acta 55 (2010) 3245–3256.

[154] V. Di Noto, E. Negro, Development of nano-electrocatalysts based on carbon nitride supports for the ORR processes in PEM fuel cells, Electrochim. Acta 55 (2010) 7564–7574.

[155] W. Zhang, J. Chen, A.I. Minett, G.F. Swiegers, C.O. Too, G.G. Wallace, Novel ACNT arrays based MEA structure-nano-Pt loaded ACNT/Nafion/ACNT for fuel cell applications, Chem Commun 46 (2010) 4824–4826.

[156] J. Zhao, A. Sarkar, A. Manthiram, Synthesis and characterization of Pd-Ni nanoalloy electrocatalysts for oxygen reduction reaction in fuel cells, Electrochim, Acta 55 (2010) 1756–1765.

[157] Z. Tang, C.K. Poh, K.K. Lee, Z. Tian, D.H.C. Chua, J. Lin, Enhanced catalytic properties from platinum nanodots covered carbon nanotubes for proton-exchange membrane fuel cells, J. Power Sources 195 (2010) 155–159.

[158] J. Lin, V. Kamavaram, A.M. Kannan, Synthesis and characterization of carbon nanotubes supported platinum nanocatalyst for proton exchange membrane fuel cells, J. Power Sources 195 (2010) 466–470.

[159] S.H. Liu, C.C. Chiang, M.T. Wu, S.B. Liu, Electrochemical activity and durability of platinum nanoparticles supported on ordered mesoporous carbons for oxygen reduction reaction, Int. J. Hydrog. Energy 35 (2010) 8149–8154.

[160] H. Lv, S. Mu, N. Cheng, M. Pan, Nano-silicon carbide supported catalysts for PEM fuel cells with high electrochemical stability and improved performance by addition of carbon, Appl. Catal. B 100 (2010) 190–196.

[161] J. Lin, A. Adame, A.M. Kannan, Development of durable platinum nanocatalyst on carbon nanotubes for proton exchange membrane fuel cells, J. Electrochem. Soc. 157 (2010) B846.

[162] B. Fang, J. Luo, P.N. Njoki, R. Loukrakpam, B. Wanjala, J. Hong, J. Yin, X. Hu, J. Last, C.J. Zhong, Nano-engineered PtVFe catalysts in proton exchange membrane fuel cells: Electrocatalytic performance, Electrochim. Acta 55 (2010) 8230–8236.

[163] R.I. Jafri, N. Rajalakshmi, S. Ramaprabhu, Nitrogen doped graphene nanoplatelets as catalyst support for oxygen reduction reaction in proton exchange membrane fuel cell, J. Mater. Chem. 20 (2010) 7114–7117.

[164] K. Leelaruji, M. Hunsom, Alcohol reduction-mediated preparation of a nano-scale Pt/C electrocatalyst for the oxygen reduction reaction in PEM fuel cells, Renew. Energy 35 (2010) 2422–2430.

[165] S. Song, Y. Liang, Z. Li, Y. Wang, R. Fu, D. Wu, P. Tsiakaras, Effect of pore morphology of mesoporous carbons on the electrocatalytic activity of Pt nanoparticles for fuel cell reactions, Appl. Catal. B 98 (2010) 132–137.

[166] K. Miyazaki, K. Kawakita, T. Abe, T. Fukutsuka, K. Kojima, Z. Ogumi, Single-step synthesis of nano-sized perovskite-type oxide/carbon nanotube composites and their electrocatalytic oxygen-reduction activities, J. Mater. Chem. 21 (2011) 1913–1917.

[167] T. Ito, U. Matsuwaki, Y. Otsuka, M. Hatta, K. Hayakawa, K. Matsutani, T. Tada, H. Jinnai, Threedimensional spatial distributions of Pt catalyst nanoparticles on carbon substrates in polymer electrolyte fuel cells, Electrochemistry 79 (2011) 374–376.

[168] T. Kottakkat, A.K. Sahu, S.D. Bhat, P. Sethuraman, S. Parthasarathi, Catalytic activity of dendrimer encapsulated Pt nanoparticles anchored onto carbon towards oxygen reduction reaction in polymer electrolyte fuel cells, Appl. Catal. B 110 (2011) 178–185.

[169] M.H. Seo, E.J. Lim, S.M. Choi, S.H. Nam, H.J. Kim, W.B. Kim, Synthesis, characterization, and electrocatalytic properties of a polypyrrole-composited Pd/C catalyst, Int. J. Hydrog. Energy 36 (2011) 11545–11553.

[170] S. Sun, G. Zhang, D. Geng, Y. Chen, R. Li, M. Cai, X. Sun, A highly durable platinum nanocatalyst for proton exchange membrane fuel cells: multiarmed starlike nanowire single crystal, Angew. Chem. 123 (2011) 442–446.

[171] C.W. Tsai, M.H. Tu, C.J. Chen, T.F. Hung, R.S. Liu, W.R. Liu, M.Y. Lo, Y.M. Peng, L. Zhang, J. Zhang, D.S. Shy, X.K. Xing, Nitrogen-doped graphene nanosheet-supported non-precious iron nitride nanoparticles as an efficient electrocatalyst for oxygen reduction, RSC Adv 1 (2011) 1349–1357.

[172] T. Oh, J.Y. Kim, Y. Shin, M. Engelhard, K.S. Weil, Effects of tungsten oxide addition on the electrochemical performance of nanoscale tantalum oxide-based electrocatalysts for proton exchange membrane (PEM) fuel cells, J. Power Sources 196 (2011) 6099–6103.

[173] J. Kim, S.W. Lee, C. Carlton, Y. Shao-Horn, Pt-covered multiwall carbon nanotubes for oxygen reduction in fuel cell applications, J. Phys. Chem. Lett. 2 (2011) 1332–1336.

[174] S.J. Aravind, R.I. Jafri, N. Rajalakshmi, S. Ramaprabhu, Solar exfoliated graphene-carbon nanotube hybrid nano composites as efficient catalyst supports for proton exchange membrane fuel cells, J. Mater. Chem. 21 (2011) 18199–18204.

[175] T. Palaniselvam, A. Irshad, B. Unni, S. Kurungot, Activity modulated low platium content oxygen reduction electrocatalysts prepared by inducing nano-order dislocations on carbon nanofiber through N_2- doping, J. Phys. Chem. C 116 (2012) 14754–14763.

[176] H.J. Zhang, X. Yuan, L. Sun, J. Yang, Z.F. Ma, Z. Shao, Synthesis and characterization of nonprecious metal binary catalyst for oxygen reduction reaction in proton exchange membrane fuel cells, Electrochim. Acta 77 (2012) 324–329.

[177] O.A. Pinchuk, F. Dundar, A. Ata, K.J. Wynne, Improved thermal stability, properties, and electrocatalytic activity of sol-gel silica modified carbon supported Pt catalysts, Int. J. Hydrog. Energy 37 (2012) 2111–2120.

[178] J. Xu, P. Gao, T. Zhao, Non-precious Co_3O_4 nano-rod electrocatalyst for oxygen reduction reaction in anion-exchange membrane fuel cells, Energy Environ. Sci. 5 (2012) 5333–5339.

[179] R. Lin, H. Zhang, T. Zhao, C. Cao, D. Yang, J. Ma, Investigation of Au@Pt/C electro-catalysts for oxygen reduction reaction, Electrochim. Acta 62 (2012) 263–268.

[180] C.T. Hsieh, Y.Y. Liu, D.Y. Tzou, W.Y. Chen, Atomic layer deposition of platinum nanocatalysts onto three-dimensional carbon nanotube/graphene hybrid, J. Phys. Chem. C 116 (2012) 26735–26743.

[181] J. Roller, R. Neagu, F. Orfino, R. Maric, Supported and unsupported platinum catalysts prepared by a one-step dry deposition method and their oxygen reduction reactivity in acidic media, J. Mater. Sci. 47 (2012) 4604–4611.

[182] A. Bauer, R. Hui, A. Ignaszak, J. Zhang, D.J. Jones, Application of a composite structure of carbon nanoparticles and Nb-TiO_2 nanofibers as electrocatalyst support for PEM fuel cells, J. Power Sources 210 (2012) 15–20.

[183] S. Bliznakov, M. Vukmirovic, L. Yang, E. Sutter, R. Adzic, Pt monolayer on electrodeposited Pd nanostructures: advanced cathode catalysts for PEM fuel cells, J. Electrochem. Soc. 159 (2012) F501.

[184] S. Sui, X. Zhuo, K. Su, X. Yao, J. Zhang, S. Du, K. Kendall, In situ grown nanoscale platinum on carbon powder as catalyst layer in proton exchange membrane fuel cells (PEMFCs), J. Energy Chem. 22 (2013) 477–483.

[185] M.A. Hoque, D.C. Higgins, F.M. Hassan, J.Y. Choi, M.D. Pritzker, Z. Chen, Tin oxide-mesoporous carbon composites as platinum catalyst supports for ethanol oxidation and oxygen reduction, Electrochim. Acta 121 (2014) 421–427.

[186] K.Y. Lee, C.Y. Liu, C.C. Sung, L.H. Hu, Influence of ink preparation with the untreated and the burned Pt/C catalysts for proton exchange membrane fuel cells, Int. J. Hydrog. Energy 39 (2014) 11454–11461.

[187] M. Sahoo, B. Vinayan, S. Ramaprabhu, Platinum-decorated chemically modified reduced graphene oxide–multiwalled carbon nanotube sandwich composite as cathode catalyst for a proton exchange membrane fuel cell, RSC Adv 4 (2014) 26140–26148.

[188] S.N. Stamatin, M. Borghei, S.M. Andersen, S. Veltze, V. Ruiz, E. Kauppinen, E. M. Skou, Influence of different carbon nanostructures on the electrocatalytic activity and stability of Pt supported electrocatalysts, Int. J. Hydrog. Energy 39 (2014) 8215–8224.

[189] J. Zhang, S. Tang, L. Liao, W. Yu, J. Li, F. Seland, G.M. Haarberg, Improved catalytic activity of mixed platinum catalysts supported on various carbon nanomaterials, J. Power Sources 267 (2014) 706–713.

[190] D. Kaewsai, H.L. Lin, Y.C. Liu, T.L. Yu, Platinum on pyridine-polybenzimidazole wrapped carbon nanotube supports for high temperature proton exchange membrane fuel cells, Int. J. Hydrog. Energy 41 (2016) 10430–10445.

[191] K. Baba, M. Nishitani-Gamo, T. Ando, M. Eguchi, Durable Marimo-like carbon support for Platinum nanoparticle catalyst in polymer electrolyte fuel cell, Electrochim. Acta 213 (2016) 447–451.

[192] P. Dhanasekaran, S.V. Selvaganesh, S.D. Bhat, Nitrogen and carbon doped titanium oxide as an alternative and durable electrocatalyst support in polymer electrolyte fuel cells, J. Power Sources 304 (2016) 360–372.

[193] U. Rost, R. Muntean, P. Podleschny, G. Marginean, M. Brodmann, V.A. Şerban, Influence of the graphitisation degree of carbon nano fibres serving as support material for noble metal electro catalysts on the performance of PEM fuel cells, Solid State Phenom 254 (2016) 27–32.

[194] S. Shin, A.R. Kim, S. Um, Integrated statistical and nano-morphological study of effective catalyst utilization in vertically aligned carbon nanotube catalyst layers for advanced fuel cell applications, Electrochim. Acta 207 (2016) 187–197.

[195] K. Yokoyama, S. Yokoyama, Y. Sato, K. Hirano, S. Hashiguchi, K. Motomiya, H. Ohta, H. Takahashi, K. Tohji, Efficiency and long-term durability of a nitrogen-doped single-walled carbon nanotube electrocatalyst synthesized by defluorination-assisted nanotube-substitution for oxygen reduction reaction, J. Mater. Chem. A 4 (2016) 9184–9195.

[196] Y. Zheng, Z. Dou, Y. Fang, M. Li, X. Wu, J. Zeng, Z. Hou, S. Liao, Platinum nanoparticles on carbon-nanotube support prepared by room-temperature reduction with H_2 in ethylene glycol/water mixed solvent as catalysts for polymer electrolyte membrane fuel cells, J. Power Sources 306 (2016) 448–453.

[197] L. Xin, F. Yang, S. Rasouli, Y. Qiu, Z.F. Li, A. Uzunoglu, C.-J. Sun, Y. Liu, P. Ferreira, W. Li, Y. Ren, L.A. Stanciu, J. Xie, Understanding Pt nanoparticle anchoring on graphene supports through surface functionalization, ACS Catal 6 (2016) 2642–2653.
[198] C. Chen, X. Zhang, Z.Y. Zhou, X.D. Yang, X.S. Zhang, S.G. Sun, Highly active Fe, N co-doped graphene nanoribbon/carbon nanotube composite catalyst for oxygen reduction reaction, Electrochim. Acta 222 (2016) 1922–1930.
[199] D. Ebenezer, K. Neelima, M. Jagannatham, P. Haridoss, Carbon nanotubes and nanohorn hybrid composite buckypaper as microporous layer for proton exchange membrane fuel cell, Fuel Cells 16 (2016) 349–355.
[200] G.V. Fortunato, F. de Lima, G. Maia, Oxygen-reduction reaction strongly electrocatalyzed by Pt electrodeposited onto graphene or graphene nanoribbons, J. Power Sources 302 (2016) 247–258.
[201] K. Mohanraju, L. Cindrella, One-pot surfactant-free synthesis of high surface area ternary alloys, PtMCo/C (M= Cr, Mn, Fe, Ni, Cu) with enhanced electrocatalytic activity and durability for PEM fuel cell application, Int. J. Hydrog. Energy 41 (2016) 9320–9331.
[202] S.P. Amyab, E. Saievar-Iranizad, A. Bayat, Platinum nanoparticles with superacid-doped polyvinylpyrrolidone coated carbon nanotubes: electrocatalyst for oxygen reduction reaction in high-temperature proton exchange membrane fuel cell, RSC Adv 6 (2016) 41937–41946.
[203] D. Puthusseri, S. Ramaprabhu, Oxygen reduction reaction activity of platinum nanoparticles decorated nitrogen doped carbon in proton exchange membrane fuel cell under real operating conditions, Int. J. Hydrog. Energy 41 (2016) 13163–13170.
[204] H.M. Barkholtz, L. Chong, Z.B. Kaiser, T. Xu, D.J. Liu, Enhanced performance of non-PGM catalysts in air operated PEM-fuel cells, Int. J. Hydrog. energy 41 (47) (2016) 22598–22604.
[205] M.J. Workman, A. Serov, L.k. Tsui, P. Atanassov, K. Artyushkova, Fe-N-C catalyst graphitic layer structure and fuel cell performance, ACS Energy Lett 2 (7) (2017) 1489–1493.
[206] G.Q. Yu, P.J. Wei, F.F. Wang, J.G. Liu, Doping copper ions into an Fe/N/C composite promotes catalyst performance for the oxygen reduction reaction, ChemElectroChem 4 (6) (2017) 1509–1515.
[207] K. Mohanraju, P. Kirankumar, L. Cindrella, O.J. Kwon, Enhanced electrocatalytic activity of Pt decorated spinals (M_3O_4, M= Mn, Fe, Co)/C for oxygen reduction reaction in PEM fuel cell and their evaluation by hydrodynamic techniques, J. Electroanal. Chem. 794 (2017) 164–174.
[208] D. Khalafallah, N. Akhtar, O.Y. Alothman, H. Fouad, K.A. Khalil, Self-assembled dopamine nanolayers wrapped carbon nanotubes as carbon-carbon bi-functional nanocatalyst for highly efficient oxygen reduction reaction and antiviral drug monitoring, Solid State Sci 71 (2017) 51–60.
[209] L. Chinchilla, D. Rossouw, T. Trefz, D. Susac, N. Kremliakova, G.A. Botton, Nanoscale analysis of structural and chemical changes in aged hybrid Pt/NbO_x/C fuel cell catalysts, J. Power Sources 356 (2017) 140–152.
[210] Z. Yang, J. Li, Q. Zhang, Y. Ling, X. Yu, W. Cai, High durability and performance of a platinum electrocatalyst supported on sulfonated macromolecules coated carbon nanotubes, ChemCatChem 9 (2017) 4005–4012.
[211] Z. Song, W. Liu, N. Cheng, M.N. Banis, X. Li, Q. Sun, B. Xiao, Y. Liu, A. Lushington, R. Li, L. Liu, Origin of the high oxygen reduction reaction of nitrogen and sulfur co-doped MOF-derived nanocarbon electrocatalysts, Mater. Horiz. 4 (2017) 900–907.
[212] A. Bharti, G. Cheruvally, Influence of various carbon nano-forms as supports for Pt catalyst on proton exchange membrane fuel cell performance, J. Power Sources 360 (2017) 196–205.
[213] K. Yang, P. Jiang, J. Chen, Q. Chen, Nanoporous PtFe nanoparticles supported on N-doped porous carbon sheets derived from metal-organic frameworks as highly efficient and durable oxygen reduction reaction catalysts, ACS Appl. Mater. Interfaces 9 (2017) 32106–32113.
[214] A. Egetenmeyer, I. Radev, D. Durneata, M. Baumgärtner, V. Peinecke, H. Natter, R. Hempelmann, Pulse electrodeposited cathode catalyst layers for PEM fuel cells, Int. J. Hydrog. Energy 42 (2017) 13649–13660.
[215] R. Singh, M. Singh, S. Bhartiya, A. Singh, D. Kohli, P.C. Ghosh, S. Meenakshi, P. Gupta, Facile synthesis of highly conducting and mesoporous carbon aerogel as platinum support for PEM fuel cells, Int. J. Hydrog. Energy 42 (2017) 11110–11117.
[216] D.G. Lee, H. Jeong, K.W. Jeon, L. Zhang, K. Park, S. Ryu, J. Kim, I.S. Lee, Carbon thin-layer-coated manganese oxide nanocrystals as an effective support for high-performance Pt electrocatalysts stabilized at a metal-metal oxide-carbon triple junction, J. Mater. Chem. A 5 (2017) 22341–22351.
[217] S. Chen, S. Thota, G. Singh, T.J. Aímola, C. Koenigsmann, J. Zhao, Synthesis of hollow Pt-Ag nanoparticles by oxygen-assisted acid etching as electrocatalysts for the oxygen reduction reaction, RSC Adv 7 (74) (2017) 46916–46924.
[218] X. Tong, J. Zhang, G. Zhang, Q. Wei, R. Chenitz, J.P. Claverie, S. Sun, Ultrathin carbon-coated Pt/carbon nanotubes: a highly durable electrocatalyst for oxygen reduction, Chem. Mater. 29 (2017) 9579–9587.
[219] X. Fu, F.M. Hassan, P. Zamani, G. Jiang, D.C. Higgins, J.Y. Choi, X. Wang, P. Xu, Y. Liu, Z. Chen, Engineered architecture of nitrogenous graphene encapsulating porous carbon with nano-channel reactors enhancing the PEM fuel cell performance, Nano Energy 42 (2017) 249–256.
[220] Y. He, S. Hwang, D.A. Cullen, M.A. Uddin, L. Langhorst, B. Li, S. Karakalos, A. J. Kropf, E.C. Wegener, J. Sokolowski, M. Chen, D. Myers, D. Su, K.L. More, G. Wang, S. Litster, G. Wu, Highly active atomically dispersed CoN_4 fuel cell cathode catalysts derived from surfactant-assisted MOFs: carbon-shell confinement strategy, Energy Environ. Sci. 12 (1) (2019) 250–260.
[221] S.B. Barim, S.E. Bozbag, H. Yu, R. Kızılel, M. Aindow, C. Erkey, Mesoporous carbon aerogel supported PtCu bimetallic nanoparticles via supercritical deposition and their dealloying and electrocatalytic behaviour, Catal. Today 310 (2018) 166–175.
[222] Z. Song, M.N. Banis, L. Zhang, B. Wang, L. Yang, D. Banham, Y. Zhao, J. Liang, M. Zheng, R. Li, S. Ye, X. Sun, Origin of achieving the enhanced activity and stability of Pt electrocatalysts with strong metal-support interactions via atomic layer deposition, Nano Energy 53 (2018) 716–725.
[223] H.H. Liu, K.L. Hsueh, C.W. Hong, DFT analysis on the Pt with nano-carbon frames for low temperature fuel cell applications, Electrochim. Acta 259 (2018) 598–605.
[224] J.L. Bott-Neto, T. Asset, F. Maillard, L. Dubau, Y. Ahmad, K. Guérin, S. Berthon-Fabry, A. Mosdale, R. Mosdale, E.A. Ticianelli, M. Chatenet, Utilization of graphitized and fluorinated carbon as platinum nanoparticles supports for application in proton exchange membrane fuel cell cathodes, J. Power Sources 404 (2018) 28–38.
[225] J.C. Calderón, L. Ndzuzo, B.J. Bladergroen, S. Pasupathi, Oxygen reduction reaction on Pt-Pd catalysts supported on carbon xerogels: Effect of the synthesis method, Int. J. Hydrog. Energy 43 (2018) 16881–16896.
[226] P. Chinnasa, W. Ponhan, E. Swatsitang, Effects of electrodes CdS/CNT/C on performance of PEMFC, Mater. Today Proc. 17 (2019) 1344–1353.
[227] H. Wang, F.X. Yin, N. Liu, R.H. Kou, X.B. He, C.J. Sun, B.H. Chen, D.J. Liu, H. Q. Yin, Engineering Fe-Fe_3C@Fe-N-C active sites and hybrid structures from dual metal-organic frameworks for oxygen reduction reaction in H_2-O_2 fuel cell and Li-O_2 battery, Adv. Funct. Mater. 29 (23) (2019), 1901531.
[228] F. Luo, C.H. Choi, M.J. Primbs, W. Ju, S. Li, N.D. Leonard, A. Thomas, F.d. r. Jaouen, P. Strasser, Accurate evaluation of active-site density (SD) and turnover frequency (TOF) of PGM-free metal-nitrogen-doped carbon (MNC) electrocatalysts using CO cryo adsorption, ACS Catal 9 (6) (2019) 4841–4852.
[229] D. Nechiyil, M.S. Garapati, R.C. Shende, S. Joulié, D. Neumeyer, R. Bacsa, P. Puech, S. Ramaprabhu, W. Bacsa, Optimizing metal-support interphase for efficient fuel cell oxygen reduction reaction catalyst, J. Colloid Interface Sci. 561 (2020) 439–448.
[230] G. Doo, S. Yuk, J.H. Lee, S. Choi, D.H. Lee, D.W. Lee, J. Hyun, S.H. Kwon, S. G. Lee, H.T. Kim, Nano-scale control of the ionomer distribution by molecular masking of the Pt surface in PEMFCs, J. Mater. Chem. A 8 (2020) 13004–13013.
[231] J. Wang, G. Wu, W. Xuan, W. Wang, W. Ding, Z. Wei, ZIF derived mesoporous carbon frameworks with numerous edges and heteroatom-doped sites to anchor nano-Pt electrocatalyst, Int. J. Hydrog. Energy 45 (2020) 22649–22657.
[232] M. Primbs, Y. Sun, A. Roy, D. Malko, A. Mehmood, M.T. Sougrati, P.Y. Blanchard, G. Granozzi, T. Kosmala, G. Daniel, P. Atanassov, J. Sharman, C. Durante, A. Kucernak, D. Jones, F. Jaouen, P. Strasser, Establishing reactivity descriptors for platinum group metal (PGM)-free Fe–N–C catalysts for PEM fuel cells, Energy Environ. Sci. 13 (8) (2020) 2480–2500.
[233] M. Qiao, Y. Wang, Q. Wang, G. Hu, X. Mamat, S. Zhang, S. Wang, Hierarchically ordered porous carbon with atomically dispersed FeN_4 for ultraefficient oxygen reduction reaction in proton-exchange membrane fuel cells, Angew. Chem. Int. Ed. 59 (7) (2020) 2688–2694.
[234] N. Coutard, B. Reuillard, T.N. Huan, F. Valentino, R.T. Jane, S. Gentil, E. S. Andreiadis, A. Le Goff, T. Asset, F. Maillard, B. Jousselme, A. Morozan, S. Lyonnard, V. Artero, P. Chenevier, Impact of ionomer structuration on the performance of bio-inspired noble-metal-free fuel cell anodes, Chem Catal 1 (1) (2021) 88–105.
[235] L. Guo, S. Hwang, B. Li, F. Yang, M. Wang, M. Chen, X. Yang, S.G. Karakalos, D. A. Cullen, Z. Feng, Promoting atomically dispersed MnN_4 sites via sulfur doping for oxygen reduction: unveiling intrinsic activity and degradation in fuel cells, ACS Nano 15 (4) (2021) 6886–6899.
[236] Z. Miao, Y. Xia, J. Liang, L. Xie, S. Chen, S. Li, H.L. Wang, S. Hu, J. Han, Q. Li, Constructing Co-N-C catalyst via a double crosslinking hydrogel strategy for enhanced oxygen reduction catalysis in fuel cells, Small 17 (29) (2021), 2100735.
[237] Q. Meyer, S. Liu, Y. Li, C. Zhao, Operando detection of oxygen reduction reaction kinetics of Fe-N-C catalysts in proton exchange membrane fuel cells, J. Power Sources 533 (2022), 231058.
[238] S. Akula, M. Mooste, B. Zulevi, S. McKinney, A. Kikas, H.M. Piirsoo, M. Rähn, A. Tamm, V. Kisand, A. Serov, E.B. Creel, D.A. Cullen, K.C. Neyerlin, H. Wang, M. Odgaard, T. Reshetenko, K. Tammeveski, Mesoporous textured Fe-N-C electrocatalysts as highly efficient cathodes for proton exchange membrane fuel cells, J. Power Sources 520 (2022), 230819.
[239] A. Wieckowski, Fuel cell catalysis: a surface science approach, John Wiley & Sons, Hoboken, New jerey, 2009.
[240] M. Kamarudin, S. Kamarudin, M. Masdar, W. Daud, Direct ethanol fuel cells, Int. J. Hydrog. Energy 38 (2013) 9438–9453.
[241] K. Elsaid, S. Abdelfatah, A.M.A. Elabsir, R.J. Hassiba, Z.K. Ghouri, L. Vechot, Direct alcohol fuel cells: Assessment of the fuel's safety and health aspects, Int. J. Hydrog. Energy 46 (2021) 30658–30668.
[242] J. Zhang, H. Liu, Electrocatalysis of direct methanol fuel cells: from fundamentals to applications, First ed., John Wiley & Sons, 2009.
[243] N. Abdullah, S. Kamarudin, L. Shyuan, Novel anodic catalyst support for direct methanol fuel cell: characterizations and single-cell performances, Nanoscale Res. Lett. 13 (2018) 1–13.
[244] I.S. Pieta, A. Rathi, P. Pieta, R. Nowakowski, M. Hołdynski, M. Pisarek, A. Kaminska, M.B. Gawande, R. Zboril, Electrocatalytic methanol oxidation over Cu, Ni and bimetallic Cu-Ni nanoparticles supported on graphitic carbon nitride, Appl. Catal. B 244 (2019) 272–283.
[245] A.I.C. Hidalgo, M.R. Aguirre, E. Valenzuela, J.Y.V. Gomez, A.C. Dávila, R. S. Varma, V.H.R. Sánchez, Sustainable application of pecan nutshell waste:

Greener synthesis of Pd-based nanocatalysts for electro-oxidation of methanol, Int. J. Hydrog. Energy 41 (2016) 23329–23335.
[246] V. Ramos-Sánchez, D. Brito-Picciotto, R. Gómez-Vargas, D. Chávez-Flores, E. Valenzuela, Carbon Supported Au-Pd-PdO with Low Metal Loading for Electro-oxidation of Methanol in Alkaline Medium, J. New Mater. Electrochem. Syst. 17 (2014) 133–138.
[247] C. Liang, L. Ding, C. Li, M. Pang, D. Su, W. Li, Y. Wang, Nanostructured WCx/CNTs as highly efficient support of electrocatalysts with low Pt loading for oxygen reduction reaction, Energy Environ. Sci. 3 (2010) 1121–1127.
[248] J. Wu, F. Hu, X. Hu, Z. Wei, P.K. Shen, Improved kinetics of methanol oxidation on Pt/hollow carbon sphere catalysts, Electrochim. Acta 53 (2008) 8341–8345.
[249] Z. Wang, M. Shoji, H. Ogata, Synthesis and characterization of platinum nanoparticles on carbon nanosheets with enhanced electrocatalytic activity toward methanol oxidation, Appl. Surf. Sci. 259 (2012) 219–224.
[250] Y. Kin, K. Saito, H. Oda, T. Ando, K. Nakagawa, Development of direct methanol fuel cell catalyst using marimo nano carbon, Catal. Lett. 149 (2019) 1–6.
[251] E. Salernitano, L. Giorgi, T.D. Makris, Direct growth of carbon nanofibers on carbon-based substrates as integrated gas diffusion and catalyst layer for polymer electrolyte fuel cells, Int. J. Hydrog. Energy 39 (2014) 15005–15016.
[252] D.H. Kim, D.Y. Shin, Y.G. Lee, G.H. An, J.H. Han, H.J. Ahn, B.J. Choi, Effects of SnO_2 layer coated on carbon nanofiber for the methanol oxidation reaction, Ceram. Int. 44 (2018) 19554–19559.
[253] C. Zhou, F. Peng, H. Wang, H. Yu, J. Yang, X. Fu, Facile preparation of an excellent Pt/RuO_2-MnO_2/CNTs nanocatalyst for anodes of direct methanol fuel cells, Fuel Cells 11 (2011) 301–308.
[254] S.H. Park, H.S. Kim, Flash light-assisted facile and eco-friendly synthesis of platinum-based alloy nanoparticle/carbon nano-tube catalysts for a direct methanol fuel cell, J. Electrochem. Soc. 162 (2014) F204.
[255] Z. Yang, F. Luo, Pt nanoparticles deposited on dihydroxy-polybenzimidazole wrapped carbon nanotubes shows a remarkable durability in methanol electro-oxidation, Int. J. Hydrog. Energy 42 (2017) 507–514.
[256] L. Liang, M. Xiao, J. Zhu, J. Ge, C. Liu, W. Xing, Low-temperature synthesis of nitrogen doped carbon nanotubes as promising catalyst support for methanol oxidation, J. Energy Chem. 28 (2019) 118–122.
[257] M. Mehrpooya, F. Valizadeh, R. Askarimoghadam, S. Sadeghi, F. Pourfayaz, S. A. Mousavi, Fabrication of nano-platinum alloy electrocatalysts and their performance in a micro-direct methanol fuel cell, Eur. Phys. J. Plus. 135 (2020) 1–17.
[258] I. Do, L.T. Drzal, Ionic liquid-assisted synthesis of Pt nanoparticles onto exfoliated graphite nanoplatelets for fuel cells, ACS Appl. Mater. Interfaces 6 (2014) 12126–12136.
[259] R. Carrera-Cerritos, V. Baglio, A. Aricò, J. Ledesma-García, M. Sgroi, D. Pullini, A. Pruna, D. Mataix, R. Fuentes-Ramírez, L. Arriaga, Improved Pd electro-catalysis for oxygen reduction reaction in direct methanol fuel cell by reduced graphene oxide, Appl. Catal. B 144 (2014) 554–560.
[260] Y. Kwok, A.C. Tsang, Y. Wang, D.Y. Leung, Ultra-fine Pt nanoparticles on graphene aerogel as a porous electrode with high stability for microfluidic methanol fuel cell, J. Power Sources 349 (2017) 75–83.
[261] P. Raghavendra, G.V. Reddy, R. Sivasubramanian, P.S. Chandana, L.S. Sarma, Reduced graphene oxide-supported Pd@Au bimetallic nano electrocatalyst for enhanced oxygen reduction reaction in alkaline media, Int. J. Hydrog. Energy 43 (2018) 4125–4135.
[262] C. Berghian Grosan, T. Radu, A.R. Biris, M. Dan, C. Voica, F. Watanabe, A.S. Biris, A. Vulcu, Platinum nanoparticles coated by graphene layers: A low-metal loading catalyst for methanol oxidation in alkaline media, J. Energy Chem. 40 (2020) 81–88.
[263] M. Eswaran, R. Dhanusuraman, P.C. Tsai, V.K. Ponnusamy, One-step preparation of graphitic carbon nitride/Polyaniline/Palladium nanoparticles based nanohybrid composite modified electrode for efficient methanol electro-oxidation, Fuel 251 (2019) 91–97.
[264] D. Sebastian, A. Serov, I. Matanovic, K. Artyushkova, P. Atanassov, A. Aricò, V. Baglio, Insights on the extraordinary tolerance to alcohols of Fe-NC cathode catalysts in highly performing direct alcohol fuel cells, Nano Energy 34 (2017) 195–204.
[265] Q. Shi, Y. He, X. Bai, M. Wang, D.A. Cullen, M. Lucero, X. Zhao, K.L. More, H. Zhou, Z. Feng, Y. Liu, G. Wu, Methanol tolerance of atomically dispersed single metal site catalysts: mechanistic understanding and high-performance direct methanol fuel cells, Energy Environ. Sci. 13 (10) (2020) 3544–3555.
[266] W.H. Cheng, K.C. Wu, M.Y. Lo, C.H. Lee, Recent advances in nano precious metal catalyst research at Union Chemical Laboratories, ITRI, Catal, Today 97 (2004) 145–151.
[267] H. Tang, J. Chen, L. Nie, D. Liu, W. Deng, Y. Kuang, S. Yao, High dispersion and electrocatalytic properties of platinum nanoparticles on graphitic carbon nanofibers (GCNFs), J. Colloid Interface Sci. 269 (2004) 26–31.
[268] Y. Li, F.P. Hu, X. Wang, P.K. Shen, Anchoring metal nanoparticles on hydrofluoric acid treated multiwalled carbon nanotubes as stable electrocatalysts, Electrochem. Commun. 10 (2008) 1101–1104.
[269] A. Sarkar, A.V. Murugan, A. Manthiram, Synthesis and characterization of nanostructured Pd-Mo electrocatalysts for oxygen reduction reaction in fuel cells, J. Phys. Chem. C 112 (2008) 12037–12043.
[270] M. Okada, Y. Konta, N. Nakagawa, Carbon nano-fiber interlayer that provides high catalyst utilization in direct methanol fuel cell, J. Power Sources 185 (2008) 711–716.
[271] S. Oke, Y. Izumi, T. Ikeda, H. Uruno, Y. Suda, H. Takikawa, S. Itoh, T. Yamaura, H. Ue, T. Sakakibara, S. Sugawara, T. Okawa, N. Aoyagi, DMFC catalyst layer prepared using arc-soot nano-carbon by dry-squeegee method and its impedance analysis, Electrochemistry 77 (2009) 210–213.
[272] D.H. Lim, D.H. Choi, W.D. Lee, H.I. Lee, A new synthesis of a highly dispersed and CO tolerant PtSn/C electrocatalyst for low-temperature fuel cell; its electrocatalytic activity and long-term durability, Appl. Catal. B 89 (2009) 484–493.
[273] J. Ye, J. Liu, Y. Zhou, Z. Zou, J. Gu, T. Yu, High catalytic performance and stability of Pt/C using acetic acid functionalized carbon, J. Power Sources 194 (2009) 683–689.
[274] M.J.F. Guinel, A. Bonakdarpour, B. Wang, P.K. Babu, F. Ernst, N. Ramaswamy, S. Mukerjee, A. Wieckowski, Carbon-supported, selenium-modified ruthenium-molybdenum catalysts for oxygen reduction in acidic media, ChemSusChem 2 (2009) 658–664.
[275] M.L. Lin, M.Y. Lo, C.Y. Mou, PtRu nanoparticles supported on ozone-treated mesoporous carbon thin film as highly active anode materials for direct methanol fuel cells, J. Phys. Chem. C 113 (2009) 16158–16168.
[276] Z. Liu, X. Zhang, L. Hong, Physical and electrochemical characterizations of nanostructured Pd/C and PdNi/C catalysts for methanol oxidation, Electrochem. Commun. 11 (2009) 925–928.
[277] J.N. Tiwari, F.M. Pan, T.M. Chen, R.N. Tiwari, K.L. Lin, Electrocatalytic activity of Pt nanoparticles electrodeposited on amorphous carbon-coated silicon nanocones, J. Power Sources 195 (2010) 729–735.
[278] L. Brandão, D.M. Gattia, R. Marazzi, M. Vittori Antisari, S. Licoccia, A. d'Epifanio, E. Traversa, A. Mendes, Improvement of DMFC electrode kinetics by using nanohorns catalyst support, Mater. Sci. Forum. (2010) 1106–1111.
[279] W. Li, Q. Xin, Y. Yan, Nanostructured Pt-Fe/C cathode catalysts for direct methanol fuel cell: The effect of catalyst composition, Int. J. Hydrog. Energy 35 (2010) 2530–2538.
[280] Y. Chen, G. Zhang, J. Ma, Y. Zhou, Y. Tang, T. Lu, Electro-oxidation of methanol at the different carbon materials supported Pt nano-particles, Int. J. Hydrog. Energy 35 (2010) 10109–10117.
[281] W.F. Chen, J.P. Wang, C.H. Hsu, J.Y. Jhan, H. Teng, P.L. Kuo, Nanostructured coral-like carbon as Pt support for fuel cells, J. Phys. Chem. C 114 (2010) 6976–6982.
[282] Y. Zhao, L. Zhan, J. Tian, S. Nie, Z. Ning, MnO_2 modified multi-walled carbon nanotubes supported Pd nanoparticles for methanol electro-oxidation in alkaline media, Int. J. Hydrog. Energy 35 (2010) 10522–10526.
[283] Z. Hamoudi, M.A. El Khakani, M. Mohamedi, Nontrivial role of carbon nanofibers morphology in binderless Pt nanocatalyst supported electrode, Int. J. Hydrog. Energy 36 (2011) 4682–4688.
[284] N. Jha, R.I. Jafri, N. Rajalakshmi, S. Ramaprabhu, Graphene-multi walled carbon nanotube hybrid electrocatalyst support material for direct methanol fuel cell, Int. J. Hydrog. Energy 36 (2011) 7284–7290.
[285] M.L. Lin, M.Y. Lo, C.Y. Mou, PtRuP nanoparticles supported on mesoporous carbon thin film as highly active anode materials for direct methanol fuel cell, Catal. Today 160 (2011) 109–115.
[286] P.K. Shen, Z. Yan, H. Meng, M. Wu, G. Cui, R. Wang, L. Wang, K. Si, H. Fu, Synthesis of Pd on porous hollow carbon spheres as an electrocatalyst for alcohol electrooxidation, RSC Adv 1 (2011) 191–198.
[287] B. Kuppan, P. Selvam, Platinum-supported mesoporous carbon (Pt/CMK-3) as anodic catalyst for direct methanol fuel cell applications: The effect of preparation and deposition methods, Prog. Nat. Sci. Mater. Int. 22 (2012) 616–623.
[288] M.S. Wietecha, J. Zhu, G. Gao, N. Wang, H. Feng, M.L. Gorring, M.L. Kasner, S. Hou, Platinum nanoparticles anchored on chelating group-modified graphene for methanol oxidation, J. Power Sources 198 (2012) 30–35.
[289] Y.S. Wu, R.G. Wu, T.K. Yeh, C.H. Tsai, Y.C. Su, F.G. Tseng, Thickness control over ionomer coatings on nano patterned three-phase zones for a highly efficient electrode, J. Electrochem. Soc. 159 (2012) F242.
[290] Z.G. Zhao, Z.J. Yao, J. Zhang, R. Zhu, Y. Jin, Q.W. Li, Rational design of galvanically replaced Pt-anchored electrospun WO_3 nanofibers as efficient electrode materials for methanol oxidation, J. Mater. Chem. 22 (2012) 16514–16519.
[291] G. Ramos-Sánchez, M.M. Bruno, Y.R. Thomas, H.R. Corti, O. Solorza-Feria, Mesoporous carbon supported nanoparticulated $PdNi_2$: a methanol tolerant oxygen reduction electrocatalyst, Int. J. Hydrog. Energy 37 (2012) 31–40.
[292] J. Zang, L. Dong, Y. Jia, H. Pan, Z. Gao, Y. Wang, Core-shell structured SiC@C supported platinum electrocatalysts for direct methanol fuel cells, Appl. Catal. B 144 (2014) 166–173.
[293] L. Giorgi, E. Salernitano, T.D. Makris, S. Gagliardi, V. Contini, M. De Francesco, Innovative electrodes for direct methanol fuel cells based on carbon nanofibers and bimetallic PtAu nanocatalysts, Int. J. Hydrog. Energy 39 (2014) 21601–21612.
[294] J. Huang, J. Zang, Y. Zhao, L. Dong, Y. Wang, One-step synthesis of nanocrystalline TiO_2-coated carbon nanotube support for Pt electrocatalyst in direct methanol fuel cell, Mater. Lett. 137 (2014) 335–338.
[295] K. Kakaei, H. Gharibi, Palladium nanoparticle catalysts synthesis on graphene in sodium dodecyl sulfate for oxygen reduction reaction, Energy 65 (2014) 166–171.
[296] S.Y. Lee, J.M. Park, S.J. Park, Roles of nitric acid treatment on PtRu catalyst supported on graphite nanofibers and their methanol electro-oxidation behaviors, Int. J. Hydrog. Energy 39 (2014) 16468–16473.
[297] Q. Liu, Y. Duan, Q. Zhao, F. Pan, B. Zhang, J. Zhang, Direct synthesis of nitrogen-doped carbon nanosheets with high surface area and excellent oxygen reduction performance, Langmuir 30 (2014) 8238–8245.
[298] A. Safavi, H. Kazemi, S. Kazemi, In situ electrodeposition of graphene/nano-palladium on carbon cloth for electrooxidation of methanol in alkaline media, J. Power Sources 256 (2014) 354–360.

[299] C. Wang, H. Gao, H. Li, Y. Zhang, B. Huang, J. Zhao, Y. Zhu, W.Z. Yuan, Y. Zhang, Graphene nanoribbons hybridized carbon nanofibers: remarkably enhanced graphitization and conductivity, and excellent performance as support material for fuel cell catalysts, Nanoscale 6 (2014) 1377–1383.
[300] T. Zhou, H. Wang, S. Ji, V. Linkov, R. Wang, Soybean-derived mesoporous carbon as an effective catalyst support for electrooxidation of methanol, J. Power Sources 248 (2014) 427–433.
[301] W. Huo, H. He, F. Sun, Microfluidic direct methanol fuel cell by electrophoretic deposition of platinum/carbon nanotubes on electrode surface, Int. J. Energy Res. 39 (2015) 1430–1436.
[302] X.L. Sui, D.M. Gu, Z.B. Wang, J. Liu, L. Zhao, L.M. Zhang, Three-dimensional TiO_2@C nano-network with high porosity as a highly efficient Pt-based catalyst support for methanol electrooxidation, RSC Adv 6 (2016) 79254–79262.
[303] D. Sebastián, A. Serov, K. Artyushkova, J. Gordon, P. Atanassov, A.S. Aricò, V. Baglio, High performance and cost-effective direct methanol fuel cells: Fe-N-C methanol-tolerant oxygen reduction reaction catalysts, ChemSusChem 9 (15) (2016) 1986–1995.
[304] Z.K. Ghouri, N.A. Barakat, H.Y. Kim, M. Park, K.A. Khalil, M.H. El-Newehy, S. S. Al-Deyab, Nano-engineered ZnO/CeO_2 dots@CNFs for fuel cell application, Arab. J. Chem. 9 (2016) 219–228.
[305] A.P. Periasamy, R. Ravindranath, P. Roy, W.P. Wu, H.T. Chang, P. Veerakumar, S.-B. Liu, Carbon–boron core–shell microspheres for the oxygen reduction reaction, J. Mater. Chem. A 4 (2016) 12987–12994.
[306] L. Song, T. Wang, H. Xue, X. Fan, J. He, In-situ preparation of Pd incorporated ordered mesoporous carbon as efficient electrocatalyst for oxygen reduction reaction, Electrochim. Acta 191 (2016) 355–363.
[307] S. Tang, X. Zhou, N. Xu, Z. Bai, J. Qiao, J. Zhang, Template-free synthesis of three-dimensional nanoporous N-doped graphene for high performance fuel cell oxygen reduction reaction in alkaline media, Appl. Energy 175 (2016) 405–413.
[308] W. Xie, F. Zhang, Z. Wang, M. Yang, J. Xia, R. Gui, Y. Xia, Facile preparation of PtPdPt/graphene nanocomposites with ultrahigh electrocatalytic performance for methanol oxidation, J. Electroanal. Chem. 761 (2016) 55–61.
[309] Q. Yi, T. Zou, Y. Zhang, X. Liu, G. Xu, H. Nie, X. Zhou, A novel alcohol/iron(III) fuel cell, J. Power Sources 321 (2016) 219–225.
[310] Y. Zhai, S. He, X. Xiao, Z. Wu, S. Li, J. Lee, A facile diethylene glycol reduction method for the synthesis of ultrafine Pd/C electrocatalyst with high electrocatalytic activity for methanol oxidation, Fuel Cells 16 (2016) 771–776.
[311] G. Zhan, Z. Fu, D. Sun, Z. Pan, C. Xiao, S. Wu, C. Chen, G. Hu, Z. Wei, Platinum nanoparticles decorated robust binary transition metal nitride-carbon nanotubes hybrid as an efficient electrocatalyst for the methanol oxidation reaction, J. Power Sources 326 (2016) 84–92.
[312] A. Zhang, X. Li, Y. He, Platinum/nitrogen-doped carbon nanoparticles synthesized in nitrogen-doped carbon quantum dots aqueous solution for methanol electro-oxidation, Electrochim. Acta 213 (2016) 332–340.
[313] M. Noroozifar, Z. Yavari, M. Khorasani-Motlagh, T. Ghasemi, S.-H. Rohani-Yazdi, M. Mohammadi, Fabrication and performance evaluation of a novel membrane electrode assembly for DMFCs, RSC Adv 6 (2016) 563–574.
[314] B. Ong, S. Kamarudin, M. Masdar, U. Hasran, Applications of graphene nano-sheets as anode diffusion layers in passive direct methanol fuel cells (DMFC), Int. J. Hydrog. Energy 42 (2017) 9252–9261.
[315] F. Fathirad, A. Mostafavi, D. Afzali, Bimetallic Pd–Mo nanoalloys supported on Vulcan XC-72R carbon as anode catalysts for direct alcohol fuel cell, Int. J. Hydrog. Energy 42 (2017) 3215–3221.
[316] A.M. Ramírez, M.V. Aguilera, C. López-Badillo, B. Ruiz-Camacho, Synthesis of FAU zeolite-C composite as catalyst support for methanol electro-oxidation, Int. J. Hydrog. Energy 42 (2017) 30291–30300.
[317] Z. Wang, C. Lu, W. Kong, Y. Zhang, J. Li, Platinum nanoparticles supported on core–shell nickel–carbon as catalyst for methanol oxidation reaction, J. Alloys Compd. 690 (2017) 95–100.
[318] J.J. Fan, Y.J. Fan, R.X. Wang, S. Xiang, H.G. Tang, S.G. Sun, A novel strategy for the synthesis of sulfur-doped carbon nanotubes as a highly efficient Pt catalyst support toward the methanol oxidation reaction, J. Mater. Chem. A 5 (2017) 19467–19475.
[319] M. Bello, S.J. Zaidi, A. Al-Ahmed, S. Basu, D.-H. Park, K.S. Lakhi, A. Vinu, Pt-Ru nanoparticles functionalized mesoporous carbon nitride with tunable pore diameters for DMFC applications, Microporous Mesoporous Mater 252 (2017) 50–58.
[320] K. Li, Z. Jin, J. Ge, C. Liu, W. Xing, Platinum nanoparticles partially-embedded into carbon sphere surfaces: a low metal-loading anode catalyst with superior performance for direct methanol fuel cells, J. Mater. Chem. A 5 (2017) 19857–19865.
[321] Y. Zhang, F. Li, X. Liu, J. Lu, G. Zhang, Promoting influence of activated carbon used in carbon paste electrode on platinum nanoparticles efficiency in methanol electrooxidation, Electrochim. Acta 242 (2017) 165–172.
[322] G.H. An, H.G. Jo, H.J. Ahn, Platinum nanoparticles on nitrogen-doped carbon and nickel composites surfaces: A high electrical conductivity for methanol oxidation reaction, J. Alloys Compd. 763 (2018) 250–256.
[323] S. Eris, Z. Daşdelen, F. Sen, Enhanced electrocatalytic activity and stability of monodisperse Pt nanocomposites for direct methanol fuel cells, J. Colloid Interface Sci. 513 (2018) 767–773.
[324] C. Domínguez, K.M. Metz, M.K. Hoque, M.P. Browne, L. Esteban-Tejeda, C. K. Livingston, S. Lian, T.S. Perova, P.E. Colavita, Continuous flow synthesis of Pt nanoparticles in porous carbon as durable and methanol-tolerant electrocatalysts for oxygen reduction reaction, ChemElectroChem 5 (2018) 62–70.
[325] D.M. Fernandes, H.C. Novais, R. Bacsa, P. Serp, B.n. Bachiller-Baeza, I. Rodríguez-Ramos, A. Guerrero-Ruiz, C. Freire, Polyoxotungstate@carbon nanocomposites as oxygen reduction reaction (ORR) electrocatalysts, Langmuir 34 (2018) 6376–6387.
[326] C. Ghiabi, A. Ghaffarinejad, H. Kazemi, R. Salahandish, In situ, one-step and co-electrodeposition of graphene supported dendritic and spherical nano-palladium-silver bimetallic catalyst on carbon cloth for electrooxidation of methanol in alkaline media, Renew. Energy 126 (2018) 1085–1092.
[327] M.G. Hosseini, R. Mahmoodi, V. Daneshvari-Esfahlan, Ni@Pd core-shell nanostructure supported on multi-walled carbon nanotubes as efficient anode nanocatalysts for direct methanol fuel cells with membrane electrode assembly prepared by catalyst coated membrane method, Energy 161 (2018) 1074–1084.
[328] K. Mohanraju, H. Lee, O.J. Kwon, High loading Pt core/carbon shell derived from platinum-aniline complex for direct methanol fuel cell application, Electroanalysis 30 (2018) 1604–1609.
[329] M. Satyanarayana, G. Rajeshkhanna, M.K. Sahoo, G.R. Rao, Electrocatalytic activity of $Pd_{20-x}Ag_x$ nanoparticles embedded in carbon nanotubes for methanol oxidation in alkaline media, ACS Appl. Energy Mater. 1 (2018) 3763–3770.
[330] D.H. Yang, X.L. Sui, L. Zhao, G.S. Huang, D.M. Gu, Z.B. Wang, Pt supported on carbon-coating antimony Tin oxide as anode catalyst for direct methanol fuel cell, Fuel Cells 18 (2018) 763–770.
[331] M. Nasrollahzadeh, M. Jahanshahi, M. Yaldagard, M. Salehi, Synthesis, characterization and comparison of polythiophene–carbon nanocomposite materials as Pt electrocatalyst supports for fuel cell applications, Bull. Mater. Sci. 41 (2018) 1–8.
[332] S. Bong, D. Han, Supercritical, freezing and thermal drying process of resorcinol-formaldehyde polymer based nano-carbons and their highly loaded PtRu anode electrocatalyst for DMFC, Electroanalysis 31 (2019) 1311–1315.
[333] N. Pongpichayakul, P. Waenkeaw, J. Jakmunee, S. Themsirimongkon, S. Saipanya, Activity and stability improvement of platinum loaded on reduced graphene oxide and carbon nanotube composites for methanol oxidation, J. Appl. Electrochem. 50 (2020) 51–62.
[334] X. Teng, A. Shan, Y. Zhu, R. Wang, W.M. Lau, Promoting methanol-oxidation-reaction by loading PtNi nano-catalysts on natural graphitic-nano-carbon, Electrochim. Acta 353 (2020), 136542.
[335] X. Guo, L. Yang, B. Shen, Y. Wei, Y. Yang, C. Yang, Q. Jiang, H. He, H. Huang, Ultrafine Pd nanocrystals anchored onto single-walled carbon nanohorns: A highly-efficient multifunctional electrocatalyst with ultra-low Pd loading for formic acid and methanol oxidation, Mater. Chem. Phys. 250 (2020), 123167.
[336] C.L. Vecchio, A. Serov, M. Dicome, B. Zulevi, A. Aricò, V. Baglio, Investigating the durability of a direct methanol fuel cell equipped with commercial Platinum Group Metal-free cathodic electro-catalysts, Electrochim. Acta 394 (2021), 139108.
[337] Y. Han, S. Yin, Y. Chen, C. Chen, W. Yan, X. Cheng, Y. Li, T. Zhang, J. Yang, Y. Jiang, Experimental and DFT studies of oxygen reduction reaction promoted by binary site Fe/Co-N-C catalyst in acid, J. Electroanal. Chem. 914 (2022), 116322.
[338] W.H. Pan, S.J. Lue, C.M. Chang, Y.L. Liu, Alkali doped polyvinyl alcohol/multi-walled carbon nano-tube electrolyte for direct methanol alkaline fuel cell, J. Membr. Sci. 376 (2011) 225–232.
[339] J.F. Wu, C.F. Lo, L.Y. Li, H.Y. Li, C.M. Chang, K.S. Liao, C.C. Hu, Y.L. Liu, S.J. Lue, Thermally stable polybenzimidazole/carbon nano-tube composites for alkaline direct methanol fuel cell applications, J. Power Sources 246 (2014) 39–48.
[340] A. Zainoodin, S. Kamarudin, M. Masdar, W. Daud, A. Mohamad, J. Sahari, Optimization of a porous carbon nanofiber layer for the membrane electrode assembly in DMFC, Energy Convers. Manag. 101 (2015) 525–531.
[341] M. Gang, G. He, Z. Li, K. Cao, Z. Li, Y. Yin, H. Wu, Z. Jiang, Graphitic carbon nitride nanosheets/sulfonated poly (ether ether ketone) nanocomposite membrane for direct methanol fuel cell application, J. Membr. Sci. 507 (2016) 1–11.
[342] W. Jia, B. Tang, P. Wu, Novel composite PEM with long-range ionic nanochannels induced by carbon nanotube/graphene oxide nanoribbon composites, ACS Appl. Mater. Interfaces 8 (2016) 28955–28963.
[343] C. Simari, V. Baglio, C.L. Vecchio, A.S. Arico, R.G. Agostino, L. Coppola, C. O. Rossi, I. Nicotera, Reduced methanol crossover and enhanced proton transport in nanocomposite membranes based on clay-CNTs hybrid materials for direct methanol fuel cells, Ionics 23 (2017) 2113–2123.
[344] N. Shaari, S. Kamarudin, Performance of crosslinked sodium alginate/sulfonated graphene oxide as polymer electrolyte membrane in DMFC application: RSM optimization approach, Int. J. Hydrog. Energy 43 (2018) 22986–23003.
[345] S. Badwal, S. Giddey, A. Kulkarni, J. Goel, S. Basu, Direct ethanol fuel cells for transport and stationary applications-A comprehensive review, Appl. Energy 145 (2015) 80–103.
[346] R. Awasthi, A. Mirzaei, R. Singh, Synthesis and characterization of nano structured Pd-Ni and Pd-Ni-C composites towards electrooxidation of alcohols, Open Catal. J. 3 (2010) 70–78.
[347] Z. Yan, H. Meng, L. Shi, Z. Li, P.K. Shen, Synthesis of mesoporous hollow carbon hemispheres as highly efficient Pd electrocatalyst support for ethanol oxidation, Electrochem. Commun. 12 (2010) 689–692.
[348] A. Elsheikh, V.L. Martins, J. McGregor, Influence of physicochemical characteristics of carbon supports on Pd ethanol oxidation catalysts, Energy Procedia 151 (2018) 79–83.
[349] A.K. Choudhary, H. Pramanik, Synthesis of low-cost HNO_3-functionalized acetylene black carbon supported Pt-Ru/C AB nano electrocatalysts for the application in direct ethanol fuel cell (DEFC), Korean J. Chem. Eng. 36 (2019) 1688–1707.
[350] M. Zhang, Z. Yan, J. Xie, Core/shell Ni@Pd nanoparticles supported on MWCNTs at improved electrocatalytic performance for alcohol oxidation in alkaline media, Electrochim. Acta 77 (2012) 237–243.

[351] J. Cai, Y. Huang, B. Huang, S. Zheng, Y. Guo, Enhanced activity of Pt nanoparticle catalysts supported on manganese oxide-carbon nanotubes for ethanol oxidation, Int. J. Hydrog. Energy 39 (2014) 798–807.

[352] H. Rostami, A.A. Rostami, A. Omrani, An electrochemical method to prepare of Pd/Cu_2O/MWCNT nanostructure as an anode electrocatalyst for alkaline direct ethanol fuel cells, Electrochim. Acta 194 (2016) 431–440.

[353] C.Y. Huang, J.S. Lin, W.H. Pan, C.M. Shih, Y.L. Liu, S.J. Lue, Alkaline direct ethanol fuel cell performance using alkali-impregnated polyvinyl alcohol/functionalized carbon nano-tube solid electrolytes, J. Power Sources 303 (2016) 267–277.

[354] A. De, R. Adhikary, J. Datta, Proactive role of carbon nanotube-polyaniline conjugate support for Pt nano-particles toward electro-catalysis of ethanol in fuel cell, Int. J. Hydrog. Energy 42 (2017) 25316–25325.

[355] A.K. Choudhary, H. Pramanik, Addition of rhenium (Re) to Pt-Ru/f-MWCNT anode electrocatalysts for enhancement of ethanol electrooxidation in half cell and single direct ethanol fuel cell, Int. J. Hydrog. Energy 45 (2020) 13300–13321.

[356] X. Wang, X. Hu, J. Huang, W. Zhang, W. Ji, Y. Hui, X. Yao, Electrospinning synthesis of porous carbon fiber supported Pt-SnO_2 anode catalyst for direct ethanol fuel cell, Solid State Sci 94 (2019) 64–69.

[357] K. Kakaei, M. Rahnavardi, Synthesis of nitrogen-doped reduced graphene oxide and its decoration with high efficiency palladium nanoparticles for direct ethanol fuel cell, Renew. Energy 163 (2021) 1277–1286.

[358] W. Zhou, S. Song, W. Li, G. Sun, Q. Xin, S. Kontou, K. Poulianitis, P. Tsiakaras, Pt-based anode catalysts for direct ethanol fuel cells, Solid State Ion 175 (2004) 797–803.

[359] F. Hu, P.K. Shen, Y.L. Li, J.Y. Liang, J. Wu, Q.L. Bao, C.M. Li, Z.D. Wei, Highly stable Pd-based catalytic nanoarchitectures for low temperature fuel cells, Fuel Cells 8 (2008) 429–435.

[360] H. Zhu, Y. Liu, L. Shen, Y. Wei, Z. Guo, H. Wang, K. Han, Z. Chang, Microwave heated polyol synthesis of carbon supported PtAuSn/C nanoparticles for ethanol electrooxidation, Int. J. Hydrog. Energy 35 (2010) 3125–3128.

[361] Z. Zhu, J. Wang, A. Munir, H.S. Zhou, Electrocatalytic activity of Pt nanoparticles on bamboo shaped carbon nanotubes for ethanol oxidation, Electrochim. Acta 55 (2010) 8517–8520.

[362] A. Dutta, S.S. Mahapatra, J. Datta, High performance PtPdAu nano-catalyst for ethanol oxidation in alkaline media for fuel cell applications, Int. J. Hydrog. Energy 36 (2011) 14898–14906.

[363] J. Tayal, B. Rawat, S. Basu, Bi-metallic and tri-metallic Pt-Sn/C, Pt-Ir/C, Pt-Ir-Sn/C catalysts for electro-oxidation of ethanol in direct ethanol fuel cell, Int. J. Hydrog. Energy 36 (2011) 14884–14897.

[364] P. dos Santos Correa, E.L. da Silva, R.F. da Silva, C. Radtke, B. Moreno, E. Chinarro, C. de Fraga Malfatti, Effect of decreasing platinum amount in Pt-Sn-Ni alloys supported on carbon as electrocatalysts for ethanol electrooxidation, Int. J. Hydrog. Energy 37 (2012) 9314–9323.

[365] V. Bambagioni, C. Bianchini, Y. Chen, J. Filippi, P. Fornasiero, M. Innocenti, A. Lavacchi, A. Marchionni, W. Oberhauser, F. Vizza, Energy efficiency enhancement of ethanol electrooxidation on Pd-CeO_2/C in passive and active polymer electrolyte-membrane fuel cells, ChemSusChem 5 (2012) 1266–1273.

[366] G. Hu, F. Nitze, H.R. Barzegar, T. Sharifi, A. Mikołajczuk, C.W. Tai, A. Borodzinski, T. Wågberg, Palladium nanocrystals supported on helical carbon nanofibers for highly efficient electro-oxidation of formic acid, methanol and ethanol in alkaline electrolytes, J. Power Sources 209 (2012) 236–242.

[367] K. Lee, S.W. Kang, S.U. Lee, K.H. Park, Y.W. Lee, S.W. Han, One-pot synthesis of monodisperse 5 nm Pd-Ni nanoalloys for electrocatalytic ethanol oxidation, ACS Appl. Mater. Interfaces 4 (2012) 4208–4214.

[368] A. Tabet-Aoul, M. Mohamedi, 3D hierarchical cauliflower-like carbon nanotubes/platinum–tin nanostructure and its electrocatalytic activity for ethanol oxidation, J. Mater. Chem. 22 (2012) 2491–2497.

[369] J. Goel, S. Basu, Effect of support materials on the performance of direct ethanol fuel cell anode catalyst, Int. J. Hydrog. Energy 39 (2014) 15956–15966.

[370] R. Cui, N. Gu, J. Shi, Z. Han, P. Guo, J. Xu, G. Zhang, Fabrication of Pd/Mn_3O_4/plait-like carbon nanocoils catalyst: A highly active catalyst for ethanol electro-oxidation in alkaline media, Electrochim. Acta 147 (2014) 778–784.

[371] N.A. Barakat, M. Motlak, A.A. Elzatahry, K.A. Khalil, E.A. Abdelghani, Ni_xCo_{1-x} alloy nanoparticle-doped carbon nanofibers as effective non-precious catalyst for ethanol oxidation, Int. J. Hydrog. Energy 39 (2014) 305–316.

[372] A. Dutta, J. Datta, Energy efficient role of Ni/NiO in PdNi nano catalyst used in alkaline DEFC, J. Mater. Chem. A 2 (2014) 3237–3250.

[373] Y. Liu, W. Wang, Y. Yang, F. Wang, X. Zhao, Z. Lei, Pd nanoparticles supported on 1H-benzotriazole functionalized carbon with enhanced catalytic performance towards ethanol oxidation, Appl. Catal. A Gen. 505 (2015) 410–415.

[374] L. Wang, A. Lavacchi, M. Bevilacqua, M. Bellini, P. Fornasiero, J. Filippi, M. Innocenti, A. Marchionni, H.A. Miller, F. Vizza, Energy efficiency of alkaline direct ethanol fuel cells employing nanostructured palladium electrocatalysts, ChemCatChem 7 (2015) 2214–2221.

[375] Y. Wang, M. Mohamedi, Hierarchically organized nanostructured TiO_2/Pt on microfibrous carbon paper substrate for ethanol fuel cell reaction, Int. J. Hydrog. Energy 42 (2017) 22796–22804.

[376] Y.H. Qin, Z.Y. Xiong, J. Ma, L. Yang, Z. Wu, W. Feng, T.L. Wang, W.G. Wang, C. W. Wang, Enhanced electrocatalytic activity and stability of Pd nanoparticles supported on TiO_2-modified nitrogen-doped carbon for ethanol oxidation in alkaline media, Int. J. Hydrog. Energy 42 (2017) 1103–1112.

[377] P. Wang, Y. Wen, S. Yin, N. Wang, P.K. Shen, PtRh alloys on hybrid TiO_2-Carbon support as high efficiency catalyst for ethanol oxidation, Int. J. Hydrog. Energy 42 (2017) 24689–24696.

[378] P. Kanninen, N.D. Luong, J. Flórez-Montaño, H. Jiang, E. Pastor, J. Seppälä, T. Kallio, Highly active platinum nanoparticles supported by nitrogen/sulfur functionalized graphene composite for ethanol electro-oxidation, Electrochim. Acta 242 (2017) 315–326.

[379] G. Li, Q. Yi, X. Yang, Y. Chen, X. Zhou, G. Xie, Ni-Co-N doped honeycomb carbon nano-composites as cathodic catalysts of membrane-less direct alcohol fuel cell, Carbon 140 (2018) 557–568.

[380] X. Sun, Y. Li, M.-J. Li, Engineering, Highly dispersed palladium nanoparticles on carbon-decorated porous nickel electrode: an effective strategy to boost direct ethanol fuel cell up to 202 mW cm^{-2}, ACS Sustain. Chem. Eng. 7 (2019) 11186–11193.

[381] B. Cermenek, J. Ranninger, B. Feketeföldi, I. Letofsky-Papst, N. Kienzl, B. Bitschnau, V. Hacker, Novel highly active carbon supported ternary PdNiBi nanoparticles as anode catalyst for the alkaline direct ethanol fuel cell, Nano Res 12 (2019) 683–693.

[382] L. Wang, M. Bevilacqua, J. Filippi, P. Fornasiero, M. Innocenti, A. Lavacchi, A. Marchionni, H. Miller, F. Vizza, Electrochemical growth of platinum nanostructures for enhanced ethanol oxidation, Appl. Catal. B 165 (2015) 185–191.

[383] O.O. Fashedemi, H.A. Miller, A. Marchionni, F. Vizza, K.I. Ozoemena, Electro-oxidation of ethylene glycol and glycerol at palladium-decorated FeCo@Fe core-shell nanocatalysts for alkaline direct alcohol fuel cells: functionalized MWCNT supports and impact on product selectivity, J. Mater. Chem. A 3 (2015) 7145–7156.

[384] Y. Chen, M. Bellini, M. Bevilacqua, P. Fornasiero, A. Lavacchi, H.A. Miller, L. Wang, F. Vizza, Direct alcohol fuel cells: Toward the power densities of hydrogen-fed proton exchange membrane fuel cells, ChemSusChem 8 (2015) 524–533.

[385] H.A. Miller, F. Vizza, A. Lavacchi, Direct alcohol fuel cells: Nanostructured materials for the electrooxidation of alcohols in alkaline media, in: Nanomaterials for Fuel Cell Catalysis. Nanostructure Science and Technology, Springer, Cham, 2016, pp. 477–516.

[386] C.H.C. Zhou, J.N. Beltramini, Y.X. Fan, G.M. Lu, Chemoselective catalytic conversion of glycerol as a biorenewable source to valuable commodity chemicals, Chem. Soc. Rev. 37 (2008) 527–549.

[387] S. Carrettin, P. McMorn, P. Johnston, K. Griffin, C.J. Kiely, G.J. Hutchings, Oxidation of glycerol using supported Pt, Pd and Au catalysts, Phys. Chem. Chem. Phys. 5 (2003) 1329–1336.

[388] K. Zakaria, M. McKay, R. Thimmappa, M. Hasan, M. Mamlouk, K. Scott, Direct glycerol fuel cells: Comparison with direct methanol and ethanol fuel cells, ChemElectroChem 6 (9) (2019) 2578–2585.

[389] Z. Pan, Y. Bi, L. An, A cost-effective and chemically stable electrode binder for alkaline-acid direct ethylene glycol fuel cells, Appl. Energy 258 (2020), 114060.

[390] K. Ishiyama, F. Kosaka, I. Shimada, Y. Oshima, J. Otomo, Glycerol electro-oxidation on a carbon-supported platinum catalyst at intermediate temperatures, J. Power Sources 225 (2013) 141–149.

[391] K. Miyazaki, T. Matsumiya, T. Abe, H. Kurata, T. Fukutsuka, K. Kojima, Z. Ogumi, Electrochemical oxidation of ethylene glycol on Pt-based catalysts in alkaline solutions and quantitative analysis of intermediate products, Electrochim. Acta 56 (2011) 7610–7614.

[392] V. Bambagioni, C. Bianchini, A. Marchionni, J. Filippi, F. Vizza, J. Teddy, P. Serp, M. Zhiani, Pd and Pt–Ru anode electrocatalysts supported on multi-walled carbon nanotubes and their use in passive and active direct alcohol fuel cells with an anion-exchange membrane (alcohol= methanol, ethanol, glycerol), J. Power Sources 190 (2009) 241–251.

[393] R.S. Siddhardha, M.B. Teja, P. Tejkiran, S.A. Ntim, P.S.S. Kumar, V. Lakshminarayanan, S. Mitra, S.S. Ramamurthy, Ultra-low casting of Pt based nano-ink for electrooxidation of glycerol and ethylene glycol fuels in alkaline medium, Fuel 158 (2015) 659–663.

[394] W. Yuan, J. Zhang, P.K. Shen, C.M. Li, S.P. Jiang, Self-assembled CeO_2 on carbon nanotubes supported Au nanoclusters as superior electrocatalysts for glycerol oxidation reaction of fuel cells, Electrochim. Acta 190 (2016) 817–828.

[395] J. Qi, N. Benipal, C. Liang, W. Li, PdAg/CNT catalyzed alcohol oxidation reaction for high-performance anion exchange membrane direct alcohol fuel cell (alcohol= methanol, ethanol, ethylene glycol and glycerol), Appl. Catal. B 199 (2016) 494–503.

[396] Z. Bai, M. Shi, Y. Zhang, Q. Zhang, L. Yang, Z. Yang, J. Zhang, Facile synthesis of silver@carbon nanocable-supported platinum nanoparticles as high-performing electrocatalysts for glycerol oxidation in direct glycerol fuel cells, Green Chem 18 (2016) 386–391.

[397] A. Marchionni, M. Bevilacqua, C. Bianchini, Y.X. Chen, J. Filippi, P. Fornasiero, A. Lavacchi, H. Miller, L. Wang, F. Vizza, Electrooxidation of ethylene glycol and glycerol on Pd-(Ni-Zn)/C anodes in direct alcohol fuel cells, ChemSusChem 6 (2013) 518–528.

[398] X. Zhang, Z. Tian, P.K. Shen, Composite of nanosized carbides and carbon aerogel and its supported Pd electrocatalyst for synergistic oxidation of ethylene glycol, Electrochem. Commun. 28 (2013) 9–12.

[399] J. Qi, L. Xin, D.J. Chadderdon, Y. Qiu, Y. Jiang, N. Benipal, C. Liang, W. Li, Electrocatalytic selective oxidation of glycerol to tartronate on Au/C anode catalysts in anion exchange membrane fuel cells with electricity cogeneration, Appl. Catal. B 154-155 (2014) 360–368.

[400] J. Song, S.W. Kang, Y.W. Lee, Y. Park, J.H. Kim, S.W. Han, Regulating the catalytic function of reduced graphene oxides using capping agents for metal-free catalysis, ACS Appl. Mater. Interfaces 9 (2017) 1692–1701.

[401] T.A.G. Silva, E. Teixeira-Neto, N. López, L.M. Rossi, Volcano-like behavior of Au-Pd core-shell nanoparticles in the selective oxidation of alcohols, Sci. Rep. 4 (2014) 1–5.
[402] J.J. Feng, S.S. Chen, X.L. Chen, X.F. Zhang, A.J. Wang, One-pot fabrication of reduced graphene oxide supported dendritic core-shell gold@gold-palladium nanoflowers for glycerol oxidation, J. Colloid Interface Sci. 509 (2018) 73–81.
[403] K. Bhunia, S. Khilari, D. Pradhan, Monodispersed PtPdNi trimetallic nanoparticles-integrated reduced graphene oxide hybrid platform for direct alcohol fuel cell, ACS Sustainable Chem. Eng. 6 (2018) 7769–7778.
[404] S. Ramakrishnan, M. Karuppannan, M. Vinothkannan, K. Ramachandran, O. J. Kwon, D.J. Yoo, Ultrafine Pt nanoparticles stabilized by MoS_2/N-doped reduced graphene oxide as a durable electrocatalyst for alcohol oxidation and oxygen reduction reactions, ACS Appl. Mater. Interfaces 11 (2019) 12504–12515.
[405] K. Krishnadevi, S. RatnaKumari, D. Prasanna, H.B.N. Prasanna, V. Anuradha, Non-covalent functionalization of triazine framework decorated over reduced graphene oxide as a novel anode catalyst support for glycerol oxidation, J. Colloid Interface Sci. 607 (2022) 1776–1785.
[406] V. Bambagioni, M. Bevilacqua, C. Bianchini, J. Filippi, A. Lavacchi, A. Marchionni, F. Vizza, P.K. Shen, Self-sustainable production of hydrogen, chemicals, and energy from renewable alcohols by electrocatalysis, ChemSusChem 3 (2010) 851–855.
[407] A. Ilie, M. Simoes, S. Baranton, C. Coutanceau, S. Martemianov, Influence of operational parameters and of catalytic materials on electrical performance of direct glycerol solid alkaline membrane fuel cells, J. Power Sources 196 (2011) 4965–4971.
[408] Z. Zhang, L. Xin, W. Li, Electrocatalytic oxidation of glycerol on Pt/C in anion-exchange membrane fuel cell: cogeneration of electricity and valuable chemicals, Appl. Catal. B 119-120 (2012) 40–48.
[409] S. Yongprapat, S. Therdthianwong, A. Therdthianwong, RuO_2 promoted Au/C catalysts for alkaline direct alcohol fuel cells, Electrochim. Acta 83 (2012) 87–93.
[410] Z. Zhang, L. Xin, W. Li, Supported gold nanoparticles as anode catalyst for anion-exchange membrane-direct glycerol fuel cell (AEM-DGFC), Int. J. Hydrog. Energy 37 (2012) 9393–9401.
[411] B.F. Machado, A. Marchionni, R.R. Bacsa, M. Bellini, J. Beausoleil, W. Oberhauser, F. Vizza, P. Serp, Synergistic effect between few layer graphene and carbon nanotube supports for palladium catalyzing electrochemical oxidation of alcohols, J. Energy Chem. 22 (2013) 296–304.
[412] Y. Holade, C. Morais, S. Arrii-Clacens, K. Servat, T.W. Napporn, K.B. Kokoh, New preparation of PdNi/C and PdAg/C nanocatalysts for glycerol electrooxidation in alkaline medium, Electrocatalysis 4 (2013) 167–178.
[413] Z. Wang, L. Xin, X. Zhao, Y. Qiu, Z. Zhang, O.A. Baturina, W. Li, Carbon supported Ag nanoparticles with different particle size as cathode catalysts for anion exchange membrane direct glycerol fuel cells, Renew. Energy 62 (2014) 556–562.
[414] O.O. Fashedemi, K.I. Ozoemena, Comparative electrocatalytic oxidation of ethanol, ethylene glycol and glycerol in alkaline medium at Pd-decorated FeCo@Fe/C core-shell nanocatalysts, Electrochim. Acta 128 (2014) 279–286.
[415] S. Dash, N. Munichandraiah, Nanoflowers of PdRu on PEDOT for electrooxidation of glycerol and its analysis, Electrochim. Acta 180 (2015) 339–352.
[416] H. Wang, L. Thia, N. Li, X. Ge, Z. Liu, X. Wang, Pd nanoparticles on carbon nitride-graphene for the selective electro-oxidation of glycerol in alkaline solution, ACS Catal 5 (2015) 3174–3180.
[417] A.N. Geraldes, D.F. da Silva, L.G. de Andrade e Silva, E.V. Spinacé, A.O. Neto, M. C. dos Santos, Binary and ternary palladium based electrocatalysts for alkaline direct glycerol fuel cell, J. Power Sources 293 (2015) 823–830.
[418] F. Munoz, C. Hua, T. Kwong, L. Tran, T.Q. Nguyen, J.L. Haan, Palladium–copper electrocatalyst for the promotion of the electrochemical oxidation of polyalcohol fuels in the alkaline direct alcohol fuel cell, Appl. Catal. B 174-175 (2015) 323–328.
[419] L.S.R. Silva, F.E. López-Suárez, M. Perez-Cadenas, S.F. Santos, L.P. da Costa, K.I. B. Eguiluz, G.R. Salazar-Banda, Synthesis and characterization of highly active Pb_x@Pt_y/C core-shell nanoparticles toward glycerol electrooxidation, Appl. Catal. B 198 (2016) 38–48.
[420] N. Li, W.Y. Xia, C.W. Xu, S. Chen, Pt/C and Pd/C catalysts promoted by Au for glycerol and CO electrooxidation in alkaline medium, J. Energy Inst. 90 (2017) 725–733.
[421] P. Lertthahan, S. Yongprapat, A. Therdthianwong, S. Therdthianwong, Pt-modified Au/C catalysts for direct glycerol electro-oxidation in an alkaline medium, Int. J. Hydrog. Energy 42 (2017) 9202–9209.
[422] H. Xu, B. Yan, K. Zhang, J. Wang, S. Li, C. Wang, Y. Shiraishi, Y. Du, P. Yang, Ultrasonic-assisted synthesis of N-doped graphene-supported binary PdAu nanoflowers for enhanced electro-oxidation of ethylene glycol and glycerol, Electrochim. Acta 245 (2017) 227–236.
[423] Y. Kang, W. Wang, Y. Pu, J. Li, D. Chai, Z. Lei, An effective Pd-NiO_x-P composite catalyst for glycerol electrooxidation: Co-existed phosphorus and nickel oxide to enhance performance of Pd, Chem. Eng. J. 308 (2017) 419–427.
[424] N. Benipal, J. Qi, J.C. Gentile, W. Li, Direct glycerol fuel cell with polytetrafluoroethylene (PTFE) thin film separator, Renew. Energy 105 (2017) 647–655.
[425] N. Benipal, J. Qi, Q. Liu, W. Li, Carbon nanotube supported PdAg nanoparticles for electrocatalytic oxidation of glycerol in anion exchange membrane fuel cells, Appl. Catal. B 210 (2017) 121–130.
[426] Z.Y. Li, J. Zhou, L.S. Tang, X.P. Fu, H. Wei, M. Xue, Y.L. Zhao, C.J. Jia, X.M. Li, H. B. Chu, Hydroxyl-rich ceria hydrate nanoparticles enhancing the alcohol electrooxidation performance of Pt catalysts, J. Mater. Chem. A 6 (2018) 2318–2326.
[427] C.A. Martins, O.A. Ibrahim, P. Pei, E. Kjeang, Towards a fuel-flexible direct alcohol microfluidic fuel cell with flow-through porous electrodes: Assessment of methanol, ethylene glycol and glycerol fuels, Electrochim. Acta 271 (2018) 537–543.
[428] X. Cui, Y. Li, M. Zhao, Y. Xu, L. Chen, S. Yang, Y. Wang, Facile growth of ultra-small Pd nanoparticles on zeolite-templated mesocellular graphene foam for enhanced alcohol electrooxidation, Nano Res 12 (2019) 351–356.
[429] N. Yahya, S.K. Kamarudin, N.A. Karim, M.S. Masdar, K.S. Loh, K.L. Lim, Durability and performance of direct glycerol fuel cell with palladium-aurum/vapor grown carbon nanofiber support, Energy Convers. Manage. 188 (2019) 120–130.
[430] C.A. Martins, O.A. Ibrahim, P. Pei, E. Kjeang, In situ decoration of metallic catalysts in flow-through electrodes: Application of Fe/Pt/C for glycerol oxidation in a microfluidic fuel cell, Electrochim. Acta 305 (2019) 47–55.
[431] P. Sangkheaw, S. Therdthianwong, A. Therdthianwong, N. Wongyao, S. Yongprapat, Enhancement of anode performance for alkaline-acid direct glycerol fuel cells, Renew. Energy 161 (2020) 395–407.
[432] J. Banjong, A. Therdthianwong, S. Therdthianwong, S. Yongprapat, N. Wongyao, High performance alkaline-acid direct glycerol fuel cells for portable power supplies via electrode structure design, Int. J. Hydrog. Energy 45 (2020) 2244–2256.
[433] H. Wang, J. Ding, P. Kannan, P. Subramanian, S. Ji, Nitrogen-doped mesoporous carbon nanosheet network entrapped nickel nanoparticles as an efficient catalyst for electro-oxidation of glycerol, Int. J. Hydrog. Energy 45 (2020) 28821–28835.
[434] S. Imhanria, X. Deng, T. Tan, J. Deng, L. Xu, W. Wang, Phosphating a Pd-rich 'dealloyed $PdCo_3$ nanoparticles': An effective electrocatalyst for glycerol oxidation reaction, J. Alloys Compd. 868 (2021), 159058.
[435] D. Chai, X. Zhang, S. Yan, G. Li, Ni_2P as an electron donor stabilizing Pt for highly efficient isopropanol fuel cell, Int. J. Hydrog. Energy. 45 (2020) 6573–6582.
[436] E. Rikkinen, A. Santasalo-Aarnio, S. Airaksinen, M. Borghei, V. Viitanen, J. Sainio, E.I. Kauppinen, T. Kallio, A.O.I. Krause, Atomic layer deposition preparation of Pd nanoparticles on a porous carbon support for alcohol oxidation, J. Phys. Chem. C 115 (2011) 23067–23073.
[437] R. Kannan, A.R. Kim, K.S. Nahm, D.J. Yoo, Facile instep synthesis of palladium nanoparticle/carbon@carbon nanotube composites for electrooxidation of xylitol, J. Nanosci. Nanotechnol. 16 (2016) 2587–2592.
[438] M. Bellini, M. Bevilacqua, J. Filippi, A. Lavacchi, A. Marchionni, H.A. Miller, W. Oberhauser, F. Vizza, S.P. Annen, H. Grützmacher, Energy and chemicals from the selective electrooxidation of renewable diols by organometallic fuel cells, ChemSusChem 7 (2014) 2432–2435.
[439] S.P. Annen, V. Bambagioni, M. Bevilacqua, J. Filippi, A. Marchionni, W. Oberhauser, H. Schönberg, F. Vizza, C. Bianchini, H. Grützmacher, A biologically inspired organometallic fuel cell (OMFC) that converts renewable alcohols into energy and chemicals, Angew. Chem. Int. Ed. 49 (2010) 7229–7233.
[440] M. Bevilacqua, C. Bianchini, A. Marchionni, J. Filippi, A. Lavacchi, H. Miller, W. Oberhauser, F. Vizza, G. Granozzi, L. Artiglia, S.P. Annen, F. Krumeich, H. Grützmacher, Improvement in the efficiency of an OrganoMetallic Fuel Cell by tuning the molecular architecture of the anode electrocatalyst and the nature of the carbon support, Energy Environ. Sci. 5 (2012) 8608–8620.
[441] H. Kivrak, D. Atbas, O. Alal, M.S. Çögenli, A. Bayrakceken, S.O. Mert, O. Sahin, A complementary study on novel PdAuCo catalysts: synthesis, characterization, direct formic acid fuel cell application, and exergy analysis, Int. J. Hydrog. Energy 43 (2018) 21886–21898.
[442] G.A. El-Nagar, K.M. Dawood, M.S. El-Deab, B.E. Al-Andouli, Efficient direct formic acid fuel cell (DFAFC) anode of nano-sized palladium complex: High durability and activity origin, Appl. Catal. B 213 (2017) 118–126.
[443] S.Z. Rejal, M.S. Masdar, S.K. Kamarudin, A parametric study of the direct formic acid fuel cell (DFAFC) performance and fuel crossover, Int. J. Hydrog. Energy. 39 (2014) 10267–10274.
[444] N.M. Aslam, M.S. Masdar, S.K. Kamarudin, W.R.W. Daud, Overview on direct formic acid fuel cells (DFAFCs) as an energy sources, APCBEE Procedia 3 (2012) 33–39.
[445] M.D. Obradović, S.L. Gojković, Electrochemical instability of Pt nanoparticles probed by formic acid oxidation, J. Electroanal. Chem. 664 (2012) 152–155.
[446] W.L. Qu, Z.B. Wang, Z.Z. Jiang, D.M. Gu, G.P. Yin, Investigation on performance of Pd/Al_2O_3-C catalyst synthesized by microwave assisted polyol process for electrooxidation of formic acid, RSC Adv 2 (2012) 344–350.
[447] B. Habibi, S. Mohammadyari, Palladium nanoparticles/nanostructured carbon black composite on carbon-ceramic electrode as an electrocatalyst for formic acid fuel cells, J. Taiwan Inst. Chem. Eng. 58 (2016) 245–251.
[448] Y. Suo, Y. Guo, C. Rong, Z. Zhang, G. Hu, Synthesis of highly active Pt-Pd-Cu/C catalysts for formic acid oxidation, Int. J. Electrochem. Sci. 12 (2017) 3561–3575.
[449] V.T. Nguyen, Q.C. Tran, N.D. Quang, N.A. Nguyen, V.T. Bui, V.D. Dao, H.S. Choi, N-doped Cdot/PtPd nanonetwork hybrid materials as highly efficient electrocatalysts for methanol oxidation and formic acid oxidation reactions, J. Alloys Compd. 766 (2018) 979–986.
[450] W. Shi, A.H. Park, H.U. Park, Y.U. Kwon, Enhancing activity and durability of Pd nanoparticle electrocatalyst by ceria undercoating on carbon support, J. Catal. 384 (2020) 22–29.
[451] D. Morales-Acosta, H. Rodríguez, L.A. Godinez, L.G. Arriaga, Performance increase of microfluidic formic acid fuel cell using Pd/MWCNTs as catalyst, J. Power Sources 195 (2010) 1862–1865.
[452] Z. Cui, P.J. Kulesza, C.M. Li, W. Xing, S.P. Jiang, Pd nanoparticles supported on HPMo-PDDA-MWCNT and their activity for formic acid oxidation reaction of fuel cells, Int. J. Hydrog. Energy 36 (2011) 8508–8517.

[453] J.Q. Zeng, S.N. Sun, J.P. Zhong, X.F. Li, R.X. Wang, L.N. Wu, L. Wang, Y.J. Fan, Pd nanoparticles supported on copper phthalocyanine functionalized carbon nanotubes for enhanced formic acid electrooxidation, Int. J. Hydrog. Energy 39 (2014) 15928–15936.
[454] H. Huang, X. Wang, Pd nanoparticles supported on low-defect graphene sheets: for use as high-performance electrocatalysts for formic acid and methanol oxidation, J. Mater. Chem. 22 (2012) 22533–22541.
[455] J. Zhong, D. Bin, F. Ren, C. Wang, C. Zhai, P. Yang, Y. Du, Graphene nanosheet-supported Pd nano-leaves with highly efficient electrocatalytic performance for formic acid oxidation, Colloids Surf. A Physicochem. Eng. Asp. 488 (2016) 1–6.
[456] W. Liu, J. Huang, Electro-oxidation of formic acid on carbon supported Pt-Os catalyst, J. Power Sources 189 (2009) 1012–1015.
[457] J. Wang, G. Yin, Y. Chen, R. Li, X. Sun, Pd nanoparticles deposited on vertically aligned carbon nanotubes grown on carbon paper for formic acid oxidation, Int. J. Hydrog. Energy 34 (2009) 8270–8275.
[458] N. Cheng, H. Lv, W. Wang, S. Mu, M. Pan, F. Marken, An ambient aqueous synthesis for highly dispersed and active Pd/C catalyst for formic acid electro-oxidation, J. Power Sources 195 (2010) 7246–7249.
[459] C. Hu, Z. Bai, L. Yang, J. Lv, K. Wang, Y. Guo, Y. Cao, J. zhou, Preparation of high performance Pd catalysts supported on untreated multi-walled carbon nanotubes for formic acid oxidation, Electrochim. Acta 55 (2010) 6036–6041.
[460] H. Gao, S. Liao, J. Zeng, Y. Xie, D. Dang, Preparation and characterization of core–shell structured catalysts using Pt_xPd_y as active shell and nano-sized Ru as core for potential direct formic acid fuel cell application, Electrochim. Acta 56 (2011) 2024–2030.
[461] T. Maiyalagan, A.B.A. Nassr, T.O. Alaje, M. Bron, K. Scott, Three-dimensional cubic ordered mesoporous carbon (CMK-8) as highly efficient stable Pd electro-catalyst support for formic acid oxidation, J. Power Sources 211 (2012) 147–153.
[462] Q. Tian, W. Chen, Y. Wu, An effective PdCo/PWA-C anode catalyst for direct formic acid fuel cells, J. Electrochem. Soc. 162 (2014) F165.
[463] M. Lou, R. Wang, L. Yang, D. Jia, Z. Sun, L. Wang, Y. Guo, X. Wang, J. Zhang, H. Shi, Ionic liquid polyoxometalate-enhanced Pd/N, P-codoped coal-based carbon fiber catalysts for formic acid electrooxidation, Appl. Surf. Sci. 516 (2020), 146137.
[464] Scott, Keith, Yu, E. Hao, M. Madhao Ghangrekar, Benjamin Erable, N. Mihai Duţeanu, Biological and microbial fuel cells, in: Comprehensive Renewable Energy, Elsevier, United States, 2012, pp. 277–300.
[465] E. Katz, P. Bollella, Fuel cells and biofuel cells: From past to perspectives, Isr. J. Chem. 61 (2021) 68–84.
[466] M. Rahimnejad, A. Adhami, S. Darvari, A. Zirepour, S.E. Oh, Microbial fuel cell as new technology for bioelectricity generation: A review, Alex. Eng. J. 54 (2015) 745–756.
[467] H.L. Song, Y. Zhu, J. Li, Electron transfer mechanisms, characteristics and applications of biological cathode microbial fuel cells-A mini review, Arab. J. Chem. 12 (2019) 2236–2243.
[468] S. Shah, V. Venkatramanan, R. Prasad, Microbial fuel cell: Sustainable green technology for bioelectricity generation and wastewater treatment, Sustainable Green Technologies for Environmental Management, Singapore, 2019, pp. 199–218.
[469] A.E. Franks, K.P. Nevin, Microbial fuel cells, a current review, Energies 3 (2010) 899–919.
[470] S. Zhong, L. Zhou, L. Wu, L. Tang, Q. He, J. Ahmed, Nitrogen-and boron-co-doped core-shell carbon nanoparticles as efficient metal-free catalysts for oxygen reduction reactions in microbial fuel cells, J. Power Sources 272 (2014) 344–350.
[471] C. Cao, L. Wei, M. Su, G. Wang, J. Shen, Spontaneous bubble-template" assisted metal-polymeric framework derived N/Co dual-doped hierarchically porous carbon/Fe_3O_4 nanohybrids: superior electrocatalyst for ORR in biofuel cells, J. Mater. Chem. A 4 (2016) 9303–9310.
[472] C. Cao, L. Wei, G. Wang, J. Liu, Q. Zhai, J. Shen, A polyaniline-derived iron-nitrogen-carbon nanorod network anchored on graphene as a cost-effective air-cathode electrocatalyst for microbial fuel cells, Inorg. Chem. Front. 4 (2017) 1930–1938.
[473] M.A.C. de Oliveira, B. Mecheri, A. D'Epifanio, F. Zurlo, S. Licoccia, Optimization of PGM-free cathodes for oxygen reduction in microbial fuel cells, Electrochim. Acta 334 (2020), 135650.
[474] D. Wang, H. Liu, Z. Cao, T. Cai, P. Han, J. Song, L. Kong, C. Liu, Ordered porous nitrogen-doped carbon with atomically dispersed FeN_4 for efficient oxygen reduction reaction in microbial fuel cell, Sci. Total Environ. 838 (2022), 156186.
[475] Z. Xing, N. Gao, Y. Qi, X. Ji, H. Liu, Influence of enhanced carbon crystallinity of nanoporous graphite on the cathode performance of microbial fuel cells, Carbon 115 (2017) 271–278.
[476] S. Singh, P.K. Bairagi, N. Verma, Candle soot-derived carbon nanoparticles: An inexpensive and efficient electrode for microbial fuel cells, Electrochim. Acta 264 (2018) 119–127.
[477] Y. Wang, C. Liu, S. Zhou, R. Hou, L. Zhou, F. Guan, R. Chen, Y. Yuan, Hierarchical N-doped C/Fe_3O_4 nanotube composite arrays grown on the carbon fiber cloth as a bioanode for high-performance bioelectrochemical system, Chem. Eng. J. 406 (2021), 126832.
[478] L. Tan, N. Li, S. Chen, Z.Q. Liu, Self-assembly synthesis of CuSe@graphene-carbon nanotubes as efficient and robust oxygen reduction electrocatalysts for microbial fuel cells, J. Mater. Chem. A 4 (2016) 12273–12280.
[479] P. Mishra, R. Jain, Electrochemical deposition of MWCNT-MnO_2/PPy nano-composite application for microbial fuel cells, Int. J. Hydrog. Energy 41 (2016) 22394–22405.
[480] X. Li, L. Ni, J. Zhou, L. Xu, C. Lu, G. Yang, W. Ding, W. Hou, Encapsulation of Fe nanoparticles into an N-doped carbon nanotube/nanosheet integrated hierarchical architecture as an efficient and ultrastable electrocatalyst for the oxygen reduction reaction, Nanoscale 12 (2020) 13987–13995.
[481] H. Luo, S. Jin, P.H. Fallgren, H.J. Park, P.A. Johnson, A novel laccase-catalyzed cathode for microbial fuel cells, Chem. Eng. J. 165 (2010) 524–528.
[482] E. Martin, B. Tartakovsky, O. Savadogo, Cathode materials evaluation in microbial fuel cells: A comparison of carbon, Mn_2O_3, Fe_2O_3 and platinum materials, Electrochim. Acta 58 (2011) 58–66.
[483] X. Xie, M. Pasta, L. Hu, Y. Yang, J. McDonough, J. Cha, C.S. Criddle, Y. Cui, Nano-structured textiles as high-performance aqueous cathodes for microbial fuel cells, Energy Environ. Sci. 4 (2011) 1293–1297.
[484] Y. Yuan, J. Ahmed, L. Zhou, B. Zhao, S. Kim, Carbon nanoparticles-assisted mediator-less microbial fuel cells using Proteus vulgaris, Biosens. Bioelectron. 27 (2011) 106–112.
[485] S. Inoue, E.A. Parra, A. Higa, Y. Jiang, P. Wang, C.R. Buie, J.D. Coates, L. Lin, Structural optimization of contact electrodes in microbial fuel cells for current density enhancements, Sens. Actuator A Phys. 177 (2012) 30–36.
[486] G. Mohanakrishna, S.K. Mohan, S.V. Mohan, Carbon based nanotubes and nanopowder as impregnated electrode structures for enhanced power generation: Evaluation with real field wastewater, Appl. Energy 95 (2012) 31–37.
[487] J. Hou, Z. Liu, S. Yang, Y. Zhou, Three-dimensional macroporous anodes based on stainless steel fiber felt for high-performance microbial fuel cells, J. Power Sources 258 (2014) 204–209.
[488] Y. Wang, B. Li, D. Cui, X. Xiang, W. Li, Nano-molybdenum carbide/carbon nanotubes composite as bifunctional anode catalyst for high-performance *Escherichia coli*-based microbial fuel cell, Biosens. Bioelectron. 51 (2014) 349–355.
[489] C. Cao, L. Wei, M. Su, G. Wang, J. Shen, Enhanced power generation using nano cobalt oxide anchored nitrogen-decorated reduced graphene oxide as a high-performance air-cathode electrocatalyst in biofuel cells, RSC Adv 6 (2016) 52556–52563.
[490] L. Zhou, P. Fu, D. Wen, Y. Yuan, S. Zhou, Self-constructed carbon nanoparticles-coated porous biocarbon from plant moss as advanced oxygen reduction catalysts, Appl. Catal. B 181 (2016) 635–643.
[491] B. Ge, K. Li, Z. Fu, L. Pu, X. Zhang, Z. Liu, K. Huang, The performance of nano urchin-like $NiCo_2O_4$ modified activated carbon as air cathode for microbial fuel cell, J. Power Sources 303 (2016) 325–332.
[492] J. Wang, P. Tian, K. Li, B. Ge, D. Liu, Y. Liu, T. Yang, R. Ren, The excellent performance of nest-like oxygen-deficient $Cu_{1.5}Mn_{1.5}O_4$ applied in activated carbon air-cathode microbial fuel cell, Bioresour. Technol. 222 (2016) 107–113.
[493] C. Cao, L. Wei, Q. Zhai, J. Ci, W. Li, G. Wang, J. Shen, Gas-flow tailoring fabrication of graphene-like Co-Nx-C nanosheet supported Sub-10 nm PtCo nanoalloys as synergistic catalyst for air-cathode microbial fuel cells, ACS Appl. Mater. Interfaces 9 (2017) 22465–22475.
[494] H.O. Mohamed, M.A. Abdelkareem, M. Obaid, S.H. Chae, M. Park, H.Y. Kim, N. A. Barakat, Cobalt oxides-sheathed cobalt nano flakes to improve surface properties of carbonaceous electrodes utilized in microbial fuel cells, Chem. Eng. J. 326 (2017) 497–506.
[495] E.T. Sayed, N. Nakagawa, Critical issues in the performance of yeast based microbial fuel cell, J. Chem. Technol. Biotechnol. 93 (2018) 1588–1594.
[496] H. Yuan, G. Dong, D. Li, L. Deng, P. Cheng, Y. Chen, Steamed cake-derived 3D carbon foam with surface anchored carbon nanoparticles as freestanding anodes for high-performance microbial fuel cells, Sci. Total Environ. 636 (2018) 1081–1088.
[497] M. Kodali, S. Herrera, S. Kabir, A. Serov, C. Santoro, I. Ieropoulos, P. Atanassov, Enhancement of microbial fuel cell performance by introducing a nano-composite cathode catalyst, Electrochim. Acta 265 (2018) 56–64.
[498] B. Mecheri, R. Gokhale, C. Santoro, M.A. Costa de Oliveira, A. D'Epifanio, S. Licoccia, A. Serov, K. Artyushkova, P. Atanassov, Oxygen reduction reaction electrocatalysts derived from iron salt and benzimidazole and aminobenzimidazole precursors and their application in microbial fuel cell cathodes, ACS Appl. Energy Mater. 1 (2018) 5755–5765.
[499] I. Gajda, J. Greenman, C. Santoro, A. Serov, C. Melhuish, P. Atanassov, I. A. Ieropoulos, Improved power and long term performance of microbial fuel cell with Fe-NC catalyst in air-breathing cathode, Energy 144 (2018) 1073–1079.
[500] G. Zhang, L. Li, M. Chen, F. Yang, Chitosan cross-linked poly (aminoanthraquinone)/Prussian blue ternary nitrogen precursor-derived Fe-N-C oxygen reduction catalysts for microbial fuel cells and zinc-air batteries, J. Mater. Chem. A 8 (2020) 9256–9267.
[501] I. Gajda, J. You, C. Santoro, J. Greenman, I.A. Ieropoulos, A new method for urine electrofiltration and long term power enhancement using surface modified anodes with activated carbon in ceramic microbial fuel cells, Electrochim. Acta 353 (2020), 136388.
[502] M. Rasmussen, S. Abdellaoui, S.D. Minteer, Enzymatic biofuel cells: 30 years of critical advancements, Biosens, Bioelectron 76 (2016) 91–102.
[503] N.A. Karim, H. Yang, Mini-Review: Recent technologies of electrode and system in the enzymatic biofuel cell (EBFC), Appl. Sci. 11 (2021) 5197.
[504] W. Zheng, H.Y. Zhao, J.X. Zhang, H.M. Zhou, X.X. Xu, Y.F. Zheng, Y.B. Wang, Y. Cheng, B.Z. Jang, A glucose/O_2 biofuel cell base on nanographene platelet-modified electrodes, Electrochem. Commun. 12 (2010) 869–871.
[505] M. Karaśkiewicz, E. Nazaruk, K. Żelechowska, J.F. Biernat, J. Rogalski, R. Bilewicz, Fully enzymatic mediatorless fuel cell with efficient naphthylated carbon nanotube-laccase composite cathodes, Electrochem. commun. 20 (2012) 124–127.
[506] F. Gouranlou, H. Ghourchian, Enhancement of ethanol-oxygen biofuel cell output using a CNT based nano-composite as bioanode, Biosensors Bioelectron 78 (2016) 337–343.

[507] S.A. Neto, J.C. Forti, V. Zucolotto, P. Ciancaglini, A.R. De Andrade, Development of nanostructured bioanodes containing dendrimers and dehydrogenases enzymes for application in ethanol biofuel cells, Biosens. Bioelectron. 26 (2011) 2922–2926.
[508] D. Selloum, S. Tingry, V. Techer, L. Renaud, C. Innocent, A. Zouaoui, Optimized electrode arrangement and activation of bioelectrodes activity by carbon nanoparticles for efficient ethanol microfluidic biofuel cells, J. Power Sources 269 (2014) 834–840.
[509] T. Garcia-Perez, S.G. Hong, J. Kim, S. Ha, Entrapping cross-linked glucose oxidase aggregates within a graphitized mesoporous carbon network for enzymatic biofuel cells, Enzyme Microb. Technol. 90 (2016) 26–34.
[510] D. Majdecka, R. Bilewicz, Nanostructuring carbon supports for optimal electrode performance in biofuel cells and hybrid fuel cells, J. Solid State Electrochem. 20 (2016) 949–955.
[511] D. Wen, L. Deng, M. Zhou, S. Guo, L. Shang, G. Xu, S. Dong, A biofuel cell with a single-walled carbon nanohorn-based bioanode operating at physiological condition, Biosens. Bioelectron. 25 (2010) 1544–1547.
[512] B. Reuillard, A.L. Goff, C. Agnès, A. Zebda, M. Holzinger, S. Cosnier, Direct electron transfer between tyrosinase and multi-walled carbon nanotubes for bioelectrocatalytic oxygen reduction, Electrochem. Commun. 20 (2012) 19–22.
[513] M.H. Koo, G. Das, H.H. Yoon, Electrochemical performance of glucose/oxygen biofuel cells based on carbon nanostructures, J. Nanosci. Nanotechnol. 16 (2016) 3054–3057.
[514] M. Bandapati, P.K. Dwivedi, B. Krishnamurthy, Y.H. Kim, G.M. Kim, S. Goel, Screening various pencil leads coated with MWCNT and PANI as enzymatic biofuel cell biocathode, Int. J. Hydrog. Energy. 42 (2017) 27220–27229.
[515] W. Sun, A. Hsu, R. Chen, Carbon-supported tetragonal MnOOH catalysts for oxygen reduction reaction in alkaline media, J. Power Sources 196 (2011) 627–635.
[516] M. Liu, Y. Song, S. He, W.W. Tjiu, J. Pan, Y.Y. Xia, T. Liu, Nitrogen-doped graphene nanoribbons as efficient metal-free electrocatalysts for oxygen reduction, ACS Appl. Mater. Interfaces 6 (2014) 4214–4222.
[517] S. Lu, D. Cao, X. Xu, H. Wang, Y. Xiang, Study of carbon black supported amorphous Ni-B nano-catalyst for hydrazine electrooxidation in alkaline media, RSC Adv 4 (2014) 26940–26945.
[518] K. Akbar, J.H. Kim, Z. Lee, M. Kim, Y. Yi, S.H. Chun, Superaerophobic graphene nano-hills for direct hydrazine fuel cells, NPG Asia Mater 9 (2017) e378.
[519] S. Lal, M. Deepa, V.M. Janardhanan, K.C. Sahu, Paper based hydrazine monohydrate fuel cells with Cu and C composite catalysts, Electrochim. Acta 232 (2017) 262–270.
[520] L. Sun, D. Liu, Chemical activation of commercial CNTs with simultaneous surface deposition of manganese oxide nano flakes for the creation of CNTs-graphene supported oxygen reduction ternary composite catalysts applied in air fuel cell, Appl. Surf. Sci. 447 (2018) 518–527.
[521] T. Zhang, Z. Li, L. Wang, P. Sun, Z. Zhang, S. Wang, Spinel $MnCo_2O_4$ nanoparticles supported on three-dimensional graphene with enhanced mass transfer as an efficient electrocatalyst for the oxygen reduction reaction, ChemSusChem 11 (2018) 2730–2736.
[522] T. Chzhao, A.E. Ukshe, L.S. Leonova, Y.A. Dobrovol'skii, Platinized-heteropolycompound-based nanostructured catalysts for low-temperature hydrogen-air fuel cells, Russ. J. Electrochem. 47 (2011) 595–604.
[523] E.V. Gerasimova, E.Y. Safronova, A.A. Volodin, A.E. Ukshe, Y.A. Dobrovolsky, A. B. Yaroslavtsev, Electrocatalytic properties of the nanostructured electrodes and membranes in hydrogen-air fuel cells, Catal, Today 193 (2012) 81–86.
[524] M.A. Abdelkareem, Y. Al Haj, M. Alajami, H. Alawadhi, N.A.M. Barakat, Ni-Cd carbon nanofibers as an effective catalyst for urea fuel cell, J. Environ. Chem. Eng. 6 (2018) 332–337.
[525] M. Ranjani, N. Senthilkumar, G.G. kumar, A. Manthiram, 3D flower-like hierarchical $NiCo_2O_4$ architecture on carbon cloth fibers as an anode catalyst for high-performance, durable direct urea fuel cells, J. Mater. Chem. A 6 (2018) 23019–23027.
[526] U.B. Demirci, Direct borohydride fuel cell: Main issues met by the membrane-electrodes-assembly and potential solutions, J. Power Sources 172 (2007) 676–687.
[527] Ç.İ. Karadağ, G. Behmenyar, F.G.B. San, T. Şener, Investigation of carbon supported nanostructured PtAu alloy as electrocatalyst for direct borohydride fuel cell, Fuel Cells 2 (2015) 262–269.
[528] J. Milikić, G. Ćirić-Marjanović, S. Mentus, D.M.F. Santos, C.A.C. Sequeira, B. Šljukić, Pd/c-PANI electrocatalysts for direct borohydride fuel cells, Electrochim, Acta 213 (2016) 298–305.
[529] I. Stoševski, J. Krstić, J. Milikić, B. Šljukić, Z. Kačarević-Popović, S. Mentus, Š. Miljanić, Radiolitically synthesized nano Ag/C catalysts for oxygen reduction and borohydride oxidation reactions in alkaline media, for potential applications in fuel cells, Energy 101 (2016) 79–90.
[530] R.C.P. Oliveira, J. Milikić, E. Daş, A.B. Yurtcan, D.M.F. Santos, B. Šljukić, Platinum/polypyrrole-carbon electrocatalysts for direct borohydride-peroxide fuel cells, Appl. Catal. B 238 (2018) 454–464.
[531] F. Asonkeng, G. Maranzana, J. Proust, M. François, L. Le Joncour, J. Dillet, S. Didierjean, G. Braesch, M. Chatenet, T. Maurer, Synthesis of metallic nanoparticles for heterogeneous catalysis: Application to the Direct Borohydride Fuel Cell, Appl. Catal. A Gen. 618 (2021), 118117.
[532] R. Ghasemi, B.K. Moghadas, I. Mohammadi, Solvothermal synthesis of Pd_{10}-Ni_{45}-Co_{45}/rGO composites as novel electrocatalysts for enhancement of the performance of DBFC, Int. J. Hydrog. Energy 45 (2020) 21808–21815.
[533] M.G. Hosseini, V. Daneshvari-Esfahlan, S. Wolf, V. Hacker, Novel bimetallic Pd-X (X= Ni, Co) nanoparticles assembled on N-doped reduced graphene oxide as an anode catalyst for highly efficient direct sodium borohydride-hydrogen peroxide fuel cells, ACS Appl. Energy Mater. 4 (2021) 6025–6039.
[534] S. Saha, P. Gayen, Z. Wang, R.J. Dixit, K. Sharma, S. Basu, V.K. Ramani, Development of bimetallic PdNi electrocatalysts toward mitigation of catalyst poisoning in direct borohydride fuel cells, ACS Catal 11 (2021) 8417–8430.
[535] S. Dey, S. Pramanik, P. Chakraborty, D.K. Rana, S. Basu, An easy synthesis of carbon-supported silver-cobalt bimetallic nanoparticles to study the electrocatalytic performance in alkaline borohydride fuel cell, J. Appl. Electrochem. 52 (2022) 247–258.
[536] A. Uzundurukan, E.S. Akça, Y. Budak, Y. Devrim, Carbon nanotube-graphene supported bimetallic electrocatalyst for direct borohydride hydrogen peroxide fuel cells, Renew. Energy 172 (2021) 1351–1364.
[537] T.H. Oh, Gold-based bimetallic electrocatalysts supported on multiwalled carbon nanotubes for direct borohydride-hydrogen peroxide fuel cell, Renew. Energy 163 (2021) 930–938.
[538] T.H. Oh, Effect of cathode conditions on performance of direct borohydride-hydrogen peroxide fuel cell system for space exploration, Renew. Energy 178 (2021) 1156–1164.
[539] S.S. Yu, T.H. Lee, T.H. Oh, Ag-Ni nanoparticles supported on multiwalled carbon nanotubes as a cathode electrocatalyst for direct borohydride-hydrogen peroxide fuel cells, Fuel 315 (2022), 123151.
[540] T.B. Ferriday, P.H. Middleton, Alkaline fuel cell technology-A review, Int. J. Hydrog. Energy. 46 (2021) 18489–18510.
[541] H.A. Miller, A. Lavacchi, F. Vizza, M. Marelli, F. Di Benedetto, F. D'Acapito, Y. Paska, M. Page, D.R. Dekel, A $Pd/CCeO_2$ anode catalyst for high-performance platinum-free anion exchange membrane fuel cells, Angew. Chem. Int. Ed. 55 (2016) 6004–6007.
[542] M. Bellini, M.V. Pagliaro, A. Lenarda, P. Fornasiero, M. Marelli, C. Evangelisti, M. Innocenti, Q. Jia, S. Mukerjee, J. Jankovic, L. Wang, J.R. Varcoe, C. B. Krishnamurthy, I. Grinberg, E. Davydova, D.R. Dekel, H.A. Miller, F. Vizza, Palladium-ceria catalysts with enhanced alkaline hydrogen oxidation activity for anion exchange membrane fuel cells, ACS Appl. Energy Mater. 2 (2019) 4999–5008.
[543] H.A. Miller, M.V. Pagliaro, M. Bellini, F. Bartoli, L. Wang, I. Salam, J.R. Varcoe, F. Vizza, Integration of a Pd-CeO_2/C anode with Pt and Pt-free cathode catalysts in high power density anion exchange membrane fuel cells, ACS Appl. Energy Mater. 3 (2020) 10209–10214.
[544] S. Kabir, K. Lemire, K. Artyushkova, A. Roy, M. Odgaard, D. Schlueter, A. Oshchepkov, A. Oshchepkov, A. Bonnefont, E. Savinova, D.C. Sabarirajan, P. Mandal, E.J. Crumlin, I.V. Zenyuk, P. Atanassov, A. Serov, Platinum group metal-free NiMo hydrogen oxidation catalysts: high performance and durability in alkaline exchange membrane fuel cells, J. Mater. Chem. 5 (2017) 24433–24443.
[545] A. Roy, M.R. Talarposhti, S.J. Normile, I.V. Zenyuk, V. De Andrade, K. Artyushkova, A. Serov, P. Atanassov, Nickel-copper supported on a carbon black hydrogen oxidation catalyst integrated into an anion-exchange membrane fuel cell, Sustain. Energy Fuels 2 (2018) 2268–2275.
[546] D. Basu, S. Basu, Synthesis, characterization and application of platinum based bi-metallic catalysts for direct glucose alkaline fuel cell, Electrochim. Acta 56 (2011) 6106–6113.
[547] L.Q. Wang, M. Bellini, J. Filippi, M. Folliero, A. Lavacchi, M. Innocenti, A. Marchionni, H.A. Miller, F. Vizza, Energy efficiency of platinum-free alkaline direct formate fuel cells, Appl, Energy 175 (2016) 479–487.
[548] O. Naumov, S. Naumov, B. Abel, A. Varga, The stability limits of highly active nitrogen doped carbon ORR nano-catalysts: a mechanistic study of degradation reactions, Nanoscale 10 (2018) 6724–6733.
[549] S.L. Scott, T.B. Gunnoe, P. Fornasiero, C.M. Crudden, To Err is human; To reproduce takes time, ACS Catal 12 (2022) 3644–3650.